Université de Montréal

Mutagénèse semi-aléatoire au site actif de la DHFR humaine : création et caractérisation de variantes hautement résistantes au MTX.

par
Jordan Volpato

Département de Biochimie
Faculté de Médecine

Thèse présentée à la Faculté des études supérieures
en vue de l'obtention du grade de *Philosophiae Doctor*
en biochimie

Décembre, 2008

Université de Montréal
Faculté des études supérieures

Cette thèse intitulée :

Mutagénèse semi-aléatoire au site actif de la DHFR humaine: création et caractérisation de variantes hautement résistantes au MTX.

présentée par :
Jordan Volpato

a été évaluée par un jury composé des personnes suivantes :

Christian Baron, président-rapporteur
Joelle Pelletier, directeur de recherche
Robert Lortie, membre du jury
Roger C. Lévesque, examinateur externe
Jurgen Sygusch, représentant du doyen de la FES

Résumé

La dihydrofolate réductase humaine (DHFRh) est une enzyme essentielle à la prolifération cellulaire. Elle réduit le dihydrofolate en tétrahydrofolate, un co-facteur impliqué dans la biosynthèse des purines et du thymidylate. La DHFRh est une cible de choix pour des agents de chimiothérapie comme le méthotrexate (MTX), inhibant spécifiquement l'enzyme ce qui mène à un arrêt de la prolifération et ultimement à la mort cellulaire. Le MTX est utilisé pour le traitement de plusieurs maladies prolifératives, incluant le cancer. La grande utilisation du MTX dans le milieu clinique a mené au développement de mécanismes de résistance, qui réduisent l'efficacité de traitement. La présente étude se penche sur l'un des mécanismes de résistance, soit des mutations dans la DHFRh qui réduisent son affinité pour le MTX, dans le but de mieux comprendre les éléments moléculaires requis pour la reconnaissance de l'inhibiteur au site actif de l'enzyme. En parallèle, nous visons à identifier des variantes plus résistantes au MTX pour leur utilisation en tant que marqueurs de sélection en culture cellulaire pour des systèmes particuliers, tel que la culture de cellules hématopoïétiques souches (CHS), qui offrent des possibilités intéressantes dans le domaine de la thérapie cellulaire.

Pour étudier le rôle des différentes régions du site actif, et pour vérifier la présence d'une corrélation entre des mutations à ces régions et une augmentation de la résistance au MTX, une stratégie combinatoire a été dévelopée pour la création de plusieurs banques de variantes à des résidus du site actif à proximité du MTX lié. Les banques ont été sélectionnées *in vivo* dans un système bactérien en utilisant des milieux de croissance contenant des hautes concentrations de MTX. La banque DHFRh 31/34/35 généra un nombre considérable de variantes combinatoires de la DHFRh hautement résistantes au MTX. Les variantes les plus intéressantes ont été testées pour leur potentiel en tant que marqueur de sélection dans plusieurs lignées cellulaires, dont les cellules hématopoïétiques transduites. Une protection complète contre les effets cytotoxiques du MTX a été observée chez ces cellules suite à leur infection avec les variantes combinatoires. Pour mieux

comprendre les causes moléculaires reliées à la résistance au MTX, des études de structure tridimensionnelle de variantes liées au MTX ont été entreprises. La résolution de la structure de la double variante F31R/Q35E lié au MTX a révélé que le phénotype de résistance était attribuable à d'importantes différences entre le site actif de la double variante et de l'enzyme native, possiblement dû à un phénomème dynamique. Une compréhension plus générale de la reconnaissance et la résistance aux antifolates a été réalisée en comparant des séquences et des structures de variantes de la DHFR résistants aux antifolates et provenant de différentes espèces.

En somme, ces travaux apportent de nouveaux éléments pour la comprehension des intéractions importantes entre une enzyme et un ligand, pouvant aider au développement de nouveaux antifolates plus efficaces pour le traitement de diverses maladies. De plus, ces travaux ont généré de nouveaux gènes de résistance pouvant être utilisés en tant que marqueurs de sélection en biologie cellulaire.

Mots-clés : dihydrofolate réductase humaine, catalyse enzymatique, inhibition, métabolisme du folate, mutagénèse combinatoire, résistance aux antifolates, méthotrexate, marqueurs de sélection, cellules hematopoïétiques, cristallographie aux rayons X.

Abstract

Human dihydrofolate reductase (hDHFR) is an enzyme that is essential to cell proliferation. It reduces dihydrofolate to tetrahydrofolate, an important cofactor involved in purine and thymidylate biosynthesis. hDHFR is a choice target for chemotherapeutic drugs like methotrexate (MTX), which specifically inhibits the enzyme, stopping cell proliferation and leading to cellular death. MTX is used for the treatment of many proliferative diseases, including cancers. Widespread use of MTX has lead to the development of resistance mechanisms appear which impair treatment efficiency. The present work focuses on a mechanism of resistance, namely mutations in hDHFR that reduce its affinity for MTX, to better understand the underlying mechanisms of inhibitor recognition at the active site of the enzyme. In parallel, we aim at identifying the most MTX-resistant variants to offer novel selectable markers for particular cell culture systems, such as hematopoietic cell culture, which offer important perspectives for cellular therapy.

To study the role of different regions of the hDHFR active site, and to verify if a correlation exists between mutations in these regions and increased resistance to MTX, a combinatorial strategy was developed enabling the creation of several hDHFR variant libraries at active site residues located in proximity to bound MTX. The libraries were selected *in vivo* in a bacterial system using culture media containing high concentration of the inhibitor. One library in particular, hDHFR 31/34/35, yielded a considerable number of highly MTX-resistant combinatorial hDHFR variants. The most interesting candidates were tested for their potential as selectable markers in various cell lines, including transduced hematopoietic cells. Complete protection from MTX-cytotoxicity was obtained for these cells following infection with the combinatorial variants. To better understand the molecular causes of MTX resistance, resolution of the crystal structures of variant proteins in presence of MTX was attempted. Resolution of the F31R/Q35E double variant revealed that the resistance phenotype was related to important differences in the active site relative to WT, possibly attributable to a dynamic motion effect. A more general comprehension of

antifolate recognition and resistance was achieved by sequence and structural comparison of antifolate-resistant DHFR variants from different species.

Overall, our work contributes to the better understanding of enzyme-inhibitor interactions, which could provide new insights into the development of more efficient clinical therapies. In addition, this work has yielded novel drug-resistance genes useful as selectable markers for cellular biology.

Keywords: human dihydrofolate reductase, enzyme catalysis, inhibition, folate metabolism, combinatorial mutagenesis, antifolate resistance, methotrexate, selectable markers, hematopoietic cells, X-ray crystallography.

Table des matières

Résumé iii
Abstract v
Table des matières vii
Liste des tableaux x
Liste des figures xii
Liste des abréviations xvi
Remerciements xxi

Préface au chapitre 1 1
Chapitre 1 - Introduction 2
1.0 Le métabolisme du folate 3
1.1 La dihydrofolate reductase humaine 6
1.1.1 – Propriétés et réaction catalytique 6
1.1.2 – Structure de la DHFR humaine et résidus du site actif 9
1.2 Les antifolates 14
1.2.1 – Les classes d'antifolates inhibant la DHFR 14
1.2.2 – Le méthotrexate 18
1.2.3 – Mécanismes de résistance au méthotrexate 22
1.3 Réduction de l'affinité au MTX par des mutations de la DHFR humaine 26
1.3.1 – Mutations de la DHFR retrouvées dans un contexte *ex vivo* 27
1.3.2 – Mutations de la DHFR identifiées dans un contexte *in vitro* 28
1.3.3 – Thérapie génique et utilisation de variantes résistantes au MTX pour la myeloprotection de cellules saines de la moelle osseuse 33
1.4 Objectifs du projet de recherche et justification des approches utilisées 39
1.4.1 – Création de banques d'ADN par mutagenèse semi-rationnelle et par saturation de sites 40

1.4.2 – Stratégie de sélection pour les banques de DHFR humaine et caractérisation des mutants actifs et résistants 41
1.4.3 – Évaluation de la protection de lignées cellulaires contre les effets cytotoxiques du MTX 42
1.4.4 – Développement d'un marqueur de sélection pour les cellules de la moelle osseuse transduites 44
1.4.5 – Cristallographie par rayons X pour élucider le mécanisme moléculaire de résistance au MTX 45

Préface au chapitre 2 47
Chapitre 2 - Augmentation de la résistance au MTX par la combinaison de substitutions au site actif de la dihydrofolate reductase humaine 48
2.1 Article 1. *Increasing MTX-resistance by combination of active-site mutations in human dihydrofolate reductase* 48

Préface au chapitre 3 90
Chapitre 3 - Développement d'un système à deux étapes pour la selection de variantes de la dihydrofolate reductase humaine actives et résistantes au MTX 92
3.1 Article 2. *2-tier bacterial and in vitro selection of active and methotrexate-resistant variants of human dihydrofolate reductase* 92

Préface au chapitre 4 125
Chapitre 4 - Sélection ex vivo de cellules hématopoiétiques transduites avec des doubles et triples variantes de la DHFRh hautement résistantes au MTX 126
4.1 Article 3. *Ex vivo* selection of hematopoietic cells using highly MTX-resistant human dihydrofolate reductase double and triple variants 126

Préface au chapitre 5 159

Chapitre 5 - Structure cristalline de la variante double F31R/Q35E de la dihydrofolate réductase humaine liée au MTX à une résolution de 1.7 Å 161

5.1 Article 4. Multiple conformers in human dihydrofolate reductase F31R/Q35E double variant suggest structural basis for methotrexate resistance 161

Préface au chapitre 6 197

Chapitre 6 - Comparaison de séquences et de structures de la dihydrofolate réductase provenant de mammifères, de bactéries et de parasites : identifiaction de régions mutées communes conférant une résistance aux antifolates 198

6.1 Article 5. Sequence and structural comparison of mammalian, bacterial and parasitic dihydrofolate reductases: cross-species 'hot-spots' provide antifolate resistance 198

Chapitre 7 - Conclusions et perspectives 255

7.0 – Conclusions générales 256

7.1 – Perspectives 260

7.1.1 – Effets des mutations sur la liaison d'autres antifolates 260

7.1.2 – Caractérisation des constantes d'isomérisation pour les mutants hautement résistantes au MTX 263

7.1.3 – Création de nouvelles banques de la DHFR humaine 265

7.1.4 – Obtention d'autres structures cristallines pour les variantes de la DHFR humaine hautement résistantes au MTX 268

7.1.5. – Études dynamiques des variantes de la DHFR humaine 269

Annexe 1 ..... A1.1

Liste des tableaux

Chapitre 2

Table 2.1. Amino acids encoded at residues 31, 34 and 35 of the hDHFR mutant library. 56

Table 2.2. Kinetic and inhibition constants for the selected MTX-resistant hDHFR mutants. 60

Table 2.3. EC_{50}^{MTX} for CHO DUKX B11 cells transfected with MTX-resistant hDHFR mutants. 65

Table 2.4. Comparison of MTX-resistant hDHFR mutated at positions F31 and F34. 67

Chapitre 3

Table 3.1. Reactivity (k_{cat}) and MTX or PMTX resistance determined in 96-well plates using crude lysates of active hDHFR variants from library 115. 110

Table 3.2. Kinetic and inhibition constants [a] of purified MTX or PMTX-resistant hDHFR mutants. 118

Chapitre 4

Table 4.1. EC_{50}^{MTX} for GP+E-86 cells transduced with hDHFR variants. 137

Chapitre 5

Table 5.1. Crystallography data. 170

Table 5.2. Kinetic and inhibitory parameters of WT hDHFR and hDHFR F31R/Q35E variant 172

Table 5.3. Polar interactions in F31R/Q35E and WT hDHFR (1U72) complexed with MTX 184

Chapitre 6

Table 6.1. Mutations providing MTX-resistance in human DHFR..... 206

Table 6.2. Substitutions providing PYR and/or CYC-resistance in *plasmodium* DHFR.. 217

Table 6.3. Homologous active site residues in DHFRs from different species..... 218

Table 6.4. Cross-species comparison of K_i for TMP and MTX, and identity at positions 22, 31 and 61 235

Chapitre 7

Tableau 7.1. Constantes d'affinité pour différents ligands chez les variantes combinatoires 31/34/35 de la DHFRh. 261

Annexe 1

Table A1.1. Crystallographic data for His6-hDHFR F31R/Q35E.....A1.7

Liste des figures

Chapitre 1

Figure 1.1. Structure chimique du folate 4
Figure 1.2. Métabolisme du folate. 5
Figure 1.3. Réaction principale catalysée par la DHFR. 8
Figure 1.4. Représentation globulaire de la structure de la DHFR humaine 10
Figure 1.5. Site actif de la DHFR humaine en présence des ligands naturels 11
Figure 1.6. Mécanisme catalytique de la DHFR humaine 13
Figure 1.7. Structure chimique d'antifolates classiques et non-classiques 16
Figure 1.8. Liaison du MTX à la DHFR humaine 21
Figure 1.9. Mécanismes de résistance au MTX 23
Figure 1.10. Schématisation des étapes de la thérapie génique appliquées dans un contexte de chimioprotection 36

Chapitre 2

Figure 2.1. Ligand binding at the active-site of WT hDHFR 52
Figure 2.2. Frequency of occurrence of the novel MTX-resistant mutants 58
Figure 2.3. Relation between the number of hDHFR mutations and k_{cat}/K_M^{DHF} or K_i^{MTX} relative to WT His_6-hDHFR 62
Figure 2.4. Survival of CHO DUKX B11 cells transfected with selected mutants in presence of MTX 64
Figure 2.5. *In silico* comparison of MTX binding between (A) WT hDHFR (1U72) and (B) mutant AVH 72

Chapitre 3

Figure 3.1. Structures of **(A)** folate (1DRF.pdb) and **(B)** MTX (1U72.pdb) bound to hDHFR active site 102

Figure 3.2. Flowchart of the 2-tier strategy to select mutated hDHFR library variants for **(A)** catalytic activity or **(B)** methotrexate (MTX) resistance 105

Figure 3.3. Comparison of hDHFR mutations that allow for conservation of activity **(A)** or MTX resistance **(B)** on the basis of the 2-tier selection strategy 106

Figure 3.4. The 2-tier selection results for library 115 107

Figure 3.5. IC_{50}^{MTX} concentration-response curves (mean ± SD; n = 3) of WT hDHFR (■), V115A (●) and V115 C (▲) using **(A)** crude lysate or **(B)** purified enzyme 116

Chapitre 4

Figure 4.1. MTX-resistance of GP+E-86 cells infected with hDHFR variants 138

Figure 4.2. Time-course of *ex vivo* MTX-selection of murine BM cells in minimal medium. BM cells infected with MIG, WT hDHFR and RFE were diluted to 15% with mock-infected BM cells according to GFP fluorescence 141

Figure 4.3. Myeloid clonogenic progenitor assays of infected BM cells following MTX selection in minimal liquid medium 142

Figure 4.4. Effect of MTX-selection on HS and progenitor cells 145

Figure 4.5. Southern blot analysis of genomic DNA from bone marrow, spleen and thymus from five mice reconstituted to > 40% $CD45.2^{+}/GFP^{+}$ cells at different LDAs 148

Chapitre 5

Figure 5.1. Chemical structures of hDHFR ligands. 165

Figure 5.2. Double variant cycle of F31R/Q35E for DHF and MTX affinity 174

Figure 5.3. Structure of hDHFR variant F31R/Q35E 176

Figure 5.4. Polar (A) and non-polar interactions (B) with bound MTX in hDHFR variant F31R/Q35E 179
Figure 5.5. Alternate side chain conformers at active site residues Tyr33 (A) and Arg31 (B) in hDHFR variant F31R/Q35E 180
Figure 5.6. Position of MTX, Arg31 and Glu35 in F31R/Q35E relative to the position observed in WT hDHFR (1U72)..... 183
Figure 5.7. Shift of loop 17-27 in hDHFR variant F31R/Q35E..... 185
Figure 5.8. Surface representation of the contacts established between residues 22 and 31 in WT hDHFR (A; 1U72), variant F31R/Q35E with Arg31B (B) and variant F31R/Q35E with Arg31A (C) bound to MTX. 187
Figure 5.9. Docking of folate onto WT hDHFR and variant F31R/Q35E 190

Chapitre 6

Figure 6.1. Chemical structures of dihydrofolate and antifolates used to inhibit DHFR activity in different species 202
Figure 6.2. Binding of MTX to the active site of human DHFR 207
Figure 6.3. Sequence alignment of DHFRs from different species 210
Figure 6.4. Superposition of hDHFR (1U72) with *pf*DHFR (A; 1J3I), *pv*DHFR (B; 1BL9) and *mt*DHFR (C; 1DG5)..... 222
Figure 6.5. 'Hot-spots' for mutations conferring resistance to antifolates in DHFRs from different species plotted on human DHFR (1U72) 226
Figure 6.6. Surface representation of hDHFR, *ec*DHFR, *pc*DHFR and *mt*DHFR complexed with MTX..... 231

Chapitre 7

Figure 7.1. A) Relation entre la perte d'affinité pour le MTX et le PMTX chez les variantes combinatoires 31/34/35 de la DHFRh. B) Arrimage moléculaire du PMTX sur la structure de la DHFRh native (1U72.pdb) 262

Figure 7.2. Schéma de l'étape d'isomérisation menant à une forte affinité entre l'enzyme (E) et l'inhibiteur (I)..... 264

Figure 7.3. Futurs sites à muter chez la DHFRh pour l'étude de la liaison du MTX 266

Annexe 1

Figure A1.1. Preliminary experiments to evaluate the efficiency of highly MTX-resistant hDHFR double and triple mutants as ex vivo selection markers for hematopoietic.....A1.3

Figure A1.2. Multiple conformers of Arg31 in the lower resolution His6-hDHFR F31R/Q35E relative to 1.7 Å resolution hDHFR F31R/Q35E.....A1.8

Liste des abréviations

ACT	*Adoptive cell therapy*
AD	*Adenosine Deaminase*
ADN	*Acide désoxyribonucléique*
ADNc	*Acide désoxyribonucléique cloné*
AICARFT	*5-aminoimidazole-4-carboxamide ribonucleotide formyltransferase*
Ala ou A	*Alanine*
AMPc	*Adénosine monophosphate cyclique*
AMT	*Aminoptérine*
Arg ou R	*Arginine*
ARN	*Acide ribonucléique*
ARNm	*Acide ribonucléique messager*
Asn ou N	*Asparagine*
Asp ou D	*Aspartate (acide aspartique)*
ATP	*Adénosine triphosphate*
BM	*Bone marrow*
CFU	*Colony forming units*
CHO	*Chinese hamster ovary*
CYC	*Cycloguanine*
Cys ou C	*Cysteine*
DHF	*Dihydrofolate*
DHFR	*Dihydrofolate reductase*
DNA	*Deoxyribonucleic acid*
dUMP	*Uridine deoxyribonucleotide monophosphate*
10-EDAM	*Edatrexate*
E. coli	*Escherichia coli*
EC_{50}	*Half maximal effective concentration for cell growth inhibition*

5-FU	*5-fluorouracil*
FPGS	*Folylpolyglutamate synthase*
GARFT	*5-phosphoribosylglycinamide formyltransferase*
GFP	*Green fluorescent protein*
Gln ou Q	*Glutamine*
Glu ou E	*Glutamate (acide glutamique)*
Gly ou G	*Glycine*
GTP	*Guanidine triphosphate*
hDHFR	*Human dihydrofolate reductase*
His ou H	*Histidine*
HS	*Hématopoïetique souche*
HSC	*Hematopoietic stem cell(s)*
IC_{50}	*Half maximal effective concentration for enzyme inhibition*
Ile ou I	*Isoleucine*
IPTG	*Isopropyl β-D-1-thiogalactopyranoside*
k_{cat}	*Constante catalytique*
K_D	*Constante de liaison*
K_i	*Constante d'inhibition*
K_M	*Constante d'affinité*
L. major	*Leishmania major*
Leu ou L	*Leucine*
LLA	*Leucémie lymphobastique aigüe*
LNLA	*Leucémie non-lymphocytaire aigüe*
Lys ou K	*Lysine*
M. tuberculosis	*Mycobacterium tuberculosis*
*m*Cl-PYR	*Metachloropyrimethamine*
MC	*Methylcellulose*
MDR	*Multi-drug resistance*

Met ou M	*Methionine*
MGMT	*O6-methylguanine-DNA methyltransferase*
mM	*Millimolaire*
µM	*Micromolaire*
MSCV	*Mouse stem cell virus*
MTHFR	*N^5, N^{10}-Methylenetetrahydrofolate reductase*
MTX	*Methotrexate*
NADPH	*Nicotinamide adenine dinucleotide phosphate*
NBMPR-P	*Nitrobenzylthioinosine 5'-monophosphate*
nM	*Nanomolaire*
P. carinii	*Pneumocystis carinii*
P. falciparum	*Plasmodium falciparum*
P. malariae	*Plasmodium malariae*
P. ovale	*Plasmodium ovale*
P. vivax	*Plasmodium vivax*
p-ABA	*para-aminobenzoyl*
PCR	*Polymerase chain reaction*
Phe ou F	*Phenylalanine*
pM	*Picomolaire*
PMTX	*Pemetrexed*
Pro ou P	*Proline*
PYR	*Pyrimethamine*
RFC	*Reduced folate carrier*
RMN	*Résonance magnétique nucléaire*
SCID	*Severe combined immunodeficiency*
SDS-PAGE	*Électrophorèse sur gel de polyacrylamide en présence de dodécylsulfate de sodium*
Ser ou S	*Serine*

SHMT	*Serine hydroxymethyltransferase*
THF	*Tetrahydrofolate*
Thr ou T	*Threonine*
TMP	*Trimethoprim*
TMTX	*Trimetrexate*
Trp ou W	*Trytophane*
TS	*Thymidylate synthase*
Tyr ou Y	*Tyrosine*
VSV-G	*Vesicular stomatitis virus G-protein*
WT	*Wild-type*

À Lise et Graciosa, qui m'ont guidé vers la voie de la recherche

Remerciements

Été 2002. Je me lance dans une aventure qui mènera ultimement à la rédaction des mots que vous êtes en train de lire et les quelques centaines de pages qui les suivent. Plus qu'une aventure, mon temps passé à l'Université de Montréal, qui totalise plus de 9 ans si l'on compte mes années au baccalauréat, aura été une véritable expérience de vie : une odyssée menant autant à l'approfondissement des connaissances académiques qu'aux choses de la vie sous ses innombrables aspects. Bien que mon nom figure seul sur la page titre de cet ouvrage, il n'en demeure pas moins que cette thèse est le fruit d'une collectivité qui m'a entouré, conseillé, écouté et appuyé tant du côté professionnel que personnel.

Si l'on me place au centre de mon entourage professionnel, on retrouve ma directrice de thèse, Joelle Pelletier, en périphérie immédiate. Sa curiosité et sa passion scientifique, sa pluridisciplinarité, ses talents de rédactrice et communicatrice et son soutien constant ont été un véritable modèle à suivre pour le développement des aptitudes essentielles menant à la formation complète d'un jeune chercheur. Malgré un horaire pouvant parfois défier le continuum espace-temps, j'ai plus souvent que jamais eu accès à une porte grande ouverte et une oreille prête à entendre (des fois malgré elle☺) mes nouvelles idées pour le projet DHFR ou le labo, mes grands théorêmes scientifiques du moment, ou encore mes pensées philosophiques sur différents aspects de la vie de tous les jours. Je tiens surtout à la remercier pour son appui et sa présence constante pendant toutes ces années.

Mes années au laboratoire Pelletier n'auraient pas été aussi mémorables sans les nombreuses personnes que j'ai eu la chance d'y côtoyer. J'ai pu rencontrer plusieurs collègues qui sont devenus pour moi des membres d'une grande famille 'scientifique', avec qui j'ai vécu plusieurs expériences mémorables dans un contexte qui n'était pas uniquement professionnel. Je tiens tout d'abord à remercier 'la vieille école', soit les gens qui ont aidé à démarrer le groupe et qui ont quitté depuis pour poursuivre leur carrière scientifique.

Nicolas Doucet, un pur homme de science, un exemple à suivre dans pratiquement tout, toujours prêt à débattre intelligemment sur à peu près n'importe quel sujet qui lui passe par la tête (fruit de longues discussions au fil des ans); Roberto Chica, un scientifique prometteur qui m'a démontré, tant au labo que pendant notre colocation, que certains (et je mets une emphase particulière sur ce mot) groupes des '70s and 80s' valent la peine d'être écoutés ('Hysteria, Yea-ah, get ready for lo-ove!!!'); PY de Waals, le 'petit frère' du groupe, qui a su garder un calme exemplaire malgré les 'attaques' fréquentes qu'il subissait des plus vieux (merci d'avoir laissé ton 'Angel King' à la maison); Elena Fossati, une brillante collaboratrice qui a su se démarquer autant par son savoir scientifique que sa capacité pour maîtriser une langue qui n'est pas la sienne en un temps record (même s'il reste à ce jour plusieurs baaaahhh au début de ses phrases); Lucie Poulin, la précision et l'exactitude incarnées en science, la gentillesse incarnée dans la vie de tous les jours, et la reine des gâteaux et des tartes maisons! Et ce que je considère être le dernier mais non le moindre de la vieille école, Jonathan Blanchet, alias 'The Crystalizer'.

Vient ensuite 'the new school', qui constitue la relève actuelle du labo Pelletier. Chris Clouthier, un mentor et ami qui ne cesse de m'épater par son intérêt dans tout et ses ambitions grandioses (you can do it Chris!); Claudio Gnaccharani, mon 'prof' d'italien, ma victime au jeu 'Briscola', qui est autant passionné par la science que par la culture nord-américaine (bah-dy!); Vanessa Guerrero, qui a comblé le départ de Lucie en étant son égale dans toutes les choses que j'ai mentionnée plus haut (il te manque juste ton petit Raphael); et la nouvelle addition du groupe, Mirja Krause, l'héritière de la continuation de ce projet de thèse, qui a su rapidement démontré qu'elle avait la motivation et le savoir scientifique pour continuer ce projet.

Je tiens aussi à remercier ma famille scientifique par extension, soit les gens avec qui j'ai collaboré de proche ou de loin sur plusieurs projets. Tout d'abord, Jeff Keillor, qui m'a aidé plus d'une fois avec des casse-têtes cinétiques de la DHFR humaine, et les gens de son groupe qui ont souvent instigué des 5 à 7 sous forme de vins et fromages (Chabot(te)!),

ce qui a permis de maintenir des liens serrés entre les deux groupes. Ensuite viennent mes collaborateurs de l'IRIC, Nadine Mayotte (une 'coach' hors-pair) et Dr. Guy Sauvageau, qui m'ont donné la chance de découvrir et de développer une véritable passion pour le monde des cellules souches hématopoïétiques. Brahm Yachnin et Dr. Albert Berghuis, qui de leur côté, ont été des collaborateurs exceptionnels pour la partie plus structurale du projet de recherche.

Étant impliqué dans les affaires étudiantes pendant toutes mes années à l'université, j'ai pu rencontrer de multiples personnes avec qui j'ai développé des liens au-delà de l'aspect académique. Ainsi, j'aimerais remercier une bonne partie de la gang de l'aile A-5 (Ti-Fred, Karine, Laurent, St-Louis, Vinny boy, Franck), JLV, Martin Audet, Félix, qui ont toujours été là pour m'entendre parler de mes aventures au doctorat et autres circonstances, ainsi que Nicolas Lahaie, que j'ai rencontré en tant que stagiaire au laboratoire Pelletier et qui est devenu un 'conseiller', un bras droit pour les affaires associatives et un véritable ami durant toutes ces années. Longue vie prospère (et scientifique) à vous tous!

Finalement, sans vouloir tomber dans le cliché total, il aurait été impossible pour moi de terminer ces longues études sans le support constant de mes amis 'non-biochimistes' et ma famille. Merci de m'avoir fait sentir que vous m'appuyiez pendant toutes ces années même si vous ne compreniez pas toujours ce que je faisais exactement. Sans vous, je ne serais pas ici. Karim, Sharif, Big Will, Michael, des amis comme vous viennent qu'une fois dans la vie. La famille Lemoine, qui m'a appuyé pendant la majeure partie de mon doctorat. Joanne et George (mes parents et co-locataires à temps partiel depuis plus d'un an), Marissa et Alex, je ne pourrais être plus choyé de vous avoir comme famille immédiate. Merci de toujours me donner un vote de confiance, un appui constant et votre amour pendant mes études doctorales qui ont parfois pu paraître interminables. Voici maintenant le début de la fin…

'Research is to see what everybody else has seen, and to think what nobody else has thought'

-Albert Szent-Gyorgy

'The war against cancer is far from over'

-John C. Bailar III.

'Every discoverer of a cancer remedy has encountered a Chinese wall of resistance'

-M. H. Clutter

Préface au chapitre 1

Le sujet de la présente thèse gravite autour d'une enzyme essentielle à la survie de toute cellule, soit la dihydrofolate reductase (DHFR) humaine. Plus précisement, l'objectif général du projet fut de contribuer à la caractérisation d'un mécanisme de résistance au méthotrexate (MTX), un agent de chimiothérapie utilisé dans le domaine clinique pour inhiber l'activité de cette enzyme. L'affinité qu'a la DHFR pour le MTX peut être grandement réduite suite à l'acquisition de certaines mutations ponctuelles dans le site actif de l'enzyme. Pour mieux caractériser ce mécanisme, des études de mutagénèse ont porté sur la majorité des résidus du site actif de l'enzyme, dans le but de mieux comprendre le rôle des différents résidus dans la liaison du MTX. En parallèle, une stratégie visant à obtenir des variantes hautement résistantes au MTX a été développée. Ces variantes ont été obtenus par la combinaison de substitutions ponctuelles à différents résidus, générant des variantes ayant grandement perdu de l'affinité pour le MTX. Les variantes hautement résistantes au MTX ont le potentiel d'être utilisés en thérapie génique pour la protection de certaines cellules saines affectées par la cytotoxicité du MTX lors d'un traitement. En plus, l'utilisation de variantes de la DHFR hautement résistantes au MTX offre une solution possible à l'un des problèmes majeurs empêchant actuellement l'application de la thérapie génique.

À titre de mise en contexte du projet, le présent chapitre décrit le rôle du folate et de la DHFR humaine dans le métabolisme cellulaire ainsi la structure moléculaire de l'enzyme et son mécanisme catalytique. En plus de décrire la chimie des molécules inhibitrices de la dihydrofolate reductase, une section est consacrée à l'inhibiteur le plus utilisé dans le domaine clinique pour contrer l'activité DHFR, le MTX. Un résumé des principaux mécanismes cellulaires de résistance au MTX est également présenté, avec une attention particulière portée sur les variantes de la DHFR résistantes au MTX et leur application potentielle dans le domaine clinique. En dernier lieu, les méthodes expérimentales utilisées pour la réalisation de cette thèse sont présentées.

Chapitre 1

Introduction

1.0 Le métabolisme du folate

En 1931, Lucy Willis démontrait que l'anémie de gestation pouvait être traitée par l'administration d'extraits de levures à des femmes enceintes[1]. Elle émit l'hypothèse qu'une molécule retrouvée dans l'extrait menait à cette guérison, qu'elle nomma le facteur Willis. En 1941, Mitchell *et al.* isolèrent le facteur Willis de feuilles d'épinards, et rebaptisèrent la molécule avec le nom folate (du latin *folium* : feuille)[2]. Ils purent aussi démontrer que le folate avait un rôle dans la prolifération cellulaire, les bactéries pouvant croître plus rapidement dans un milieu de croissance contenant la molécule. Le folate fût classifié comme une vitamine (vitamine B9), étant donné ses propriétés de guérison et de prolifération cellulaire.

La détermination de la structure du folate et l'établissement de la synthèse chimique du folate[3] ont permis d'élucider le rôle métabolique du folate dans la cellule. Le folate est constitué de trois parties chimiques distinctes, soit un noyau ptérine, une partie *p*-aminobenzoyle et une partie glutamate (**Figure 1.1**). Le noyau ptérine peut être réduit pour former les dérivés foliques dihydrofolate (DHF) et tétrahydrofolate (THF). Ce sont ces dérivés du folate qui jouent un rôle important dans le maintien et la prolifération cellulaire de tous les organismes vivants[4].

Chez les mammifères, le folate pénètre dans le cytoplasme des cellules *via* le récepteur du folate[5]. Une fois dans la cellule, le folate est polyglutamylé au carbonyle γ de sa queue glutamate par la folylpolyglutamate synthétase (FPGS)[6]. La polyglutamation permet une rétention prolongée du folate dans la cellule puisque le folate polyglutamylé n'est plus un substrat pour le récepteur du folate[7]. En parallèle, la polyglutamation augmente aussi l'affinité de diverses enzymes pour les dérivés métaboliques du folate[8] (**Figure 1.2**). Le folate polyglutamylé est alors réduit en DHF, substrat de la dihydrofolate reductase (DHFR), qui réduit le DHF en THF. Le THF sera enzymatiquement modifié pour porter des groupements monocarbonées aux atomes N_5 ou N_{10} qui seront utilisés lors de la

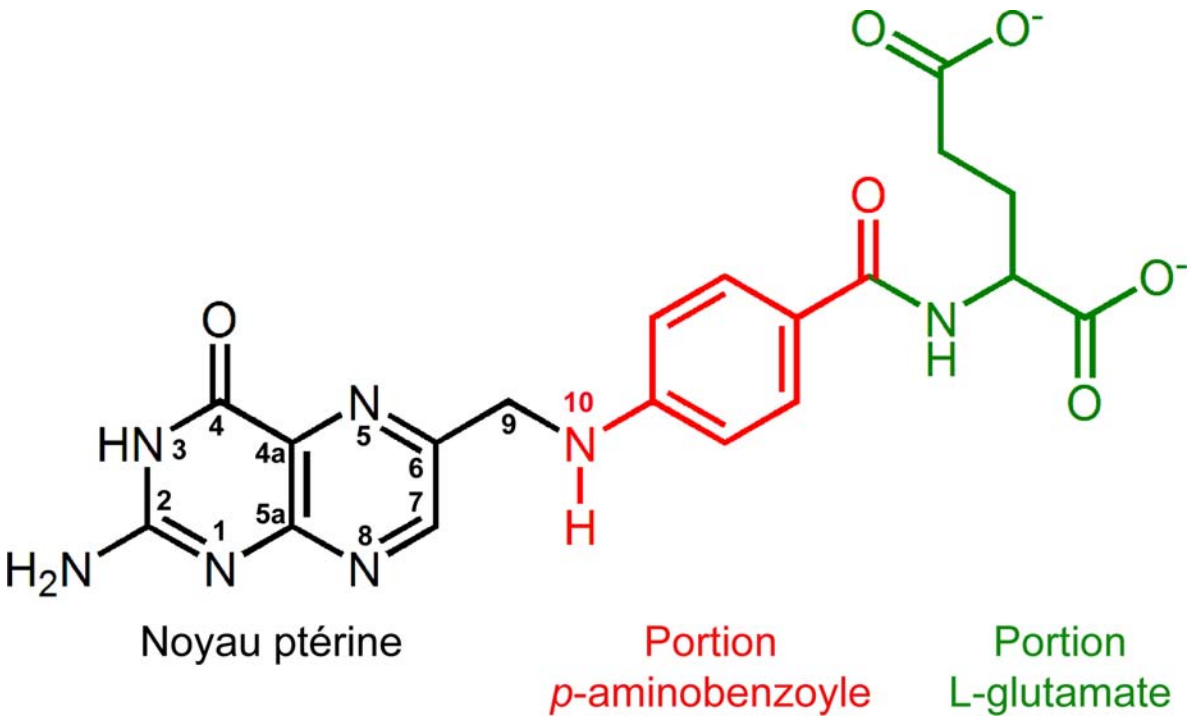

Figure 1.1. Structure chimique du folate. Le folate est une molécule composée de trois portions, soit un noyau ptérine (en noir), une portion *p*-aminobenzoyle (en rouge) et une portion L-glutamate (en vert).

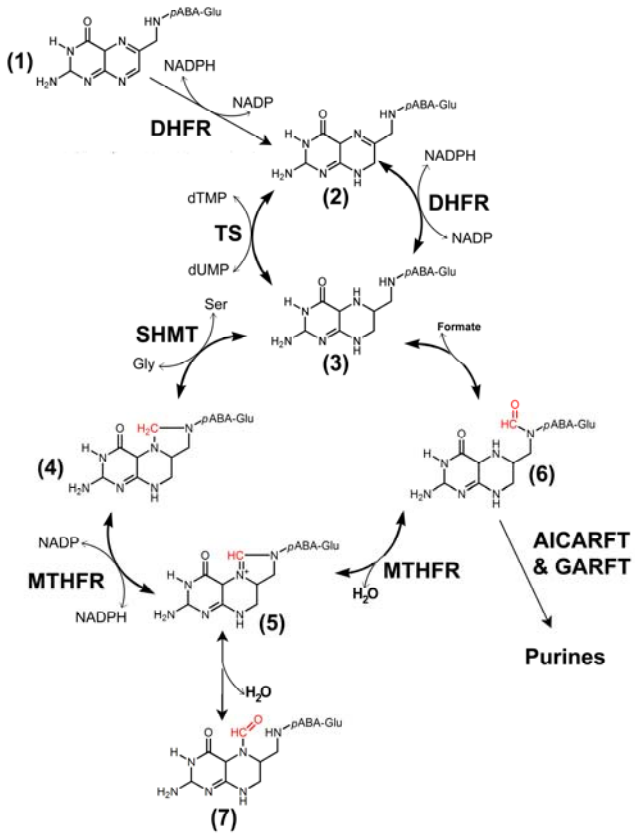

Figure 1.2. Métabolisme du folate. Le folate (1) est converti en DHF (2) puis THF (3) par la DHFR. Le THF sert de cofacteur à la TS pour la synthèse de dTMP, ou de substrat à la SHMT pour la formation de 5,10-méthylène-THF (4), initiant le cycle des dérivés du THF. L'enzyme multifonctionnelle MTHFR oxide le composé (4) pour donner le 5,10-méthényl-THF (5), qui est converti en 10-formyl-THF (6) par l'action de la même enzyme. Le 10-formyl-THF (6) est un cofacteur des enzymes AICARFT et GARFT, impliquées dans la voie de la biosynthèse des purines. La MTHFR peut aussi catalyser la formation de 10-formyl-THF (6) directement à partir de THF (3). En cas d'inhibition de la DHFR, le cycle des dérivés du THF peut être 'sauvé' par l'administration de 5-formyl-THF (Leucovorine; (7)). Les différents groupements d'intérêts présents sur les dérivés de THF sont en rouge. Adapté de [4].

biosynthèse de nucléotides *de novo*[4]. Ainsi, le THF peut servir de substrat à l'enzyme sérine hydroxyméthyltransférase (SHMT), qui transfère le carbone β de la sérine sur le THF, formant ainsi le 5,10-méthényl-THF et la glycine. Le 5,10-méthényl-THF est le co-facteur de l'enzyme thymidylate synthase (TS), qui transfert le groupement méthényl sur le dUMP, générant ainsi une molécule de dTMP, qui servira à la synthèse d'ADN *de novo*[4]. Le 5,10-méthényl-THF et le THF sont aussi impliqués dans la synthèse des purines. Ces deux composés peuvent être transformés en 10-formyl-THF par l'enzyme trifonctionnelle 5,10-méthylène-THF déshydrogénase (MTHFR)[9]. Le 10-formyl-THF sert de co-facteur dans les réactions catalysées par la 5-phosphoribosylglycinamide formyltransferase (GARFT) et l'aminoimidazole carboxamide ribonucleotide formyltransferase (AICARFT), deux enzymes impliquées dans la voie métabolique de la synthèse des purines, qui mènera à la formation de GTP et d'ATP. Ces deux molécules sont destinées à servir de source d'énergie métabolique à la cellule en plus d'être des blocs de construction nécessaires à la réplication de l'ADN lors de la division cellulaire[4]. L'ensemble de ces réactions ne serait pas possible sans l'activité de la première enzyme impliquée dans le métabolisme du folate, soit la dihydrofolate réductase (DHFR).

1.1 La dihydrofolate reductase humaine

1.1.1 – Propriétés et réaction catalytique

La présence d'une enzyme pouvant réduire le folate en THF fut initialement proposée suite à des observations de microorganismes bactériens[10, 11] et d'extraits de cellules de mammifères[12]. Osborn et Huennekens[13] furent les premiers à démontrer que cette réaction se déroulait en deux étapes, en isolant une déshydrogénase de foie de poulet qui réduisait le DHF en THF, mais pas le folate en THF. C'était la découverte de l'enzyme dihydrofolate réductase.

La dihydrofolate réductase est présente chez tous les organismes procaryotes et eucaryotes, où elle est exprimée constitutivement dans le cytosol. Chez l'humain, le gène de la DHFR se retrouve sur le chromosome 5 et encode une enzyme constituée de 186 acides aminés[14]. Bien que la DHFR humaine soit considérée comme une enzyme exprimée constitutivement, son expression peut être modulée par les concentrations cellulaires de certains facteurs de croissance et/ou d'AMPc[15]. Comme d'autres enzymes pouvant lier des co-facteurs nucléotidiques[16, 17], la DHFR humaine peut lier son ARN messager au niveau du site actif pour réguler son activité, empêchant ainsi la liaison des substrats[18].

Tel que mentionné précedemment, la DHFR catalyse une réaction primordiale dans le métabolisme du folate, soit la réduction du 7,8-DHF en 5,6,7,8-THF. La réaction est dépendante du co-facteur NADPH qui est oxydé en $NADP^+$ lors de la réaction[13] (**Figure 1.3**). Des études *in vitro* avec l'enzyme recombinante ont permis de déduire le schéma réactionnel complet, en mesurant les vitesses d'association et de dissociation de chaque substrat et produit[19]. À des concentrations de substrats imitant les conditions cellulaires, le NADPH initie le cycle catalytique en se liant au site actif de l'enzyme. Le DHF se lie et la réduction est catalysée par la protonation de l'atome N_5 du noyau ptérine et un transfert d'hydrure de l'atome C_4 de la portion ribonicotinamide du NADPH vers l'atome C_6 du noyau ptérine du DHF. La vitesse du transfert d'hydrure varie selon le pH. Toutefois, à pH physiologique, le transfert d'hydrure est l'une des étapes les plus rapides du schéma réactionnel global, tel que démontré par l'effet isotopique négligeable observé lorsque l'agent réducteur est le NADPD[20]. Le relâchement des produits constitue l'étape limitante du cycle catalytique à pH physiologique. Actuellement, il n'est toujours pas clair quel produit est relâché en premier pour la reprise d'un nouveau cycle catalytique étant donné que les vitesses de dissociation du THF et du $NADP^+$ sont pratiquement identiques[19].

Le mécanisme catalytique entourant la réaction de réduction a longtemps été un sujet de débat chez l'enzyme humaine. Pour que le transfert d'hydrure entre les atomes C_4 du NADPH et C_6 du DHF s'effectue, l'atome N_5 du DHF doit être protonné, générant ainsi

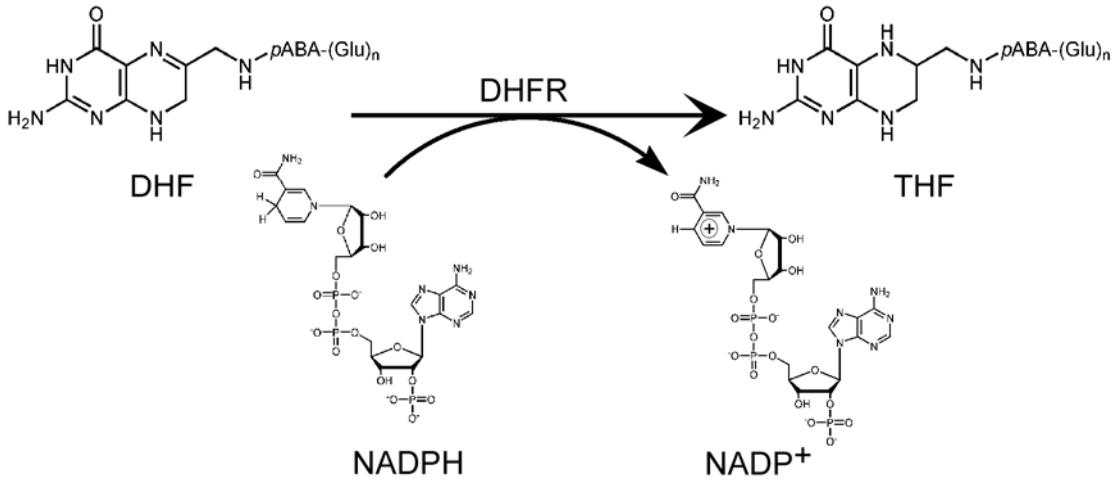

Figure 1.3. Réaction principale catalysée par la DHFR.

un carbocation au C_6 du noyau pterine. Deux hypothèses principales furent émises quant à la protonation de l'atome N_5 : 1- présence d'un acide aminé avec une fonction carboxylique au site actif de l'enzyme pouvant protonner N_5 du noyau pterine[21]; 2- protonation du DHF avant son entrée dans le site actif de la DHFR[22]. La première hypothèse fut généralement plus acceptée, puisqu'une mutation de l'acide aminé Asp27 en Asn abolissait l'activité enzymatique de la DHFR d'*Escherichia coli* (*E. coli)*[21]. Un alignement de séquences révélait que le résidu humain homologue à l'Asp27 était le Glu30, pouvant aussi potentiellement protonner le DHF au site actif de l'enzyme. Il est à noter que l'enzyme est également présumée responsable de la réduction du folate en 7,8-DHF, bien que les données cinétiques *in vitro* avec le folate semblent indiquer que cette réaction se produit beaucoup plus lentement que la réduction du DHF en THF[23].

1.1.2 – Structure de la DHFR humaine et résidus du site actif

La résolution par cristallographie aux rayons X de la structure tridimensionnelle de la DHFR humaine démontrait qu'elle présentait une forte homologie de structure avec les DHFRs d'autres espèces eucaryotes et procaryotes[24-35]. La DHFR humaine est formée d'un feuillet β central constitué de 8 brins β (7 parallèles et 1 anti-parallèle ; β1 à 8), flanqués de 4 hélices α (α1 à 4) en surface, les structures secondaires étant reliées entre elles par des boucles (**Figure 1.4**). Le site actif, qui est au cœur de l'enzyme, contient deux sites de liaison, un pour le substrat et l'autre pour le co-facteur (**Figure 1.5A**).

La partie ribonicotinamide du NADPH se lie dans un sillon créé à l'interface des hélices α2, α4, le brin β1 et une partie de la boucle reliant le brin β1 à l'hélice α1 (**Figure 1.5B**). Cette portion du co-facteur forme des ponts hydrogène avec le squelette peptidique du résidu Ala9[36], et des contacts hydrophobes avec les résidus Ile16 et Leu22[31, 36]. Les portions diphosphate et riboadénine sont en surface du site actif, et forment des ponts hydrogène avec les résidus Lys55, Ser119 (portion diphosphate)[36] et Arg77 (portion

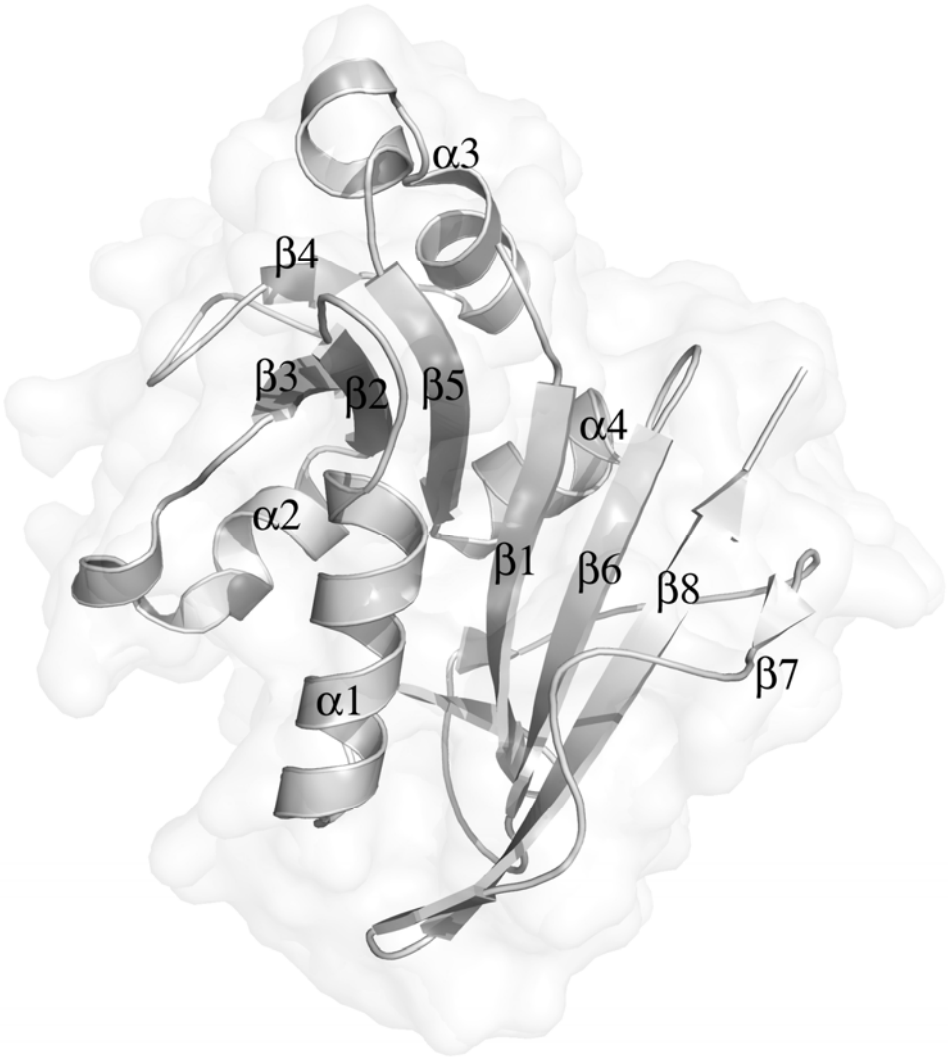

Figure 1.4. Représentation globulaire de la structure de la DHFR humaine. La DHFR humaine comporte 4 hélices α (α1 à α4), entourant un feuillet β central composé de 8 brins (β1 à β8). Cette image a été créée à partir du fichier 1U72.pdb[34].

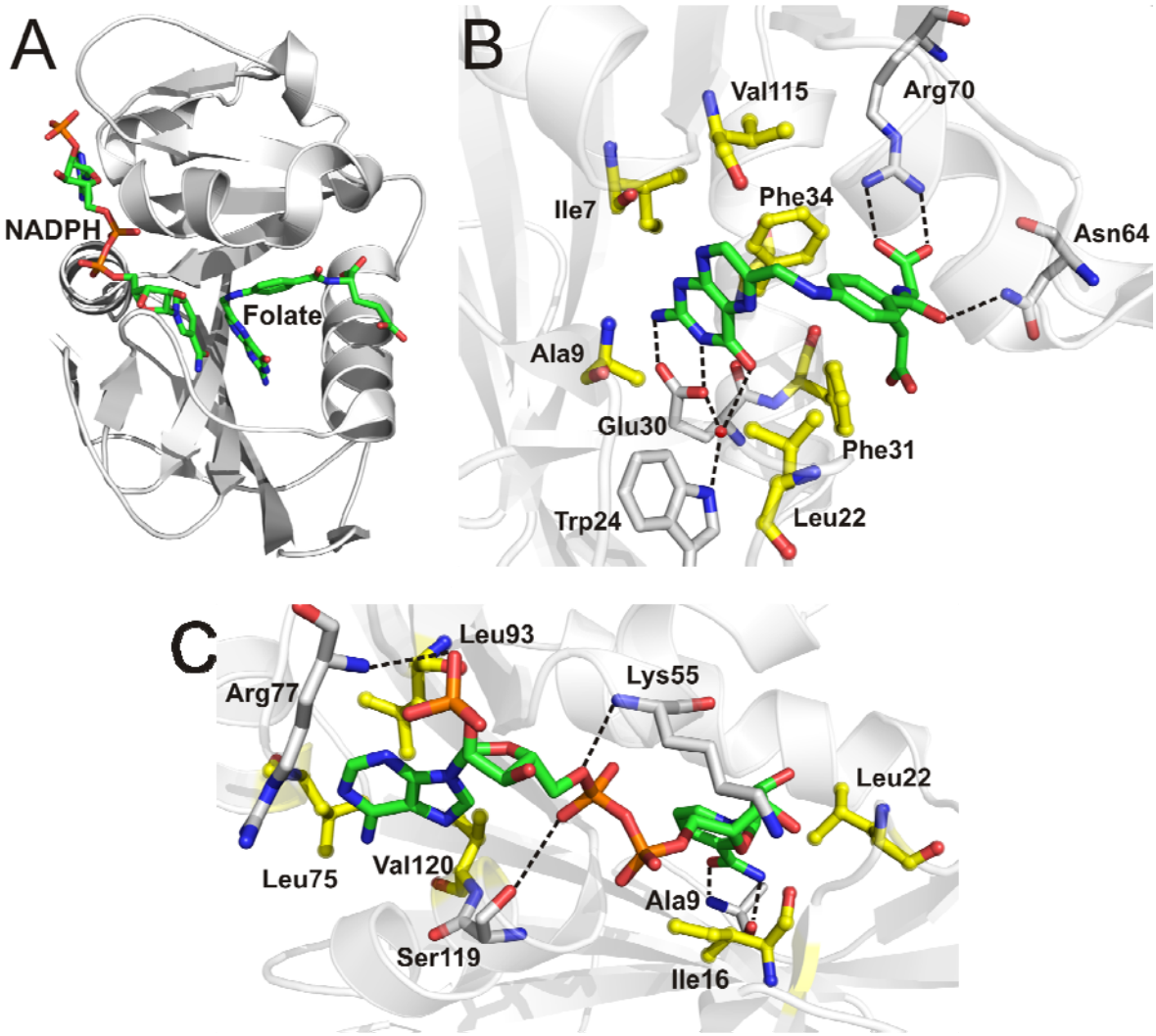

Figure 1.5. Site actif de la DHFR humaine en présence des ligands naturels (superposition des structures 1U72.pdb[34] et 1DRF.pbd[24]). A : Vue globale de la DHFR complexée au folate et au NADPH. B : Site de liaison du folate. C : Site de liaison du NADPH. Les ligands et les résidus d'intérêt sont tous représentés sous forme de bâtonnets selon le code suivant : carbones des résidus hydrophobes (boules jaunes) ; carbone des résidus formant des ponts H (blanc) ; carbones des ligands (vert). Les atomes d'oxygène sont en rouge, les atomes d'azote en bleu et les atomes de phosphore sont en orange. Les ponts H sont illustrés par des traits hachurés noirs.

riboadénine)[31]. Des contacts hydrophobes sont aussi formés entre la portion riboadénine et la poche hydrophobe formée par les résidus Leu75, Leu93 et Val120[36].

Le folate (et présumément le DHF) se lie face à la portion ribonicotinamide du NADPH, dans un sillon formé principalement par l'hélice α1, la boucle entre le brin β1 à l'hélice α1 et l'hélice α2 (**Figure 1.5C**). Le noyau pterine se lie au fond de la cavité du site actif, où l'atome N_5 (accepteur de proton) est positionné à moins de 3.1 Å de l'atome C_4 de la portion ribonicotinamide du NADPH (donneur d'hydrure). Le noyau ptérine forme des contacts hydrophobes aves les résidus Phe31 et Phe34. D'autres interactions apolaires sont formées entre le noyau ptérine et les chaînes latérales des résidus Ile7, Ala9, Leu22 et Val115, ainsi qu'avec les atomes du squelette peptidique du résidu Ala9. Le groupement 2-amino et l'atome N_3 du noyau ptérine forment des ponts hydrogène avec le résidu Glu30, considéré comme le donneur de proton lors de la réaction. Toutefois, l'atome N_5 n'est pas à proximité du résidu Glu30 dans la structure cristalline, et ne serait pas directement protonné par Glu30. L'obtention de la structure cristalline de la DHFR humaine liée au folate a permis de mieux élucider le mécanisme par lequel l'atome N_5 peut être protonné[24] (**Figure 1.6**). Une molécule d'eau, qui est hautement conservée dans les structures cristallines de la DHFR humaine obtenues à ce jour[24-30, 32-34], participe à la formation d'un réseau de ponts hydrogènes avec les résidus Glu30, Trp24 et le groupement 4-oxo du noyau ptérine[24, 37]. La stabilisation créée par le réseau de ponts hydrogènes donnerait un caractère plus acide à cette molécule d'eau, qui donnerait un proton au groupement 4-oxo du noyau pterine. La protonation de N_5 pourrait alors se faire directement ou via une autre molécule d'eau, générant ainsi une espèce carbocation en C_6. Selon ce mécanisme, le transfert d'hydrure se ferait avant ou après la protonation du noyau pterine, mais ne pourrait se faire en même temps que la protonation[38].

Les portions *p*-aminobenzoyle et glutamate du DHF se retrouvent majoritairement à la surface du site actif, où se forment des interactions avec plusieurs résidus. La portion ρ-aminobenzoyl forme un pont hydrogène avec le résidu Asn64, et des contacts hydrophobes

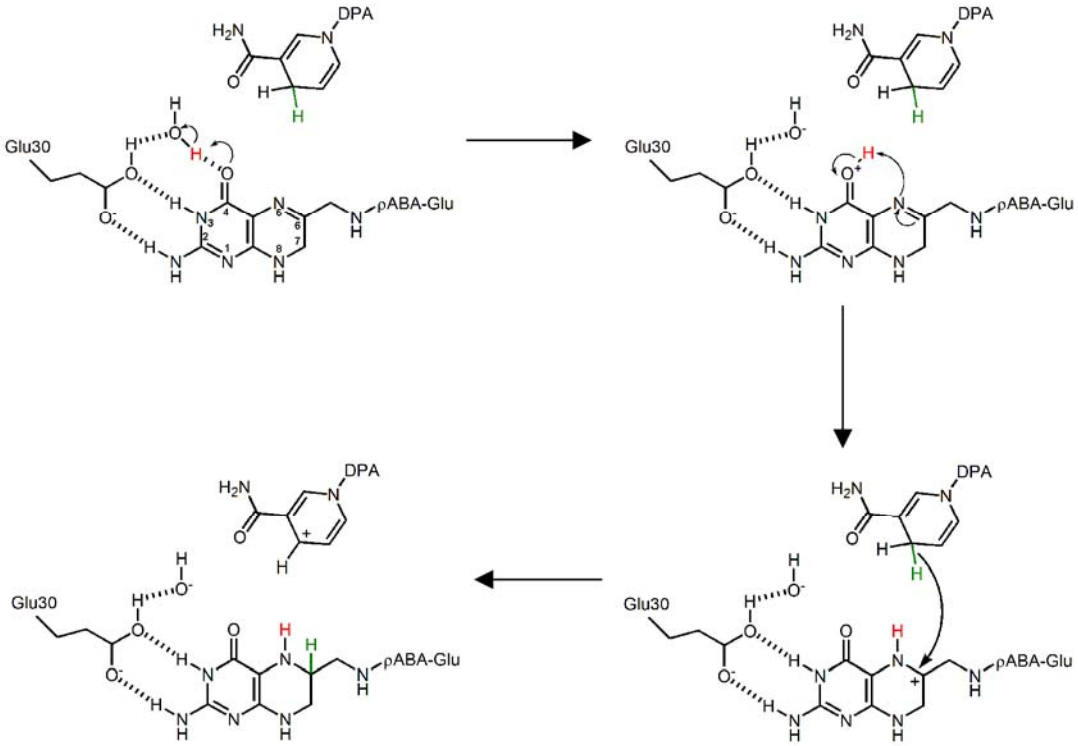

Figure 1.6. Mécanisme catalytique de la DHFR humaine. Dans ce schéma, la protonation du DHF *via* la molécule d'eau et le résidu Glu30 se fait avant le transfert d'hydrure du NADPH vers l'atome C_6 du DHF. Seuls les noyaux nicotinamide du NADPH et ptérine du DHF sont dessinés. DPA : portion ribodiphosphate riboadénine du NADPH ; *p*-ABA-Glu : portions *p*-aminobenzoyle - L-glutamate du DHF. Les liens hachurés représentent des ponts H. Adapté de [22].

avec les résidus Phe31, Ile60 et Leu67. Le groupement α-carboxylate de la portion glutamate forme des interactions électrostatiques avec le groupement guanidium de la chaîne latérale du résidu Arg70. Ce même groupement peut former un pont hydrogène avec la chaine latérale du résidu Gln35[34].

1.2 Les antifolates

Dû à leur rôle prépondérant dans la synthèse de l'ADN et de la prolifération cellulaire, les enzymes impliquées dans le métabolisme du folate sont rapidement devenues des cibles thérapeutiques pour le traitement de maladies dont les mécanismes d'invasion sont basés sur la prolifération cellulaire. Une des premières stratégies envisagées pour le traitement de ces maladies a été de concevoir des analogues du folate (nommés antifolates) pouvant inhiber la DHFR et d'autres enzymes importantes du métabolisme du folate. Parce que la biosynthèse du THF est primordiale pour la synthèse du thymidylate et des purines, la DHFR est devenue une cible préférée pour la conception d'antifolates pour le traitement de divers types de cancers ainsi que des infections parasitaires et bactériennes.

1.2.1 – Les classes d'antifolates inhibant la DHFR

Les antifolates sont catégorisés en deux grandes classes, selon leur structure générale. Ainsi, nous retrouvons les antifolates classiques et les antifolates non-classiques[39] (**Figure 1.7**). Ces composés donnent lieu à un mode d'inhibition compétitif, signifiant qu'ils compétitionnent avec le substrat DHF pour se lier au site actif de l'enzyme. Les antifolates classiques sont des analogues du folate qui contiennent des variantes des trois portions de la molécule, soit un noyau ptérine, une portion *p*-aminobenzoyle et une queue glutamate. Les différences structurales entre le folate et les antifolates classiques se retrouvent principalement au niveau du noyau ptérine. Typiquement, les antifolates classiques comportent un groupement amino à l'atome C_4 du noyau ptérine, qui remplace le groupement 4-oxo retrouvé chez le folate, générant ainsi un noyau 2,4 diaminoptérine. Les

atomes N_5 et/ou N_8 du noyau pterine peuvent aussi être substitués par des atomes de carbone chez certains antifolates[40, 41]. Les parties *p*-aminobenzoyle et glutamate comportent parfois des modifications chimiques, surtout au niveau de l'atome N_{10} de la portion *p*-aminobenzoyle et au niveau du γ-carboxylate de la portion glutamate[40, 42, 43].

Les antifolates non-classiques sont nommées ainsi parce qu'ils ne comportent que certains groupements chimiques retrouvés soit sur le folate ou sur les inhibiteurs classiques[39]. Ainsi, ces inhibiteurs ne contiennent pas de portion glutamate, et présentent souvent un groupement benzyle substitué à la place de la portion *p*-aminobenzoyle. De plus, le noyau 2,4-diaminoptérine retrouvé sur les inhibiteurs classiques est souvent remplacé par un noyau 2,4-diaminopyrimidine. L'absence de la portion glutamate et le caractère apolaire de ces molécules fait en sorte qu'elles peuvent diffuser passivement à travers la membrane plasmique pour se rendre au cytosol des cellules pour inhiber l'activité DHFR[44].

La variété chimique retrouvée chez les antifolates non-classiques donne lieu à des inhibiteurs ayant une certaine sélectivité pour des DHFRs d'espèces données. À titre d'exemple, les antifolates non-classiques comportant un noyau 2,4-diaminopyrimidine n'inhibent pas efficacement les DHFR des vertébrés, et peuvent être utilisés pour inhiber sélectivement les DHFR bactériennes ou parasitaires. Le pyriméthamine (PYR) (**Figure 1.7**) est un antifolate non-classique pouvant sélectivement inhiber la DHFR d'organismes parasitaires tels *Plasmodium falciparum* ou *Plasmodium vivax*, qui sont la principale cause de la malaria dans les pays sous-développés[45]. Le triméthoprime (TMP), un autre antifolate non-classique ayant un squelette 2,4-diaminopyrimidine (**Figure 1.7**), inhibe sélectivement la DHFR d'organismes bactériens comme *E. coli*, et est couramment utilisé pour traiter les infections uninaires causées par les bactéries *Enterobacter*[46]. L'enzyme humaine a 60 000 fois moins d'affinité pour cet inhibiteur, malgré une forte conservation des résidus du site actif entre les deux espèces[47]. Cet exemple de sélectivité est devenu un modèle d'étude classique quant à la compréhension structurale des contacts importants lors de la liaison

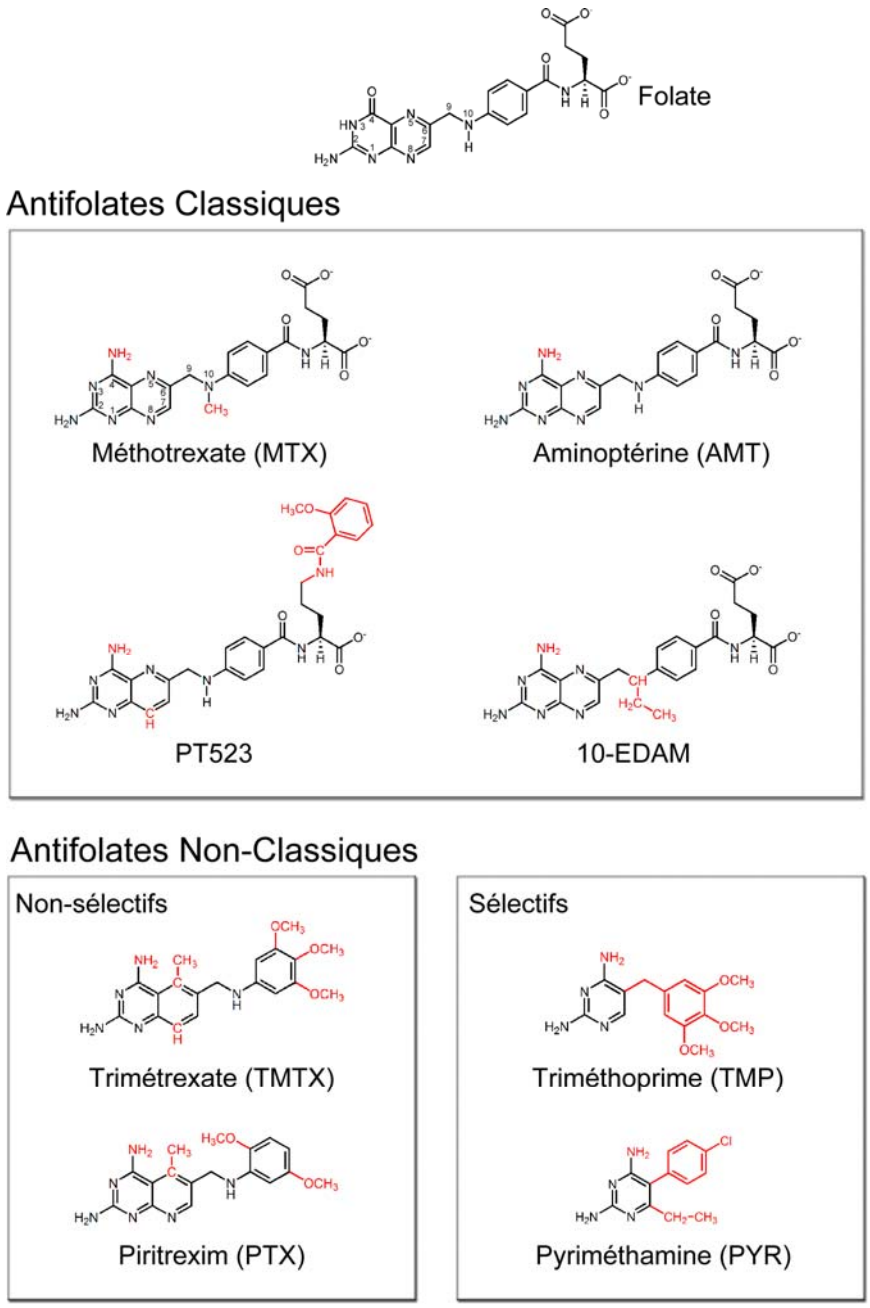

Figure 1.7. Structure chimique d'antifolates classiques et non-classiques. Les groupements chimiques des antifolates différents du folate sont en rouge. La numérotation du noyau ptérine est donnée pour le folate et le méthotrexate.

d'inhibiteurs à une cible thérapeutique donnée. La superposition des structures cristallines de la DHFR humaine et bactérienne a démontré que le site actif de l'enzyme humaine était plus étroit et moins volumineux que le site actif de la DHFR bactérienne. Le plus petit volume chez la DHFR humaine pouvait potentiellement engendrer des encombrements stériques avec des chaînes latérales du site actif lors de la liaison du TMP. Toutefois, cette observation n'expliquait pas complètement la sélectivité du TMP pour l'enzyme bactérienne, puisque la DHFR aviaire, qui présentait une affinité semblable à l'enzyme humaine pour le TMP, possédait une structure et une séquence hautement homologue à l'enzyme humaine tout en ayant un volume de site actif comparable à l'enzyme bactérienne[48, 49]. À ce jour, la liaison sélective du TMP à l'enzyme bactérienne reste mal comprise[36].

Contrairement aux inhibiteurs non-classiques, les antifolates classiques sont plus fréquemment utilisés pour traiter des maladies affectant les cellules de mammifères. Même si leur ressemblance au folate fait en sorte que les DHFRs de toutes espèces peuvent être inhibées *in vitro* par cette famille de molécule[50-52], il reste que certaines composantes retrouvées uniquement chez les cellules eucaryotes sont essentielles pour permettre l'incorporation de ces inhibiteurs dans la cellule. Tout comme le folate, les antifolates classiques s'introduisent dans les cellules des eucaryotes par différents transporteurs membranaires[4]. Le transporteur le plus fréquemment utilisé par ces inhibiteurs est le 'Reduced Folate Carrier protein' (RFC), qui permet le transport passif des antifolates classiques dans le cytosol[53]. La portion extracellulaire du RFC reconnaît les antifolates classiques, permettant ainsi le passage des molécules à travers un pore formé par les 12 hélices transmembranaires du transporteur[53]. Le RFC est exprimé dans tous les tissus primaires des cellules de mammifères, rendant le traitement de maladie à caractère prolifératif avec les antifolates classiques efficace[54]. Les antifolates classiques peuvent aussi s'introduire dans le cytosol des cellules de mammifères en utilisant le récepteur du folate. Toutefois, l'affinité de ce récepteur pour les antifolates classiques est beaucoup plus

basse que le RFC[55], indiquant que le RFC est la voie principale d'entrée des antifolates classiques. Contrairement aux cellules de mammifères, les bactéries ont la capacité de synthétiser le folate *de novo*[56], éliminant ainsi la nécessité de système d'importation du folate chez ces organismes. De plus, certaines bactéries comme *E. coli* possèdent des protéines membranaires pouvant expulser des molécules comme les antifolates classiques à l'extérieur de la cellule[57]. Ces mécanismes rendent le traitement des maladies bactériennes avec les antifolates classiques inefficaces.

Les antifolates classiques sont des molécules qui peuvent présenter un long temps de vie à l'intérieur de la cellule, procurant ainsi un effet thérapeutique prolongé[58]. Cette rétention cellulaire est assurée par le polyglutamation du groupement γ-carboxylate de la portion glutamate de ces molécules. Tout comme les folates présents dans la cellule, les antifolates classiques peuvent servir de substrat à la FPGS étant donné la présence de la queue glutamate. Bien qu'une vaste gamme d'antifolates classiques soit disponible, seuls quelques inhibiteurs sont présentement utilisés dans le domaine médical pour le traitement de plusieurs types de cancers[59-62] et certaines maladies auto-immunes[63, 64]. Malgré la création et la caractérisation de divers antifolates classiques au cours des dernières années[39], le méthotrexate (MTX), un des premiers antifolates synthétisés, demeure le plus utilisé pour le traitement de diverses maladies chez l'humain.

1.2.2 – Le méthotrexate

En 1947, la synthèse du premier antifolate fut réalisée[65]. En remplaçant le groupement 4-oxo du folate par un groupement 4-amino, il était possible d'obtenir un inhibiteur puissant de la croissance cellulaire. C'est ainsi que l'aminoptérine (AMT) fut développé. Des premiers tests cliniques avec l'AMT pour le traitement de la leucémie lymphocytaire aigüe (LLA) infantile démontrèrent pour la première fois une rémission transitoire de la maladie suite à l'administration de l'inhibiteur[66]. L'ensemble de ces travaux démontra qu'il était possible de traiter le cancer avec des molécules pouvant

inhiber la croissance cellulaire, et permit d'établir les bases de la chimiothérapie moderne pour le traitement de cancers.

Dans cette même étude[66], le dérivé N_{10}-méthyle de l'AMT fut synthétisé et testé contre la LLA. Le dérivé N_{10}-méthyl donna une rémission qui durait plus longtemps que celle conférée par l'AMT, tout en étant moins cytotoxique pour les patients recevant le traitement. Cette molécule fut initialement baptisée améthoptérine, puis son nom changea à méthotrexate (MTX). Peu longtemps après, il fut démontré que le MTX et l'AMT étaient des inhibiteurs compétitifs de la DHFR humaine[67], compétitionnant avec le folate et le dihydrofolate pour le même site de liaison au site actif. Outre le traitement de la LLA, le MTX est couramment utilisé seul ou en cocktail pour le traitement de cancers de la tête et du cou[61], le cancer du sein[60] et l'ostéosarcome[59]. Des études *ex vivo* ont permis de démontrer que le MTX agissait principalement sur des cellules en phase S du cycle mitotique, correspondant à l'étape où la synthèse de purines et de thymidine est cruciale pour la division cellulaire[68]. Le MTX est efficace pour inhiber la croissance de cellules cancéreuses, qui sont en division constante, mais démontre aussi une cytotoxicité pour des cellules saines du corps qui se divisent fréquemment. Plus précisément, la croissance des cellules hématopoïétiques souches (HS) est inhibée lors d'un traitement au MTX[69]. Ces cellules se trouvent dans la moelle osseuse où elles peuvent se différencier pour donner des érythrocytes, des lymphocytes B et des lymphocytes T, ces dernières étant à la base du système immunitaire[70]. Les patients recevant un traitement au MTX sont donc immuno-supprimés, un des désavantages majeurs du traitement avec les antifolates classiques. Pour réduire cet effet, le MTX est co-administré avec la leucovorine (5-formyl-THF), permettant ainsi une production basale de THF dans les cellules saines envers le maintien de ces cellules[71] (**Figure 1.2**). Toutefois, les propriétés d'immunosuppression du MTX font en sorte qu'il peut être utilisé à de très faible doses pour traiter certaines maladies auto-immunes, telles le psoriasis[63] et l'arthrite rhumatoïde juvénile[64].

La détermination des paramètres cinétiques et d'inhibition pour les différents ligands de la DHFR ont révélé que le MTX se lie plus fortement au site actif de l'enzyme (K_i^{MTX} = 3.4 pM) que le substrat DHF (K_M^{DHF} = 100 nM)[19], soit une différence d'affinité de près de 30 000 entre les deux ligands, expliquant en partie l'efficacité du traitement de cancers avec le MTX. Cette différence d'affinité peut être expliquée en partie par des interactions spécifiques existant entre le site actif de la DHFR humaine et le MTX, qui ne sont pas présentes lors de la liaison du DHF. La résolution de la structure cristalline de l'enzyme complexée avec le MTX et le co-facteur NADPH[34] a permis d'éclaircir les différences entre la liaison du DHF et du MTX au site actif de l'enzyme[24, 34]. Bien que le MTX soit en compétition avec le DHF pour le même site de liaison sur la DHFR, le noyau 2,4-diaminoptérine du MTX se lie dans une orientation opposée au noyau ptérine du DHF (**Figure 1.8A**). Une rotation de 180º au niveau du lien C_6-C_9 assure cette différence de liaison. Dans cette orientation, le groupement 4-amino est à proximité des groupements carbonyles du squelette peptidique des résidus Ile7 et Val115 (2.7 Å et 3.21 Å respectivement), formant des ponts hydrogène avec ces deux résidus (**Figure 1.8B**). Ces deux ponts hydrogène sont hautement conservés chez tous les inhibiteurs portant un groupement 2,4-diamino. L'orientation du noyau ptérine semble être uniquement dépendante du groupement présent à l'atome C_4, puisque les structures cristallines de la DHFR contenant des inhibiteurs possédant un groupement 4-oxo[25, 35, 72] ont un noyau pterine orienté de la même façon que le DHF, alors que les inhibiteurs possédant un groupement 4-amino[25, 28, 30, 73] ont un noyau pterine orienté de la même façon que le MTX. Les inhibiteurs contenant un groupement 2,4-diamino au noyau ptérine ont généralement des valeurs de K_i très basses (entre 0,3 et 5 pM)[74, 75], alors que les inhibiteurs contenant un groupement 4-oxo au noyau ptérine ont des valeurs de K_i plus élevées (>7 nM)[76, 77]. Les résidus Ile7 et Val115 n'ont que la capacité de former des contacts hydrophobes avec le noyau pterine du DHF et des inhibiteurs contenant un groupement 4-oxo, étant donné l'orientation du noyau de ces ligands lors de la liaison au site actif. Les contacts hydrophobes forment des énergies de liaison plus faibles que les ponts hydrogènes[78], et

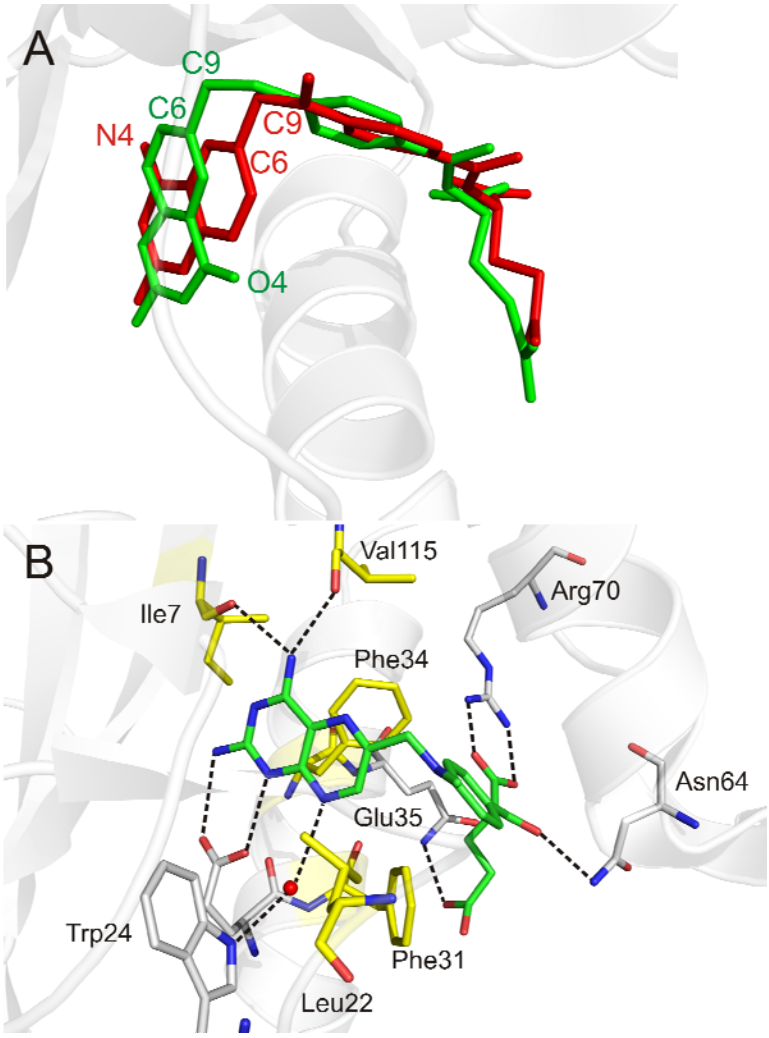

Figure 1.8. Liaison du MTX à la DHFR humaine (1U72.pdb). A : Le noyau ptérine du MTX (rouge) se lie dans une orientation inverse au noyau ptérine du folate (vert; 1DRF.pdb) dû à une rotation de 180º du lien C_6-C_9. Le groupement 4-amino du MTX (N4) pointe dans une direction opposée du site actif par rapport au groupement 4-oxo du folate (O4). B : Interactions entre le MTX et les résidus du site actif. La molécule d'eau conservée du site actif est représentée par une sphère rouge. Les résidus et le MTX sont représentés sous forme de bâtonnets (azote en bleu, oxygène en rouge, carbone du MTX en vert, carbone de résidus hydrophobes en jaune et carbone de résidus hydrophiles en blanc). Les ponts H sont illustrés par des traits hachurés.

l'inversion de l'orientation du noyau ptérine entre les deux molécules expliquerait l'affinité plus grande pour des inhibiteurs comportant des fonctions 2,4-diamino comme le MTX.

D'autres ponts hydrogène sont formés entre le groupement 2-amino et l'atome N_1 du noyau ptérine et la chaîne latérale du résidu catalytique Glu30. L'atome N_8 du noyau ptérine est impliqué dans un réseau de ponts H impliquant une molécule d'eau hautement conservée au site actif, la chaîne latérale du résidu Trp24 et la chaîne latérale du résidu Glu30. Les chaînes latérales des résidus Phe34 et Leu22 forment des contacts hydrophobes avec le noyau ptérine du MTX. Les portions *p*-aminobenzoyle et glutamate de l'inhibiteur se lient sensiblement dans la même orientation que ces mêmes portions pour le DHF. Ainsi, la portion *p*-aminobenzoyle forme des contacts hydrophobes avec les chaînes latérales des résidus Phe31 et Phe34. Il existe un pont hydrogène entre le groupement carbonyle de la portion *p*-aminobenzoyle et la chaîne latérale du résidu Asn64. La portion glutamate se trouve principalement à la surface du site actif où le groupement α-carboxylate forme un pont salin avec la chaîne latérale du résidu Arg70. La chaîne latérale du résidu Gln35 peut former un pont hydrogène avec le groupement γ-carboxylate de la portion glutamate.

1.2.3 – Mécanismes de résistance au méthotrexate

L'efficacité clinique du MTX pour le traitement de cancers a rapidement été atténuée par l'acquisition de divers mécanismes de résistance dans les cellules cancéreuses. Dès 1962, soit près de 12 ans après l'introduction du MTX dans les traitements cliniques, une première étude rapportait la perte d'efficacité du MTX dans la lignée lymphoblastique murine L5178Y, expliquée par un mauvais fonctionnement du mécanisme de transport du MTX[79]. Depuis cette découverte, trois mécanismes de résistance indépendants ont été identifiés dans les cellules néoplasiques humaines, soit la diminution de la diffusion intracellulaire du MTX, la diminution du temps de rétention du MTX dans le cytosol et la diminution de l'efficacité du MTX envers la DHFR humaine (**Figure 1.9**). Ces trois

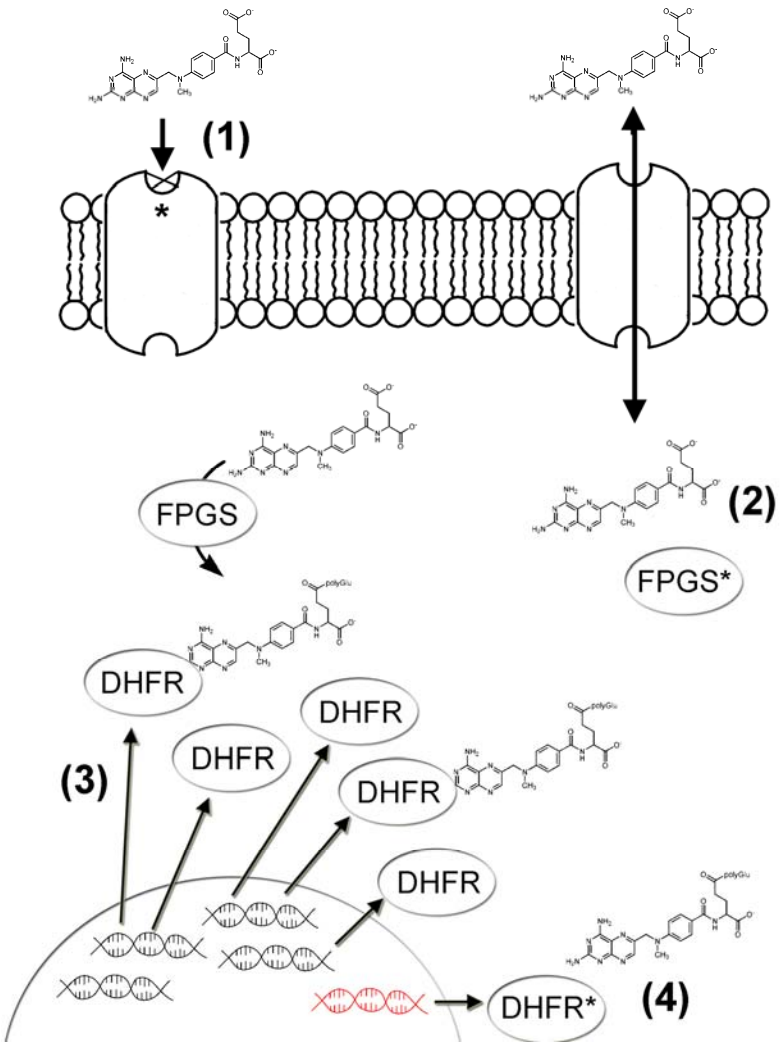

Figure 1.9. Mécanismes de résistance au MTX. (1) Réduction du transport du MTX dans la cellule. (2) Réduction de la polyglutamylation du MTX par la FPGS. (3) Amplification du gène de la DHFR, menant à une surexpression de la DHFR et à la séquestration du MTX. (4) Mutations dans le gène de la DHFR générant une DHFR mutante avec une affinité plus faible pour le MTX. Les (*) symbolisent la présence d'acides aminés substitués au niveau des différentes protéines suite à des mutations génétiques. Adapté de [4].

mécanismes peuvent être présents individuellement ou en concert et mènent généralement à une rechute pendant la période de rémission suite à un traitement au MTX[80].

La diminution de l'incorporation du MTX dans le cytosol de cellules néoplasique a été le premier mécanisme de résistance rapporté dans la littérature[79]. Toutefois, les causes moléculaires de ce type de résistance n'étaient pas clairement établies. Le rôle du RFC dans ce type de résistance fût démontré suite au rétablissement du transport du MTX dans des cellules de cancer du sein humaines dépourvues de mécanisme de transport du MTX et ayant été transfectées avec l'ADNc du RFC[81]. Divers types de mutations dans le gène encodant le RFC seraient à l'origine de la diminution du transport du MTX dans la cellule. Les premiers variants du RFC furent identifiés *ex vivo* en exposant différentes lignées leucémiques murines et humaines à des concentrations croissantes de MTX. Plusieurs mutations furent associées à une déficience du transport du MTX dans la cellule, due à l'expression d'un transporteur moins efficace pour l'incorporation du MTX[82, 83], à l'absence d'expression du RFC due à une mutation non-sens[84], ou à une baisse du niveau d'expression du RFC relié à des mutations dans les regions non-codantes du RFC[54, 85]. L'utilisation de lignées cellulaires pour caractériser ce mode de résistance s'est avérée représentative puisque certaines mutations du RFC sont retrouvées au sein d'isolats cliniques provenant de patients étant traités avec le MTX pour certains types de cancers[86, 87]. Une modification génétique au niveau du RFC n'est pas la seule cause possible d'une diminution de l'incorporation du MTX dans la cellule. Plus récemment, des protéines membranaires de type 'multi-drug resistance proteins' (MDR) ont été retrouvées dans des cellules cancereuses exposées au MTX[88, 89]. Ces pompes membranaires expulsent un large spectre de composés utilisés pour le traitement du cancer dont les antifolates, et constituent un fléau actuel pour l'efficacité de plusieurs traitements anti-néoplasiques[90]. Toutefois, dans le cas du MTX, les MDR ne reconnaissent que la forme monoglutamylée de l'inhibiteur, la forme diglutamylée ne pouvant être expulsée de la cellule[91].

La polyglutamylation du MTX est essentielle pour sa rétention prolongée à suite à son entrée au cytosol[92]. Les antifolates classiques comme le MTX contiennent une portion glutamate qui sert de substrat à la FPGS, une enzyme cytosolique réalisant la polyglutamation du folate et ses dérivés. Tout comme le folate, le MTX se fait polyglutamyler sur son groupement γ-carboxylate par la FPGS[93]. Une déficience de la polyglutamation du MTX mène à une moins bonne rétention cellulaire résultant en une diminution de l'efficacité de traitement[94]. Cette déficience est attribuable à une diminution de l'expression de l'enzyme, réduisant ainsi l'activité de polyglutamylation du MTX[95, 96]. Tout comme pour le RFC, les causes moléculaires de la diminution de l'activité intracellulaire de la FPGS furent identifiées par l'exposition de lignées cellulaires cancéreuses à des concentrations croissantes de MTX. La caractérisation de l'activité FPGS venant d'isolats cliniques de différents types de cancers a été d'autant plus importante puisque ces études ont démontré que la polyglutamylation pouvait être naturellement variable d'un type cellulaire à l'autre. Ainsi, le MTX est un inhibiteur efficace pour le traitement de la LLA, puisque les cellules lymphocytaires présentent une forte activité de polyglutamylation intracellulaire[86]. Toutefois, le MTX s'avère inefficace pour le traitement des types de leucémies non-lymphocytaire aigue (LNLA)[97] et myélocytaire aigue[98], car les cellules myéloïdes présentent naturellement une faible activité FPGS.

Les deux mécanismes de résistance décrits ci-haut peuvent être contournés en administrant une concentration élevée de MTX. Ainsi, une plus grande concentration de MTX permet une meilleure diffusion au cytosol, assurant ainsi une concentration suffisante de MTX dans la cellule, indépendemment de l'état de polyglutamylation des molécules[99]. Dans ce cas, un autre mécanisme de résistance peut assurer la survie des cellules néoplasiques. Une augmentation de la concentration cellulaire de DHFR permet une titration du MTX circulant dans le cytosol tout en assurant une activité DHFR suffisante à la prolifération de la cellule. L'augmentation de la concentration intracellulaire de la DHFR est attribuable à deux mécanismes distincts. En premier lieu, une amplification du gène

encodant la DHFR a été associée à une résistance au MTX dans plusieurs lignées cellulaires lors d'études *ex vivo*[100-102] ainsi que dans des isolats cliniques de patients traités au MTX[80, 103-105]. Le phénomène d'amplification peut être dû à une duplication du chromosome 5, contenant la séquence codante de la DHFR[106], ainsi qu'à la présence de chromosomes double minutes encodant la DHFR[107, 108]. Une concentration élevée en DHFR peut aussi être observée sans l'amplification du gène. L'ARN messager encodant la DHFR humaine se fixe au niveau du site actif pour moduler l'expression de l'enzyme[109]. Il est postulé qu'un changement de conformation de l'enzyme suite à la liaison du MTX au complexe enzyme-ARNm rendrait l'ARN messager libre pour la traduction, induisant une augmentation de l'expression basale de la DHFR sans modification génétique[110].

1.3 Réduction de l'affinité au MTX par des mutations de la DHFR humaine

En 1976, Jackson *et al.*[111] rapportèrent des lignées cellulaires résistantes au MTX, ne démontrant aucun des mécanismes de résistance précédemment mentionnés. L'isolement des DHFRs et la caractérisation des constantes d'inhibition pour les enzymes des différentes lignées leur permis de conclure que la résistance observée était due à une moins bonne affinité envers le MTX chez les DHFR isolées. Dans une étude subséquente, il fut démontré qu'une mutation au site actif de la DHFR contenue dans une lignée cellulaire murine résistante au MTX était à la base de la résistance observée chez ces cellules[112]. Ces études démontraient l'existence d'un nouveau mécanisme de résistance au MTX, pouvant donner de plus amples informations sur les contacts moléculaires essentiels existant entre la DHFR et le MTX. Plusieurs travaux subséquents ont suivi dans le but d'identifier l'ensemble des mutations ponctuelles pouvant générer une moins bonne affinité au MTX chez la DHFR, selon des designs expérimentaux réalisés dans un contexte *ex vivo* ou *in vitro*.

1.3.1 – Mutations de la DHFR retrouvées dans un contexte *ex vivo*

Simonsen et Levinson furent les premiers à identifier un mutant de la DHFR ayant une moins grande affinité pour le MTX[112]. La substitution par une arginine au résidu natif Leu22 (mutant Leu22Arg) était responsable d'une perte d'affinité au MTX (augmentation de la valeur de K_D^{MTX} de 270 fois comparativement à la valeur de l'enzyme native) et de la résistance observée chez ces cellules[113]. Un mutant Leu22Phe fut identifié dans deux lignées différentes de cellules de hamster chinois résistantes au MTX[114, 115]. La caractérisation de la constante d'inhibition de ce mutant révélait que l'affinité était diminuée de plus de deux ordres de grandeur par rapport à l'enzyme native[115]. Le résidu Leu22 est hautement conservé chez les DHFR des mammifères, et se situe à l'interface des sites de liaison du DHF et du NADPH. Tel que révélé par la structure cristalline de l'enzyme humaine et de l'enzyme murine complexée avec le MTX[34], la chaîne latérale de ce résidu a la possibilité de former des contacts van der Waals avec le noyau ptérine de l'inhibiteur. Le remplacement d'un résidu hydrophobe comme Leu22 par des résidus polaires ou aromatiques pourrait rompre les interactions présentes chez l'enzyme native et ainsi réduire l'affinité pour le MTX.

Des mutations au résidu Phe31, un autre résidu du site actif de la DHFR, ont été identifiées comme étant responsables de la diminution de l'affinité de l'enzyme pour le MTX. Le mutant Phe31Ser fut identifié dans des cellules humaines du cancer du colon exposées à des doses croissantes de MTX[116]. La caractérisation des constantes de liaison au MTX de la DHFR révélait que le K_D^{MTX} était près de 100 fois plus élevé chez le mutant Phe31Ser que chez l'enzyme native. Le mutant Phe31Trp, identifié dans une lignée cellulaire leucémique murine, conférait une résistance à des concentrations modérées de MTX (< 0.1 μM) lorsque transfecté dans des cellules CHO *dhfr*-[117]. Le résidu Phe31 est conservé chez les mammifères, et sa chaîne latérale est impliquée dans des contacts van der Waals avec la portion *p*-aminobenzoyle du MTX et du DHF[24, 34]. L'obtention de la

structure cristalline du mutant Phe31Ser complexé au MTX a permis d'établir les bases moléculaires de la résistance retrouvées chez ce mutant. La substitution d'une chaîne aromatique par un résidu à petite chaîne latérale modifie le volume du site actif, et rompt les interactions hydrophobes existantes entre le résidu Phe31 et l'anneau aromatique de la portion *p*-aminobenzoyle de l'inhibiteur[118]. Toutefois, cette structure ne sert pas à expliquer la résistance conférée par le maintien d'un résidu aromatique dans le mutant Phe31Trp, dont les paramètres cinétiques et d'inhibition n'ont pas été caractérisés suite à son identification.

Une dernière mutation a été identifiée dans des études *ex vivo*. Le mutant Gly15Trp a été caractérisé suite à son identification dans des cellules leucémiques murine résistantes au MTX[119]. Ce mutant est particulier, puisque contrairement aux résidus 22 et 31, le résidu Gly15 se trouve à l'extérieur du site actif, sur une boucle loin du site de liaison du MTX. La boucle contenant le résidu Gly15 est homologue à la boucle Met20 chez la DHFR d'*E. coli*. Cette boucle est hautement mobile et cette mobilité a été démontrée comme étant importante pour l'accès des ligands au niveau du site actif de l'enzyme[120, 121]. L'introduction d'un résidu volumineux comme le Trp dans cette boucle pourrait donc réduire la mobilité, gênant ainsi l'accès du MTX au site actif de la DHFR[119].

1.3.2 – Mutations de la DHFR identifiées dans un contexte *in vitro*

La première étude de mutagénèse dirigée sur la DHFR humaine marqua le début de l'identification d'autres mutations et de l'approfondissement des connaissances sur les facteurs moléculaires pouvant réduire l'affinité de l'enzyme pour le MTX, et l'effet de ces mutations sur la reconnaisance du substrat DHF et l'efficacité catalytique de la DHFR[122]. Tel que mentionné précédemment, le MTX et le DHF compétitionnent pour le même site de liaison sur la DHFR, et s'y lient selon une conformation similaire. Par contre, la présence d'un groupement 4-amino sur le noyau ptérine du MTX favorise des liaisons spécifiques entre le MTX et la DHFR, qui ne sont pas présentes lorsque l'enzyme lie le

DHF. Cette différence d'orientation contribue à la plus forte affinité qu'a la DHFR humaine pour le MTX (K_i^{MTX} = 3.4 pM *vs* K_M^{DHF} = 100 nM). Les expériences de mutagenèse tentèrent d'identifier les régions critiques communes à la liaison des deux ligands, tout en identifiant les régions de contacts spécifiques promouvant une liaison plus forte pour le MTX chez la DHFR humaine.

Les mutations *ex vivo* étant principalement retrouvées au niveau des résidus 22 et 31 du site actif, plusieurs mutations furent testées à ces deux codons. Ainsi, une première étude rapportait l'effet des mutations Phe31Leu, Phe31Val, Phe31Thr, Phe31Ser, Phe31Ala et Phe31Gly[118]. La caractérisation des constantes cinétiques révélait que les efficacités catalytiques de ces différentes variantes (k_{cat}/K_M^{DHF}) étaient 3 (Phe31Ala) à 25 fois (Phe31Val) plus faibles que chez l'enzyme native, attribuable principalement à une réduction de l'affinité pour le substrat DHF. L'affaiblissement de la liaison du substrat DHF lors de la substitution de la chaîne latérale aromatique du résidu Phe31 par des acides aminés moins volumineux fut attribué à une perte des contacts van der Waals entre le résidu Phe31 et la portion *p*-aminobenzoyle du DHF[24, 35]. En revanche, seules les variantes Phe31Ser, Phe31Ala et Phe31Gly étaient résistantes au MTX, avec des valeurs de K_i^{MTX} étant respectivement 70, 78 et 100 fois plus élevée que la valeur de l'enzyme native. Les trois autres variantes générées comportaient des valeurs de K_i^{MTX} comparables au type natif, signifiant que la résistance au MTX n'était pas simplement dépendante de la réduction du volume ou de la polarité de la chaîne latérale au résidu 31, et que certains contacts spécifiques pouvaient exister entre ce résidu et le MTX. Ce constat fut appuyé par la caractérisation de la variante Phe31Arg, présentant 2000 fois moins d'affinité pour le MTX que la DHFR native suite à l'introduction de la chaîne latérale volumineuse chargée de l'arginine[123]. Comme pour les autres substitutions au résidu 31, l'efficacité catalytique de la variante Phe31Arg était réduite, ayant une valeur de k_{cat}/K_M^{DHF} 100 fois plus petite que l'enzyme native. Toutefois, cette diminution d'efficacité était principalement attribuable à une diminution du k_{cat} de la variante enzymatique, l'affinité du DHF n'étant réduite que de 5 fois chez la variante Phe31Arg[123].

Des observations semblables purent être portées suite à la caractérisation des variations au résidu Leu22. Les variantes Leu22Arg, Leu22Phe, Leu22Tyr et Leu22Trp furent caractérisés pour leur efficacité catalytique et leur affinité envers le MTX et d'autres antifolates classiques et non-classiques pouvant inhiber la DHFR humaine native[29]. L'efficacité catalytique était réduite chez toutes les variantes, principalement dû à une affinité plus faible pour les substrats DHF et NADPH. Le résidu 22 étant à l'interface des sites de liaison de ces deux substrats, ce résultat n'était pas inattendu. La diminution de l'efficacité catalytique était accompagnée d'une diminution plus importante de l'affinité pour le MTX chez tous les mutants à l'exception de la variante Leu22Arg, qui présentait une perte d'affinité égale à la perte d'efficacité catalytique par rapport à la DHFR native (diminution de 2500 fois pour les deux paramètres). La variante Leu22Tyr s'avérait être la plus résistante (K_i^{MTX} = 10.9 nM), affichant une perte d'affinité de 3200 fois par rapport à l'enzyme native (K_i^{MTX} = 3.4 pM). Chez cette variante particulière, l'efficacité catalytique n'était diminuée que par un facteur de 10 par rapport à l'enzyme native. L'obtention de la structure cristalline de la variante Leu22Tyr complexé au MTX suggérait que la chaîne latérale de l'acide aminé aromatique était trop volumineuse pour s'orienter comme le résidu natif dans le site actif. Il a été proposé que ce changement d'orientation réduisait les interactions van der Waals entre le ligand et le résidu 22 substitué, menant à une réduction de l'affinité pour le MTX[29]. Une étude subséquente démontra que les variations conservatrices Leu22Met et Leu22Ile conservaient des propriétés semblables à l'enzyme native par rapport à l'efficacité catalytique et l'affinité pour le MTX, l'AMT, le piritrexim et le trimetrexate[124] (**Figure 1.7**). Cette observation mena à la conclusion que seuls les résidus volumineux et/ou aromatiques avaient un effet de diminution de l'affinité pour le MTX et les autres antifolates à la position 22. Pris dans l'ensemble, ces études indiquaient que le résidu 22 était crucial pour la liaison d'autres antifolates, puisque les variantes résistantes au MTX étaient toutes résistantes aux antifolates classiques AMT et 10-EDAM, ainsi qu'aux antifolates non-classiques piritrexim et trimétrexate[29, 124].

Finalement, ces travaux démontraient pour la première fois que les substitutions conférant une résistance au MTX *ex vivo* dans des cellules murines généraient aussi une résistance au MTX chez l'enzyme humaine (variantes Leu22Phe et Leu22Arg). La forte homologie de structure et la similarité retrouvée entre les résidus du site actif des enzymes murine et humaine laissaient présager ce résultat[115]. La confirmation de la résistance au MTX des variantes Gly15Trp et Phe31Trp chez l'enzyme humaine[125], initialement identifiées dans des DHFR des lignées cellulaires murines[117, 119], appuya cette hypothèse.

La DHFR murine a aussi été assujettie à des études de mutagénèse dirigée pour déterminer l'effet de mutations sur la résistance au MTX. Les variantes Leu22Arg, Phe31Ser et Phe31Arg murines furent démontrées comme étant résistantes au MTX, tout comme leurs homologues respectives chez l'humain[126]. D'autres substitutions à des résidus non-caractérisés chez l'enzyme humaine furent identifiées comme conférant la résistance au MTX chez la DHFR murine. Ainsi, les variantes Ile7Ser, Trp24Arg, Phe34Leu, Gln35Arg, Gln35Pro et Val115Pro démontrèrent toutes une diminution de l'affinité pour le MTX[126]. Ces résultats étaient intéressants dans la mesure où tous ces résidus étaient situés autour du site de liaison du DHF/MTX et étaient hautement conservés chez l'enzyme humaine[24] (**Figure 1.5B**). Ainsi, il fut possible d'obtenir de nouvelles variantes résistantes au MTX chez la DHFR humaine en ciblant certains de ces résidus. La variante Ile7Phe chez l'enzyme humaine possédait un K_i^{MTX} = 24 nM, soit une augmentation de 7000 fois la valeur de l'enzyme native (K_i^{MTX} = 0.0034 nM)[123]. Dans la structure cristalline de la DHFR humaine complexée au MTX, le groupement carbonyl du squelette peptidique du résidu Ile7 forme un pont hydrogène avec le groupement 4-amino du noyau ptérine du MTX[34] (**Figure 1.8B**). Cette interaction ne peut être présente entre l'enzyme et le substrat DHF, puisque le noyau ptérine du DHF se lie dans une orientation opposée à celui du MTX[34, 35]. Il était donc présumé que des substitutions au résidu Ile7 pouvaient potentiellement générer des variantes de la DHFR humaine ayant une affinité réduite pour le MTX sans toutefois avoir perdu de l'affinité pour le substrat DHF. Toutefois, contrairement au raisonnement

structural, la valeur du K_M^{DHF} de la variante Ile7Phe (K_M^{DHF} = 20 μM) était 200 fois plus élevée que la valeur de l'enzyme native (K_M^{DHF} = 0.1 μM), signifiant que le résidu Ile7 était important pour la liaison du DHF et du MTX malgré les interactions spécifiques présentes entre ce résidu et le MTX.

Des substitutions au résidu 34 de l'enzyme humaine générèrent aussi des variantes qui ne liaient plus aussi efficacement le MTX[127, 128]. Les variantes Phe34Ala, Phe34Ile, Phe34Ser, Phe34Thr et Phe34Val possédaient des valeurs de K_D^{MTX} entre 2 800 fois (Phe34Val) et 60 000 fois (Phe34Ser) plus élevées que l'enzyme native, signifiant que le MTX se liait moins fortement aux variantes du résidu Phe34 qu'à l'enzyme native ou à tout autre variante de la DHFR humaine générée à d'autres résidus[127]. L'efficacité catalytique était drastiquement réduite chez toutes les variantes, principalement dû à une réduction de l'affinité des enzymes variantes pour le DHF (diminution du K_M^{DHF} de 31 à 850 fois par rapport à l'enzyme native). Le résidu Phe34 est strictement conservé dans les DHFR de toutes espèces confondues, où il forme des contacts hydrophobes avec le noyau ptérine et la partie *p*-aminobenzoyle des ligands dans le site de liaison du DHF. Les études de mutagénèse au résidu Phe34 permirent de confirmer l'importance de ce résidu dans la liaison du DHF et des antifolates en général.

Une autre interaction retrouvée dans la structure cristalline de la DHFR humaine complexée au MTX fut également démontrée comme étant importante pour la liaison du DHF. La variante Arg70Lys fut créée et caractérisée pour évaluer l'importance du pont salin formé entre le groupement α-carboxylate de la portion glutamate des ligands et le groupement guanidium du résidu Arg70[129]. Le K_D^{MTX} pour la variante Arg70Lys était 22 000 fois plus élevé que celui retrouvé chez la DHFR native, démontrant l'importance de cette interaction dans la liaison du MTX. Parallèlement, cette variante avait une efficacité catalytique réduite à 3% de la valeur de l'enzyme native, principalement dû à une réduction de l'affinité pour le DHF chez l'enzyme mutante *(*K_M^{DHF} = 3.72 μM *versus* 0.1 μM pour l'enzyme native)[129].

1.3.3 – Thérapie génique et utilisation de variantes résistantes au MTX pour la myeloprotection de cellules saines de la moelle osseuse

Au début des années 80, une nouvelle forme de thérapie promettait de guérir certaines maladies congénitales affectant les cellules sanguines. Outre les débats religieux et éthiques associés aux perspectives eugéniques de ce traitement, la thérapie génique des cellules sanguines offrait la possibilité de corriger les défauts reliés à un gène non-fonctionnel dans la cellule en insérant dans le génome de cellules hématopoïétiques souches (HS) une copie du gène fonctionnel. Les cellules HS sont présentes dans la moelle osseuse, où elles ont la capacité de se renouveller par division ou se différencier en différents types de cellules progénitrices importantes pour la formation des cellules sanguines, telles que les lymphocytes B et T, essentiels au système immunitaire[70]. Pour incorporer le gène d'intérêt, une partie de la moelle osseuse d'un patient est prélevée, maintenue en culture et infectée avec un rétro-virus contenant le gène fonctionnel. Les cellules de moelle osseuse infectées sont par la suite greffées chez le patient, où elles ont l'occasion de repeupler la moelle osseuse pour corriger le défaut génétique.

Les premières études cliniques de thérapie génique se concentrèrent sur le traitement de la maladie SCID ('Severe Combined ImmunoDefiency'), causée soit par un défaut dans le gène de l'adénosine désaminase (AD-SCID) ou dans le gène encodant la partie γ du récepteur de l'interleukine 2 (X-SCID), menant à un défaut dans la différentiation et la fonction de lymphocytes T[130]. Le premier traitement clinique de thérapie génique rapportait l'intégration du gène AD dans des cellules lymphocytes T humaines, qui étaient ensuite injectées dans des patients souffrant de AD-SCID[131]. Malgré le succès de ce traitement, les patients devaient continuellement recevoir des injections de cellules T transduites, les lymphocytes T ayant un court temps de vie dans le corps[131]. Étant donné leur rôle dans la production de toutes les cellules sanguines, les cellules HS devinrent une cible idéale de traitement par thérapie génique. Des études rapportèrent un

traitement efficace des différentes formes de SCID avec des cellules HS transduites et greffées chez des patients souffrant de cette maladie, portant à croire qu'une guérison complète pouvait être réalisée par cette thérapie[132-134]. Toutefois, les espoirs de guérison pour la SCID et d'autres maladies sanguines par cette thérapie ont rapidement été freinés lorsque des études rapportèrent que certains patients traités pour la X-SCID avaient développé des leucémies dues à une intégration aléatoire du rétro-virus, générant un événement oncogénique dans les cellules transduites[135, 136]. Présentement, des études sont consacrées à optimiser les deux problèmes principaux de l'application de la thérapie génique. Premièrement, les virus utilisés pour l'intégration de matériel génétique sont peu spécifiques, pouvant s'intégrer à plusieurs endroits dans le génome d'une cellule, menant au développement potentiel d'événements oncogéniques[135, 137]. Le développement de systèmes viraux ayant des sites d'intégrations plus spécifiques est présentement en cours[138-141]. Deuxièmement, l'efficacité de transduction dans les cellules HS est souvent très basse, ce qui réduit l'efficacité de repopulation de la moelle osseuse par les cellules transduites. Il est estimé que les cellules transduites doivent constituer près de 30 % à 40% de la moelle osseuse pour conférer un effet thérapeutique chez la majorité des maladies traitables par thérapie génique[70]. Même à ce pourcentage, l'effet thérapeutique est considéré à court terme, puisque les cellules transduites, qui se retrouvent en plus petite proportion que les cellules non-transduites, sont en compétition avec les cellules non-transduites de l'hôte pour la population de la moelle osseuse. Ceci nécessiterait donc plusieurs interventions pour maintenir un effet à plus long terme. Diverses méthodes sont présentement à l'étude pour augmenter le pourcentage de repopulation des cellules transduites[142-146], dont une impliquant des variantes de la DHFR humaine résistantes au MTX[147]. Ces méthodes visent l'enrichissement de la population de cellules transduites, prolongeant ainsi l'effet thérapeutique suite à une greffe de moelle transduite.

Hock et Miller rapportèrent une nouvelle application potentielle de la thérapie génique, celle de protéger les cellules HS saines contre les effets cytotoxiques d'agents de chimiothérapie[148]. Le MTX inhibe la croissance de toute cellule en phase S de division[68].

Parce que la DHFR se trouve dans toutes les cellules, le MTX inhibe autant la croissance de certaines cellules saines qui sont en division constante que la progression de cellules tumorales lors d'un traitement de chimiothérapie. L'effet secondaire le plus néfaste du MTX est l'immunosuppression, causée par le déplétion des cellules hématopoïétiques souche (HS), sensibles au effet cytotoxique du MTX. Le fait de rendre les cellules HS résistantes à un agent de chimiothérapie donné atténuerait l'effet d'immunosuppression lors du traitement, et permettrait de poursuivre des protocoles plus aggressifs en augmentant la concentration administrée de l'agent de chimiothérapie[69] (**Figure 1.10**). En incorporant le gène encodant pour la variante Leu22Arg de la DHFR murine dans un vecteur rétro-viral, il fut possible de démontrer que l'intégration de la DHFR résistante au MTX dans les cellules HS murines permettait une survie des cellules HS exposées *in vitro* au MTX (10% de survie à 0,1 μM de MTX). Depuis cette étude, plusieurs variantes de la DHFR humaine ont été testées pour cette application dans deux modèles cellulaires distincts, soit les cellules CHO DUKX B11 (*dhfr*$^-$) et les cellules HS murines.

Les cellules CHO DUKX B11 (*dhfr*$^-$) constituent un modèle simple et efficace pour tester l'activité DHFR des variantes et le niveau de résistance au MTX que ces variantes peuvent conférer aux cellules. Seules les variantes actives et résistantes au MTX permettent la croissance des cellules dans un milieu de culture dépourvu en nucléotides contenant l'inhibiteur. La transfection des variantes humaines Gly15Trp[149], Leu22Phe[124], Leu22Arg[124], Phe31Ser et Phe34Ser[150] dans les cellules CHO DUKX B11 a démontré que toutes ces variantes étaient actives dans un contexte *ex vivo* et procuraient une résistance modérée au MTX (moins de 10% de survie à une concentration de 1 μM de MTX, seuil auquel l'enzyme native ne peut conférer de résistance). En parallèle, les variantes humaines Gly15Trp, Leu22Arg, Phe31Ser et Phe34Ser[149, 150] furent transduites dans des cellules HS murines. L'exposition des cellules transduites à 0,1 μM de MTX donna des pourcentages de survie situés entre 6 et 31%[149, 150].

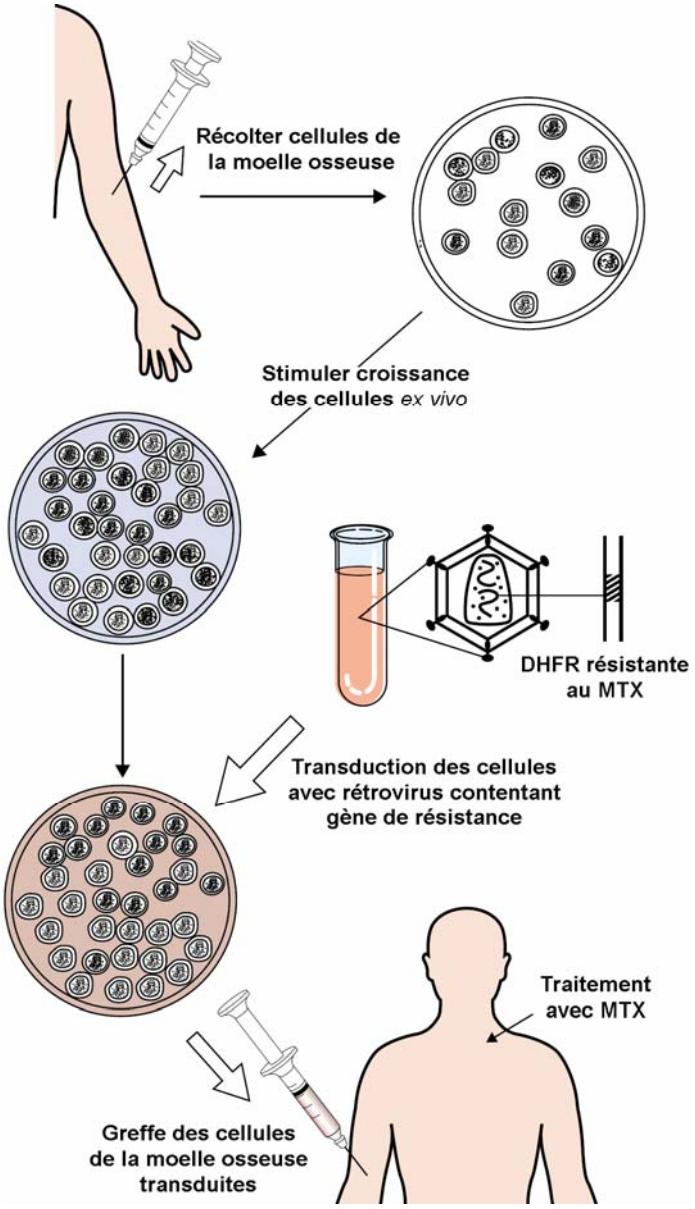

Figure 1.10. Schématisation des étapes de la thérapie génique appliquées dans un contexte de chimioprotection. Adapté de [170].

Les bas pourcentages de survie avec les variantes ponctuelles de la DHFR humaine ne rendaient pas leur utilisation dans un contexte clinique possible, puisque les doses de MTX circulant dans le plasma sanguin se situent entre 0,5 et 1 μM lors de traitement de chimiothérapie[151, 152]. Le bas niveau de résistance conféré par ces variantes ponctuelles était attribuable soit à la baisse d'efficacité catalytique (e.g. mutant Leu22Arg) ou à une réduction trop modérée de l'affinité pour le MTX (e.g. mutant Phe31Ser). Il fut postulé qu'une variante résistante pouvant servir à la chimioprotection des cellules HS devait avoir une efficacité catalytique suffisante pour assurer la survie et la division des cellules, tout en ayant une très faible affinité pour le MTX[118]. Parmi toutes les variantes ponctuelles caractérisées, seule Leu22Tyr semblait offrir un bon compromis pour ces deux paramètres, avec une efficacité catalytique réduite de 10 fois et une réduction de l'affinité pour le MTX de plus de 3000 fois par rapport à l'enzyme native[29]. La protection des cellules HS murines transduites avec la variante Leu22Tyr était près de 75% à 0,1 μM de MTX, et près de 20% à 1 μM de MTX, démontrant que cette variante protégeait mieux les cellules HS que les autres variantes ponctuelles[153]. La variante Leu22Tyr fut aussi utilisée pour un autre type d'application, visant à améliorer un des problèmes réduisant l'efficacité d'un traitement par thérapie génique, soit le bas taux de repopulation des cellules transduites. Il fut possible d'enrichir *in vivo* la proportion de cellules de moelle osseuse transduites avec la variante Leu22Tyr suite à l'administration de l'antifolate TMTX à des souris ayant reçu une greffe de moelle préalablement transduite avec la variante[147]. Ce résultat démontrait qu'il était possible d'augmenter le nombre de cellules transduites dans un organisme suite à la greffe de cellules transduites, indépendamment du taux de transduction obtenu avant la greffe. En administrant des doses régulières de l'antifolate TMTX, il fut possible d'enrichir la proportion de cellules transduites dans la moelle osseuse de souris à des taux situés entre 23 et 83%, ce qui corrélait avec la résistance conférée par cette variante dans un contexte *ex vivo*.

Un dernier effort pour améliorer l'efficacité de protection au MTX fut entrepris, en créant des variantes doublement substituées de la DHFR humaine résultant de la combinaison de variantes ponctuelles aux résidus 22 et 31[154]. En combinant les variantes Leu22Tyr et Leu22Phe avec les variantes Phe31Ser ou Phe31Gly, il fut possible d'obtenir des doubles variantes actives (Leu22Tyr/Phe31Ser, Leu22Tyr/Phe31Gly, Leu22Phe/Phe31Ser et Leu22Phe/Phe31Gly) possédant de faibles affinités pour le MTX. Les efficacités catalytiques de ces variantes étaient réduites de 24 à 66 fois, alors que les valeurs d'affinité pour le MTX étaient réduites de 7600 à 44 000 fois par rapport à l'enzyme native. La combinaison de deux variations ponctuelles conférant une résistance modérée au MTX (e.g. Leu22Phe, K_i^{MTX} = 0.55 nM et Phe31Ser, K_i^{MTX} = 0.24 nM) résultait en une augmentation drastique de la valeur de K_i^{MTX} chez la double variante (e.g. Leu22Phe/Phe31Ser, K_i^{MTX} = 26 nM). L'effet de la combinaison de deux variantes ponctuelles sur la réduction de l'efficacité catalytique était plus modérée, la plus faible efficacité catalytique rapportée pour la double variante Leu22Tyr/Phe31Gly (k_{cat}/K_M^{DHF} = 1.4 $\mu M^{-1}s^{-1}$) étant réduite de 8 fois par rapport à la variante Leu22Tyr (k_{cat}/K_M^{DHF} = 12 $\mu M^{-1}s^{-1}$) et de 18 fois par rapport à la variante Phe31Gly (k_{cat}/K_M^{DHF} = 26 $\mu M^{-1}s^{-1}$). Les doubles variantes offraient donc une plus grande résistance au MTX que les variantes ponctuelles, ce qui pourrait conférer une protection complète à l'inhibiteur. Les doubles variantes furent transduites dans des cellules de moelle osseuse murine et testés *ex vivo* pour leur résistance au MTX[155-157]. Ces études démontrèrent que la double variante Leu22Phe/Phe31Ser était la meilleure candidate pour la myeloprotection, conférant une résistance au MTX permettant la survie de 14 à 75% des cellules transduites à 0,1 μM de MTX, mais ne pouvait procurer une résistance aussi élevée que la variante L22Y dans le même contexte[153].

1.4 Objectifs du projet de recherche et justification des approches utilisées

L'acquisition par les cellules tumorales de divers mécanismes de résistance clinique au MTX a mené au développement de nouvelles molécules inhibitrices ciblant le métabolisme du folate. Étant donné le rôle primordial de la DHFR dans le métabolisme du folate, plusieurs composés analogues au MTX ont été synthétisés pour contourner les mécanismes de résistance cliniques en plus de contrer l'activité de l'enzyme dans les cellules, avec peu de succès[39]. Une meilleure connaissance des contacts essentiels entre l'enzyme et le MTX pourrait mener au développement de nouveaux inhibiteurs de la DHFR humaine. La caractérisation des paramètres cinétiques et d'inhibition des variantes de la DHFR humaine a permis de mieux comprendre l'effet de certaines mutations sur la reconnaissance du MTX et la réduction catalytique du substrat DHF, suggérant des rôles pour certains résidus dans la liaison des ligands. De plus, la combinaison de variations ponctuelles aux résidus Leu22 et Phe31 a généré des variantes hautement résistantes au MTX, suggérant qu'une combinaison d'autres variantes du site actif de la DHFR pourrait augmenter la résistance au MTX en maintenant une activité suffisante à la survie cellulaire. Toutefois, l'approche utilisée pour la création des variantes était basée sur le design rationnel, où les variations incorporées à des sites spécifiques de l'enzyme étaient choisies selon des présomptions issues des interactions entre l'enzyme et le ligand. Seuls les résidus Leu22 et Phe31 ont été les sujets de plusieurs études de mutagenèse, où un petit nombre de mutations ont été explorées. Les autres résidus du site actif ont été peu caractérisés et pourraient jouer un rôle important dans la liaison du MTX et/ou du DHF. Les variantes utilisées pour la protection de cellules HS sont issus de ces études, mais n'ont pas la capacité de conférer une résistance élevée à de grandes concentrations de MTX (> 0,1 μM), qu'elles soient ponctuelles (Leu22Tyr) ou combinatoires (Leu22Phe/Phe31Ser). Ainsi, la caractérisation de nouvelles variantes ponctuelles et combinatoires pourrait générer de nouveaux gènes de résistance procurant une meilleure protection aux cellules HS.

Basé sur ces considérations, le but de ce projet fut d'élucider le rôle de l'ensemble des résidus du site actif de la DHFR humaine dans la liaison du MTX en créant de nouvelles variantes combinatoires et ponctuelles de la DHFR humaine actives et résistantes au MTX par mutagenèse semi-rationnelle ou par saturation de sites. En parallèle, la caractérisation des constantes cinétiques et d'inhibition des variantes générées servi à identifier de nouvelles variantes hautement résistantes au MTX, pouvant offrir la myeloprotection aux cellules HS. Plusieurs principes théoriques et méthodes expérimentales furent conjointement employés pour la réalisation globale de ce projet.

1.4.1 – Création de banques d'ADN par mutagenèse semi-rationnelle et par saturation de sites

Contrairement au design rationel, l'évolution dirigée[158] est une méthode qui permet d'explorer un grand nombre de possibilités de mutations chez un gène donné, dans le but d'obtenir un phénotype désiré. Toutefois, les banques d'ADN générées par cette méthode sont parfois trop grandes pour être criblées de façon représentative. La mutagenèse semi-rationnelle[159] représente un bon compromis entre les deux approches, où certains résidus d'intérêt sont substitués par plusieurs possibilités d'acides aminés et combinés entre eux pour rechercher un phénotype désiré. Ainsi, dans le chapitre 2, nous avons créé une première banque combinatoire par mutagenèse semi-rationelle, en incorporant de concert une variété d'acides aminés aux résidus Phe31, Phe34 et Gln35, qui appartiennent tous à l'hélice α1 de la DHFR humaine. Cette banque combinatoire a été créée pour élucider le rôle des substitutions aux résidus Phe34 et Gln35 pouvant conférer une résistance au MTX, tout en évaluant l'effet de variations combinatoires entre ces deux résidus et le résidu Phe31 sur la reconnaissance du MTX. Cette banque a aussi servie comme preuve de concept pour l'établissement des diverses méthodes développées au cours du projet.

En parallèle, le chapitre 3 décrit la création et la caractérisation de variantes aux résidus Ile7, Gly15, Trp24, Arg70 et Val115 par mutagénèse par saturation de sites,

permettant l'incorporation des 20 acides aminés à ces différents résidus. Ces résidus étant peu caractérisés dans la littérature, nous avons jugé que des études structure/fonction approfondies sur chacun de ces résidus seraient essentielles pour atteindre les objectifs du projet.

1.4.2 – Stratégie de sélection pour les banques de DHFR humaine et caractérisation des mutants actifs et résistants

L'identification de variantes possédant un phénotype désiré à partir d'une banque d'ADN nécessite une méthode de criblage ou de sélection. Dans le cadre de notre projet, nous voulions identifier des variantes de la DHFR humaine résistantes au MTX qui conservaient une activité suffisante pour la survie cellulaire. Ainsi, nous avons développé une stratégie de sélection *in vivo* basée sur la complémentation de l'activité et la résistance au MTX de variantes de la DHFR humaine chez des bactéries *E. coli*. Cet organisme fût choisi car son taux de croissance en culture est rapide comparé à d'autres bactéries et à des cellules eucaroytes. De plus, la transformation de l'ADN plasmidique peut donner lieu à plus de 10^7 transformants, permettant le criblage de grandes banques de mutants. Toutefois, la majorité des souches d'*E. coli* commercialement disponibles sont intrinsèquement résistantes à de hautes concentration de MTX. Pour pallier ce problème, la souche SK037 fut utilisée pour ces expériences, parce qu'elle est plus sensible au MTX, résultat d'une délétion génétique dans la pompe membranaire AcrAB[57]. Les banques ont été transformées dans la souche SK037, qui a été exposé à un milieu de culture minimal solide contenant de très hautes concentrations en MTX et du TMP pour inhiber sélectivement la DHFR bactérienne. Les colonies bactériennes présentent sur le milieu minimal contenaient ainsi des variantes de la DHFR humaine actives et résistantes au MTX (Chapitre 2 et Chapitre 3). La banque combinatoire Phe31/Phe34/Gln35 et les banques individuelles ont été sélectionnées ainsi.

Les valeurs des paramètres cinétiques et d'inhibition ont été déterminées pour les variantes actives et résistantes suite à l'étape de sélection, dans le but de d'évaluer l'effet des substitutions sur les constantes d'affinité pour le DHF (K_M^{DHF}) et le MTX (K_i^{MTX}), ainsi que la constante catalytique (k_{cat}). Ces paramètres ont été déterminés par spectrophotométrie, dans des conditions répondant aux critères de la cinétique Michaelis-Menten[160]. À partir de ces méthodes, une stratégie de criblage à haut débit en plaques 96 puits fut établit en utilisant les banques individuelles, pour amener le processus de caractérisation cinétique à une plus grande échelle (Chapitre 3). Il fût ainsi possible de déterminer rapidement les valeurs de k_{cat} et d'IC_{50}^{MTX} pour toutes les variantes actives des banques individuelles. Les constantes de liaison du MTX (K_D^{MTX}) furent mesurées par fluorimétrie, pour confirmer que la perte d'affinité chez les variantes était uniquement reliée à un phénomène de perte de contacts entre le MTX et certains résidus du site actif de la DHFRh (Chapitre 2).

1.4.3 – Évaluation de la protection de lignées cellulaires contre les effets cytotoxiques du MTX

Les variantes combinatoires possédant une bonne activité DHFR et une faible affinité pour le MTX issus de la banque Phe31/Phe34/Gln35 furent transfectées dans des cellules CHO *dhfr*$^-$ (Chapitre 2) ou transduites dans des cellules de moelle osseuse murines (Chapitre 4), pour évaluer l'effet protecteur de ces nouvelles variantes comparativement aux mutants précédemment rapportés pour cette même application. Les cellules CHO *dhfr*$^-$ transfectées avec les variantes les plus résistantes de la banque combinatoire ont été exposées à différentes concentrations de MTX dans un milieu de culture minimal ne contenant pas de nucléotides, rendant la survie et la prolifération de ces cellules dépendantes de l'activité DHFR des variantes transfectées. Les cellules CHO *dhfr*- représentent un système simple et efficace pour l'évaluation de la résistance au MTX,

puisque les variantes conférant une résistance au MTX dans ce système semblent aussi procurer un effet protecteur aux cellules de la moelle osseuse[149, 150].

La transduction de cellules de moelle osseuse nécessite plusieurs étapes avant d'exposer les cellules transduites au MTX (Chapitre 4). Pour incorporer les variantes combinatoires dans les cellules de moelle osseuse, nous avons tout d'abord cloné chaque variante dans un vecteur proviral contenant des éléments du virus des cellules souches murines (MSCV)[161]. Ce vecteur a été choisi car les éléments viraux qu'il contient sont très efficaces pour l'infection des cellules de la moelle osseuse. Le vecteur proviral a ensuite été transfecté dans des cellules d'empaquetage 293 spécialement modifiées pour la production de rétrovirus (VSV-G)[162]. Ces cellules ont été modifiées pour contenir les gènes rétroviraux encodant les protéines fonctionnelles, de structure et de l'enveloppe virale dans leur génome. Suite à la transfection, l'ARNm encodé par le vecteur proviral est encapsidé dans un des vaisseaux viraux produits par les cellules 293 modifiées. L'utilisation de ce système est avantageuse puisque les titres viraux sont élevés comparativement à d'autres types de cellules d'empaquetage, et les virus produits sont amphotropiques, signifiant qu'ils ont la capacité d'infecter des cellules issues de différentes espèces. Toutefois, l'utilisation de ce système n'est que transitoire, puisque l'expression de la glycoprotéine VSV est cytotoxique, menant à une mort des cellules d'empaquetage après quelques jours de culture. Le virus amphotropique a été utilisé pour infecter un autre type de cellules d'empaquetage, les cellules GP+E86, produisant un virus pouvant infecter des cellules de la moelle osseuse murines. Les GP+E86 sont des cellules 3T3 dérivées contenant dans leur génome les gènes nécessaires à la fonction et la structure d'un virus, et un gène encodant une glycoprotéine de surface spécifique à un récepteur membranaire des cellules murines (virus écotropique pseudotypé).

Avant leur infection, les cellules de la moelle osseuse ont été isolées fraîchement des fémurs et des tibias de souris, et pré-stimulées pour entrer en cycle dans un milieu de culture contenant des interleukines et facteurs de croissance spécifiques. Ceci assure un

taux d'infection maximal pendant la co-culture des cellules de la moelle avec les cellules GP+E86 infectées. Les cellules de la moelle infectées ont été mises en culture dans des milieux semi-solides, dans des conditions semblables à celles utilisées pour les autres mutants de la DHFR humaine résistants au MTX, dans le but de comparer l'effet protecteur des variantes combinatoires avec les données retrouvées dans la littérature[147, 149, 150, 155]. La culture en milieu semi-solide est fréquemment utilisée car elle permet de faire une estimation rapide *ex vivo* du nombre de cellules pouvant potentiellement reconstituer la moelle osseuse d'un animal qui recevrait une greffe de ces cellules.

1.4.4 – Développement d'un marqueur de sélection pour les cellules de la moelle osseuse transduites

Un des problèmes majeurs reliés à l'application de la thérapie génique est le faible taux de transduction d'un gène thérapeutique dans les cellules de la moelle osseuse lors de l'étape d'infection *ex vivo*[163]. Le faible nombre de cellules transduites mène à une faible reconstitution de ces cellules dans la moelle osseuse d'un patient ayant reçu une greffe, à des niveaux qui sont parfois trop bas pour donner l'effet thérapeutique désiré[164]. Des stratégies de sélection ont été développées pour augmenter la proportion des cellules transduites au sein des niches de moelle osseuse. La transduction de cellules de la moelle osseuse avec un rétrovirus constitué d'un gène thérapeutique et d'un gène de résistance à un agent myelotoxique offre le potentiel d'enrichir le nombre de cellules transduites chez des animaux recevant une greffe de moelle osseuse. Dans un premier temps, il a été démontré qu'il était possible d'enrichir *in vivo* la population de cellules transduites dans la moelle osseuse suite à l'administration d'agents myelotoxiques[143, 147]. La sélection *in vivo* est toutefois limitée par deux facteurs. L'efficacité de la sélection varie selon l'animal modèle testé, la sélection étant plus efficace chez les petits mammifères que chez les mammifères plus semblables à l'homme, attribuable à des différences dans la régulation des cellules HS chez ces différentes espèces[165]. De plus, certains agents myelotoxiques sont mutagènes, et les effets à long terme suite à leur administration sont méconnus[166].

Pour pallier ces problèmes, nous avons développé une stratégie de sélection *ex vivo* pour augmenter le nombre de cellules transduites avant la greffe (Chapitre 4). Une population de cellules de moelle osseuse murine infectée avec un gène de résistance au MTX a été exposée en culture au MTX, permettant d'éliminer les cellules non-transduites. L'enrichissement des cellules transduites offre la possibilité d'augmenter les probabilités de reconstitution de la moelle d'un animal par ces cellules suite à une greffe. L'avantage principal de ce type de sélection réside dans le fait que l'efficacité de sélection n'est pas dépendante de l'origine des cellules de la moelle osseuse, puisque les cellules de la moelle osseuse des différentes espèces se comportent de façon semblable *ex vivo*[167]. Une sélection *ex vivo* efficace utilisant le MTX pourrait donc être utilisée pour enrichir des cellules humaines transduites avant une greffe, menant ainsi à une meilleure repopulation de la moelle osseuse par des cellules contenant un gène thérapeutique.

1.4.5 – Cristallographie par rayons X pour élucider le mécanisme moléculaire de résistance au MTX

L'élucidation des interactions moléculaires existantes entre une protéine et un ligand peut s'avérer très informative pour la compréhension d'un mécanisme catalytique, d'un mécanisme de signalisation ou pour le design de molécules analogues pouvant inhiber certaines activités cellulaires. La cristallographie par rayons X est une méthode très utilisée pour la détermination de la structure tridimensionnelle d'une protéine complexée à des ligands, menant à une meilleure caractérisation des interactions gouvernant la liaison et l'affinité des biomolécules envers leurs ligands[168, 169].

La DHFR humaine native a précédemment été cristallisée en présence de divers ligands[24, 26, 27, 30, 31]. Ces études ont entre autre permis de démontrer que certains inhibiteurs, comme le MTX, ne se liaient pas dans la même orientation que le substrat et formaient des interactions spécifiques avec l'enzyme, connaissances pouvant être exploitées pour le design de nouveaux antifolates. De plus, quelques variantes de la DHFR résistantes au

MTX ont aussi été cristallisées en présence d'inhibiteurs, dans le but de mieux comprendre les interactions spécifiques gérant l'affinité de l'enzyme pour les antifolates[25, 29]. Toutefois, ces études ont été faites avec des variantes ponctuelles de la DHFR ayant une résistance modérée à l'inhibiteur, ne permettant pas de voir de voir des changements évidents dans la liaison du MTX.

Ainsi, nous avons appliqué les méthodes reliées à la cristallographie des protéines sur les variantes combinatoires de la DHFR hautement résistants au MTX, pour mieux élucider les interactions moléculaires responsables de la perte d'affinité pour le MTX. Une description détaillée des procédures et des résultats obtenus pour ces études se retrouve au chapitre 5. Ainsi, nous avons pu produire et purifier des DHFR humaines substitutées, obtenir des cristaux de ces protéines en présence de ligands, et résoudre la structure cristalline pour une des variantes combinatoires (F31R/Q35E) à l'étude. En combinant des observations faites à partir de la structure cristalline avec des données cinétiques obtenues, nous avons pu proposer que la cause de la résistance élevée au MTX chez la double variante F31R/Q35E est attribuable à un phénomène biophysique encore peu caractérisé à ce jour.

Préface au chapitre 2

Partant de la prémisse que la combinaison de variantes ponctuelles résistantes au MTX de la DHFR générerait des variantes combinatoires hautement résistantes au MTX, nous avons créé et caractérisé une banque combinatoire incorporant des substitutions aux résidus Phe31, Phe34 et Gln35, tous retrouvés sur l'hélice α1 du site actif de la DHFR humaine. Le développement d'un système de sélection basé sur la survie de bactéries *E. coli* a permis l'identification de 10 variantes hautement résistantes au MTX provenant de la banque combinatoire. La caractérisation des paramètres cinétiques et d'inhibition pour chacune des variantes a démontré que l'importance de la perte d'affinité au MTX corrélait avec le nombre de substitutions retrouvées aux résidus 31, 34 et 35 dans l'échantillon sélectionné, les variantes triples démontrant la plus grande perte d'affinité au MTX. En revanche, la perte d'affinité au MTX corrélait aussi avec une perte d'efficacité catalytique, les variantes triples démontrant la plus basse efficacité catalytique. Toutefois, la perte d'affinité pour le MTX était généralement plus importante que la perte d'efficacité catalytique, signifiant que les substitutions affectaient plus la liaison du MTX que du substrat DHF. La transfection des variantes les plus résistantes dans des cellules CHO *dhfr*$^-$ exposées à de hautes concentrations de MTX assurait une survie aux cellules, la variante triple F31A/F34V/Q35H permettant une survie maximale à la plus haute concentration de MTX utilisée. Une étude de modélisation *in silico* de cette variante a permis de proposer que la perte d'affinité pour le MTX chez cette variante était due à une perte de contacts hydrophobes entre le ligand et les résidus 31 et 34 du site actif.

Ce chapitre est présenté sous forme d'article scientifique publié dans la revue *Journal of Molecular Biology* en octobre 2007. Ayant participé à tous les aspects de recherches expérimentales et théoriques de cette étude, ma contribution à ce projet est majeure. Une aide technique offerte par Elena Fossati pour les travaux de modélisation moléculaire justifie sa présence en tant que deuxième auteure.

Chapitre 2

Augmentation de la résistance au MTX par la combinaison de substitutions au site actif de la dihydrofolate reductase humaine

2.1 Article 1. *Increasing MTX-resistance by combination of active-site mutations in human dihydrofolate reductase*

Increasing MTX-resistance by combination of active-site mutations in human dihydrofolate reductase

Jordan P. Volpato[1], Elena Fossati[1] & Joelle N. Pelletier[1,2]

[1]Département de Biochimie and [2]Département de Chimie

Université de Montréal

C.P. 6128, Succursale Centre-Ville

Montréal (Québec)

H3C 3J7 CANADA

J. Mol. Biol., 2007, 373 (3), 599-611

ABSTRACT

Methotrexate-resistant forms of human dihydrofolate reductase have the potential to protect healthy cells from the toxicity of methotrexate (MTX), to improve prognosis during cancer therapy. It has been shown that synergistic MTX-resistance can be obtained by combining two active-site mutations that independently confer weak MTX-resistance. In order to obtain more highly MTX-resistant human dihydrofolate reductase (hDHFR) variants for this application, we used a semi-rational approach to obtain combinatorial active-site mutants of hDHFR that are highly resistant towards MTX. We created a combinatorial mutant library encoding various amino acids at residues Phe31, Phe34 and Gln35. *In vivo* library selection was achieved in a bacterial system on media containing high concentrations of MTX. We characterized ten novel MTX-resistant mutants with different amino acid combinations at residues 31, 34 and 35. Kinetic and inhibition parameters of the purified mutants revealed that higher MTX-resistance roughly correlated with a greater number of mutations, the most highly-resistant mutants containing three active site mutations (K_i^{MTX} = 59 to 180 nM; wild-type K_i^{MTX} < 0.03 nM). An inverse correlation was observed between resistance and catalytic efficiency, which decreased mostly as a result of increased K_M toward the substrate dihydrofolate. We verified that the MTX-resistant hDHFRs can protect eukaryotic cells from MTX toxicity by transfecting the most resistant mutants into DHFR-knock-out CHO cells. The transfected variants conferred survival at MTX concentrations between 100-fold and >4000-fold higher than the wild-type enzyme, the most resistant triple mutant offering protection beyond the maximal concentration of MTX that could be included in the medium. These highly resistant variants of hDHFR offer potential for myeloprotection during administration of MTX in cancer treatment.

INTRODUCTION

hDHFR (EC 1.5.1.3) is a ubiquitous cytosolic enzyme that catalyzes the reduction of 5,6-dihydrofolate (DHF) to 5,6,7,8-tetrahydrofolate (THF) in a nicotinamide adenine dinucleotide phosphate (reduced form) (NADPH)-dependent reaction. THF is an essential cofactor in several metabolic pathways, including purine and thymidylate biosynthesis. As a result of its importance in cellular proliferation, hDHFR has long been a key pharmacological target for the treatment of various types of cancer.[1] Methotrexate is a folate analogue that acts as a slow, tight binding competitive inhibitor of hDHFR, thereby inhibiting cellular THF synthesis and cellular proliferation. MTX is widely used for the treatment of acute lymphoblastic leukemia,[2] osteosarcoma,[3] breast cancer[4] and head and neck cancer.[5]

Efficacy of MTX in cancer treatment is largely attributed to the high affinity of the drug for hDHFR (K_i = 3.4 pM).[6] Crystal structures of the wild-type (WT) hDHFR complexed with MTX have shown that, despite its high structural similarity to folate, MTX and folate bind at the active site in a different orientation.[7] Although the *p*-aminobenzoic acid and glutamate (*p*-ABA-Glu) portions of both ligands bind at the active site in a similar orientation, the pteroyl moiety of MTX is flipped 180° around the C6-C9 bond (Figure 2.1(a)), such that its 4-amino group forms specific hydrogen bonds with the backbone carbonyls of residues Ile7 and Val115 (Figure 2.1(b)), in contrast to bound folate, which does not form hydrogen bonds with these residues. The pteroyl moiety of MTX is also involved in hydrogen bonding with residue Trp24 *via* a conserved water molecule and with residue Glu30,[8] while the side chain of residues Leu22 and Phe34 are within van der Waals distance of this portion of the inhibitor (Figure 2.1(b)).[9, 10] These interactions are also formed with the pteroyl moiety of folate, albeit with the opposite side of the pterin ring. The *p*-ABA moiety of MTX and DHF mainly interact *via* van der Waals interactions with residues Phe31 and Phe34 of α-helix 1 (residues 27-40), which also contains Gln35 that is

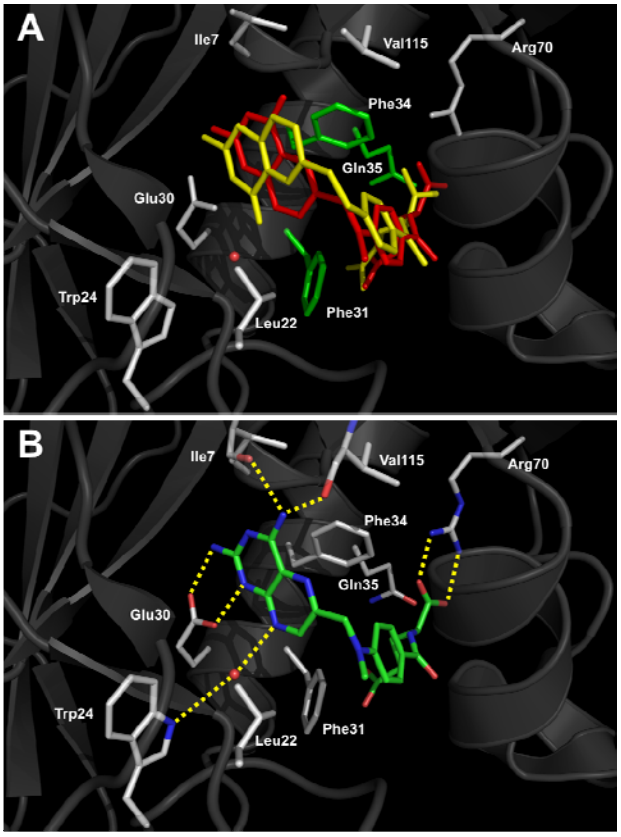

Figure 2.1. Ligand binding at the active-site of WT hDHFR. A: Superimposition of hDHFR with bound folate (yellow; 1DRF.pdb[62]) and its competitive inhibitor methotrexate (red; 1U72.pdb[7]). The active site is shown, highlighting the flip of the bicyclic pteroyl ring. Stick representations of side-chains from Ile7, Leu22, Trp24, Glu30, Arg70 and Val115 are shown in white. The residues targeted for mutation, Phe31, Phe34 and Gln35, are in green. A conserved active-site water molecule is depicted as a red sphere. B: Hydrogen bonding network of bound MTX at the active site of hDHFR. Side-chains and MTX are in sticks representation, coloured by atom (nitrogen (blue), oxygen (red) and carbon (white for side chains and green for MTX)). A conserved active-site water molecule is depicted as a red sphere. For clarity, only the coordinates of 1U72.pdb are represented.

proximal to the γ-glutamate moiety of the bound ligands. The glutamate moiety also forms a salt bridge with the guanidinium side chain of Arg70.

Previous studies of hDHFR and murine DHFR have shown that certain mutations at residues Leu22, Phe31, Phe34, Gln35 and Arg70 (Figure 2.1) can yield catalytically-active, MTX-resistant mutants.[11-17] Identification of MTX-resistant hDHFR mutants has been performed either *ex vivo* in cultured cells exposed to MTX[18-20] or by performing site-directed mutagenesis at the active site of hDHFR by rational design.[9, 11-15, 21] These studies have mostly yielded point mutants that maintain good catalytic efficiency while displaying moderate MTX resistance (e.g. F31S, K_i = 0.240 nM; L22R : K_i = 4.6 nM).[14, 15] However, some point mutations confer high MTX resistance (e.g. F34S : ternary K_D^{MTX} = 210 nM), albeit with considerably reduced catalytic efficiency.[10] These studies led to a better understanding of ligand binding at the enzyme active site and contributed to structure-based design of new antifolate inhibitors.[22]

Identifying more highly MTX-resistant hDHFR mutants offers important applications in the medical field. Because MTX-resistant hDHFRs have not been observed in clinical studies of acquired MTX-resistance in cancer patients,[23] MTX-resistant hDHFRs have the potential to protect healthy haematopoietic stem cells from MTX toxicity during chemotherapy,[24] thus protecting patients from immunosuppression. Gene therapy strategies have been used to transfer MTX-resistant hDHFRs into mouse and human bone marrow progenitor cells, efficiently ensuring stem cell survival upon exposure to MTX.[25, 26] Resistant cells transplanted in the bone marrow of mice ensured myeloprotection during treatment with MTX.[27, 28] For this application, ideal candidate hDHFR mutants should have a very high K_i for MTX (in the high nanomolar range), while maintaining the catalytic properties, including DHF binding , required to ensure cell survival.

Highly MTX-resistant hDHFR genes with good catalytic efficiencies have been obtained by the combination of the moderately MTX-resistant point mutants at active-site

residues 22 and 31,[29] which generated synergistically resistant hDHFRs (e.g. L22Y-F31G, K_i = 150 nM *versus* L22Y, K_i = 11 nM and F31G, K_i = 0.35 nM) that conferred high MTX resistance in human and mouse stem cell lines. While those results are promising, variants that are yet more highly resistant and/or more active would hold greater potential for clinical application, by increasing the difference in cellular survival between cells harboring MTX-resistant hDHFR and those with native hDHFR (target of MTX).

On the basis of these considerations, we have devised a strategy based on directed evolution for the identification of novel hDHFR combinatorial mutants that are highly active and resistant to MTX. Directed evolution of ligand binding in an enzyme generally requires structure-based knowledge to pinpoint residues in the vicinity of the active site. These residues are mutated in combination and the resulting combinatorial mutant libraries are screened for a desired property. Application of such methods has provided new structural insight into ligand binding,[30,31] engineered new substrate specificity,[32] and resulted in the development of efficient biomarkers.[33,34] Using a semi-rational approach, we created a combinatorial library encoding mutations at residues Phe31, Phe34 and Gln35 of the hDHFR gene. These residues belong to α-helix 1 and are individually known to confer MTX resistance upon mutation.[10,14,17] We performed *in vivo* library selection in a bacterial system propagated on media containing a high concentration of MTX. Characterization of selected variants yielded novel MTX-resistant hDHFR mutants, including a variety of combinatorial mutants that displayed an important decrease in MTX binding, comparable to the weakest-binding hDHFR mutant reported to date, albeit with a greater residual specific activity. As a result, we obtained very efficient protection of a relevant mammalian cell model, *dhfr* $^-$ CHO DUKX B11 cells.

RESULTS

Creation of the hDHFR mutant library

A combinatorial library encoding 567 different mutants was created by mutating amino acids Phe31, Phe34 and Gln35 to a selection of amino acids, in order to identify novel MTX-resistant hDHFR mutants (Table 2.1). The number of possibilities encoded was restricted in view of future recombination with other mutant hDHFR libraries. The three positions chosen for mutation belong to α-helix 1 (residues 27-40), which contains the catalytic residue Glu30, a highly-conserved residue that protonates N_5 of DHF prior to hydride transfer,[8] as well as residues Phe31, Phe34, Gln35, that have been shown to be important for substrate and/or inhibitor binding.[10,14,17] The selection of amino acids to be encoded at positions 31, 34 and 35 was based either on known mutations that individually confer resistance to MTX or on the basis of *in silico* observations of hDHFR with bound MTX. We encoded the desired mutations at the three positions using a single degenerate oligonucleotide primer. As a result of codon degeneracy, other amino acids were encoded in addition to the amino acid variety of interest (Table 2.1). Site-directed mutagenesis studies at residues 31 and 34 have shown that MTX-resistant mutants generally contain small polar or non-polar amino acids at these positions. Consequently, these types of residues were encoded in addition to the phenylalanine present at these positions in WT hDHFR. As noted in previous reports,[7,35-37] visualization of bound MTX or folate in the native enzyme (Figure 2.1) suggests that these substitutions can reduce the contact surface with bound ligand, therefore reducing affinity for MTX and/or DHF. For residue 35, earlier studies of the murine DHFR gene have shown that the mutation Q35P can confer moderate resistance to MTX.[17] The location of the Q35P mutation in the middle of α-helix 1 suggests a change in α-helix geometry. Consequently, we mutated Gln 35 to amino acids with low α-helical propensity,[38] without encoding proline due to low stability of the Q35P point mutant.[17]

Table 2.1. Amino acids encoded at residues 31, 34 and 35 of the hDHFR mutant library.

Native residue	Encoded amino acids	Justification
F31	**F**, **A**, **G**, **R**,**S**, C, L, P, V	Reducing contact surface with inhibitor
F34	**F**, **A**, **I**, **S**, **T**, **Q** L	Reducing contact surface with inhibitor
Q35	**Q**, **D**, **G**, **N**, **R**, **S**, E, H, K,	Changing helical propensity

Wild-type residues at positions 31, 34 and 35 are underlined. Intended substitutions are in bold. The remaining amino acids were encoded as a result of the degeneracy of the genetic code.

Selection and identification of MTX-resistant mutants

The hDHFR mutant library was transformed in *Escherichia coli* SK037, a MTX-sensitive strain. This strain is a knock-out for *tolC*, which encodes a protein essential to the function of a multi-drug-resistance (MDR) efflux pump.[39] The quality of the library was assessed by sequencing 70 clones that grew on non-selective media (LA-100). Nucleotide representation for each of the degenerate codons used at residues 31, 34 and 35 followed the expected statistical distribution, and no non-specific mutation was observed. The library was then selected on M9 minimal medium containing 1 mM MTX (ATM-1000). As negative controls for MTX-resistance, *E. coli* SK037 transformed with pQE32 or WT hDHFR-pQE32 were also plated on the selective medium. The survival rate of the library was 0.2%, whereas no bacterial growth was observed for the negative controls. *E. coli* SK037 transformed with hDHFR L22Y-pQE32, which encodes a MTX-resistant point mutant of hDHFR, were plated on the selective ATM-1000 medium as a positive control. This yielded a 100% survival rate relative to non-selective medium, demonstrating that the selection stringency was appropriate for identification of MTX-resistant hDHFR mutants. Seventy colonies were picked following selection to identify the mutations at positions 31, 34 and 35. As shown in Figure 2.2, ten different mutants were identified post-selection. The mutants are designated by the one-letter code of the amino acid occurring at positions 31, 34 and 35. The selection yielded 1 point mutant, five double mutants and four triple mutants. Mutant PFE was the most frequently selected combination (30%), followed by SFE (27%), RFE (20%) and PFH (11%). These variants, which are all double mutants, represent 88% of the selected clones and all contain the native Phe residue at codon 34. The last double mutant identified, GFN, also conserves the native Phe at position 34, but was identified only once (1%). The most frequently observed triple mutant is AVH, identified 5 times (7%), followed by RTR (1%), RTS (1%) and RAN (1%). Finally, a point mutant, PFQ (F31P) was identified once (1%). This point mutant had not yet been characterized in MTX-resistance studies. Retransformation and plating in the presence (ATM-1000) or

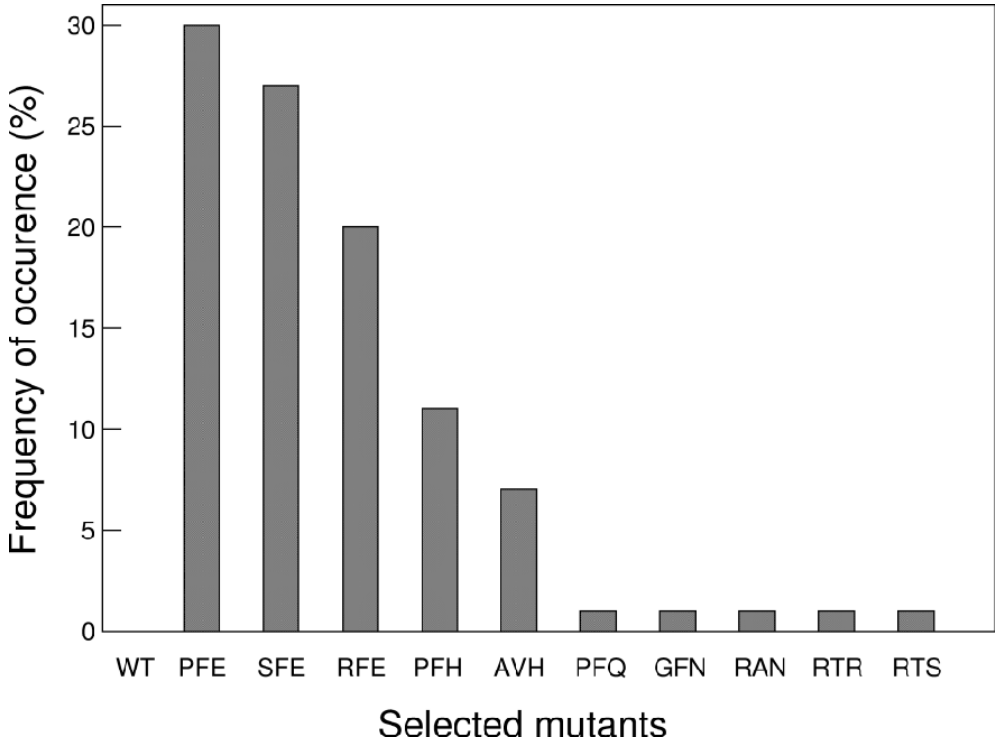

Figure 2.2. Frequency of occurrence of the novel MTX-resistant mutants. Seventy mutants were isolated following selection of the hDHFR mutant library on ATM-1000 medium. Mutants are designated by the one-letter code of the amino acid occurring at positions 31, 34 and 35, respectively. Mutant PFQ corresponds to point mutant F31P.

absence (LA-100) of MTX gave rise to a similar number of colonies for all selected variants, confirming that the observed resistance is solely due to the MTX-resistant hDHFRs.

Binding and kinetic characterization of MTX-resistant hDHFR mutants

For determination of kinetic and binding parameters, the retransformed MTX-resistant hDHFR variants were purified in one step to 90-95% purity, with yields ranging between 1-30 mg/L of culture (data not shown). Solubility and relative expression level of all variants upon over-expression was verified by loading volume-equivalent amounts of total cell extracts, cell pellet and supernatant for resolution by SDS-PAGE. All His_6-hDHFR variants were approximately 50% soluble, as reported for the native recombinant hDHFR,[40] ruling out solubility differences in explaining the observed variations in yield of purified variants. In addition, all mutants (soluble + insoluble) were expressed at similar levels. The mock-purified supernatant of *E. coli* SK037 transformed with the vector pQE32 served as a negative control in all kinetic and binding experiments.

Michaelis constants for the substrate DHF (K_M^{DHF}) and reactivity (k_{cat}) were determined for the ten selected mutants and for WT His_6-hDHFR. K_M^{DHF} of WT His_6-hDHFR was determined to be <75 nM. At this concentration of DHF, the enzyme was already saturated. It was not possible to obtain a more precise value due to the weak signal observed at such a low concentration of substrate. Previously reported K_M^{DHF} values for recombinant, native (non-His-tagged) WT hDHFR are in the range of 33 to 120 nM,[6,15,20] suggesting that the His_6-tag has little effect on DHF affinity. K_M^{DHF} was increased at least ninefold to 57-fold for the selected mutants relative to WT His_6-hDHFR as a result of the mutations introduced at positions 31, 34 and/or 35. This was not unexpected, as the residues chosen for mutagenesis are known to be involved in DHF binding. As shown in Table 2.2, k_{cat} values were reduced by at most a factor of 10, except for mutant RAN (20-fold decrease); mutants PFQ, GFN and SFE displayed k_{cat} values similar to that of native

Table 2.2. Kinetic and inhibition constants for the selected MTX-resistant hDHFR mutants.

Enzyme[a]	k_{cat} (s^{-1})	K_M^{DHF} (μM)	k_{cat}/K_M^{DHF} (s^{-1} μM^{-1})	IC_{50}^{MTX} (nM)	K_i^{MTX} (nM)	K_D^{MTX} [b] (nM)
WT (FFQ)	10±2	≤0.075	≥140	41±14	≤0.031	<2
Point mutant						
F31P (PFQ)	6.4±1.0	1.5±0.30	4.3	110±40	1.7±0.6	<2
Double mutants						
GFN	4.3±1.0	1.7±0.39	2.6	570±180	9±3	16±5
PFH	1.7±0.12	2.1±0.51	0.80	470±70	10±1	6.9±1.4
PFE	1.7±0.05	2.7±0.63	0.60	470±170	12±4	4.1±1.6
RFE	1.3±0.17	0.69±0.13	1.9	3100±1600	21±11	21±0.2
SFE	9.4±0.31	3.3±0.70	2.8	930±340	30±11	25±4
Triple mutants						
RAN	0.50±0.06	2.2±0.62	0.20	550±80	12±2	<2
RTS	1.0±0.09	1.7±0.27	0.60	4500±2500	59±26	110±12
RTR	1.0±0.10	2.0±0.25	0.50	3500±1600	86±49	11±0.9
AVH	1.1±0.39	4.3±1.3	0.30	4400±1700	180±69	150±44

[a] hDHFR variants are designated by the one-letter code of the amino acids occurring at positions 31, 34 and 35.
[b] K_D^{MTX} for the ternary complex.

enzyme. The lowest reactivities were generally displayed by mutants containing a F31R substitution, which is consistent with previous reports of this point mutant (k_{cat} = 0.93 s^{-1}).[41] As a result of the k_{cat} and K_M^{DHF}variations, the catalytic efficiencies (k_{cat}/K_M^{DHF}) for all selected mutants were reduced, ranging from a 30-fold decrease for point mutant PFQ to a 700-fold decrease for triple mutant RAN (Table 2.2).

The inhibition constants for MTX (K_i^{MTX}; Table 2.2) reveal that all selected mutants were resistant to MTX, the most highly resistant being the AVH triple mutant (K_i^{MTX} = 180 nM), with K_i^{MTX} almost 4 orders of magnitude greater than WT. The mutant with the lowest K_i is the point mutant PFQ (K_i^{MTX} = 1.7 nM), which was inhibited 50-fold less efficiently by MTX than the WT enzyme, while the other combinatorial double and triple mutants showed K_i increases of at least 2 orders of magnitude (Table 2.2, Figure 2.3). Ternary binding constants for MTX were also determined, to verify that the observed loss of inhibition correlated with reduced binding. The ternary K_D^{MTX} values obtained were similar to the K_i^{MTX} values for all mutants (Table 2.2), indicating a direct relation between binding and inhibition in all cases. The greatest difference between K_i and K_D was for mutant RTR (eightfold). It was not possible to determine the K_D values precisely for WT His_6-hDHFR, PFQ and RAN mutants by this method, the fluorescence quenching detection limit being ~2 nM MTX in our system. Binary K_D^{MTX} values were also obtained in absence of NADPH for the MTX-resistant mutants (results not shown). In all cases, the value for the binary K_D^{MTX} was greater than the ternary K_D^{MTX} (fourfold to 19-fold difference for tested mutants RTR, RTS, RFE and AVH). This is consistent with bound NADPH promoting tighter binding of MTX to the selected hDHFR variants, as demonstrated for the native enzyme.[6]

Protection of mammalian cells with mutant hDHFRs

We verified the efficacy of eukaryotic cell protection with four of the selected mutants (Table 2.3). CHO DUKX B11 cells (*dhfr*$^-$) were transfected with mutant RFE, SFE, RTS or AVH. These variants were chosen because they displayed the highest K_i^{MTX}

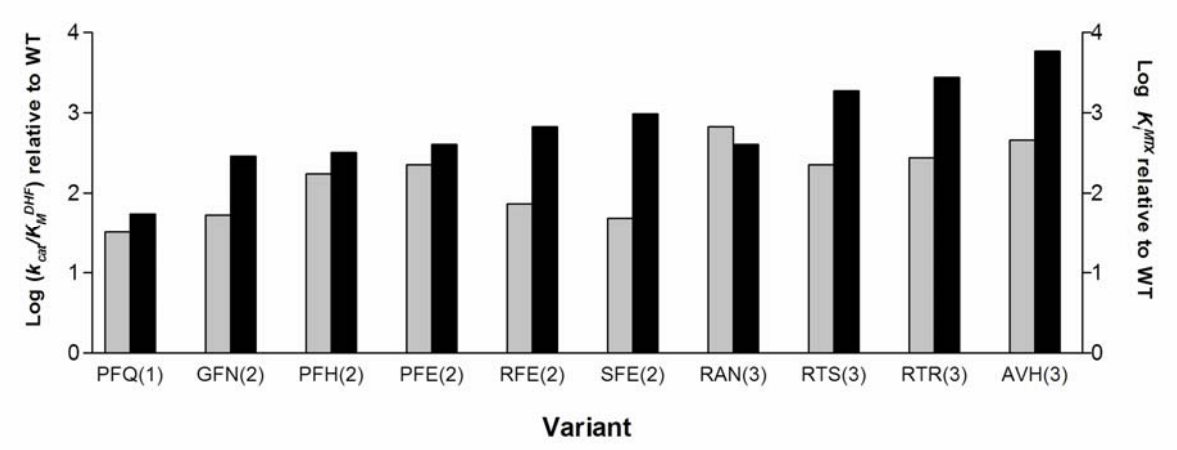

Figure 2.3. Relation between the number of hDHFR mutations and k_{cat}/K_M^{DHF} or K_i^{MTX} relative to WT His_6-hDHFR. Mutants are designated by the one-letter code of the amino acid occurring at positions 31, 34 and 35, respectively. Numbers in parentheses correspond to the number of mutations in the variant. Log k_{cat}/K_M^{DHF} relative to WT is shown in grey while log K_i^{MTX} relative to WT is in black.

values while maintaining catalytic efficiency comparable to MTX-resistant hDHFRs used in similar studies.[42-44] WT hDHFR and the MTX-resistant point-mutant L22Y served as negative and positive controls, respectively. A mock experiment consisted in transfecting pcDNA 3.1 vector (null). Transfection efficiency was evaluated at approximately 50% for all constructs. Transfected cells were exposed to various concentrations of MTX for 48 hrs in α-MEM medium containing no nucleotides, ensuring that cell survival was based solely on activity of the transfected hDHFRs. Figure 2.4 presents cell survival data; EC_{50}^{MTX} values are given in Table 2.3. All mutants tested conferred MTX-resistance to CHO DUKX B11 cells. The point mutant L22Y (EC_{50}^{MTX} = 12 μM) provided a 220-fold increase in EC_{50}^{MTX} relative to the WT hDHFR (EC_{50}^{MTX} = 0.054 μM). The double mutants RFE (EC_{50}^{MTX} = 31 μM) and SFE (EC_{50}^{MTX} = 32 μM) provided a 570-fold increase, while the triple mutant RTS (EC_{50}^{MTX} = 56 μM) provided a 1030-fold increase relative to WT. The EC_{50}^{MTX} for the triple mutant AVH (>4000-fold increase) could not be determined because dissolution of higher concentrations of MTX in the medium perturbed the pH. Mutant AVH allowed survival of 73% of the cell population at 200 μM MTX. Enzyme expression under these conditions was confirmed by Western blot analysis (data not shown). The null control showed no cell survival, confirming that survival was due solely to the presence of MTX-resistant hDHFRs, and that no secondary resistance mechanism had been acquired upon exposure to MTX. Cells expressing WT hDHFR were sensitive to low concentrations of MTX, ruling out gene amplification.

DISCUSSION

Of 567 possibilities encoded in the hDHFR mutant library, ten MTX-resistant mutants were identified following selection on solid media containing 1 mM MTX. The chosen selection strategy yielded one novel single mutant and nine novel combinatorial MTX-resistant mutants, providing new insight into the role of residues at positions 31, 34

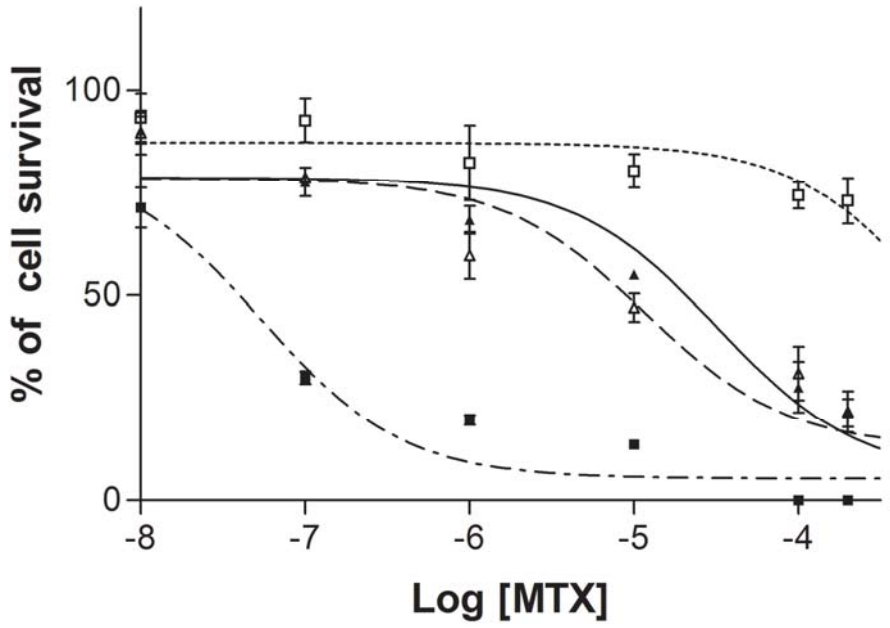

Figure 2.4. Survival of CHO DUKX B11 cells transfected with selected mutants in presence of MTX. Data is presented for two representative mutants: double mutant SFE (▲) and triple mutant AVH (□). The positive control L22Y (△) and the negative control WT hDHFR (■) are given as references. SFE and AVH are designated by the one-letter code of the amino acid occurring at positions 31, 34 and 35, respectively. Percentage of cell survival represents the ratio of cells counted in presence and absence of MTX after 48hrs at 37ºC, 5% CO_2.

Table 2.3. EC_{50}^{MTX} for CHO DUKX B11 cells transfected with MTX-resistant hDHFR mutants.

Transfected variant	EC_{50}^{MTX} (μM)
Null	0
WT	0.054
L22Y	12
RFE	31
SFE	32
RTS	56
AVH	>200

Combinatorial mutants are designated by the one-letter code of the amino acids occurring at positions 31, 34 and 35.

and 35 in ligand binding and selectivity, while generating novel hDHFR mutants that efficiently protect CHO (*dhfr-)* eukaryotic cell line from MTX-cytotoxicity. All of the resistant mutants displayed reduced catalytic efficiencies compared to WT His_6-hDHFR (30 to 700-fold decrease), mainly as a result of decreased productive binding of DHF (tenfold to 60-fold K_M^{DHF} increase). The reduction in MTX affinity was much greater, with K_i^{MTX} increased 54 to 5800-fold. Thus, we identified a variety of patterns of mutations at active-site residues 31, 34 and/or 35 that greatly reduce the binding of MTX while maintaining sufficient affinity for DHF to provide the level of catalytic activity required for bacterial propagation. The various sequence patterns obtained are indicative of significant plasticity and robustness in these active-site residues: a low number of mutations were sufficient to induce a new phenotype (high MTX resistance resulting from plasticity) while the native function, THF synthesis, endured the effect of the mutations to an important degree as a result of robustness.[45]

Consistent with previous reports of hDHFR point mutants of Phe31,[14] we observed the bulky, positively-charged Arg and small residues, whether polar or non-polar (Gly, Ala and Ser) at position 31 (Table 2.4). The variety of amino acids identified at position 31 (five of the nine encoded) confirms that this position can tolerate a variety of side-chain volumes and functional groups. Arg31 was encoded in four of the resistant mutants, consistent with F31R being the most resistant Phe31 point mutant reported (K_i^{MTX} = 7.2 nM).[41] In addition, we observed the structurally-constraining proline at position 31 (point mutant F31P, or PFQ). Never previously reported, this MTX-resistant point mutant exhibits resistance and catalytic efficiency intermediate between the previously-reported F31R and F31S point mutants.[14,41]

Phe34 was the most strongly conserved native residue, consistent with previous studies qualifying the importance of Phe34 in binding either MTX or DHF at the active site.[10] Three of the four amino acids encoded were observed in the four triple mutants we identified (Ala, Thr or Val). Previously-characterized point mutants were not identified by

Table 2.4. Comparison of MTX-resistant hDHFR mutated at positions F31 and F34.

hDHFR variant	K_i^{MTX} (nM)	k_{cat}/K_M^{DHF} ($\mu M^{-1}\ s^{-1}$)	Reference
WT (FFQ)	≤0.031	≥140	This work
L22Y[a]	11	10	29
F31X			
F31S	0.24	16	14
F31A	0.27	30	14
F31G	0.35	26	14
F31P (PFQ)	1.7	4.3	This work
F31R	7.2	1.5	41
F34X			
F34T	9.6[b]	0.11	10
F34V	10[b]	0.49	10
F34A	34[b]	0.24	10
Combinatorial mutants[c]			
GFN	9	2.6	This work
RAN	12	0.2	″
RFE	21	1.9	″
SFE	30	2.8	″
RTS	59	0.6	″
RTR	86	0.5	″
AVH	180	0.3	″

[a] Variant L22Y was used as a positive control for MTX resistance.

[b] Values of ternary K_D^{MTX}.

[c] Combinatorial mutants are designated by the one-letter code of the amino acids occurring at positions 31, 34 and 35.

our screening strategy, likely because the *in vivo* MTX-resistance trait that we selected for is complex, requiring low MTX binding combined with sufficiently high specific activity as well as good expression and stability. The F34S mutant is an important example: despite having the highest ternary K_D^{MTX} reported for any hDHFR mutant (210 nM), its very poor catalytic efficiency (0.017 $\mu M^{-1}s^{-1}$)[10] apparently decreases enzyme function to a level too low for cellular propagation.

A diversity of mutations was also observed at position 35 (five out of nine amino acids encoded); no resistant point mutants were identified. The Gln35Glu substitution occurred in the three most frequently observed selected mutants (Figure 2.2), that all conserved Phe34. The introduction of a negative charge at this location may introduce electrostatic repulsion of the γ-glutamate tail (Figure 2.1(b)).While this effect is also expected to reduce DHF binding, we note that MTX binding is more importantly reduced than productive DHF binding (K_M^{DHF}), by a factor of at least 10 (mutant PFE) to more than 70 (mutant RFE). The differing binding and kinetic properties of mutants PFE, RFE and SFE highlight the impact of combining mutations at position 31 (Pro, Arg or Ser) with the Gln35Glu substitution. A positively charged residue at position 35 also supports MTX-resistance, as evidenced by the Gln35Arg (mutant RTR) and the Gln35His substitutions (mutants AVH and PFH). The side chain of Gln35 has been proposed to hydrogen bond with the guanidinium group of Arg70 in the ligand-free enzyme or when the ligand does not contain a *p*-aminobenzoyl function,[7,46,47] while in the presence of ligands Arg70 forms a conserved salt bridge with the α-carboxylate of the glutamate moiety.[12] The mutations selected at position 35 may render the active site less propitious to ligand binding, by forming a Glu35-Arg70 salt-bridge in the apoenzyme or as a result of electrostatic repulsion with Arg70 in the case of an Arg35 or His35 mutation. Structural data are required to confirm these hypotheses.

In addition to the correlation of the conserved Phe34 with Q35E, other correlations were observed. Mutants PFQ, PFE and PFH equally conserve Phe34 while displaying a

Phe31 to Pro substitution. Mutants RTR and RTS, two triple mutants, also displayed correlation at positions 31 and 34. In no case was a strict co-variation observed. Considering the restricted subset of amino acids encoded at each of the three positions, it is likely that greater sequence diversity at positions 31, 34 and 35 can promote resistance.

How effective is the accumulation of mutations in providing increased MTX resistance? Combining the F31P substitution with mutations at position 35 (mutants PFE and PFH) resulted in a six-to seven-fold increase in K_i^{MTX} accompanied by a five-to seven-fold decrease in catalytic efficiency (Table 2.4). Double mutant GFN displayed a nearly 40-fold increase in K_i^{MTX} and a tenfold decrease in catalytic efficiency relative to the point mutant F31G, contributed mainly by a sixfold increase in K_M^{DHF}.[14] The point mutant F31S[14] provides only modest MTX-resistance; the addition of mutation Q35E (mutant SFE) resulted in a 125-fold increase in K_i^{MTX}. In counterpart, the catalytic efficiency was reduced sixfold relative to F31S, due solely to decreased DHF affinity. The same Q35E mutation had a smaller effect when combined with mutation F31R (mutant RFE; Table 2.4). Comparison of these double mutants highlights the complexity of cumulating active-site mutations: the effect of mutation Q35E differs according to its environment (i.e. the amino acid at position 31).

The selected triple mutants provided further evidence of the impact of multiple mutations on resistance: the most highly MTX-resistant hDHFR variants were all triple mutants (Table 2.2; Figure 2.3). While the F31R point mutant alone provides good MTX resistance (K_i^{MTX} = 7.2 nM)[41], additional mutations increased resistance, as evidenced by triple mutants RTS (K_i^{MTX} = 59 nM) and RTR (K_i^{MTX} = 86 nM). The frequently observed F31R appears to provide a good basis for further mutations to increase resistance.

The current data set is consistent with synergistic effects of many of the mutations toward MTX binding, as opposed to additive effects.[48] A striking example is triple mutant AVH, which displayed the weakest MTX binding out of the selected mutants (K_i^{MTX} = 180 nM), an almost 6000-fold increase in K_i^{MTX} relative to the WT. This combinatorial mutant

nearly matches the best-reported K_D^{MTX} (F34S = 210 nM).[10] However, it boasts a catalytic efficiency that is almost 20-fold superior to the F34S point mutant. The point mutant Q35H was not selected, suggesting that it does not confer a high level of resistance. Nonetheless, Q35H increased the K_i^{MTX} of the point mutant F31P in mutant PFH; combined with F31A (K_i^{MTX} = 0.27 nM)[14] and F34V (K_i^{MTX} = 10 nM)[10], it contributed to the highest resistance in mutant AVH. In a similar fashion, the Q35R mutation (the murine Q35R mutant displays only a tenfold increase in K_i^{MTX}),[17] combined with F31R (K_i^{MTX} = 7.2 nM)[41] and F34T (K_i^{MTX} = 9.6 nM),[10] contributed to resistance in mutant RTR (K_i^{MTX} = 86 nM). No resistant triple mutant was identified that was only one mutation away from a characterized double mutant, precluding a direct assessment of the effect of one additional mutation in these cases. It is not currently possible to predict synergistic effects of mutations on specific protein functions; our success in identifying multiple active-site environments providing the desired properties resulted from searching an area of sequence space that was likely, according to prior knowledge, to harbour positive solutions. Despite the fact that F34 was highly conserved during selection, likely as a result of its role in DHF binding, mutations at this position in the context of neighbouring mutations provided the highest level of resistance. We are currently combining this triply-mutated library with further libraries mutated at active-site residues previously shown to specifically interact with MTX, to attempt to further increase MTX resistance while maintaining catalytic efficiency. Rather than restricting the identity of mutations to specific point mutants known to confer resistance, each position encodes a variety of amino acids, allowing for the possibility of unpredicted combinatorial effects.

As made evident above, the trade-off to decreased MTX binding with the greater number of mutations was a general correlation with decreased catalytic efficiency. The most important contributor to decreased catalytic efficiency was decreased productive binding of DHF: the variation in K_M^{DHF} was 1.5 to 44-fold greater than the change in k_{cat}. Surprisingly, while the impact of point mutations at positions 31 and 34 on K_M^{DHF} was great, there was no significant further increase of K_M^{DHF} upon accumulating mutations. The

additional mutations did, however, greatly increase K_i^{MTX}. These differences in the effect of the mutations toward either ligand may result from the different binding modes for the pteroyl moiety of DHF and MTX at the active site of hDHFR (Figure 2.1), despite the fact that residues 31 and 35 do not directly interact with the pteroyl moiety. We are currently testing further ligands of DHFR to verify whether there is a relation between the decreased MTX and DHF affinity, and affinity for other ligands. Trimethoprim (TMP), an antibiotic that targets bacterial DHFR with a high degree of specificity (K_i^{TMP} *E. coli* DHFR: 80 pM) binds hDHFR 12,000-fold more weakly,[49] justifying its use in our selection strategy to knock out background *E. coli* DHFR activity. While most of the mutants selected for MTX resistance showed no change of *in vitro* resistance to TMP relative to the WT hDHFR, double mutant RFE and triple mutants RTR and RTS showed significant resistance (data not shown). Our results are consistent with the observation that the Leu28Arg substitution in *E. coli*, homologous to hDHFR mutation Phe31Arg, contributes to TMP-resistance in addition to MTX resistance.

The AVH mutant bound to MTX was created *in silico* to gain insight into the effects of the mutations on MTX binding (Figure 2.5). While this simple molecular visualization does not provide structural evidence, it is clear that the combinatorial F31A/F34V mutations enlarge the volume of the active-site cavity proximal to MTX, simply as a consequence of the smaller volumes of the substituted amino acids.[50] The F31A mutation is likely to reduce van der Waals interactions with the *p*-ABA moiety of MTX relative to the WT. The F34V mutation likely has a similar effect in addition to reducing van der Waals interactions with the pterin moiety. The effect of the Q35H mutation is not as apparent in this visualization. We are presently obtaining structural information for mutant AVH by X-ray crystallography.

We have shown that CHO *dhfr*$^-$ cells containing double mutants RFE or SFE and triple mutants RTS or AVH were all protected, to some extent, from the toxic effects of MTX (Table 2.3; Figure 2.4). The positive control, point mutant L22Y, confers good MTX-

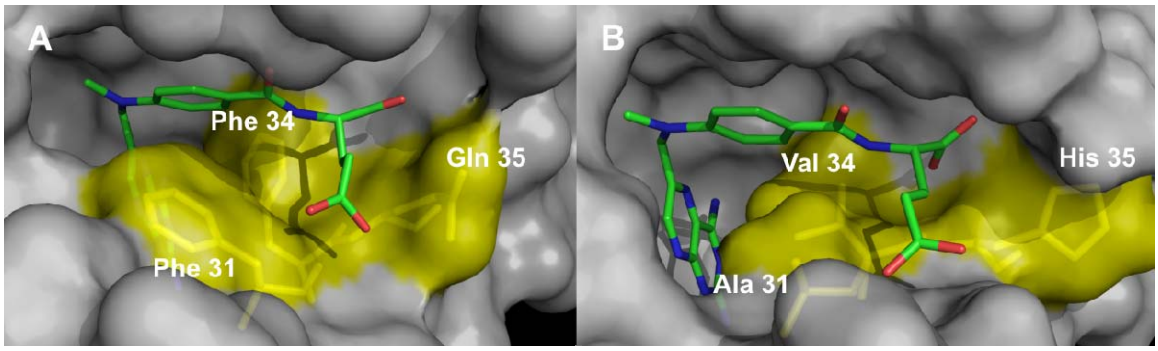

Figure 2.5. *In silico* comparison of MTX binding between (A) WT hDHFR (1U72) and (B) mutant AVH. Protein structures are shown in surface representation with residues 31, 34 and 35 coloured yellow, and MTX coloured by atom (nitrogen, blue; oxygen, red; and carbon, green), in sticks representation. AVH coordinates were obtained by mutating residues 31, 34, 35 using PDB file 1U72 as starting coordinates, followed by minimization in presence of bound MTX and NADPH. NADPH is not shown

resistance in mammalian cells as a result of its good catalytic efficiency (12 $s^{-1}\mu M^{-1}$) and high K_i^{MTX} (10.9 nM).[15] Previously reported transfections of hDHFR point mutants (F31S, F34S, G15W and L22R) in CHO *dhfr*$^-$ cells[43,44] yielded between 2 to 7% cell survival in presence of 1 μM MTX. In our similar system, the resistance conferred by our double mutants was greater than that for any of the point mutants. In turn, the triple mutants offered a better protection than the double mutants. The triple mutant AVH, exhibiting the highest K_i^{MTX}, conferred the best protection with 70% cell survival at 200 μM MTX, despite the fact that it displayed the lowest catalytic efficiency among our sample. This suggests that weak MTX binding is a more important feature than catalytic efficiency in protecting the CHO cells. This result provides an interesting tool for further increasing MTX resistance, given that most MTX-resistant mutants previously used to protect mammalian cells had catalytic efficiencies at least tenfold higher than the AVH mutant.[51]

Combining active-site mutations in hDHFR yielded novel insights concerning increased MTX resistance. Ideally, one would like to predict the capacity of a mutant to confer MTX resistance to mammalian cells from assessment of a specific *in vitro* parameter, be it K_i^{MTX}, IC_{50}^{MTX} or K_D^{MTX}, or yet a combination such as K_i^{MTX} × catalytic efficiency.[10,14,16] While each of these provided a rough estimate of resistance, we did not succeed in ranking the *in vivo* effect of the MTX resistant mutants according to *in vitro* parameters. We believe factors such as expression level, folding, stability and cell type all contribute to the *in vivo* effect. Given the correlation between the efficiency of MTX-protection in CHO *dhfr*$^-$ and in haematopoietic stem cells for a given MTX-resistant mutant,[43,52] we are currently investigating the potential for the most highly MTX-resistant combinatorial mutants to protect haematopoietic stem cells, *via* retroviral infections. Preliminary results in haematopoietic stem cells (J.P.V. *et al.,* unpublished results) suggest that, despite the fact that mutant AVH confers a high level of MTX-resistance, it is not our most effective mutant at conferring resistance in that specific *in vivo* context. This underscores the difficulty of identifying an *in vitro* indicator for ranking *in vivo* effects, and

supports further identification of a variety of MTX-resistant hDHFR variants for application in different contexts.

MATERIALS AND METHODS

Reagents

Restriction and DNA modifying enzymes were purchased from MBI Fermentas (Burlington, ON). Folic acid, methotrexate, β-NADPH, adenine, deoxyadenine and thymidine were purchased from Sigma-Aldrich (Oakville, ON). Dihydrofolic acid (DHF) was synthesized from folic acid as described.[53] Ni-NTA was purchased from Qiagen (Mississauga, ON). Cell culture media and reagents were purchased from Invitrogen (Burlington, ON), with the exception of dialyzed fetal bovine serum (FBS), which was obtained from HyClone (Logan, UT), and 5-bromo-4-chloro-3-indoyl-β-D-galactopyranoside (X-Gal), which was purchased from US biological (Swampscott, MA). CHO DUKX B11 (*dhfr*-) cells were a generous gift from Ingrid Remy and Stephen W. Michnick (Université de Montréal, Montréal, QC).

Bacterial strains and plasmids

E. coli strain SS320 was used for propagation of the DNA library.[54] *E. coli* strain SK037,[39] which was used for selection and over-expression of MTX-resistant mutants, was a generous gift from Gwen S. Snapp and James C. Hu (Texas A&M University, College Station, TX). The pQE32 expression vector was purchased from Qiagen. The WT hDHFR (MRA-91) and hDHFR L22Y (MRA-90) genes contained in pBluescript vector[55] were obtained from the Malaria Research and Reference Reagent Resource center (Manassas, VA).

Oligonucleotides and DNA constructions

Standard oligonucleotide primers used for mutagenesis were purchased from Alpha DNA (Montréal, QC). Primers containing degenerate codons were purchased from Integrated DNA Technologies (Coralville, IA). Dye-labelled oligonucleotide primers for DNA sequencing were purchased from Li-Cor Biotechnology (Lincoln, NB). The external primer set 1 (primer 1A: *fwd* $^{5'}$ ACACAC*GGATCC*AAATGGTTGGTTCGCTAAACTGCATC (BamHI restriction site in italics) and primer 1B: *rev* $^{5'}$ CAATTTCACACAGGAAACAGCT) was designed for PCR amplification of the entire coding region of the WT hDHFR and hDHFR L22Y genes and subcloning into pQE32 vector between the BamHI and HindIII restriction sites. An AflII restriction site (in italics) was introduced for ulterior recombination work *via* silent mutations between codons 26 and 28 of WT hDHFR by mega-primer PCR,[56] using primer 2: *rev* $^{5'}$ TGGAAATATCTAAATTCGTTC*CTTAAG*GGTGGCCACGGCAGGT and the external primer set 1. The resulting construct, WT hDHFR-pQE32, expressed WT His_6-hDHFR (N-terminally His_6-tagged) and served as a template for the creation of the hDHFR mutant library as well as for the creation of eukaryotic transfection DNA constructs.

Creation of the hDHFR mutant library at positions Phe31, Phe34 and Gln35

The hDHFR mutant library was created by megaprimer PCR,[56] using degenerate primers encoding a variety of amino acids at positions Phe31, Phe34 and Gln35 (see Table 1) using primer 3: *rev* $^{5'}$ AGAGGTTGTGGTCATTCT*SYBKRH*ATATCT*GVV*TTCGTTCCTTAAGGGTGG (degenerate codons in italics) as well as primer 1A and primer 4B: *rev* $^{5'}$ GTTCTGAGGTCATTACTGG as external primers (external primer set 2). The resulting library was cloned into pQE32 using the BamHI and HindIII restriction sites and transformed in *E. coli* SS320, yielding approximately 1×10^4 colonies. The quality of the library was evaluated by sequencing the entire hDHFR gene from 70 colonies picked on

Luria-Bertani (LB) medium containing 100 μg/mL ampicillin (LA-100; non-selective conditions). Sequencing was performed by the dideoxy-chain termination method using a Thermo Sequenase Cycle Sequencing kit (GE Healthcare, Piscataway, NJ) and a dye-labelled primer with a Li-Cor 4200 automated sequencer (Lincoln, NB).

Selection and identification of highly MTX-resistant mutants

Plasmid DNA from the pooled hDHFR mutant library was isolated and transformed into electrocompetent *E. coli* SK037 cells for selection. The cells were plated in equal dilutions on LA-100 (non-selective) or on M9 minimal medium containing 0.08% (w/v) casamino acids, 100 μg/mL ampicillin, 1 μg/mL trimethoprim (TMP) and 1 mM MTX (dissolved in 0.05M KOH) (ATM-1000 medium; selective conditions). Colony formation took place at 37°C for 16 hrs on the non-selective medium and for 36 hrs on the selective medium. The survival rate of the library was calculated from the ratio of colonies formed on selective ATM-1000 relative to non-selective LA-100 medium. Seventy colonies were picked on ATM-1000 media, and the plasmid DNA was sequenced to identify mutations at positions 31, 34 and 35. In all cases, the entire coding sequence was verified.

Expression and purification of selected hDHFR variants

For expression of both WT His_6-hDHFR and MTX-resistant mutants identified by selection, the plasmids of interest were isolated and retransformed into *E. coli* SK037 cells. Overnight cultures were used to inoculate 50 mL of LB media and were propagated at 37°C until $A_{600\ nm} \approx 0.7$. Protein expression was induced with the addition of 1 mM isopropyl 1-thio-β-D-galactopyranoside (IPTG), after which cells were further propagated for 3 hrs at 37°C. Induced cells were harvested by centrifugation (4000*g* for 30 min at 4°C). The cell pellet was resuspended in 0.1M potassium phosphate buffer (pH 8.0), 5 mM imidazole. The cells were lysed on ice using a Branson sonicator (three pulses at 200 W for 30 s with a tapered micro-tip). Cellular debris were pelleted by centrifugation (4000*g* for 30 min at 4 °C) and 1 mL of pre-equilibrated Ni-NTA resin (Qiagen) was added to the supernatant. The

slurry was mixed by inversion at 4°C for 1 h, after which it was transferred to a column (Bio-Rad Polyprep Chromatography columns, 0.8 x 4 cm) for gravity-flow purification. The column was washed with 5 mL each of 0.1M phosphate buffers (pH 8.0) containing increasing concentrations of imidazole (5, 10, 15 and 20 mM). Elution of bound protein was achieved using 2 mL of 0.1M phosphate buffer (pH 7.5), 50 mM imidazole. Eluted protein was dialyzed overnight against 0.1M phosphate buffer (pH 7.5) at 4°C for 16 hrs. Expression pattern and purity of enzymes were evaluated using the public domain image analysis software Scion Image (NIH, rsb.info.nih.gov/nih-image) following separation by SDS-PAGE (15% (w/v) polyacylamide gel) stained by the zinc-imidazole method.[57] Protein concentration was determined using the Bradford assay (Bio-Rad, Hercules, CA).

Determination of kinetic and inhibition parameters

All kinetic and inhibition assays were conducted in MATS buffer (25 mM Mes, 25 mM acetate, 50 mM Tris, 100 mM sodium acetate and 0.02% (w/v) sodium azide) (pH 7.6) at 23°C. Substrates were dissolved in MATS buffer and quantified by spectrophotometry ($\varepsilon_{340\ nm}$ = 6200 $M^{-1}cm^{-1}$ for NADPH and $\varepsilon_{282\ nm}$ = 28,400 $M^{-1}cm^{-1}$ for DHF). MTX was dissolved in 0.05M KOH and quantified by spectrophotometry in 0.1M NaOH using $\varepsilon_{258\ nm}$ = 22 100 $M^{-1}cm^{-1}$ and $\varepsilon_{302\ nm}$ = 23 300 $M^{-1}cm^{-1}$. Kinetic parameters for the hDHFR mutants were determined with a Cary 100 Bio UV/Vis spectrophotometer (Varian Canada Inc., Montréal, QC) by monitoring the NADPH and DHF depletion ($\Delta\varepsilon_{340\ nm}$ = 12 800 $M^{-1}cm^{-1}$)[58] in 1-cm cells with 10 nM enzyme, unless otherwise stated. All assays were performed in at least 4 independent experiments and the average values are reported. The initial rates during the first 15% of substrate conversion were recorded for all assays. Kinetic and inhibition parameters were obtained from a non-linear regression fit to the Michaelis-Menten equation using Graphpad Prism (Graphpad Software, San Diego, CA). The k_{cat} values were determined in presence of saturating substrate concentrations (100 μM each of DHF and NADPH) in 1-cm cells according to $k_{cat} = V_{max}/[E]$. K_M values for DHF (K_M^{DHF}) for the MTX-resistant mutants were determined in presence of 20 μM NADPH by varying

the concentration of DHF (0.5 μM to 20 μM). For WT His_6-hDHFR, K_M^{DHF} was obtained by spectrophotometric determination in 10-cm cells containing 1 nM enzyme, 10 μM NADPH and a range of DHF concentrations (0.05 μM to 10 μM). The kinetic parameters of two mutants determined in 1-cm cells were also confirmed in 10-cm cells. IC_{50}^{MTX} for WT His_6-hDHFR and mutants were determined in presence of saturating concentrations of substrates (100 μM each of DHF and NADPH) and increasing concentrations of MTX (0.025 μM to 100 μM). Inhibition constants for MTX (K_i^{MTX}) were calculated from the determined IC_{50}^{MTX} according to the equation for competitive inhibitor binding.[59]

Determination of equilibrium dissociation constants

Ternary equilibrium dissociation constants for MTX (K_D^{MTX}) were determined in a 1-cm path-lenght quartz cell using a Cary Eclipse Bio fluorometer (Varian Canada Inc., Montréal, QC), by titrating the fluorescence quenching resulting from formation of the enzyme-ligand complex with increasing concentrations of MTX. For each variant tested, enzyme and NADPH were mixed at final concentrations of 200 nM and 5 μM (saturating concentration), respectively, and serial additions of MTX were added (0 to 1600 nM) in a final volume of 3 mL. The total volume of added MTX represented approximately 10% of the entire sample volume. After each addition of MTX, the solution was mixed with a magnetic stirrer for 2 minutes. Fluorescence quenching was monitored at λ_{ex} = 280 nm and λ_{em} = 435 nm. All assays were performed in at least 3 independent experiments, and the average values are reported. The K_D^{MTX} values for each variant were obtained by fitting relative fluorescence (ΔF) to the following equation:[60]

$$\Delta F = \frac{\Delta F_{\max}\left([hDHFR]_0 + [MTX] + K_D - \sqrt{([hDHFR]_0 + [MTX] + K_D)^2 - (4[hDHFR]_0[MTX])}\right)}{2[hDHFR]_0}$$

Molecular modelling

Molecular modelling was performed using the InsightII package (version 2000, Accelerys), with 1U72.pdb (WT hDHFR with bound MTX and NADPH)[7] as starting coordinates. Following removal of the crystallographic water molecules, the BIOPOLYMER module was used to mutate residues 31, 34 and 35 and to add hydrogen atoms at the normal ionization state of amino acids at pH 7. Energy minimization of the enzyme-ligand complex was performed using 1000 steps of steepest descents minimization, followed by a conjugate gradient minimization until convergence of 0.001 kcal/mol/Å. Minimizations were performed with no constraints, using a dielectric constant of 80 and a cut-off value of 100 Å.

Protection of eukaryotic cells with MTX-resistant hDHFRs

Genes encoding the MTX-resistant mutants with the highest K_i^{MTX} values were amplified by PCR with primer 5A: *fwd* $^{5'}$ ACACAC*GAATTC*ATCCACCATGGTTGGTTCGCTAAACTGCAT and primer 5B: *rev* $^{5'}$ ACACAC*CTCGAG*AGCTTAATCATTCTTCTC and sub-cloned into pcDNA3.1 (+)-Zeo (Invitrogen) using the *Eco*RI and *Xho*I restriction sites (in italics). The WT and L22Y hDHFR genes were also amplified and cloned as described above, to serve as negative and positive controls for MTX resistance, respectively. The resulting constructs do not encode a His_6 tag. A mock transfection with pcDNA3.1 (+)-Zeo also served as a negative control. Cells were stained using trypan blue and counted using a Bright-Line hemacytometer (American Optical Corporation, Buffalo, NY). CHO DUKX B11 cells were propagated at 37°C, 5% CO_2 (v/v) in 10-cm plates and passaged every 48 h at 1.5×10^6 cells per plate in α-MEM containing 10% (v/v) dialyzed FBS, 4 mM glutamine, 10 μg/mL each of adenine, deoxyadenosine and thymidine, 100 units/mL penicillin and 100 μg/mL streptomycin (complete α-MEM medium). For passages, cells were washed twice with 1 × PBS and trypsinized for 5 min at 37 °C. Before transfection, 5×10^5 cells at passage 10 or less were

propagated for 18 h on 10-cm plates (70% confluence). A 3µg sample of plasmid DNA was mixed with 20 µL of Lipofectamine 2000 (Invitrogen) and incubated at room temperature for 45 min in 800 µL Opti-MEM. The mixture was added to the cells, which were further incubated at 37 °C with 5% CO_2 for 4 h. The transfection media was replaced by α-MEM media for 36 h. The transfected cells were split into 6 cm plates containing approximately 1×10^5 cells. The cells were exposed to different concentrations of MTX (0 - 200 µM) in α-MEM media in the absence of adenine, deoxyadenine and thymidine. As a reference, the same number of cells was plated in complete α-MEM medium. The stock solution (2 mM MTX) was prepared in 0.05M KOH to ensure dissolution; MTX could not be added at a higher concentration than 200 µM as this marked the limit of the buffering capacity of the medium. The cells were counted after 48 h. Transfection efficiency was evaluated first by transfecting the *lacZ* reporter gene (pBabe-LacZ)[61] and by counting the number of blue cells in the presence of X-Gal; and secondly by comparing the number of cells in absence and in presence of nucleotides in the media. The percentage of cell survival is given as the ratio of cells counted in the presence or in the absence of MTX (in absence of nucleotides). EC_{50}^{MTX} were generated with a non-linear sigmoidal fit using Graphpad Prism software. All MTX-resistance studies were performed in at least 3 independent experiments and the average EC_{50}^{MTX} values are reported. Expression of hDHFR variants was verified by Western blotting, following resolution of supernatant from transfected CHO DUKX B11 cells by SDS-PAGE (15% (w/v) polyacrylamide gel) and semi-dry transfer on PVDC membrane. The membranes were blocked with 5% (w/v) powdered milk before overnight incubation at 4 ºC with primary polyclonal anti-mDHFR antibody from rabbit. Membranes were washed twice with PBS, 0.5% (v/v) Tween before incubation for 1 h at 4 °C with the secondary monoclonal anti-rabbit-alkaline phosphatase coupled antibody (Sigma-Aldrich). Protein bands were revealed with BCIP/NBT (Sigma-Aldrich) for 10 min at room temperature.

ACKNOWLEDGMENTS

The authors thank Frédérick-Antoine Mallette and Gerardo Ferbeyre for discussions and suggestions concerning cell culture, Stéphane Roy for the use of cell culture facilities, Huy Ong for the use of a Cary 100 spectrophotometer, as well as Krista Morley, Lucie Poulin, Roberto A. Chica and Nicolas Doucet for critical reading of the manuscript. This work was supported by Canadian Institutes of Health Research (CIHR) grant 68851.

REFERENCES

1. Chu, E. & Allegra, C. J. (1996). Antifolates. *In Cancer Chemotherapy and Biotherapy* (Chabner, B. A. & Longo, D. L., eds.), 2nd edit., pp. 149-212. Lippincott-Raven, Philadelphia, PA.

2. Mennes, M., Stiers, P., Vandenbussche, E., Vercruysse, G., Uyttebroeck, A., De Meyer, G. & Van Cool, S. W. (2005). Attention and information processing in survivors of childhood acute lymphoblastic leukemia treated with chemotherapy only. *Pediatr. Blood Cancer* 44, 478-486.

3. Daw, N. C., Billups, C. A., Rodriguez-Galindo, C., McCarville, M. B., Rao, B. N., Cain, A. M., Jenkins, J. J., Neel, M. D. & Meyer, W. H. (2006). Metastatic osteosarcoma. *Cancer* 106, 403-412.

4. Slamon, D. J., Romond, E. H. & Perez, E. A. (2006). Advances in adjuvant therapy for breast cancer. *Clin. Adv. Hematol. Oncol.* 4(Suppl. 7), 4-9.

5. Strojan, P., Soba, E., Budihna, M. & Auersperg, M. (2005). Radiochemotherapy with Vinblastine, Methotrexate, and Bleomycin in the treatment of verrucous carcinoma of the head and neck. *J. Surg. Oncol.* 92, 278-283.

6. Appleman, J. R., Prendergast, N., Delcamp, T. J., Freisheim, J. H. & Blakley, R. L. (1988). Kinetics of the formation and isomerization of methotrexate complexes of recombinant human dihydrofolate reductase. *J. Biol. Chem.* 263, 10304-10313.

7. Cody, V., Luft, J. R. & Pangborn, W. (2005). Understanding the role of Leu22 variants in methotrexate resistance: comparison of wild-type and Leu22Arg variant mouse and human dihydrofolate reductase ternary crystal complexes with methotrexate and NADPH. *Acta Crystallogr. Sect. D.* 61, 147-155.

8. Meiering, E. M., Li, H., Delcamp, T. J., Freisheim, J. H. & Wagner, G. (1995). Contributions of tryptophan 24 and glutamate 30 to binding long-lived water molecules in the ternary complex of human dihydrofolate reductase with methotrexate and NADPH studied by site-directed mutagenesis and nuclear magnetic resonance spectroscopy. *J. Mol. Biol.* 247, 309-325.

9. Ercikan, E., Waltham, M., Dicker, A., Schweitzer, B. & Bertino, J. R. (1993). Effect of codon 22 mutations on substrate and inhibitor binding for human dihydrofolate reductase. *Advan. Expt. Med. Biol.* 338, 515-519.

10. Nakano, T., Spencer, H. T., Appleman, J. R. & Blakley, R. L. (1994). Critical role of phenylalanine 34 of human dihydrofolate reductase in substrate and inhibitor binding and in catalysis. *Biochemistry* 33, 9945-9952.

11. Schweitzer, B. I., Srimatkandada, S., Gritsman, H., Sheridan, R., Venkataraghavan, R. & Bertino, J. R. (1989). Probing the role of two hydrophobic active site residues in the human dihydrofolate reductase by site-directed mutagenesis. *J. Biol. Chem.* 264, 20786-20795.

12. Thompson, P. D. & Freisheim, J. H. (1991). Conversion of arginine to lysine at position 70 of human dihydrofolate reductase: generation of a methotrexate-insensitive mutant enzyme. *Biochemistry* 30, 8124-8130.

13. Blakley, R. L., Appleman, J. R., Chunduru, S. K., Nakano, T., Lewis, W. S. & Harris, S. E. (1993). Mutations of human dihydrofolate reductase causing decreased inhibition by methotrexate. *Advan. Expt. Med. Biol.* 338, 473-479.

14. Chunduru, S. K., Cody, V., Luft, J. R., Pangborn, W., Appleman, J. R. & Blakley, R. L. (1994). Methotrexate-resistant variants of human dihydrofolate reductase. Effects of Phe31 substitutions. *J. Biol. Chem.* 269, 9547-9555.

15. Lewis, W. S., Cody, V., Galitsky, N., Luft, J. R., Pangborn, W., Chunduru, S. K., Spencer, H. T., Appleman, J. R. & Blakley, R. L. (1995). Methotrexate-resistant variants of human dihydrofolate reductase with substitutions of leucine 22. Kinetics, crystallography, and potential as selectable markers. *J. Biol. Chem.* 270, 5057-5064.

16. Ercikan-Abali, E. A., Waltham, M. C., Dicker, A. P., Schweitzer, B. I., Gritsman, H., Banerjee, D. & Bertino, J. R. (1996). Variants of human dihydrofolate reductase with substitutions at leucine-22: effect on catalytic and inhibitor binding properties. *Mol. Pharmacol.* 49, 430-437.

17. Thillet, J., Absil, J., Stone, S. R. & Pictet, R. (1988). Site-directed mutagenesis of mouse dihydrofolate reductase. Mutants with increased resistance to methotrexate and trimethoprim. *J. Biol. Chem.* 263, 12500-12508.

18. Melera, P. W., Davide, J. P. & Oen, H. (1988). Antifolate-resistant Chinese hamster cells. Molecular basis for the biochemical and structural heterogeneity among dihydrofolate reductases produced by drug-sensitive and drug-resistant cell lines. *J. Biol. Chem.* 263, 1978-1990.

19. Srimatkandada, S., Schweitzer, B. I., Moroson, B. A., Dube, S. & Bertino, J. R. (1989). Amplification of a polymorphic dihydrofolate reductase gene expressing an enzyme with decreased binding to methotrexate in a human colon carcinoma cell line, HCT-8R4, resistant to this drug. *J. Biol. Chem.* 264, 3524-3528.

20. Dicker, A. P., Waltham, M. C., Volkenandt, M., Schweitzer, B. I., Otter, G. M., Schmid, F. A., Sirotnak, F. M. & Bertino, J. R. (1993). Methotrexate resistance in an in vivo mouse tumor due to a non-active-site dihydrofolate reductase mutation. *Proc. Natl. Acad. Sci. USA* 90, 11797-11801.

21. Chunduru, S. K., Appleman, J. R. & Blakley, R. L. (1993). Kinetic investigation of methotrexate resistant human dihydrofolate reductase (hDHFR) mutants at Phe31. *Advan. Expt. Med. Biol.* 338, 507-510.

22. Wyss, P. C., Gerber, P., Hartman, P. G., Hubschwerlen, C., Locher, H., Marty, H. P. & Stahl, M. (2003). Novel dihydrofolate reductase inhibitors. Structure-based versus diversity-based library design and high-throughput synthesis and screening. *J. Med. Chem.* 46, 2304-2312.

23. Spencer, H. T., Sorrentino, B. P., Pui, C. H., Chunduru, S. K., Sleep, S. E. & Blakley, R. L. (1996). Mutations in the gene for human dihydrofolate reductase: an unlikely cause of clinical relapse in pediatric leukemia after therapy with methotrexate. *Leukemia* 10, 439-446.

24. Lynch, G., Magill, G. B., Sordillo, P. & Golbey, R. B. (1982). Combination chemotherapy of advanced sarcomas in adults with "CYOMAD" (S7). *Cancer* 50, 1724-1727.

25. Sauerbrey, A., McPherson, J. P., Zhao, S. C., Banerjee, D. & Bertino, J. R. (1999). Expression of a novel double-mutant dihydrofolate reductase-cytidine deaminase fusion gene confers resistance to both methotrexate and cytosine arabinoside. *Hum. Gene Ther.* 10, 2495-2504.

26. Capiaux, G. M., Budak-Alpdogan, T., Alpdogan, O., Bornmann, W., Takebe, N., Banerjee, D., Maley, F. & Bertino, J. R. (2004). Protection of hematopoietic stem cells from pemetrexed toxicity by retroviral gene transfer with a mutant dihydrofolate reductase-mutant thymidylate synthase fusion gene. *Cancer Gene Ther.* 11, 767-773.

27. Zhao, S. C., Banerjee, D., Mineishi, S. & Bertino, J. R. (1997). Post-transplant methotrexate administration leads to improved curability of mice bearing a mammary tumor transplanted with marrow transduced with a mutant human dihydrofolate reductase cDNA. *Hum. Gene Ther.* 8, 903-909.

28. May, C., Gunther, R. & McIvor, R. S. (1995). Protection of mice from lethal doses of methotrexate by transplantation with transgenic marrow expressing drug-resistant dihydrofolate reductase activity. *Blood* 86, 2439-2448.

29. Ercikan-Abali, E. A., Mineishi, S., Tong, Y., Nakahara, S., Waltham, M. C., Banerjee, D., Chen, W., Sadelain, M. & Bertino, J. R. (1996). Active site-directed double mutants of dihydrofolate reductase. *Cancer Res.* 56, 4142-4145.

30. Rui, L., Cao, L., Chen, W., Reardon, K. F. & Wood, T. K. (2005). Protein engineering of epoxide hydrolase from Agrobacterium radiobacter AD1 for enhanced activity and enantioselective production of (R)-1-phenylethane-1,2-diol. *Appl. Environ. Microbiol.* 71, 3995-4003.

31. Schmitzer, A. R., Lepine, F. & Pelletier, J. N. (2004). Combinatorial exploration of the catalytic site of a drug-resistant dihydrofolate reductase: creating alternative functional configurations. *Protein Eng. Des. Sel.* 17, 809-819.

32. Santoro, S. W. & Schultz, P. G. (2002). Directed evolution of the site specificity of Cre recombinase. *Proc. Natl. Acad. Sci. USA* 99, 4185-4190.

33. Tsutsui, H., Karasawa, S., Shimizu, H., Nukina, N. & Miyawaki, A. (2005). Semi-rational engineering of a coral fluorescent protein into an efficient highlighter. *EMBO Rep.* 6, 233-238.

34. Shaner, N. C., Campbell, R. E., Steinbach, P. A., Giepmans, B. N., Palmer, A. E. & Tsien, R. Y. (2004). Improved monomeric red, orange and yellow fluorescent proteins derived from Discosoma sp. red fluorescent protein. *Nature Biotechnol.* 22, 1567-1572.

35. Davies, J. F., 2nd, Delcamp, T. J., Prendergast, N. J., Ashford, V. A., Freisheim, J. H. & Kraut, J. (1990). Crystal structures of recombinant human dihydrofolate reductase complexed with folate and 5-deazafolate. *Biochemistry* 29, 9467-9479.

36. Williams, E. A. & Morrison, J. F. (1992). Human dihydrofolate reductase: reduction of alternative substrates, pH effects, and inhibition by deazafolates. *Biochemistry* 31, 6801-6811.

37. Klon, A. E., Heroux, A., Ross, L. J., Pathak, V., Johnson, C. A., Piper, J. R. & Borhani, D. W. (2002). Atomic structures of human dihydrofolate reductase complexed with NADPH and two lipophilic antifolates at 1.09 Å and 1.05 Å resolution. *J. Mol. Biol.* 320, 677-693.

38. Chou, P. Y. & Fasman, G. D. (1974). Prediction of protein conformation. *Biochemistry* 13, 222-245.

39. Kopytek, S. J., Dyer, J. C., Knapp, G. S. & Hu, J. C. (2000). Resistance to methotrexate due to AcrAB-dependent export from *Escherichia coli*. *Antimicrob. Agents Chemother.* 44, 3210-3212.

40. Prendergast, N. J., Delcamp, T. J., Smith, P. L. & Freisheim, J. H. (1988). Expression and site-directed mutagenesis of human dihydrofolate reductase. *Biochemistry* 27, 3664-3671.

41. Patel, M., Sleep, S. E., Lewis, W. S., Spencer, H. T., Mareya, S. M., Sorrentino, B. P. & Blakley, R. L. (1997). Comparison of the protection of cells from antifolates by transduced human dihydrofolate reductase mutants. *Hum. Gene Ther.* 8, 2069-2077.

42. Thillet, J. & Pictet, R. (1990). Transfection of DHFR- and DHFR+ mammalian cells using methotrexate-resistant mutants of mouse dihydrofolate reductase. *FEBS Letters* 269, 450-453.

43. Banerjee, D., Schweitzer, B. I., Volkenandt, M., Li, M. X., Waltham, M., Mineishi, S., Zhao, S. C. & Bertino, J. R. (1994). Transfection with a cDNA encoding a Ser31 or Ser34 mutant human dihydrofolate reductase into Chinese hamster ovary and mouse marrow progenitor cells confers methotrexate resistance. *Gene* 139, 269-274.

44. Banerjee, D., Zhao, S. C., Tong, Y., Steinherz, J., Gritsman, K. & Bertino, J. R. (1994). Transfection of a nonactive site mutant murine DHFR cDNA (the tryptophan 15 mutant) into Chinese hamster ovary and mouse marrow progenitor cells imparts MTX resistance *in vitro*. *Cancer Gene Ther.* 1, 181-184.

45. Aharoni, A., Gaidukov, L., Khersonsky, O., Mc, Q. G. S., Roodveldt, C. & Tawfik, D. S. (2005). The 'evolvability' of promiscuous protein functions. *Nature Genet.* 37, 73-76.

46. Cody, V., Luft, J. R., Pangborn, W. & Gangjee, A. (2003). Analysis of three crystal structure determinations of a 5-methyl-6-N-methylanilino pyridopyrimidine antifolate complex with human dihydrofolate reductase. *Acta Crystallogr. sect. D.* 59, 1603-1609.

47. Cody, V., Galitsky, N., Luft, J. R., Pangborn, W. & Gangjee, A. (2003). Analysis of two polymorphic forms of a pyrido[2,3-d]pyrimidine N9-C10 reversed-bridge antifolate binary complex with human dihydrofolate reductase. *Acta Crystallogr. Sect. D.* 59, 654-661.

48. Mildvan, A. S. (2004). Inverse thinking about double mutants of enzymes. *Biochemistry* 43, 14517-14520.

49. Baccanari, D. P., Stone, D. & Kuyper, L. (1981). Effect of a single amino acid substitution on *Escherichia coli* dihydrofolate reductase catalysis and ligand binding. *J. Biol. Chem.* 256, 1738-1747.

50. Chothia, C. (1976). The nature of the accessible and buried surfaces in proteins. *J. Mol. Biol.* 105, 1-12.

51. Blakley, R. L. & Sorrentino, B. P. (1998). In vitro mutations in dihydrofolate reductase that confer resistance to methotrexate: potential for clinical application. *Hum. Mutat.* 11, 259-263.

52. Flasshove, M., Banerjee, D., Bertino, J. R. & Moore, M. A. (1995). Increased resistance to methotrexate in human hematopoietic cells after gene transfer of the Ser31 DHFR mutant. *Leukemia,* 9(Suppl. 1), S34-S37.

53. Blakley, R. L. (1960). Crystalline dihydropteroylglutamic acid. *Nature*, 231.

54. Sidhu, S. S., Lowman, H. B., Cunningham, B. C. & Wells, J. A. (2000). Phage display for selection of novel binding peptides. *Methods Enzymol.* 328, 333-363.

55. Fidock, D. A. & Wellems, T. E. (1997). Transformation with human dihydrofolate reductase renders malaria parasites insensitive to WR99210 but does not affect the intrinsic activity of proguanil. *Proc. Natl. Acad. Sci. USA* 94, 10931-10936.

56. Sarkar, G. & Sommer, S. S. (1990). The "megaprimer" method of site-directed mutagenesis. *Biotechniques* 8, 404-407.

57. Fernandez-Patron, C., Castellanos-Serra, L. & Rodriguez, P. (1992). Reverse staining of sodium dodecyl sulfate polyacrylamide gels by imidazole-zinc salts: sensitive detection of unmodified proteins. *Biotechniques* 12, 564-573.

58. Hillcoat, B. L., Nixon, P. F. & Blakley, R. L. (1967). Effect of substrate decomposition on the spectrophotometric assay of dihydrofolate reductase. *Anal. Biochem.* 21, 178-189.

59. Segel, I. H. (1993). Simple inhibition systems. In *Enzyme Kinetics: Behavior and Analysis of Rapid Equilibrium and Steady-State Enzyme Systems*, pp. 100-160, John Wiley and Sons, New York.

60. Kawaura, T., Inagaki, M., Tanaka, A., Kato, M., Nishikawa, S. & Kashimura, N. (2003). Contributions of polysaccharide and lipid regions of lipopolysaccharide to the recognition by spike G protein of bacteriophage phi X174. *Biosci. Biotechnol. Biochem.* 67, 869-876.

61. Mallette, F. A., Goumard, S., Gaumont-Leclerc, M. F., Moiseeva, O. & Ferbeyre, G. (2004). Human fibroblasts require the Rb family of tumor suppressors, but not p53, for PML-induced senescence. *Oncogene,* 23, 91-99.

62. Oefner, C., D'Arcy, A. & Winkler, F. K. (1988). Crystal structure of human dihydrofolate reductase complexed with folate. *Eur. J. Biochem.* 174, 377-385.

Préface au chapitre 3

Pour caractériser l'effet de substitutions à d'autres régions du site actif, nous avons procédé à la mutagénèse par saturation des résidus Ile7, Gly15, Trp24, Arg70 et Val115 de la DHFRh, créant ainsi 5 nouvelles banques de mutants. Ces résidus, situés dans ou en périphérie du site actif de la DHFRh, sont hautements conservés et peu caractérisés quant à leurs rôles pour l'activité et la reconnaissance des ligands par la DHFRh. Étant donné le grand nombre de banques à cribler et la quantité d'informations structure-fonction pouvant ressortir du criblage, nous avons développé un système de sélection et de caractérisation rapide des variantes, plus élaboré que celui décrit au chapitre précédent, constitué de deux étapes. Une étape de sélection *in vivo* permettant l'identification de variantes conservant une activité DHFR a été réalisée, en parallèle avec la sélection *in vivo* pour identifier les mutants actifs et résistants au MTX. Les variantes sélectionnées lors de la première étape du criblage sont sujets à un essai de criblage à haut débit *in vitro* (en plaques en 96-puits), permettant de confirmer les résultats de phénotypes obtenus pour les différentes variantes lors de l'étape de sélection *in vivo*, ainsi que d'obtenir des valeurs préliminaires de paramètres catalytiques et d'inhibition pour chaque variante active. Cette étape permet aussi l'identification de faux-positifs venant de l'étape de sélection. Le système à deux étapes fut appliqué aux banques de mutants, ce qui a permis de démontrer que seul le résidu 115 tolérait une grande variété de substitutions permettant de maintenir une activité catalytique, parmi lesquelles deux variantes permettaient une haute résistance au MTX. De plus, nous avons démontré que le système se prêtait bien à la caractériserisation de la liaison d'autres antifolates, tel le pemetrexed, une molécule pouvant inhiber plusieurs cibles dans la cellule.

Les résultats de ce chapitre sont présentés sous forme d'article scientifique dans la revue *Journal of Biomolecular Screening* parue en juillet 2008. J'ai contribué à une partie des recherches théoriques et à quelques aspects expérimentaux de cette étude (création des banques DHFRh mut24, mut70 ; caractérisation des paramètres cinétiques et d'inhibition des mutants V115A et V115C). La participation de Lucie Poulin et Vanessa Guerrero dans le développement d'une stratégie de criblage à haut débit, ainsi que David-Antoine Dugas

dans la création de la banque mut115, justifie leur présence en tant que troisième, quatrième et cinquième auteurs respectivement.

Chapitre 3

Développement d'un système à deux étapes pour la selection de variantes de la dihydrofolate reductase humaine actives et résistantes au MTX

3.1 Article 2. *2-tier bacterial and in vitro selection of active and methotrexate-resistant variants of human dihydrofolate reductase*

2-tier bacterial and *in vitro* selection of active and methotrexate-resistant variants of human dihydrofolate reductase

Elena Fossati[1], Jordan P. Volpato[1], Lucie Poulin[2], Vanessa Guerrero[1], David-Antoine Dugas[1] and Joelle N. Pelletier[1,2]

[1]Département de Biochimie and [2]Département de Chimie

Université de Montréal

C.P. 6128, Succursale Centre-Ville

Montréal (Québec)

H3C 3J7 CANADA

J. Biomol. Scr., 2008, 13 (6), 504-514

ABSTRACT

We report a rapid and reliable 2-tier selection and screen for detection of activity as well as drug-resistance in mutated variants of a clinically-relevant drug-target enzyme. Human dihydrofolate reductase point-mutant libraries were subjected to a 1st-tier bacterial complementation assay, such that bacterial propagation served as an indicator of enzyme activity. Alternatively, when selection was performed in the presence of the inhibitor methotrexate (MTX), propagation indicated MTX resistance. The selected variants were then subjected to a 2nd-tier *in vitro* screen in 96-well plate format using crude bacterial lysate. Conditions were defined to establish a threshold for activity or for MTX resistance. The 2nd-tier assay allowed rapid detection of the best variants among the leads and provided reliable estimates of relative reactivity, (k_{cat}) and IC_{50}^{MTX}. Screening saturation libraries of active-site positions 7, 15, 24, 70 and 115 revealed a variety of novel mutations compatible with reactivity as well as 2 novel MTX-resistant variants: V115A and V115C. Both variants displayed K_i^{MTX} = 20 nM, a 600-fold increase relative to the wild-type. We also present preliminary results from screening against further antifolates following simple modifications of the protocol. The flexibility and robustness of this method will provide new insights into interactions between ligands and active-site residues of this clinically relevant human enzyme.

INTRODUCTION

Dihydrofolate reductase (DHFR, EC 1.5.1.3) catalyzes the NADPH-dependent reduction of 7,8-dihydrofolate (DHF) to 5,6,7,8-tetrahydrofolate (THF), an essential metabolite involved in the biosynthesis of purines and thymidylate.[1] Due to its crucial role in cell proliferation, human DHFR (hDHFR) has long been a target in the treatment of psoriasis,[2] rheumatoid arthritis[2,3] and neoplastic diseases.[4] A specific competitive inhibitor of hDHFR, the antifolate methotrexate (MTX), has been extensively used to treat various cancers.[4] Limitations to cancer treatment with MTX include lack of specificity for cancerous cells[1] and development of drug resistance.[5]

Among the recognized MTX-resistance mechanisms,[5] we are specifically interested in mutations that weaken MTX binding. Despite their structural similarity, the substrate DHF and the inhibitor MTX bind to the active site in different orientations, making different contacts with the enzyme.[6,7] Active-site mutations may thus reduce MTX binding while maintaining sufficient DHF affinity for catalysis.[8-10] Gaining a better understanding of substrate and inhibitor binding at the hDHFR active site by characterizing ligand binding in active-site variants will offer insight toward the synthesis of alternative antifolates.[4,10] In a clinical context, MTX-resistant hDHFR variants can offer protection of haematopoietic stem cells from the cytotoxicity of MTX *via* gene therapy.[11] Furthermore, MTX-resistant hDHFR variants show excellent potential as selectable markers for gene transfer in stem cells, improving the outcome of gene therapy.[11] For these applications, ideal hDHFR variants should possess a high K_i for MTX (weak binding) and efficient catalytic properties (low K_M^{DHF} and high k_{cat}) in addition to good stability, solubility and high expression levels.

We previously performed directed evolution to identify highly MTX-resistant variants of hDHFR from a combinatorial library of mutants using a rapid bacterial selection strategy.[8] The strategy relies on the capacity for variants of human DHFR to allow bacterial

propagation in the presence of high MTX concentrations. While characterization of the selected variants confirmed successful identification of active and highly MTX-resistant hDHFR variants with no significant background from false-positive hits, there remain issues to be addressed to allow its broader application. First, we need to assess if the bacterial-based selection strategy is robust; that is, what is the incidence of false-negatives? While bacterial selection offers the undeniable advantage of speed, it is challenging to tune the sensitivity to specific enzyme properties. Differences in mutant enzyme stability, expression levels and limitations set by bacterial metabolic requirements (upper or lower threshold for requirement of a specific metabolite) contribute to phenotypic responses that do not reflect kinetic properties of the enzyme variants. Second, classic methods for characterizing the kinetic parameters defining activity and MTX-resistance of the selected variants were lengthy and labour-intensive, precluding application at a larger scale. Finally, the selection assay had been designed exclusively for the purpose of identifying the phenotype of MTX-resistance. However, a further phenotype of interest is that of conservation of native-like activity upon mutation.

Herein, we present a streamlined, 2-tier selection and screening protocol to rapidly identify hDHFR variants that are active and/or MTX-resistant and that possess properties justifying further, more detailed kinetic characterization. As a 1st step, the bacterial selection strategy was expanded to select either for native-like activity or for a combination of activity and MTX-resistance. Then, an *in vitro* activity assay was conveniently performed directly on cell lysates in 96-well plate format to rapidly provide a reliable estimate of catalytic activity and/or MTX-resistance. Toward this goal, active-site residues 7, 15, 24, 70 and 115 of hDHFR, each known or suspected to affect ligand binding, were subjected to saturation mutagenesis. The 5 libraries were selected for conservation of native-like activity and for MTX resistance. A variety of mutations compatible with activity were identified and 2 novel MTX-resistant variants were identified and characterized. Preliminary results from screening against further antifolates are also reported, demonstrating the adaptability of the approach.

MATERIALS AND METHODS

Reagents

Restriction and DNA modifying enzymes and dNTPs were purchased from MBI Fermentas (Burlington, ON). Folic acid, methotrexate (MTX), β-NADPH, trimethoprim (TMP), buffers and CelLytic™ B Cell Lysis Reagent were from Sigma-Aldrich (Oakville, ON). Pemetrexed (ALIMTA) was from Eli Lilly (Toronto, ON). Alimta was supplied as 1:1 mixture of pemetrexed and D-mannitol. Dihydrofolate (DHF) was synthesized from folic acid.[12] Standard mutagenic oligonucleotide primers were from Alpha DNA (Montréal, QC), while primers containing degenerate codons were from Integrated DNA Technologies (Coralville, IA). The QIAquick® Gel extraction kit, QIAprep® Spin plasmid purification kits, and Ni-NTA agarose were from Qiagen (Mississauga, ON). Isopropyl 1-thio-β-D-galactopyranoside (IPTG) was from BioShop Canada (Burlington, ON). DNA sequencing was performed by dideoxy-chain termination using a Thermo Sequenase Cycle Sequencing Kit (GE healthcare) and dye-labelled primers (*fwd* $^{5'}$CGGATAACAATTTCACACAG$^{3'}$ or *rev* $^{5'}$GTTCTGAGGTCATTACTGG$^{3'}$) (Li-Cor Biotechnology, Lincoln, NB) with a Li-Cor 4200 automated sequencer. *Escherichia coli* strain SK037[13] was a generous gift from Gwen Snapp and James Hu (Texas A&M).

Creation of the hDHFR saturation mutant libraries

The construct WT hDHFR-pQE32 encoding WT human DHFR cloned into pQE32 (Qiagen) between the BamHI and HindIII sites was previously described.[8] It expresses WT His_6-hDHFR (*N*-terminally 6-histidine tagged) and was the template in creation of the mutated libraries. The external primer set 1 (primer 1A: *fwd* $^{5'}$ ACACAC<u>GGATCC</u>AAATGGTTGGTTCGCTAAACTGCATC$^{3'}$ [BamHI restriction site underlined]; primer 1B: *rev* $^{5'}$GTTCTGAGGTCATTACTGG$^{3'}$) allowed for PCR amplification of the entire coding region. Libraries 7 and 15, named according to the numbering of the mutated residue, were constructed in a single-step PCR using primers

*fwd*7 (5'ACCATGGGATCCAAATGGTTGGTTCGCT**T**AACTGCNNSGTCGCTGTG TCCCAGA3'; a silent mutation [bold] was introduced as a tracer) or *fwd*15 (5'ACCATGGGATCCAAATGGTTGGTTCGCTAAACTGCATCGTCGCTGTGTCCCA GAACATGNNSATCGGCAAGAACGG3'), respectively, with primer 1B. Library 24 was constructed by 2-step megaprimer PCR[14] using primer 24 (*rev* 5'TCCTTAAGGGTGGSNNCGGCAGGTCCCCGT3') and external primer set 1. Libraries 70 and 115 were created by 3-step overlap extension PCR[15] using primers 70A (*fwd* 5'CGACCTTTAAAGGGTNNSATTAATTTAGTTAG3') and 70B (*rev* 5'CTGAGAACTAAATTAATSNNACCCTTTAAAGGTCG3') or primers 115A (*fwd* 5'GACATGGTCTGGATANNSGGTGGCAGTTCTGTTTATAAGG3') and 115B (*rev* 5'CCTTATAAACAGAACTGCCACCSNNTATCCAGACCATGTC3'), and the external primer set 1. Degenerate codons are underlined. The resulting libraries were cloned into pQE32 between BamHI and HindIII and transformed into electrocompetent *E. coli* SK037, yielding approximately 1×10^4 colonies per library. The quality of each library was verified by sequencing DNA from clones propagated on LB agar containing 100 μg/ml ampicillin.

Selection for activity and MTX resistance

Library-transformed *E. coli* SK037 was selected first for hDHFR activity, then for MTX resistance. *E. coli* SK037 transformed with pQE2 (Qiagen) was the negative control. Cells were plated in equal dilutions on M9 minimal agar containing 0.08% w/v casamino acids and 100 μg/ml ampicillin (MM_A; non-selective conditions), on MM_A containing 0.1 μg/ml trimethoprim (TMP) (MM_AT; selective conditions for hDHFR activity) and MM_AT containing 1 mM MTX (ATM_1000;[8] selective conditions for MTX resistance). Colony formation took place at 37 °C over 18 h on both MM_A and MM_AT and over 22 h on ATM_1000. The survival rate for each library was the ratio of colonies observed on selective MM_AT or ATM_1000 relative to non-selective MM_A medium. Following selection, plasmid DNA was sequenced to identify the mutations at the targeted positions.

In all cases, the entire coding sequence was verified, and in certain cases, both strands were verified.

Protein expression and cell lysis

For expression, transformed *E. coli* SK037 were propagated in LB (100 μg/ml ampicillin) at 37 °C, 225 rpm in 96-well assay blocks with 2 ml wells (Costar, Cambridge, MA). Fresh LB medium (1 ml) was inoculated with overnight cultures (25 μl) and propagated until $OD_{600} \approx 0.6$. Protein expression was induced by addition of IPTG to a final concentration of 1 mM and further propagation for 3 hrs. The assay blocks were centrifuged (30 min, 2700 × *g,* 4 °C), the supernatant was removed and the pellets were resuspended in 150 μl of lysis reagent (15 min, 225 rpm, room temperature). The lysates were clarified by centrifuging as above and were preserved on ice until required.

Determination of activity and antifolate resistance from crude cell lysates in 96-well plates

All rate measurements were in MATS buffer (25 mM MES, 25 mM acetic acid, 50 mM Tris, 100 mM sodium acetate and 0.02% w/v sodium azide) pH 7.6, 23 °C. Substrates were dissolved in buffer and quantified by spectrophotometry ($\varepsilon_{340\ nm}$ = 6 200 $M^{-1}cm^{-1}$ for NADPH; $\varepsilon_{282\ nm}$ = 28 400 $M^{-1}cm^{-1}$ for DHF). MTX was dissolved in 0.05 M KOH and quantified in 0.1 M NaOH ($\varepsilon_{258\ nm}$ = 22 100 $M^{-1}cm^{-1}$ and $\varepsilon_{302\ nm}$ = 23 300 $M^{-1}cm^{-1}$). Pemetrexed (ALIMTA) was dissolved and quantified in 0.9 % w/v NaCl ($\varepsilon_{226\ nm}$ = 31200 $M^{-1}cm^{-1}$). Catalytic activity of mutants was determined in 96-well flat-bottom plates (Costar #3595, Cambridge, MA) with a FLUOstar OPTIMA UV-Vis plate reader (BMG Laboratories, Offenburg) by monitoring concurrent NADPH and DHF depletion ($\Delta\varepsilon_{340\ nm}$ = 12 800 $M^{-1}\ cm^{-1}$).[16] Reaction rates were determined in a final volume of 300 μl using crude cell lysate and 100 μM each DHF and NADPH. To evaluate the background due to bacterial DHFR, reactions were conducted in presence or absence of 1 μg/ml TMP.

To ensure high signal to background while keeping the reaction sufficiently slow to allow measurement of initial rates, an initial estimate of reaction rate was obtained using various dilutions of the lysates. The dilutions were then adjusted for rate measurement of each variant. These dilutions were also used for determination of k_{cat} according to $k_{cat} = V_{max}$ / [hDHFR], where the concentration of soluble hDHFR variant in each lysate was estimated following migration on 15 % SDS-PAGE and Coomassie blue staining. Protein quantification was performed using the image analysis software Scion Image (NIH, rsb.info.nih.gov/nih-image) from digitalized images of the stained gels.

For assessment of MTX resistance, residual activities were determined as the ratio of activity in presence of 200 or 1000 nM MTX *versus* activity in absence of MTX. The concentration of hDHFR variant in each lysate was verified to ensure that saturating concentrations of MTX were used. For library 115, the approximate IC_{50}^{MTX} values of active mutants were determined from cell lysates by monitoring initial reaction rates in presence of 100 µM each DHF and NADPH and increasing concentrations of MTX: 0, 50, 500, 1000, 5000 and 10000 nM. IC_{50}^{MTX} values were obtained from a non-linear regression fit to the hyperbolic model for one-site binding using Graphpad Prism (Graphpad Software, San Diego, CA) and the data from three independent experiments.

For assessment of PMTX resistance, residual activities were determined as the ratio of activity in presence of 5 µM or 20 µM PMTX *versus* activity in absence of PMTX. For assessment of TMP sensitivity, reactions were conducted in presence or absence of 0.1 µg/ml (0.34 µM) and 1 µg/ml (3.4 µM) TMP.

Purification and characterization of individual selected variants

The MTX-resistant and the PMTX-resistant mutants identified by screening as well as mutant I7F were expressed and purified by Ni-NTA affinity chromatography as previously described[8] from 50 ml of culture medium. Solubility and relative expression level were verified by loading volume-equivalent amounts of total cell extracts, cell pellet

and lysis supernatant for resolution by 15 % SDS-PAGE. Purity was evaluated using the Scion Image software following separation by 15 % SDS-PAGE and Coomassie blue staining. Protein concentration was determined using the Bradford assay (Bio-Rad, Hercules, CA). Kinetic and inhibition constants were determined in presence DHF and NADPH (100 μM each) in 1-cm cells with a Cary 100 Bio UV/Vis spectrophotometer (Varian Canada, Montréal, QC).[8] For determination of K_M^{DHF}, the concentration of DHF was varied (0.5 μM to 20 μM). For determination of IC_{50}^{MTX}, the following MTX concentrations were used: 0, 0.025, 0.050, 0.1, 0.5, 1, 10 μM. For determination of IC_{50}^{PMTX}, the following PMTX concentrations were used: 0, 0.1, 0.5, 1, 5, 10, 100 μM. K_i^{MTX} and K_i^{PMTX} were calculated from IC_{50}^{MTX} and IC_{50}^{PMTX}, respectively, according to the equation for competitive inhibitor binding.[17] DHF was held constant at 100 μM for all IC_{50} determinations. The mock-purified *E. coli* SK037 expressing no hDHFR served as a negative control.

RESULTS AND DISCUSSION

Selection of target residues for mutagenesis

In silico visualization of active-site hDHFR residues known to interact with DHF and/or MTX was performed to identify residues for mutation. The crystal structure coordinates of the ternary complex of hDHFR with MTX and NADPH (1U72.pdb)[7] and the binary complex of hDHFR with folic acid (1DHF.pdb)[6] were visualized. Folate and MTX are constituted of a pteridine ring moiety, a *p*-aminobenzoyl group (*p*-ABA) and a L-glutamyl γ-carboxylate tail. The molecules are chemically and sterically similar. However, because of their differences, MTX binds to DHFR with its pteroyl moiety flipped 180° about the C_6-C_9 bond relative to folate (**Fig. 3.1A, 3.1B**). As a result, active-site residues form different contacts with the two molecules and binding of the inhibitor MTX is 2000-fold stronger than binding of the substrate DHF.

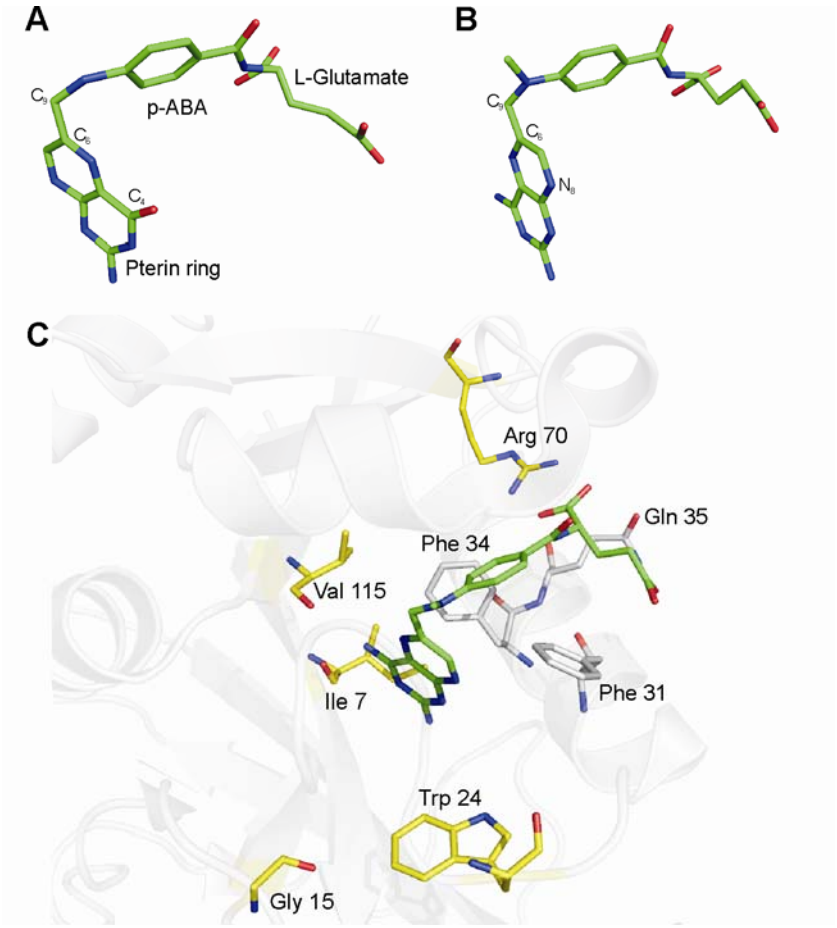

Figure 3.1. Structures of **(A)** folate (1DRF.pdb) and **(B)** MTX (1U72.pdb) bound to hDHFR active site, with atom numbering. **(C)** The active-site area of hDHFR with bound MTX (1U72.pdb), illustrating the residues targeted for saturation mutagenesis (yellow sticks) as well as residues mutated in a previous study[8] (white sticks).

MTX-resistant point mutants of DHFR from human or other mammalian sources have been identified either in vitro, in vivo or ex-vivo. Point mutations at residues Ile7,[18,19] Gly15,[20] Leu22,[21,22] Trp24,[19] Phe31,[8,23] Phe34,[24] Gln35,[19] Arg70[25] and Val115[19] have yielded DHFR variants with decreased MTX-affinity. In particular, saturation mutagenesis[26] and in vitro characterization of mutants at residues 22[21,22] and 31[8,23] have identified the specific mutations at these positions that confer MTX-resistance in vitro.

Herein, we investigated five non-contiguous positions where no saturation mutagenesis had been performed previously: Ile7, Gly15, Trp24, Arg70 and Val115 (**Fig. 3.1C**). The backbone carbonyl groups of Ile7 and Val115 form hydrogen bonds with the 4-amino pteroyl group of bound MTX; these bonds are not formed with folate.[7] Trp24 and Arg70 are strictly invariant residues in all vertebrate and bacterial DHFRs. The indole nitrogen of Trp24 is hydrogen-bonded to the C_4-oxygen of folate (N_8 of MTX) via a conserved water molecule. Arg70 makes ionic interactions with the α-carboxylate of the L-glutamate moiety of both folate and MTX. The mutation R70K weakens binding to both ligands.[25] Gly15, also selected for mutagenesis, is a highly conserved residue located on a loop outside the active site (**Fig. 3.1C**). It has no known interaction, direct or indirect, with NADPH, DHF or MTX. Nonetheless, mutant G15W was isolated in vivo from a MTX-resistant subline of murine leukemic cells implanted in mice,[27] justifying further investigation.

Mutagenesis and expression

Saturation mutagenesis was performed to obtain individual libraries encoding the 20 amino acids at positions 7, 15, 24, 70 and 115 of hDHFR (libraries 7, 15, 24, 70 and 115, respectively). The libraries were subcloned into pQE32 to provide His_6-tagged variants for ease of purification. The His_6-tag causes no detectable variation in WT hDHFR kinetic parameters.[8] The libraries were transformed into *E. coli* SK037, a MTX-sensitive strain that is a knock-out of the *tolC* component of a multi-drug-resistance (MDR) efflux pump.[13]

Approximately 1×10^4 colonies were obtained per library. DNA sequencing of randomly chosen clones propagated on non-selective medium revealed little or no sequence biases and no non-specific mutations. For library 115, DNA sequencing of 42 clones selected for activity and 46 nonselected clones allowed identification of 18 out of the 20 possible variants (mutants V115D and V115E were not identified).

Selection and screening for catalytically active mutants

The 2-tier selection strategy to identify catalytically active mutants is depicted in **Fig. 3.2A**. To verify whether the 2-tier strategy could reliably select active variants, we validated it against library 115. This library had shown a range of activity levels upon preliminary screening and was judged a good candidate to assess sensitivity and prevalence of false positives or false negatives. The 1st-tier assay is a bacterial complementation assay allowing high-throughput selection of active variants. For this assay, the library was plated on selective MM_AT medium containing trimethoprim (TMP). TMP inhibits the endogenous bacterial DHFR, making bacterial propagation on minimal medium obligatorily dependent on the activity of the expressed variant of hDHFR. *E. coli* SK037 transformed with pQE2 or with WT hDHFR-pQE32 was used as negative and positive controls, respectively. No bacterial growth was observed for the negative control whereas a survival rate varying between 88% and 100% was observed for the positive control. DNA sequencing of 42 selected colonies yielded 8 unique hDHFR variants (7 mutants and the WT) (**Fig. 3.3A**). The WT (Val115) was the most frequently selected variant (48%), followed by V115I (32%), V115M (10%) and V115C, V115L, V115F, V115Y and V115A (2% each) (**Fig. 3.4A**). We observed no bias resulting from the distribution of the 32 codons of the 'NNS' approach to saturation mutagenesis. Thus, the NNS codon encodes the WT Val at a frequency of 2/32, the V115I, M, C, F and Y at a frequency of 1/32 and the V115L at a frequency of 3/32; nonselected mutations are also encoded at frequencies varying between 1/32 and 3/32.

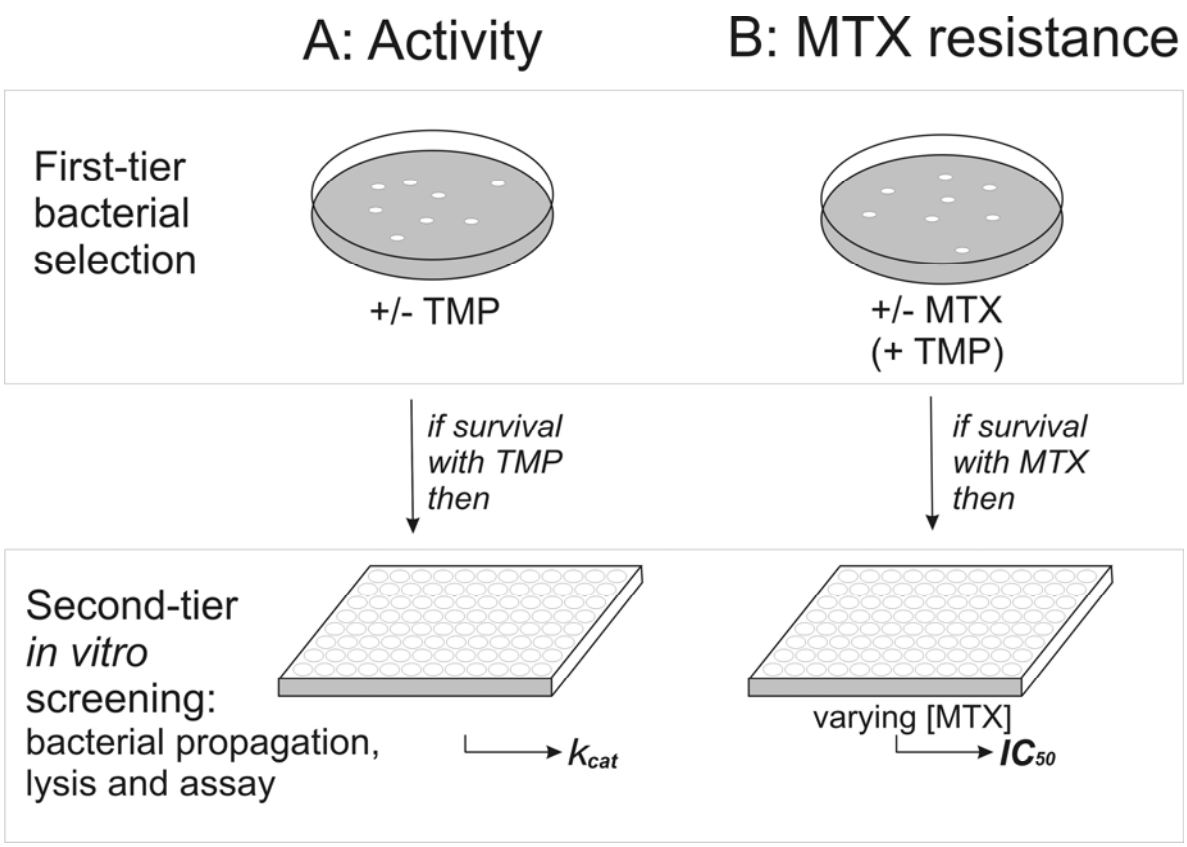

Figure 3.2. Flowchart of the 2-tier strategy to select mutated hDHFR library variants for **(A)** catalytic activity or **(B)** methotrexate (MTX) resistance. The 1st-tier selection relies on bacterial propagation in the presence of trimethoprim (TMP). Colonies are picked into 96-well plates for 2nd-tier screening using crude bacterial lysate.

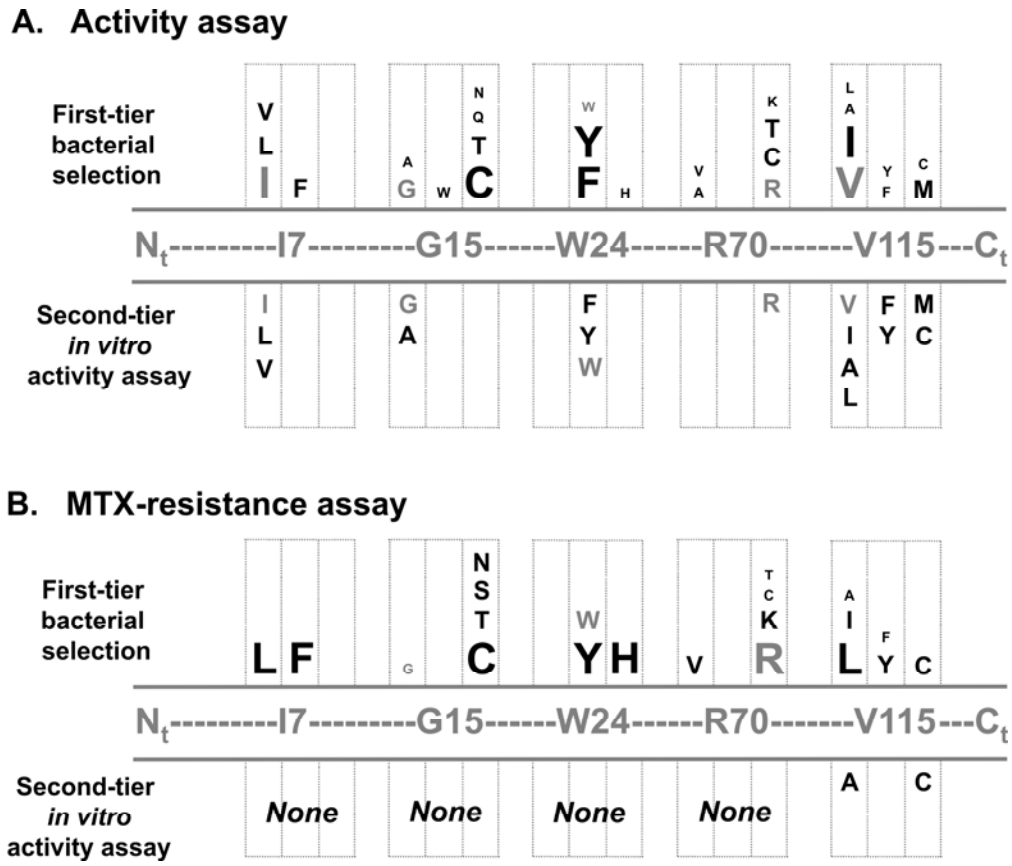

Figure 3.3. Comparison of hDHFR mutations that allow for conservation of activity **(A)** or MTX resistance **(B)** on the basis of the 2-tier selection strategy. Residues subjected to mutagenesis are depicted relative to the WT hDHFR primary sequence. Above the sequence are the mutants identified in the 1st-tier bacterial selection. The size of the font is related to the frequency of occurrence in the selection: small (< 10 %), medium (10 to 30%), large (> 30%). Below the sequence are the mutations identified in the 2nd-tier *in vitro* assay. Clones with **(A)** > 2-fold the *in vitro* activity of the negative control were considered active and clones with **(B)** residual activity > 40% at 200 nM MTX were considered MTX-resistant. Mutations at each targeted position are grouped as follows: small, hydrophobic (1st column); aromatic (2nd column); polar and charged (3rd column). The WT residue at each targeted position is shown in gray.

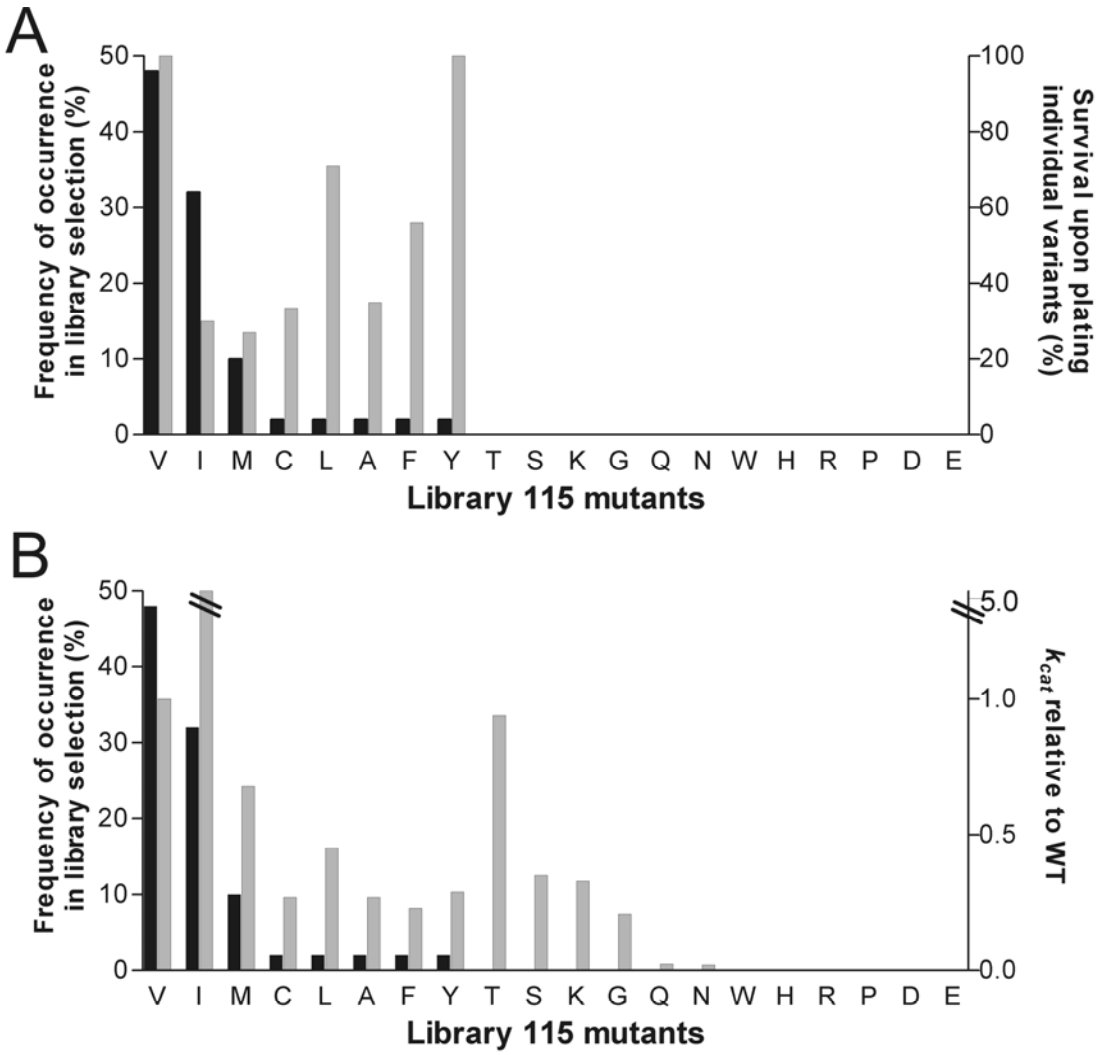

Figure 3.4. The 2-tier selection results for library 115. **(A)** Comparison of the frequency of occurrence of mutations following bacterial library selection (black bars) and bacterial survival rates from plating individual variants (gray bars). Variants T, S, K, G, Q and N showed negligible selection rates (between 0.02 % and 0.002 %) while variants W, H, R and P were not selected (= 0). All variants showing *in vitro* activity (see Panel B) were individually plated. **(B)** Frequency of occurrence of mutations following bacterial library selection (black bars) and k_{cat} relative to WT (Val115) for individual variants (gray bars). Variants D and E were not individually tested.

Not all variants identified as active by bacterial complementation were necessarily suitable for *in vitro* characterization. If the threshold for significant activity is higher *in vitro* than *in vivo*, some variants that allow cellular propagation may appear to be inactive *in vitro* and would thus constitute false positive hits from bacterial selection. Factors such as expression level, solubility and stability may have differing effects *in vivo* and *in vitro*. Moreover, if a greater number of selected colonies had been sequenced, further active variants at position 115 may have been identified. Failure to identify these would result in false negatives from bacterial selection.

To evaluate prevalence of false negatives, both the active, selected variants as well as the active but non-selected variants (14 variants in total, see **Fig. 3.4**) were individually plated under the bacterial selective conditions. All variants identified in the 1st-tier selection step conferred high survival rates while all others resulted in negligible or no survival (**Fig. 3.4A**). Thus, bacterial selection of library 115 gave no false negatives.

To evaluate prevalence of false-positive hits in the 1st-tier selection, the 2nd-tier 96-well plate-based screening assay was applied to library 115 variants. Despite having lower throughput than the selection step, it has the advantage of rapidly providing an estimate of the kinetic constant k_{cat}. To assess activity independently of bacterial selection, the selected variants as well as the nonselected variants were subjected to the *in vitro* activity assay (18 variants). DHFR activity was assayed directly from cell lysates in 96-well plate-based assays. When available, at least 2 clones were assayed per mutant. No significant differences in reaction rates were observed in absence or presence of TMP. This indicates that there is no significant background due to endogenous bacterial DHFR. *E. coli* SK037 transformed with pQE2 also served as a negative control. Again, the bacterial DHFR gave a negligible signal relative to the overexpressed hDHFR variants. The WT was always identified as being active both in bacterial selection and *in vitro*, which was an essential validation of the reliability of the method.

Clones with > 2-fold the *in vitro* activity of the negative control pQE2/SK037 were considered active. This threshold was established on the basis of the reproducibly weak signal obtained for the negative controls (at least 2 negative controls were included on each 96-well plate) as well as the sensitivity of plate-reader. Because the assay was performed with crude lysate rather than purified enzyme, any active but poorly expressed, poorly soluble or unstable mutant would be classified as inactive if the overall activity were < 2-fold pQE2/SK037. All library 115 variants that were identified in the first-tier bacterial selection were also active *in vitro*, confirming that the selection yielded no false positive hits (**Fig. 3.3A and 3.4B**). The k_{cat} for all active variants from library 115 roughly correlated with the frequency of occurrence of the mutants during bacterial selection (**Fig. 3.4B** and **Table 3.1**). When more than 1 clone was assayed for a given mutation, the data were generally in agreement. However, mutants V115T, V115Q, V115N, V115S, V115K and V115G, which had not been selected *in vivo* and which yielded no significant cellular propagation when individually plated (**Fig. 3.4A**), were also identified as active *in vitro*. The most active mutant, V115T, exhibited a native-like k_{cat}. While these mutants possessed readily assayed activity, their overall properties (potentially including K_M changes) did not provide sufficient turnover to support bacterial growth. These variants were not false negatives according to the criteria required for bacterial propagation, which is the ultimate goal of our work. Nonetheless, they illustrate that there can be a loss of underlying structure-activity information if only the bacterial-selected variants are subjected to the 2nd-tier assay for *in vitro* activity, as this assay can reveal individual properties of specific interest.

Having validated the reliability of the 2-tier selection procedure, it was applied to the remaining libraries. Following 1st-tier selection for activity, 16 selected clones per library were subjected to DNA sequencing analysis, allowing identification of mutations compatible with cell survival (**Fig. 3.3A**). Survival rates for the different libraries varied between 3% and 7% and a variety of mutations were tolerated at each targeted position.

Table 3.1. Reactivity (k_{cat}) and MTX or PMTX resistance determined in 96-well plates using crude lysates of active hDHFR variants from library 115.

Library 115 Variants[a]	k_{cat} *Relative to WT*	*Residual Activity (%) at 200 nM MTX*[b]	IC_{50}^{MTX} *(nM)*[c]	*Residual Activity (%) at 5 μM PMTX*[d]
V (WT)	1	11	20 ± 12	30
I	5.0	8	0.4 ± 0.3	**49**
M	0.68	12	19 ± 4	11
C	0.27	**67**	**400 ± 69**	**51**
L	0.45	30	130 ± 25	**80**
A	0.27	**49**	**220 ± 17**	**50**
F	0.23	–[e]	47 ± 41	–
Y	0.29	18	38 ± 8	16
T	0.94	35	76 ± 13	30
S	0.35	24	76 ± 7	22
K	0.33	34	96 ± 18	28
G	0.21	30	67 ± 5	30
Q	0.024	–	27 ± 7	–
N	0.020	–	51 ± 18	–

Variants are grouped according to frequency of bacterial selection for activity (**Fig. 4**).
a. IC_{50}^{MTX} could be calculated only where a non-negligible k_{cat} was recorded.
b. Variants in bold were considered MTX resistant according to the user-defined threshold of residual activity at 200 nM MTX being greater than 40%, as defined under Results.
c. Mean ± SD; $n = 3$. Variants in bold were considered MTX resistant according to the user-defined threshold of $IC_{50}^{MTX} \geq$ μ200 nM, as defined under Results.
d. Variants in bold were considered PMTX resistant according to the user-defined threshold of residual activity at 5 μM PMTX being significantly greater than the WT residual activity.
e. "–" indicates that activity was not detectable.

The mutants conferring survival were then tested *in vitro* in the 2nd-tier assay, allowing for identification of stable, soluble and active mutants (**Fig. 3.3A**). For libraries 7 and 24, most of the bacterial-selected mutants were active *in vitro*, with elimination of at most 1 false positive hit per library. Five false-positive mutants were eliminated from each of library 15 and 70. In library 70 only the native Arg showed detectable activity *in vitro*. Contrary to the results of library 115, where no false-positives were identified, not all mutants obtained in the 1st-tier selection showed significant *in vitro* activity. The correlation between *in vivo* and *in vitro* activity appears to depend on the particular library and on the threshold chosen to define activity, where mutations at the different positions have differing effects on the overall properties of the enzyme.

Mutations that support catalytic activity

Position 115 tolerated the greatest number of mutations. The active variant V115P was previously reported in the highly homologous mouse DHFR (mDHFR) but was unstable,[27] and its hDHFR counterpart was incompatible with bacterial propagation in this study. Positions 7 and 15 tolerated only a restricted subset of conservative mutations. Gly15, located farther from the active site than the other targeted residues, tolerated the conservative mutation G15A. The only reported mutation of hDHFR at position 15, G15W, was described as active but unstable.[20] This is consistent with it having been identified in the 1st-tier bacterial selection but eliminated in the 2nd-tier *in vitro* assay. Position 7 tolerated only the conservative mutations I7L and I7V. As in the case of Val115, the main-chain carbonyl of Ile7 is hydrogen-bonded to MTX but not to DHF.[7] The only active hDHFR mutation previously described at position 7 was I7F.[18] This mutant was identified in the 1st-tier bacterial selection but was rejected in the *in vitro* assay, its activity being slightly inferior to the chosen threshold. Considering that its expression level and solubility were comparable to the WT (data not shown), its low *in vitro* activity is likely a result of its reported instability and its high K_M^{DHF}.[18] Because its activity *in vitro* was not negligible, we determined its kinetic parameters using purified enzyme (k_{cat} = 2.1 ± 0.1 s^{-1}, K_M^{DHF} = 14.9

± 3.6 μM; k_{cat}/K_M^{DHF} = 0.16 $\mu M^{-1}s^{-1}$), confirming the reported data (k_{cat} = 5.0 ± 0.2 s^{-1}, K_M^{DHF} = 20 ± 2.1 μM; k_{cat}/K_M^{DHF} = 0.25 $\mu M^{-1}s^{-1}$).[18] The exclusion of this variant following the *in vitro* assay does not point to disagreement with previous studies but highlights the advantage of comparing all variants on the basis of a user-defined threshold for a specific parameter, where only variants surpassing that value are considered to be sufficiently fit for a given application.

Residues Trp24 and Arg70 are highly conserved in various species and are known to be important for DHF binding.[25,28] Moreover, Arg70 appears to be involved in maintaining the structure of the binding site.[25] Position 70 tolerated no substitution that allowed significant *in vitro* catalytic activity. The conservative hDHFR mutation R70K has been previously described (k_{cat} = 1.75 s^{-1}, K_M^{DHF} = 0.47 μM; k_{cat}/K_M^{DHF} = 3.7 $\mu M^{-1}s^{-1}$ at pH 7.5).[25] Its stability was comparable to the WT.[25] The mutation R70K was identified in the 1st-tier bacterial selection, but was then eliminated in the following step (**Fig. 3.3A**; 2 independent clones tested). Factors such as lower expression level or solubility may have contributed to reduce its *in vitro* fitness below the established threshold. Position 24 tolerated the conservative substitutions W24F and W24Y (**Fig. 3.3A**). The hDHFR mutation W24F was previously described as being compatible with activity (K_M^{DHF} increased 25-fold and a 3-fold increase in k_{cat} relative to WT) but its stability was 3-fold lower than the WT. NADPH binding was also weakened and the rate of hydride transfer was markedly decreased, illustrating its importance for substrate binding and catalysis;[28] nonetheless, its resulting activity was above the threshold. Mutation W24R in mDHFR was reported to be very poorly active,[19] and was not tolerated by hDHFR in this study (**Fig. 3.3A**).

Overall, the parallel comparison of a large number of mutations of a human gene by the rapid means of bacterial propagation was shown to provide a reliable indicator of global activity. Further sorting by the 2nd-tier *in vitro* assay allowed efficient retention of the variants that best met the user-specified parameters. The selected variants were

overwhelmingly in agreement with published data and readily allowed identification of novel, active point mutants of hDHFR.

Selection and screening for MTX resistance

In parallel with the activity assay, a 2-tier selection strategy was developed to identify MTX-resistant hDHFR mutants (**Fig. 3.2B**). In the 1st-tier bacterial selection step, the 5 libraries were selected on medium containing 1 mM MTX (ATM-1000). MTX inhibits the hDHFR variants that are not resistant, making the survival of bacteria on minimal medium dependent on the activity of the hDHFR variants that are active as well as MTX-resistant. It should be noted that, despite the increased MTX sensitivity of *E. coli* SK037, it exhibited relatively high intrinsic MTX resistance such that > 200 μM MTX was required for efficient bacterial selection. No bacterial growth was observed for the negative control expressing only endogenous bacterial DHFR. When the WT hDHFR was expressed, very low survival was observed (0.002%), consistent with its sensitivity to MTX. Survival of all libraries was low (≤ 0.03%), suggesting that few MTX-resistant variants were present and highlighting the importance of verifying the occurrence of false-positives. DNA sequencing following selection allowed identification of 2 to 6 mutations at each targeted position (**Fig. 3.3B**).

The 2nd-tier screening step using the 96-well plate screening assay was used to eliminate false positives. The clones identified as being MTX-resistant by bacterial selection were assayed for residual activity in the presence of 200 nM MTX (**Table 3.1**) or 1000 nM MTX (not shown), relative to activity in the absence of MTX. These 2 concentrations were selected based on IC_{50}^{MTX} (estimated at 100 μM DHF) for previously-characterized, MTX-resistant point mutants: L22Y ($IC_{50}^{MTX} \cong 2000$ nM, where K_M^{DHF} = 0.53 μM and K_i^{MTX} = 10.9 nM);[22] L22W ($IC_{50}^{MTX} \cong 1000$ nM, where K_M^{DHF} = 0.42 μM and K_i^{MTX} = 4.31 nM);[22] L22R ($IC_{50}^{MTX} \cong 290$ nM, where K_M^{DHF} = 1.6 and K_i^{MTX} = 4.57)[22] as well as I7F ($IC_{50}^{MTX} \cong 272 \pm 72$ nM, this study). The assays were conducted using the same

cell-lysate dilutions as for the activity test. Cell lysate from SK037 expressing no hDHFR or expressing WT hDHFR-pQE32 were used as negative controls for MTX-resistance. Previously characterized hDHFR mutants displaying a broad range of MTX-resistance levels were used as positive controls: mutant F31A/F34V/Q35H (AVH; K_i^{MTX}= 180 nM), mutant F31R/F34T/Q35R (RTR; K_i^{MTX}= 86 nM) and point-mutant F31P (K_i^{MTX}= 1.7 nM).[8] Mutants AVH and RTR showed residual activity higher than 40% at both concentrations of MTX tested, consistent with their high IC_{50}^{MTX} under these conditions (4400 nM and 3500 nM, respectively). F31P showed a residual activity > 40% at 200 nM MTX but not at 1000 nM, consistent with its IC_{50}^{MTX} under these conditions (110 nM). On the basis of these observations, a threshold of residual activity > 40% at 200 nM MTX was established as being minimally required to consider a mutant as MTX-resistant.

Two mutants from library 115 (V115A and V115C) were effectively resistant to MTX on the basis of the threshold (**Fig. 3.3B** and **Table 3.1**). These had never been previously reported. Other mutants had residual activities higher than WT hDHFR but were rejected because these values were below the established threshold. Previously reported MTX-resistant mutants of hDHFR I7F[18] and R70K[25] were identified at the 1st-tier level but rejected at the 2nd-tier screening as their overall activity *in vitro* did not meet the required criteria, as discussed above. Despite the fact that the purified I7F mutant was effectively MTX-resistant, with a K_i^{MTX} = 31.9 ± 8.5 nM (> 1000-fold increase relative to WT), the > 200-fold increase in K_M^{DHF} [18] and/or further modified properties contributed to decrease *in vitro* activity below the established threshold. G15W has also been reported as being MTX-resistant but unstable;[20] its fitness was too low even to allow 1st-tier selection for resistance.

As a further control for robustness of the strategy, the mutants encoded in library 115 (18 variants) were all individually tested for residual activity at 200 and 1000 nM MTX. The only mutants with a residual activity > 40% in presence of 200 nM MTX were

V115A and V115C. Thus, the bacterial selection for MTX-resistance yielded no false negatives in library 115.

The IC_{50}^{MTX} values for all library 115 mutants that showed non-negligible *in vitro* activity were measured in 96-well plates directly from cell lysates (**Table 3.1** and **Fig. 3.5A**). This assay was less rapid but more precise than the simple assay of residual activity. Only mutants V115A and V115C presented an IC_{50}^{MTX} higher than 200 nM. Other mutants (e.g V115L, V115K, V115T and V115G) had an IC_{50}^{MTX} higher than the WT hDHFR but lower than the established threshold of resistance (200 nM MTX). These results confirm the validity of relying on the simple indicator of residual activity to reliably identify MTX resistance. Thus, the rapid 2-step protocol consisting of bacterial selection followed by *in vitro* measurement of residual activity provided sufficient information to identify hDHFR variants satisfying our specific requirements for resistance.

Screening for modified binding to additional antifolate compounds

To verify the flexibility of the method, it was applied to testing against the antifolate TMP. Because human DHFR is intrinsically resistant to TMP (K_i^{TMP} WT hDHFR = 960 ± 30 nM relative to K_i^{TMP} WT *E. coli* DHFR = 0.08 nM)[29], we screened for increased sensitivity rather than resistance. The 1st-tier bacterial selection step cannot be applied to this compound because the endogenous bacterial DHFR will confer bacterial growth in absence of TMP. We performed the 2nd-tier *in vitro* reaction rate measurements for library 115 in absence or presence of 0.34 μM and 3.4 μM TMP. As mentioned previously, there was no significant background *in vitro* due to endogenous bacterial DHFR. In no case was a significant difference in reaction rates observed, indicating that no library 115 variants tested were rendered TMP-sensitive as a result of mutation. This confirmed that TMP sensitivity was not the cause of reduced cellular propagation in the bacterial selection presented above.

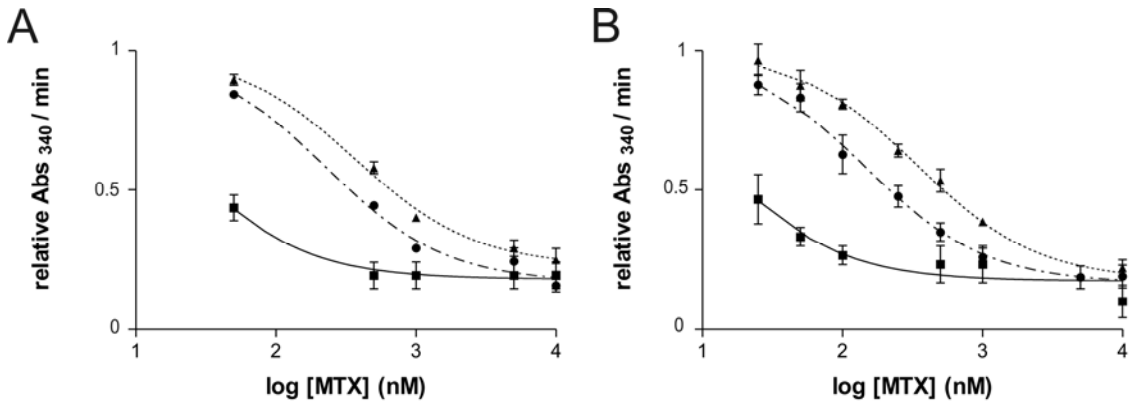

Figure 3.5. IC_{50}^{MTX} concentration-response curves (mean ± SD; n = 3) of WT hDHFR (■), V115A (●) and V115 C (▲) using **(A)** crude lysate or **(B)** purified enzyme.

Preliminary tests were performed to assess resistance to the clinically relevant antifolate pemetrexed (PMTX). Pemetrexed inhibits multiple folate-utilizing enzymes, including thymidylate synthase and hDHFR[4]. Because bacterial selection using pemetrexed could not be interpreted solely on the basis of hDHFR resistance, only the 2nd-tier *in vitro* screen was performed. Active clones from the 5 libraries considered in this study were assayed in crude lysate for residual activity in the presence of 5 μM PMTX (**Table 3.1**) or 20 μM (not shown) PMTX, relative to activity in the absence of PMTX. These concentrations were selected based on the value of $IC_{50}^{PMTX} \cong 0.75 \pm 0.3\mu M$ determined for the purified WT hDHFR. Using the same negative controls as for MTX-resistance, mutants with residual activity significantly greater than the WT residual activity at 5 μM PMTX were considered PMTX-resistant (**Table 3.1**). Screening results suggest that, as for MTX, variants V115A and V115C may be PMTX-resistant. Variants V115L and V115I also showed potential PMTX resistance according to residual activity.

Kinetic and inhibition parameters of the novel antifolate-resistant mutants

The WT and the novel MTX and/or PMTX-resistant mutants (V115A and V115C, V115I, V115L) identified in the 2nd-tier screen were expressed, purified to 90-95% purity and characterized according to their kinetic and inhibition parameters (**Table 3.2**). Their expression levels were comparable, and as for WT hDHFR, mutants were approximately 50% soluble (data not shown). Catalytic efficiencies (k_{cat}/K_M^{DHF}) for variants V115A and V115C were reduced by approximately 700 and 1400-fold, respectively, relative to WT. K_M^{DHF} for V115A and V115C was increased at least 100-fold relative to WT while turnover (k_{cat}) was reduced only 4 and 15-fold, respectively, relative to WT. The inhibition constants confirmed that both variants were effectively MTX-resistant, having $K_i^{MTX} = 20$ nM, which is > 600-fold higher than the WT and compares favorably to the well-characterized resistant point mutant L22Y ($K_i^{MTX} = 10.9$ nM).[22] It should be noted that IC_{50}^{MTX} for V115A and V115C from crude lysate or in purified form were comparable (**Table 3.1** and **Table 3.2; Fig. 3.5**). This demonstrates the accuracy of the rapid determination of IC_{50}^{MTX} directly

Table 3.2. Kinetic and inhibition constants [a] of purified MTX or PMTX-resistant hDHFR mutants.

hDHFR Variant	k_{cat} *(s^{-1})*	K_M^{DHF} *(μM)*	k_{cat}/K_M^{DHF} *($\mu M^{-1}s^{-1}$)*	IC_{50}^{MTX} *(nM)*	K_i^{MTX} *(nM)*	IC_{50}^{PMTX} *(μM)*	K_i^{PMTX} *(nM)*
Wild-type	10 ± 2.0	< 0.075	>138	41 ± 14	<0.031	0.75 ± 0.3	<0.5
V115C	0.65 ± 0.02	7 ± 1	0.1	330 ± 29	20 ± 4	4.3 ± 1.6	283 ± 44
V115A	2.8 ± 0.2	15 ± 2	0.2	150 ± 18	20 ± 5	1 ± 0.3	131 ± 87
V115L	ND[b]	4 ± 0.5	ND	190 ± 60	7.3 ± 2.7	9 ± 4	378 ± 118
V115I	1.3 ± 0.05	<1	>1.3	20 ± 8	<0.2	0.2 ± 0.03	<2

a. Mean ± SD, $n = 3$, except for mutant V115L, where $n = 2$.
b. ND, not determined.

from cell lysate in the 96-well plate format. Variants V115A and V115C were also shown to be PMTX-resistant as their K_i^{PMTX} values were > 250-fold greater than the WT hDHFR.

Variant V115L showed ~ 5-fold increase in IC_{50}^{MTX} relative to WT (**Table 3.1**; **Table 3.2**), which was below our user-defined threshold for resistance. Nonetheless, determination of its K_i^{MTX} confirmed that it confers MTX-resistance, albeit at a lower level than variants V115A and V115C (**Table 3.2**). This variant showed the greatest increase in K_i^{PMTX}, with a > 700-fold increase relative to WT. Taken with the results for variant V115A, which shows high MTX resistance and moderate PMTX resistance, our results suggest that variants at position 115 may confer a differential degree of resistance to the specific antifolates tested, despite the structural similarity of the compounds. We are pursuing more detailed studies relative to this question.

Variant V115I was not MTX resistant but was identified as being potentially PMTX resistant according to residual activity (**Table 3.1**). However, further analysis demonstrated that it is not PMTX resistant and thus constitutes a false-positive hit from the second-tier residual activity screen.

CONCLUSIONS

An efficient 2-tier selection strategy was applied to the selection of active and MTX-resistant hDHFR variants from 5 hDHFR libraries created by saturation mutagenesis of active-site residues. This allowed, for the 1st time, exhaustive screening and identification of mutations compatible with hDHFR activity at these positions. The 2 tiers showed reliability and complementarity with respect to identification of active hDHFR variants. The 1st-tier bacterial selection results of library 115 confirmed that the most frequently selected variants conferred better survival rates. All selected mutants from library 115 were also active in the 2nd tier, *in vitro* assay. Because the 2nd-tier assay has

user-defined parameters, varying the threshold for activity or the assay conditions (substrate and cofactor concentrations) will yield additional information relative to the effect of mutations on catalytic activity. In general, where active, stable and soluble variants have been reported, they were selected in the 2nd-tier activity assay, further validating the selection strategy. Thus, the bacterial selection for activity was shown to be robust and the *in vitro* screening allowed rapid preliminary kinetic characterization of novel active hDHFR variants.

The addition of MTX to the 2-tier procedure allowed identification of MTX-resistant point mutants at these positions, among which 2 are novel variants. There was no evidence of false-negatives upon bacterial selection. False-positives were readily eliminated upon *in vitro* screening, for which the IC_{50}^{MTX} values obtained from crude lysate were comparable to those obtained with purified enzyme. The concentrations of MTX for tests of residual growth were set by the operator and determined the extent of resistance that was sought. In this work, the concentrations of MTX were selected according to properties of previously-characterized point mutants, since our aim was to match or surpass that level of resistance. By increasing the threshold, only the most highly resistant mutants would be identified.

The method described is ideal for screening large libraries, the 1st-tier bacterial selection being high-throughput and the 2nd-tier assay allowing rapid detection of the best variants among the leads, according to user-defined parameters. The approach has proven efficient in rapidly assessing key kinetic parameters in enzyme variants. Simple modification of the protocol readily allowed screening against further compounds; preliminary screening has allowed identification of three novel pemetrexed-resistant variants by this approach. The 2-tier strategy should also prove adaptable to screening other metabolically-essential enzymes that can complement a bacterial strain rendered metabolically deficient via chemical or genetic methods, and where a colorimetric or fluorogenic assay can reliably report activity in crude bacterial lysate.

ACKNOWLEDGMENTS

The authors thank Christopher Clouthier for critical reading of the manuscript. This work was supported by Canadian Institutes of Health Research (CIHR) grant 68851.

REFERENCES

1. Schweitzer BI, Dicker AP, Bertino JR: Dihydrofolate reductase as a therapeutic target. *Faseb J* 1990; 4:2441-2452.

2. International Bone Marrow Transplant Registry: Effect of methotrexate on relapse after bone marrow transplantation for acute lymphoblastic leukemia. *Lancet* 1989; 1:535-537.

3. Kremer JM, Lee JK: A long-term prospective study of the use of methotrexate in rheumatoid arthritis: update after a mean of fifty-three months. *Arthritis Rheum* 1988; 31:577-584.

4. Walling J: From methotrexate to pemetrexed and beyond: a review of the pharmacodynamic and clinical properties of antifolates. *Invest New Drugs* 2006; 24:37-77.

5. Zhao R, Goldman ID: Resistance to antifolates. *Oncogene* 2003; 22:7431-7457.

6. Davies JF, 2nd, Delcamp TJ, Prendergast NJ, Ashford VA, Freisheim JH, Kraut J: Crystal structures of recombinant human dihydrofolate reductase complexed with folate and 5-deazafolate. *Biochemistry* 1990; 29:9467-9479.

7. Cody V, Luft JR, Pangborn W: Understanding the role of Leu22 variants in methotrexate resistance: comparison of wild-type and Leu22Arg variant mouse and human dihydrofolate reductase ternary crystal complexes with methotrexate and NADPH. *Acta Crystallogr D Biol Crystallogr* 2005; 61:147-155.

8. Volpato JP, Fossati E, Pelletier JN: Increasing methotrexate resistance by combination of active-site mutations in human dihydrofolate reductase. *J Mol Biol* 2007; 373:599-611.

9. Blakley RL, Sorrentino BP: In vitro mutations in dihydrofolate reductase that confer resistance to methotrexate: potential for clinical application. *Hum Mutat* 1998; 11:259-263.

10. Gangjee A, Jain HD, Phan J, Lin X, Song X, McGuire JJ, Kisliuk RL: Dual inhibitors of thymidylate synthase and dihydrofolate reductase as antitumor agents: design, synthesis, and biological evaluation of classical and nonclassical pyrrolo[2,3-d]pyrimidine antifolates(1). *J Med Chem* 2006; 49:1055-1065.

11. Budak-Alpdogan T, Banerjee D, Bertino JR: Hematopoietic stem cell gene therapy with drug resistance genes: an update. *Cancer Gene Ther* 2005; 12:849-863.

12. Blakley R: Crystalline dihydropteroylglutamic acid. *Nature* 1960; 188:231-232.

13. Kopytek SJ, Dyer JC, Knapp GS, Hu JC: Resistance to methotrexate due to AcrAB-dependent export from Escherichia coli. *Antimicrob Agents Chemother* 2000; 44:3210-3212.

14. Sarkar G, Sommer SS: The "megaprimer" method of site-directed mutagenesis. *Biotechniques* 1990; 8:404-407.

15. Ho SN, Hunt HD, Horton RM, Pullen JK, Pease LR: Site-directed mutagenesis by overlap extension using the polymerase chain reaction. *Gene* 1989; 77:51-59.

16. Hillcoat BL, Nixon PF, Blakley RL: Effect of substrate decomposition on the spectrophotometric assay of dihydrofolate reductase. *Anal Biochem* 1967; 21:178-189.

17. Segel IH: *Enzyme Kinetics: Behaviour and Analysis of Rapid Equilibrium and Steady-State Enzyme Systems*. New York: John Wiley and Sons, 1993.

18. Patel M, Sleep SE, Lewis WS, Spencer HT, Mareya SM, Sorrentino BP, Blakley RL: Comparison of the protection of cells from antifolates by transduced human dihydrofolate reductase mutants. *Hum Gene Ther* 1997; 8:2069-2077.

19. Thillet J, Absil J, Stone SR, Pictet R: Site-directed mutagenesis of mouse dihydrofolate reductase. Mutants with increased resistance to methotrexate and trimethoprim. *J Biol Chem 1988*; 263:12500-12508.

20. Spencer HT, Sorrentino BP, Pui CH, Chunduru SK, Sleep SE, Blakley RL: Mutations in the gene for human dihydrofolate reductase: an unlikely cause of clinical relapse in pediatric leukemia after therapy with methotrexate. *Leukemia* 1996; 10:439-446.

21. Ercikan-Abali EA, Waltham MC, Dicker AP, Schweitzer BI, Gritsman H, Banerjee D, Bertino JR: Variants of human dihydrofolate reductase with substitutions at leucine-22: effect on catalytic and inhibitor binding properties. *Mol Pharmacol* 1996; 49:430-437.

22. Lewis WS, Cody V, Galitsky N, Luft JR, Pangborn W, Chunduru SK, Spencer HT, Appleman JR, Blakley RL: Methotrexate-resistant variants of human dihydrofolate reductase with substitutions of leucine 22: kinetics, crystallography, and potential as selectable markers. *J Biol Chem* 1995; 270:5057-5064.

23. Chunduru SK, Cody V, Luft JR, Pangborn W, Appleman JR, Blakley RL: Methotrexate-resistant variants of human dihydrofolate reductase: effects of Phe31 substitutions. *J Biol Chem* 1994; 269:9547-9555.

24. Nakano T, Spencer HT, Appleman JR, Blakley RL: Critical role of phenylalanine 34 of human dihydrofolate reductase in substrate and inhibitor binding and in catalysis. *Biochemistry* 1994; 33:9945-9952.

25. Thompson PD, Freisheim JH: Conversion of arginine to lysine at position 70 of human dihydrofolate reductase: generation of a methotrexate-insensitive mutant enzyme. *Biochemistry* 1991; 30:8124-8130.

26. Morris JA, McIvor RS: Saturation mutagenesis at dihydrofolate reductase codons 22 and 31: a variety of amino acid substitutions conferring methotrexate resistance. *Biochem Pharmacol* 1994; 47:1207-1220.

27. Dicker AP, Waltham MC, Volkenandt M, Schweitzer BI, Otter GM, Schmid FA, Sirotnak FM, Bertino JR: Methotrexate resistance in an in vivo mouse tumor due to a non-active-site dihydrofolate reductase mutation. *Proc Natl Acad Sci U S A* 1993; 90:11797-11801.

28. Beard WA, Appleman JR, Huang SM, Delcamp TJ, Freisheim JH, Blakley RL: Role of the conserved active site residue tryptophan-24 of human dihydrofolate reductase as revealed by mutagenesis. *Biochemistry* 1991; 30:1432-1440.

29. Appleman JR, Prendergast N, Delcamp TJ, Freisheim JH, Blakley RL: Kinetics of the formation and isomerization of methotrexate complexes of recombinant human dihydrofolate reductase. *J Biol Chem* 1988; 263:10304-10313.

Préface au chapitre 4

Les variantes de la DHFRh hautement résistantes au MTX offrent la possibilité d'améliorer les techniques actuelles de sélection de cellules hématopoïétiques souches transduites avec un gène thérapeutique. Ayant obtenu de nouvelles variantes combinatoires procurant une résistance accrue au MTX dans un modèle cellulaire (chapitre 2), nous avons testé le potentiel des variantes hautement résistantes au MTX en tant que marqueurs de sélection pour enrichir les cellules hématopoiétiques transduites. Ces cellules offrent plusieurs perspectives cliniques pour le traitment de maladies du système sanguin et certains types de cancers. En transduisant les variantes de la DHFRh hautement résistantes au MTX dans des cellules de la moelle osseuse isolées de souris, nous avons démontré qu'il était possible d'enrichir sélectivement les cellules transduites contenues dans une population de cellules hématopoïétiques lors d'expériences de compétition *ex vivo,* en présence d'une forte concentration de MTX. La sélection *ex vivo* devenait plus stringente en utilisant des milieux de culture dépourvus de nucléotides. De plus, nous avons démontré que la sélection se produisait également au niveau des cellules hématopoïétiques souches, essentielles à l'application clinique de la thérapie génique pour corriger des maladies du système sanguin. Les cellules hématopoiétiques souches transduites ont pu reconstituer de façon considérable la moelle osseuse de souris ayant reçu des greffes des cellules soumises au processus de sélection. L'application des variantes de la DHFRh hautement résistantes au MTX en tant que marqueurs de sélection pour les cellules de la moelle osseuse offre des perspectives intéressantes pour amplifier la proportion de cellules transduites avant la greffe, augmentant les chances de reconstitution de la moelle par ces cellules.

Ce chapitre est présenté sous forme d'article scientifique soumis à la revue *Experimental Hematology* en mars 2009. Ayant participé à tous les aspects de recherches expérimentales et théoriques de cette étude, ma contribution à ce projet est majeure. Une aide et des conseils techniques offerts par Nadine Mayotte, agente de recherche au laboratoire de notre collaborateur, le Dr. Guy Sauvageau, justifie sa présence en tant que deuxième auteure.

Chapitre 4

Sélection *ex vivo* de cellules hématopoiétiques transduites avec des doubles et triples variantes de la DHFRh hautement résistantes au MTX

4.1 Article 3. *Ex vivo* selection of hematopoietic cells using highly MTX-resistant human dihydrofolate reductase double and triple variants

Ex vivo selection of hematopoietic cells using highly MTX-resistant human dihydrofolate reductase double and triple variants

Jordan P. Volpato[1], Nadine Mayotte[2], Guy Sauvageau[2] and Joelle N. Pelletier[1,3]

[1]Département de Biochimie, [2]Institut de recherche en cancérologie et immunologie (IRIC) and [3]Département de Chimie

Université de Montréal

C.P. 6128, Succursale Centre-Ville

Montréal (Québec)

H3C 3J7 CANADA

Submitted to *Experimental Hematology* (March 2009)

Summary

Objective. Ex vivo selection of transduced HSC with drug-resistance genes offers the possibility to enrich transduced cells prior to engraftment, toward increased reconstitution in transplant recipients. We have evaluated the potential of methotrexate (MTX)-resistant variants of human dihydrofolate reductase (hDHFR) for this application in murine hematopoietic cells.

Materials and Methods. Wild-type hDHFR, MTX-resistant hDHFR double or triple mutants or the control point mutant L22Y were transduced into murine bone marrow cell populations. *Ex vivo* selection was performed against MTX. Repopulation potential of transduced HSC following selection was evaluated in recipient mice.

Results. MTX-resistant hDHFR variant F31R/Q35E, F31A/F34V/Q35H and F31R/F34T/Q35S conferred full protection from MTX-cytotoxicity to transduced myeloid progenitors following 10 days exposure to MTX. Bone marrow cells including 15% cells infected with F31R/Q35E were enriched to 98% transduced cells within 6 days of *ex vivo* selection. In a preliminary experiment, SLAM cells including 19% cells infected with F31R/Q35E, selected for 2 days with MTX and transduced with Nup98-HoxA10HD, allowed long-term reconstitution of murine recipients to 40% at a dilution of 1:4.

Conclusion. Myeloid progenitors and more differentiated hematopoietic cells transduced with MTX-resistant hDHFR variants were enriched *ex vivo* after a short selection with MTX. HSC were also enriched following selection.

Introduction

A major obstacle to effective gene therapy for treatment of hematologic disorders is low transduction efficiency, translating into low repopulation of transduced hematopoietic stem cells (HSC) in bone marrow niches following engraftment in irradiated recipients [1]. Transduction of a drug-resistance gene in HSC offers the possibility to enrich the transduced cells, by administration of the corresponding myelo-suppressive chemotherapy agent prior to or following engraftment. The transduced cells have a selective advantage and withstand cytotoxic effects, thereby enriching the transduced population.

A number of drug-resistance enzymes, and particularly drug resistant O^6-methylguanine-DNA-methyltransferase (MGMT) [2-4] and human dihydrofolate reductase (hDHFR) variants [5-7], have been tested for these applications. Although those two systems confered chemoprotection as well as enrichment of transduced hematopoietic cells *in vivo*, safety concerns have halted the clinical application of MGMT, as the selective drugs are DNA-alkylating agents for which the long-term side effects are poorly documented [8]. Enrichment of HSC transduced with drug-resistant hDHFRs offers a greater clinical potential: antifolates are widely used and their side effects are well characterized and readily minimized with leucovorin rescue treatment [9,10].

hDHFR catalyzes the reduction of 7,8-dihydrofolate (DHF) to 5,6,7,8-tetrahydrofolate (THF). THF is an essential cofactor for *de novo* synthesis of nucleotides in proliferating cells. Antifolates are chemotherapy agents that target folate utilizing-enzymes such as hDHFR. Targeting DHFR activity has proven effective for inhibiting cell proliferation, making antifolates key compounds for treatment of cancers and other proliferative diseases [11]. The most clinically-relevant antifolate is methotrexate (MTX), currently used to treat various forms of cancers [12-15] and auto-immune diseases [16,17]. MTX exhibits cytotoxicity toward hematopoietic cell lines [10,18], making it a candidate drug for enrichment of bone marrow populations transduced with a MTX-resistance gene.

Ideal MTX-resistant hDHFR variants must maintain sufficient catalytic activity to ensure cell survival, while displaying important decreases in MTX affinity to ensure drug-resistance. Efficient *in vivo* enrichment of bone marrow cells transduced with hDHFR variant L22Y has been demonstrated in the mouse model using MTX or trimetrexate (TMTX) combined with nucleoside transport inhibitors [6,19,20]. Variant L22Y is a benchmark, being the first drug-resistance gene to allow selection of transduced HSC. However, *in vivo* enrichment was only transient when assayed in non-human primates [21]. The ineffective selection was attributed to differences in the frequency of HSC cell cycling, which is higher in mice than in primates [22]. Given the similar properties of non-human primate and human HSC [22], *in vivo* enrichment of transduced bone marrow cells may not be efficient for clinical enrichment of engrafted stem cells. Enriching transduced cells in bone marrow populations *ex vivo* prior to engraftment could bypass current transduction efficiency setbacks.

In that approach, HSC from isolated bone marrow cells are expanded *ex vivo*, infected with a retrovirus harbouring a drug-resistance gene, selected with a cytotoxic drug, and engrafted into lethally irradiated animal recipients. The main limitation is the time during which *ex vivo* cultured HSC maintain self-renewal properties: only 4-8 days for muring HSC following retroviral transduction [23]. Thus, successful *ex vivo* selection must occur within this timeframe.

Prior *ex vivo* selection studies on transduced bone marrow cells were performed with various hDHFR variants, mostly as a model to evaluate the potential of *in vivo* chemoprotection or enrichment of hematopoietic cells for a given variant [24-28]. A promising variant was the doubly-substituted L22F/F31S [29]. This variant displayed a greater decrease in MTX-affinity than variant L22Y [30], while maintaining sufficient catalytic activity to ensure cell proliferation. Approximately 75% of L22F/F31S transduced murine hematopoietic cells survived at a moderate dose of MTX (100 nM) after 12 days of *ex vivo* MTX-selection on myeloid progenitor assays [31]. Human $CD34^+$ cells transduced

with that variant and selected against MTX in liquid culture were fully protected from cytotoxicity at a moderate concentration (50 to 200 nM). Long-term culture-initiating cells were present after selection, suggesting that *ex vivo* selection could be used to enrich cells with reconstitutive potential [32,33]. Nonetheless, *ex vivo* MTX-selection of murine or human hematopoietic cells has never led to increased reconstitution of transduced cells in myelo-ablated animal recipients [34-36]. It appears that the time required for efficient selection exceeded the *ex vivo* life-span of HSC. To be successful, more rapid *ex vivo* selection is required. hDHFR variants with weaker MTX-affinity may enable more rapid *ex vivo* selection of HSC at high MTX concentrations. In addition, MTX-resistant variants ensuring cell survival at high MTX concentrations could also be applied to hematopoietic cell gene therapy to protect bone marrow cells from MTX cytotoxicity during chemotherapy, and could increase the clinical index of the inhibitor.

We recently reported highly MTX-resistant hDHFRs obtained *via* semi-random mutagenesis [37]. The most highly resistant variants contained combinatorial substitutions at active-site residues F31, F34 and/or Q35. CHO *dhfr*$^-$ cells transfected with variants F31R/Q35E (RFE), F31S/Q35E (SFE), F31R/F34T/Q35S (RTS) and F31A/F34V/Q35H (AVH) survived and proliferated at high concentrations of MTX. In the case of variant AVH, >70% of the cell population survived at 200 μM MTX within 48 hrs of selection, during which the negative control cells had died. This constituted the most resistant hDHFR variant reported in the CHO *dhfr*$^-$ cell line. Here, we evaluate the level of protection conferred by combinatorial hDHFR variants RFE, SFE, RTS and AVH as well as their application as *ex vivo* selection markers for enrichment of murine hematopoietic cells, including HSC. We demonstrate that the hDHFR variants used in this study are suited for *ex vivo* selection of hematopoietic cells prior to engraftment as well as for myeloprotection applications.

Materials and methods

Reagents - Cell culture liquid media were purchased from Invitrogen (Burlington, ON), unless stated otherwise. Restriction enzymes were purchased from MBI Fermentas (Burlington, ON) or Invitrogen. Methotrexate (MTX) was purchased from Sigma-Aldrich (Oakville, ON).

Animals – Bone marrow donors were C57BL/6J (CD45.2) mice, competitor/recipients were C57BL6/Pep3b (CD45.1) and helper cell donors were c-kit $^{w41-/w41-}$ (CD45.2) mice. Animals were housed in ventilated micro-isolator cages and provided with sterilized food and acidified water.

Retroviral vector constructs - The cDNAs encoding WT hDHFR and hDHFR variants L22Y, RFE, SFE, RTS and AVH were initially in vector pcDNA3.1(+) as described in [37]. The cDNAs were subcloned between *Eco*RI and *Xho*I sites of MSCV(-) retroviral vector (Clontech Laboratories, Mountain View, CA) containing an IRES-GFP insertion between the *Xho*I and *Cla*I sites (MIG vector) [38]. The Nup98-HoxA10HD-MIG construct is described in [39].

Amphotropic and ecotropic virus production - MIG vectors harbouring hDHFR variants were transfected into amphotropic vesicular stomatitis virus (VSV) pseudotyped retrovirus packaging cells 293 GPG [40] using Lipofectamine 2000 (Invitrogen). The MIG vector (no insert) was used as a negative control for all experiments. Prior to transfection, 5×10^5 packaging cells were propagated for 18 hrs on 10-cm plates (to 70% confluence) in Dulbecco's Modified Eagle Medium (DMEM) + 10% heat-inactivated fetal bovine serum (HIFBS) + 5 μg/mL tetracycline (Sigma). Plasmid DNA (20 μg) was mixed with 2.5 μg each of *gag-pol* and *VSV-G* vectors [40] and 40 μL of Lipofectamine 2000 in Opti-MEM (2 mL final volume). The mixture was incubated at room temperature for 20 minutes and was added to the cells, which were further incubated at 37°C / 5% CO_2 for 5 hrs. The media was replaced by DMEM + 10% HIFBS media and changed daily. GFP signalling was observed

daily for 7 days post-transfection. Viral supernatants were harvested by collecting virus-containing media and storing at 4ºC. Harvesting continued for 7 days, when less than 30% of transfected VSV-G cells remained attached.

The viral supernatants from VSV-G cells were filtered through 0.22µ filters for infection of high-titer, helper free, GP+E-86 ecotropic virus producer cells [41]. GP+E-86 cells were plated at 30% confluence with amphotropic viral supernatant and incubated at 37°C / 5% CO_2 for 72 hrs. Following infection, cells were observed under a UV-lamp inversed microscope for GFP signal. The infected GP+E-86 cells were expanded post-infection in DMEM + 10% newborn calf serum (NCS) and stocks were frozen at -80ºC.

MTX selection of infected GP+E-86 virus producer cells - Infected GP+E-86 cells containing hDHFR variants were plated at 1×10^3 cells/mL in 6-well plates in presence of DMEM containing 10% NCS with increasing concentrations of MTX (0, 10^1, 10^2, 10^3, 10^4 and 10^5 nM). Cells were incubated for 12 days at 37°C / 5% CO_2 with replacement of medium every 3 days. Following MTX-selection, cells were washed three times with 1× PBS and trypsinized using TrypLE. Cells were pelleted at 800 rpm, 8 min, resuspended in 2 mL DMEM + 10% NCS, and counted in presence of trypan blue with a hemacytometer to assess survival.

Retroviral infection of primary bone marrow cells - Bone marrow (BM) cells were harvested from C57BL/6J mice 4 days after intravenous injection of 5-fluorouracil (5-FU; Faulding, Lake Forest, IL) by flushing femurs and tibias with DMEM containing 2% FBS. Flushed cells were pelleted at 800 rpm, 8 min, and resuspended in DMEM containing 15% FBS, 6 ng/mL IL-3, 10 ng/mL IL-6, 100 ng/mL steel factor, 10^{-4} M β-mercaptoethanol, 10 µg/mL ciprofloxacin (Fluka, Oakville, ON) and 50 µg/mL gentamycin (BM medium). Cells were pre-stimulated at a density of 1×10^6 cells/mL in BM medium for 48 hrs at 37°C / 5% CO_2. Cells were recounted in 3% acetic acid solution with a hemacytometer and plated at 1×10^6 cells/mL in co-culture with a monolayer of irradiated GP+E-86 virus producer cells in the presence of 6 µg/mL hexadimethrine bromide (polybrene) (Sigma) for 48 hrs at 37°C /

5% CO_2. Following co-culture, cells were harvested and recounted for clonogenic progenitor assays and selection in presence of MTX.

Ex vivo MTX selection using myeloid clonogenic progenitor assays - Infected BM cells were plated in 35 mm dishes at a concentration of 5×10^3 cells/mL in 1.1 mL of 1.1% methylcellulose in DMEM medium supplemented with 3% fetal calf serum (FCS), 6% deionized bovine serum albumine (BSA), 2 mM L-glutamine, 200 μg/mL transferrin, 5 U/mL erythropoietin, 50 ng/mL steel factor, 10 ng/mL IL-3, 10 ng/mL IL-6 and 10^{-4} M β-mercaptoethanol (MC media), in presence or absence of 500 nM MTX. Colonies were scored after 12 days incubation at 37°C / 5% CO_2 using normal and GFP-fluorescence microscopy.

Ex vivo competition assay using MTX selection in minimal BM media - MIG, WT hDHFR-MIG or hDHFR RFE-MIG transduced BM cells from C57BL/6J mice were diluted to 15% with mock-infected BM cells from C57BL/6J mice. Prior to dilution, GFP signal of co-cultured BM cells was analyzed by flow cytometry to assess the percentage of infection of each construct. The cell population was plated at 2×10^5 cells/mL in 35 mm plates, in α-MEM containing 15% dialyzed FBS, 6 ng/mL IL-3, 10 ng/mL IL-6, 100 ng/mL steel factor, 10^{-4} M β-mercaptoethanol, 10 μg/mL ciprofloxacin and 50 μg/mL gentamycin (minimal BM medium) in presence or absence of 1 μM MTX. Cells counts at 0, 2, 4, 6 and 8 days were performed as described above. Myeloid clonogenic progenitor assays were performed for all time points, by plating 5×10^3 cells/mL in 35 mm plates. Colonies were scored after 10 days incubation at 37°C / 5% CO_2 using normal and GFP-fluorescence microscopy.

Dilution repopulation assay in murine recipients for sorted SLAM cells following MTX selection in minimal BM medium - Total BM populations from C57BL/6J and Pep3B mice were incubated with anti-Gr1-APC, anti-Ter119-APC, anti-B220-APC, anti-CD48-FITC, anti-Sca-PE and anti-CD150-PE antibodies at 4ºC for 1h. Following incubation, APC-positive cells were sorted out. PE-positive cells ($CD150^+CD48^-$) were isolated from the

remaining population (SLAM cells [42]). Sorted BM C57BL (CD45.2) cells were infected by co-culture with GP+E-86(hDHFR RFE) while sorted BM Pep3B (CD45.1) cells were mock-infected, in a 96-well format, and incubated at 37°C / 5% CO_2 for 72 h in BM medium + polybrene (6 μg/mL). GFP^+ (Ly5.2) BM C57BL/6J (CD45.2) cells were sorted by flow cytometry, and diluted to 19% infected cells with mock-infected Pep3B (CD45.1) BM cells (competitors). This cell population was incubated in a 96-well format at 37°C / 5% CO_2 for 2, 4 or 6 days of selection in minimal BM medium containing 1μM MTX. Following MTX selection, cells were harvested by centrifugation (500 rpm, 5 min at 4ºC) and resuspended in BM medium. Cells were then co-cultured with GP+E (Nup98-HoxA10HD) in a 96-well format and incubated at 37°C / 5% CO_2 for 48 h in BM medium + polybrene (6 μg/mL). Cells were harvested as described above and resuspended in BM medium. Cell populations were diluted to 1:4 and 1:25 with BM medium and injected in the tail-vein of sub-lethally irradiated Pep3B mice (2 mice per dilution). All dilutions were mixed with 2×10^5 c-kit $^{W41-/W41-}$ mouse helper cells. Myeloid clonogenic progenitor assays were conducted in parallel, to evaluate infection rate and survival of cells after selection. For these assays, cells were plated on MC medium at 1:50 and 1:12.5 dilutions from the initial populations in 24-well plates. Colonies were scored after 10 days incubation at 37°C / 5% CO_2 using normal and GFP-fluorescence microscopy. Repopulation experiments were performed in triplicate, in three independent experiments (A, B and C).

The presence of GFP^+ CD45.2 and CD45.1 cells was evaluated by monitoring GFP signalling in peripheral blood samples isolated from the tail-vein of recipient mice, at 12 weeks post-injection. Blood samples were treated with 1× erythrocyte lysis buffer for 10 minutes at 4°C and washed twice with 1× PBS + 2% FCS. Prior to FACS analysis, cells were stained with anti-CD45.1-PE and anti-CD45.2-APC for 30 minutes at 4°C and washed with 1× PBS + 2% FCS to discard unbound antibodies.

Retroviral integration was verified in NheI-digested genomic DNA from BM, spleen and thymus cells by Southern blot using a ^{32}P-labelled GFP probe. Number of

integrations and clonality were similarly assessed using EcoRI-digested DNA. Cell morphology was assessed by Wright staining of cytospin preparations of BM cells.

Results

MTX selection of infected GP+E-86 virus producer cells and infected bone marrow (BM) cells – The effect of the highly MTX-resistant hDHFR variants RFE, SFE, RTS or AVH was evaluated towards transduced GP+E-86 ecotropic virus producer cells and isolated hematopoietic cells. The hDHFR variant L22Y was the positive control for MTX-resistance. hDHFR L22Y has been shown to confer MTX-resistance in various cell lines, including 3T3 cells [28,29,43]. MIG and MIG-WT hDHFR served as negative controls. Infection efficiency was >99% for all constructs as assessed by GFP fluorescence. No significant difference in GFP fluorescence intensity was observed, suggesting that the bicistronic vector was expressed at similar levels by all constructs. MTX resistance in GP+E-86 cells was determined by plating infected cells with increasing concentrations of MTX (0-100 μM). The EC_{50}^{MTX} for cells infected with any hDHFR variant were > 2 orders of magnitude higher than the negative controls (Figure 4.1A; Table 4.1). Double mutant SFE conferred MTX-resistance in the same range as the benchmarking variant L22Y, while variants RTS, RFE and AVH conferred higher MTX resistance (> 1 order of magnitude higher). Previous reports have shown that the degree of chemoprotection conferred by a given MTX-resistant variant in adherent cells correlated well with that obtained in bone marrow cells [27,28,44]. The results obtained for the GP+E-86 cells suggested that variants RFE, RTS and AVH could confer greater myeloprotection at high MTX concentrations than variant L22Y.

To verify the level of chemoprotection conferred by the highly MTX-resistant hDHFR variants, bone marrow (BM) cells harvested from 5-FU treated mice were infected with the variants. Infection rates ranged between 50-60% for each construct (data not

Table 4.1. EC_{50}^{MTX} for GP+E-86 cells transduced with hDHFR variants.

Construct	EC_{50}^{MTX} (μM)[a]
MIG	0.017 ± 0.001
WT-MIG	0.096 ± 0.064
L22Y-MIG	4.7 ± 1.6
SFE-MIG	6.8 ± 1.8
RFE-MIG	>100
RTS-MIG	>100
AVH-MIG	>100

[a] Mean ± SD, based on 3 independent experiments.

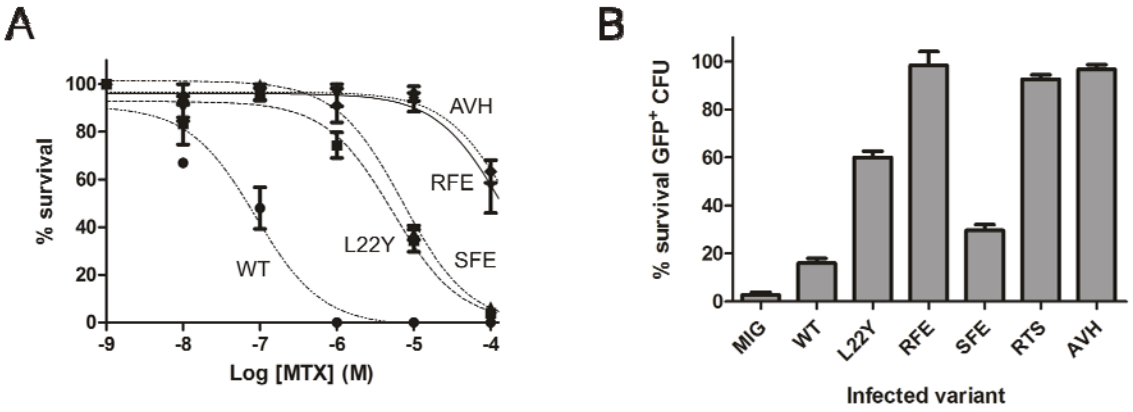

Figure 4.1. MTX-resistance of GP+E-86 cells infected with hDHFR variants. A) GP+E-86 cells infected with WT hDHFR, L22Y, SFE, RFE, or AVH were exposed to MTX for 12 days. GP+E-86 cells infected with MIG vector or mock-infected cells were used as negative controls (not shown). The percentage of survival is the ratio of cells counted in presence *vs* absence of MTX. Variant RTS (data not shown) gave results similar to those of variant RFE. Results are given for the average of 3 independent experiments. B) Clonogenic progenitor assays of infected BM cells exposed to 500 nM MTX. Bone marrow (BM) cells infected with WT hDHFR, point mutant L22Y or variants SFE, RFE, RTS or AVH were plated at 5×10^3 cells/mL on semi-solid methylcellulose media in presence or absence of 500 nM MTX. BM cells infected with MIG vector or mock-infected (not shown) were used as negative controls. After 12 days incubation, colonies were scored using GFP-fluorescence microscopy. The percentage of survival is the ratio of GFP^+ colonies in presence *vs* absence of MTX. Results are given for the average of 3 independent experiments.

shown). In parallel, infected BM populations were subjected to myeloid progenitor assays with 500 nM MTX to evaluate the myeloprotection conferred by the hDHFR variants. Following a 12-day incubation, GFP^+ colony-forming units (CFU) were scored. BM progenitor cells infected with hDHFR variants RFE, RTS and AVH were fully protected from cytotoxicity (Figure 4.1B). The L22Y positive control conferred partial protection, allowing 60% survival of the infected CFU, while variant SFE conferred the lowest protection (< 30% survival), barely greater than WT hDHFR (< 20% protection). This confirms that MTX-resistance genes can provide high survival of myeloid cells in the presence of MTX. The number and size of CFU scored in absence of MTX was comparable for all constructs, indicating that the MTX-resistant variants did not hinder cell survival and proliferation despite their lower catalytic efficiencies relative to WT DHFR [37]. Survival of mock-infected (data not shown) and MIG-infected CFU was evaluated at < 2% under the same conditions.

Ex vivo MTX selection of BM cells in liquid culture – Preliminary experiments (Annexe 1, Figure A1.1) toward using the hDHFR variants as *ex vivo* selection markers for BM cells demonstrated that mutant RFE was the best candidate for *ex vivo* BM cell-selection, as it conferred full protection to infected BM cells at a high dose of MTX after a 4-day selection period. The short selection period was chosen to maintain the self-replication properties of HSC for bone marrow repopulation following engraftment [23]. Another series of experiments (Annexe 1, Figures A1.1B and A1.1C) suggested that it was possible to enrich infected HSC and progenitor cells *ex vivo* in a cell population initially containing 25% infected BM cells, and engraft the selected cells into host mice. Despite apparent selection of infected BM cells, uninfected BM cells were still present after the 4-day selection, albeit in a lower proportion.

The *ex vivo* selection strategy was fine-tuned to reduce background survival of uninfected BM cells. Previous results *in vivo* selection in mice using MTX-resistant genes were improved by co-administering a nucleoside inhibitor during antifolate selection [6,19]. HSC and early progenitor cells have a thymidine rescue pathway allowing host stem cells to tolerate the doses of antifolate administered during *in vivo* enrichment [45]. The medium used in the selection experiment described above contained nucleotides, potentially contributing to the survival of uninfected BM cells. Liquid medium lacking nucleotides was thus used to improve selection stringency. BM cells infected with MIG, WT hDHFR or variant RFE were exposed to 1 μM MTX for up to 8 days. The selection was undertaken after dilution of infected cells to 15% with mock-infected BM cells, to investigate competition by the infected cells. The absence of nucleotides in the medium did not hinder cell proliferation, as the cell population increased in absence of MTX for all constructs, the highest cell density being reached after 6 days (Figure 4.2A). In presence of 1 μM MTX, BM cells infected with MIG and WT hDHFR decreased with time, whereas cells infected with RFE proliferated steadily (Figure 4.2B). Flow cytometry confirmed that infected, GFP^+ cells comprised ≥ 92% of the RFE-selected sample after 4 days (Figure 4.2C).

To quantify the myeloid progenitor cells remaining after exposure to MTX, selected BM populations were subjected to myeloid progenitor assays after each day of selection. In contrast to the propagation of BM cells in absence of MTX (Figure 4.2A), CFU increased between days 0 and 2, then decreased until day 8 (Figure 4.3). The effects of MTX on myeloid progenitor cells were seen at the onset of selection, as the CFU after 2 days exposure to MTX was < 50% of CFU in absence of MTX for all constructs. Despite the decreasing CFU, an enrichment of GFP^+ cells was observed in myeloid progenitors transduced with RFE following MTX-selection (Figure 4.3, days 2 to 6). However, the low number of myeloid progenitor cells remaining after ≥ 6 of selection suggested that the number of HSC remaining would be insufficient for engraftment; a shorter selection period

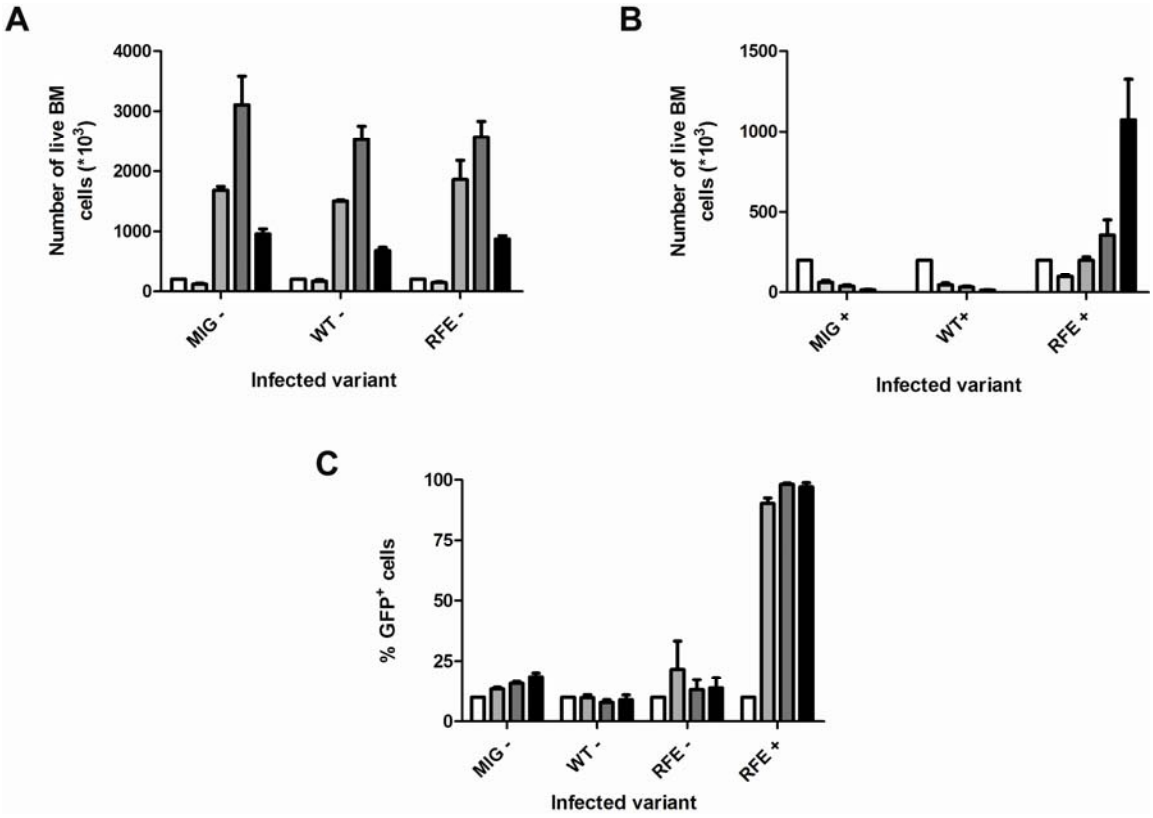

Figure 4.2. Time-course of *ex vivo* MTX-selection of murine BM cells in minimal medium. BM cells infected with MIG, WT hDHFR and RFE were diluted to 15% with mock-infected BM cells according to GFP fluorescence. Cells were plated in minimal BM medium, in the absence (-; Panel A) or presence (+;Panel B) of 1 μM MTX. Live cells were scored with trypan blue (average of 3 independent experiments). In the presence of MTX, only the cells infected with the MTX-resistant RFE variant of hDHFR survived and replicated (Panel B). Selection of resistant *vs* sensitive cells was significant at day 2 (□), important at days 4 (▒) and 6 (■) and essentially complete at day 8 (■) relative to initial conditions at day 0 (□) (Panel A *vs* Panel B). Flow cytometry analysis confirmed that the RFE-infected, selected cells were ≥ 92% GFP^+ from 4 days on (Panel C).

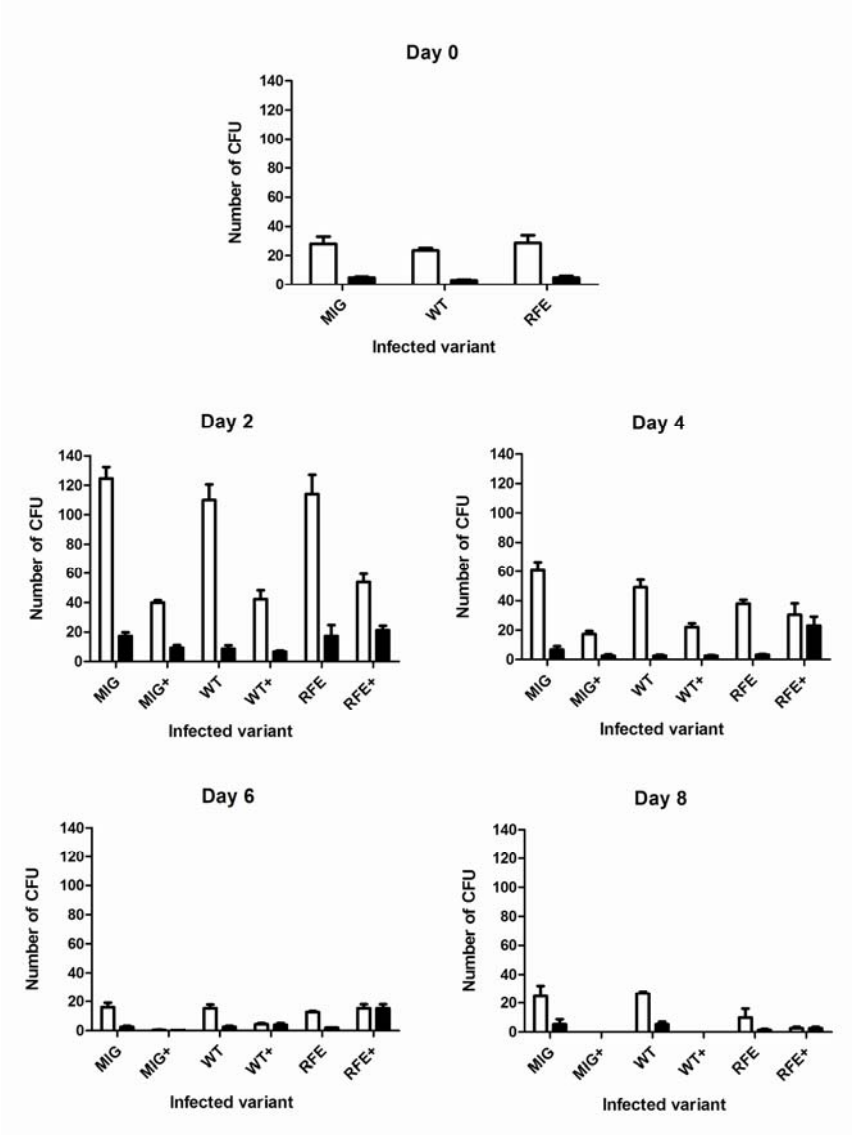

Figure 4.3. Myeloid clonogenic progenitor assays of infected BM cells following MTX selection in minimal liquid medium. Myeloid clonogenic progenitor assays were performed to quantify the survival of myeloid progenitor cells after MTX selection in minimal BM medium. Visible colonies (white bars) and GFP^+ colonies (black bars) were scored for days of selection 0, 2, 4, 6 and 8.

(< 6 days) may present a better balance between enrichment of the transduced cells and cell fitness for this population.

Efficiency of MTX selection on HSC and progenitor cells – As demonstrated above, myeloid progenitors were selected in the population of BM cells. However, the effect of the selection on HS cells, which dictate reconstitution of engrafted animals, was not directly demonstrated. To gain insight into the effect of MTX selection on HS cells, we performed a preliminary experiment toward engraftment of mice with selected cells. SLAM cells [42] were isolated by flow cytometry in BM populations from C57BL/6J mice and infected with variant RFE. Transduction efficiency was evaluated to be 70%, indicating that SLAM cells were in cycle during the infection period. In parallel, SLAM cells were isolated from Pep3B mice and mock-infected with GP+E-86 cells. The infected GFP^+ C57BL/6J ($CD150^+CD48^-$) cells were sorted by flow cytometry and mixed with Pep3B mock-infected ($CD150^+CD48^-$) cells to provide approximately 20% GFP^+ cells in the mixed populations. This dilution was undertaken to verify competition by the RFE-infected cells during selection.

The mixed populations were exposed to 1 μM MTX in medium lacking nucleotides for 2, 4 or 6 days. Following selection, cells were co-cultured with GP+E-86 cells producing Nup98-HoxA10HDHD-MIG virus. Nup98-HoxA10HD encodes a transcription factor that promotes HSC self-renewal *ex vivo* and following engraftment [39] [46]. Because the selection had proven to be stringent on myeloid progenitor and presumably on HS cells (Figures 4.2 and 4.3), infection with Nup98-HoxA10HD was added to the selection protocol to amplify HSCs surviving the selection procedure. After infection with Nup98-HoxA10HD, the reconstitution potential of 2 and 4-day MTX-selected cells was assessed by engrafting two cell dilutions (1:4, 1:25) into irradiated Pep3B mice. *c-kit*$^{-/-}$cells from $W41^-/W41^-$ mice were co-engrafted as helper cells [47], to give an additional reconstitution advantage to the selected cells.

Following infection with RFE, MTX selection and infection with Nup98-HoxA10HD, a fraction of the cells were subjected to myeloid progenitor assays to evaluate the effect of the selection protocol on myeloid cells (Figure 4.4A). Myeloid progenitor assays at a dilution of 1:12.5 showed a decrease in CFU according to the length of MTX selection, seen markedly between days 4 and 6 of selection. Enrichment of GFP^+ cells was observed after only 2 days of MTX selection, where more than 88% of cells were GFP^+ (relative to 19% at day 0). After 4 and 6 days of MTX-selection, > 99% myeloid progenitors were GFP^+. This did not confirm that the selection of BM C57BL cells was efficient, as the Nup98-HoxA10HD retrovirus also contained a GFP cassette.

Peripheral blood from engrafted mice was collected at 12 weeks post-injection and analyzed by flow cytometry (Figure 4.4B). Blood cells were doubly-labelled with anti-CD45.1-PE and anti-CD45.2-APC to discriminate between cells originating from Pep3B and C57BL/6J mice, respectively. Four distinct cell populations were observed: $CD45.2^+$ cells, $CD45.2^+/GFP^+$ cells, $CD45.1^+$ cells and $CD45.1^+/GFP^+$. Considering that engrafted cells were essentially all GFP^+ after 2 days selection with MTX, we concluded that $CD45.2^+$ cells without GFP signal resulted from reconstitution with $W41^-/W41^-$ mouse helper cells, while $CD45.1^+$ cells without GFP signal resulted from reconstitution by the endogenous BM Pep3B cells. To evaluate the enrichment of RFE-infected HS cells following engraftment, the ratio of $CD45.2^+/GFP^+$: $CD45.1^+/GFP^+$ was calculated for each dilution for the two *ex vivo* MTX-selection periods. At dilution 1:4, the ratio of $CD45.2^+/GFP^+$: $CD45.1^+/GFP^+$ was roughly 1:1 for all selection periods. Because the original ratio of RFE-infected $CD45.2^+$ cells to uninfected $CD45.1^+$ cells had been 1:4, this illustrated that even the 2-day MTX-selection had been efficient, allowing approximately 4-fold enrichment of $CD45.2^+/GFP^+$ cells relative to $CD45.1^+/GFP^+$ cells. At LDA 1:25, the ratio of $CD45.2^+/GFP^+$: $CD45.1^+/GFP^+$ increased to (3:1) at 2 days of MTX selection. Similar ratios were observed at 4 days of MTX selection (2:1). The percentage of reconstitution by GFP^+ cells decreased with increasing length of *ex vivo* selection (2 day

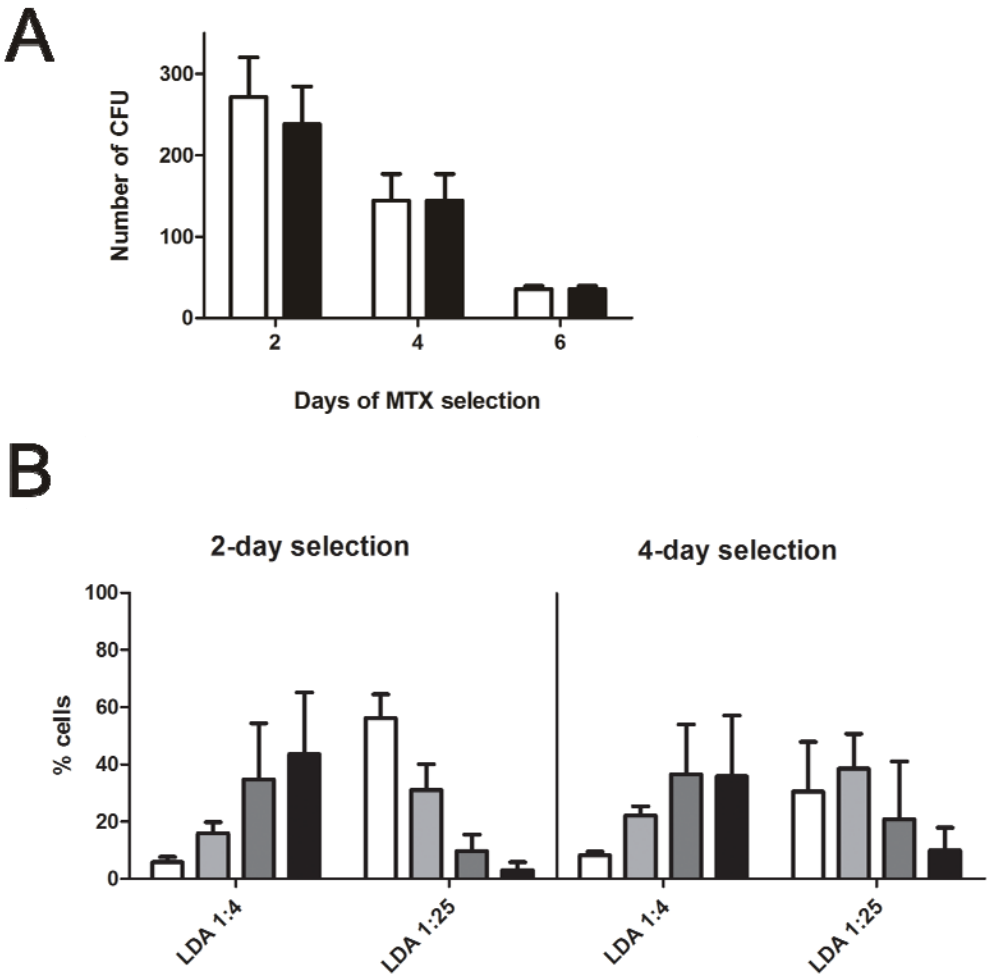

Figure 4.4. Effect of MTX-selection on HS and progenitor cells. A) Myeloid clonogenic progenitor assays of $CD150^{+}CD48^{-}$ cells infected with mutant RFE, selected with MTX, and infected with Nup98-HoxA10HD. Results are shown for LDA of 1:12.5. Visible colonies (white bars) and GFP^{+} colonies (black bars) were scored after 2, 4 and 6 days of selection with 1 μM MTX, in three independent experiments. B) Flow cytometry analysis of murine peripheral blood samples 12 weeks post-injection with $CD150^{+}CD48^{-}$ cells infected with mutant RFE, selected with 1 μM MTX, and infected with Nup98-

HoxA10HD. Cells were labelled with anti-CD45.2 (LY5.2)-APC and anti-CD45.1 (LY5.1)-PE antibodies prior to flow cytometry analysis. Percentages for $CD45.2^+$ (□), $CD45.1^+$ (▒), $CD45.2^+/GFP^+$ (▓) and $CD45.1^+/GFP^+$ (■) cells are reported. Analysis was conducted on mice having received different cell dilutions (1:4 or 1:25; 2 mice per dilution) following 2-day or 4-day *ex vivo* selection with 1 μM MTX. Results are given for the average of three independent experiments.

selection > 4 day selection), consistent with the supposition that the number of HSC decreased during *ex vivo* selection (Figure 4.5).

Southern blot analysis of 5 animals with high $CD45.2^{+}/GFP^{+}$ reconstitution (> 40%) demonstrated that the RFE and Nup98-HoxA10HD transgenes were present in BM, spleen and thymus cells following long-term reconstitution (Figure 4.5). Some rearrangements were observed when probing with GFP for viral integration of both constructs (Figure 4.5A). However, cytospin preparations of BM cells revealed no pre-leukemic or leukemic cells, suggesting that these rearrangements were benign. The number of integrations suggests that the animals were reconstituted by polyclonal cell populations (Figure 4.5B).

Discussion

We have successfully demonstrated that highly MTX-resistant hDHFR variants can be used as selectable markers for rapid *ex vivo* enrichment of hematopoietic cells following transduction of a MTX-resistance gene and selection with a high concentration of MTX. As a prelude to the experiments with bone marrow cells, GP+E-86 virus producer cells infected with variants RFE, RTS and AVH and exposed to 10 μM MTX proliferated as well as untreated cells following a 12-day selection experiment (Figure 4.1A). EC_{50}^{MTX} values (Table 4.1) for GP+E-86 cells infected with these variants were greater than the highest concentration of MTX used (100 μM). While those results were obtained following a 12-day selection, the effects of MTX toxicity on negative controls were seen within 2 days of selection (data not shown). The variants that conferred the highest EC_{50}^{MTX} values in GP+E-86 cells also conferred the greatest chemoprotection from MTX to transduced BM cells, as determined by myeloid progenitor assays (Figure 4.1B). Cells transduced with mutants RFE, RTS and AVH formed colonies on methylcellulose medium containing 500 nM MTX, a concentration ≥ 5-fold higher than similar experiments performed with other MTX-resistant DHFR mutants [24,26,27,31,44]. The previously described variant L22Y

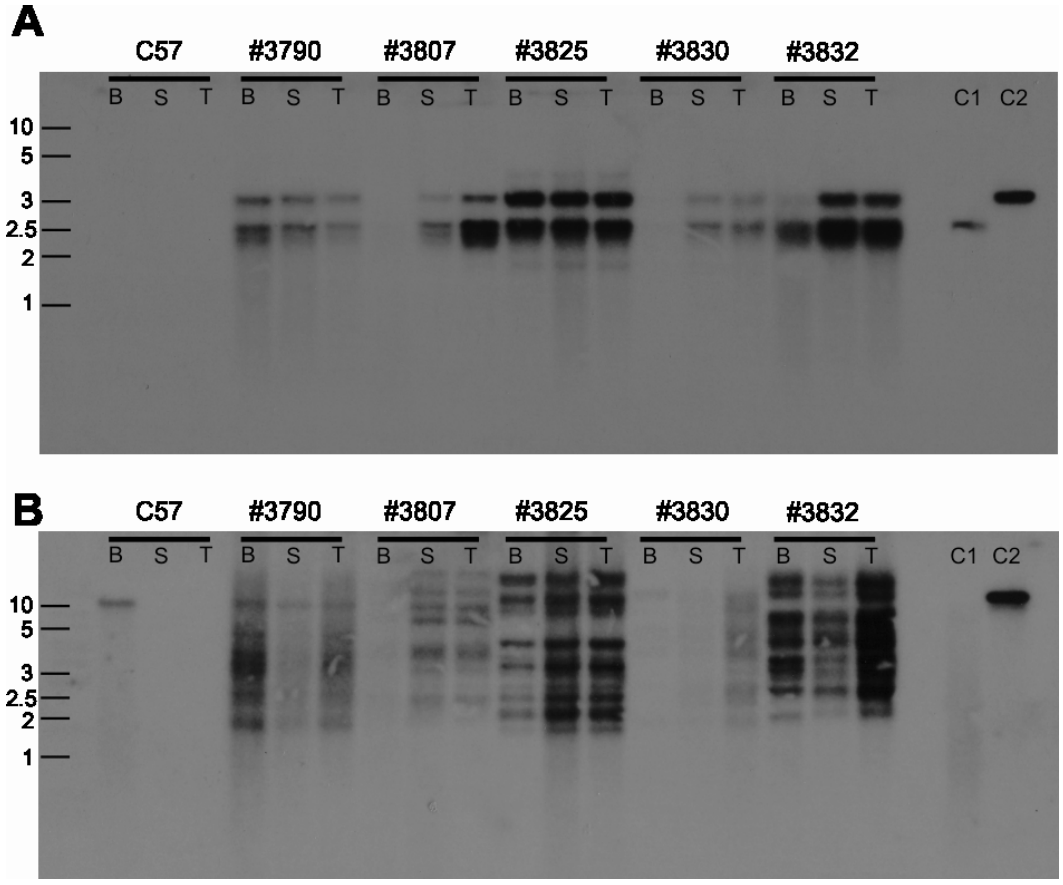

Figure 4.5. Southern blot analysis of genomic DNA from bone marrow, spleen and thymus from five mice reconstituted to > 40% CD45.2^{+}/GFP^{+} cells at different LDAs. Control C57BL/6J and mice # 3790 (2-day selection, dilution 1:4), #3807 (4-day selection, dilution 1:4), #3825 (2-day selection, dilution 1:4), #3830 (4-day selection, dilution 1:4) and #3832 (4-day selection, dilution 1:25) were sacrificed. 15 μg of DNA from bone marrow (B), spleen (S) and thymus (T) was digested with NheI (panel A; pro-viral integration) or EcoRI (panel B; number of insertions) and a ^{32}P-labelled GFP probe was used for detection of DNA. 10 pg of NheI (Panel A) or EcoRI (Panel B) -digested hDHFR RFE-MIG (C1) and Nup98-HoxA10HD-MIG (C2) proviral constructs were the positive controls. Molecular weight of the DNA ladder (in kDa) is indicated on the left side of the blots.

displayed a lower EC_{50}^{MTX} (4.7 μM) than the double and triple mutants in GP+E-86 cells, while it conferred ≈ 60% protection to transduced BM cells at 500 nM MTX. This indicated that higher concentrations of MTX could be used to accelerate selection of cells transduced with the double and triple hDHFR mutants. Accordingly, we had previously observed efficient selection of CHO *dhfr*$^-$ cells transfected with variants RFE, RTS and AVH within 48 hrs of MTX exposure. These data demonstrate that the highly MTX-resistant mutants enable selection of infected cells on a short timespan, an important feature for efficient *ex vivo* enrichment of hematopoietic stem cells prior to engraftment.

Of the three highly MTX-resistant mutants shown to confer high levels of chemoprotection in the myeloid progenitor assay, variant RFE was selected for *ex vivo* selection experiments based on the high survival to transduced BM cells that variant RFE conferred at a high concentration of MTX (1 μM), relative to the benchmark L22Y. The concentration of MTX for *ex vivo* liquid culture selection was increased two-fold relative to the myeloid progenitor assays to increase the selection stringency. Thorough *ex vivo* selection of transduced bone marrow cells was achieved in nucleotide-free liquid culture medium. While cell populations transduced with the different constructs behaved similarly in absence of MTX (Figure 4.2A), only cells transduced with RFE proliferated in presence of 1 μM MTX (Figure 4.2B). From a starting culture of 2×10^6 bone marrow cells containing 15% transduced cells, more than 1×10^6 cells were obtained following 8 days of exposure to MTX (Figure 4.2B). All surviving cells (> 99%) were GFP^+ as confirmed by flow cytometry, demonstrating that only RFE-transduced cells remained following MTX-selection (Figure 4.2C). This indicated that the expression of an active and MTX-resistant hDHFR was the source of the observed survival and proliferation of RFE-transduced cells. Myeloid progenitor assays showed that, despite GFP^+ enrichment in RFE-transfected CFU, the number of CFU decreased as the selection progressed (Figure 4.3). Nevertheless, RFE-transduced CFU were better protected from exposure to MTX relative to control populations.

The effect of *ex vivo* selection on HSC was evaluated *via* a preliminary competitive survival assay, where sorted SLAM cells from donor C57BL/6J mice (CD45.2) were infected with RFE and diluted to 20% with mock-transduced SLAM cells from Pep3B mice (CD45.1) for selection with 1 μM MTX in absence of nucleotides. After 2 days of selection, the relative ratio of CD45.2/GFP$^+$ cells was equal to (LDA 1:4) or greater than (LDA 1:25) CD45.1/GFP$^+$ cells (Figure 4.4B). Considering that the initial ratio of CD45.2/GFP$^+$: CD45.1/GFP$^+$ had been 1:4 (20% RFE-infected cells), an enrichment of ≥ 4-fold took place for RFE-infected HSC during *ex vivo* MTX-selection, though untransduced HSC were not entirely eliminated. To our knowledge, this is the first time that MTX has been reported as an agent that impedes proliferation of untransduced HSC *ex vivo*. Previous studies have proposed that the myelo-ablative effect of MTX is primarily due to the cytotoxic effects of the drug on mature, non-stem cell progenitors and their progeny [48]. These promising results provide us with the information required to conduct a more thorough investigation of the engraftment potential of the *ex vivo*-selected cells.

Some parallels can be drawn between the *ex vivo* selection strategy described here and the *in vivo* strategy described by Allay *et al.* [6]. The combination of an antifolate with a nucleoside transport inhibitor has previously been shown to select and enrich transduced HSC *in vivo* in the murine model [6,19]. The results presented here demonstrate that MTX enables *ex vivo* enrichment of transduced HSC in the absence of nucleotides. In both cases, drug-exposure did not eliminate all untransduced HSC. This is an intrinsic limitation of cell-cycle drugs like MTX. Although most HSC are in cycle in presence of cytokines [49], a subpopulation of HSC may remain quiescent and is therefore not affected by MTX cytotoxicity. Another striking similarity involves the decrease in GFP signal from peripheral blood after cessation of drug treatment observed during *in vivo* selection, which suggested that selection was more efficient for transduced differentiated progenitors rather than for transduced HSC [6]. This correlates well with our results of myeloid progenitor

assays following *ex vivo* selection, where high numbers of GFP^+ CFU were scored after 2 and 4 days, but not 6 days, of MTX-selection (Figure 4.4A).

We have demonstrated the selection of hematopoietic cells transduced with highly MTX-resistant hDHFR variants using an *ex vivo* selection strategy. We rapidly enriched transduced HSC in a competition experiment. Hematopoietic cell lineages, such as more differentiated progenitor cells, were considerably enriched and continued to proliferate following MTX selection. We propose that the *ex vivo* strategy with MTX-resistant hDHFR mutants described herein will be useful for enrichment of transduced hematopoietic cells used for adoptive cell transfer (ACT) [50] or in strategies that use progenitor cells for targeting cancer tumors [51,52]. Approaches such as ACT require a high proportion of transduced T-lymphocytes for effective cancer treatment, and lympho-depletion in the host is required to limit competition for homeostatic cytokines by host lymphocytes [53]. MTX has been shown to deplete lymphocytes following administration at low doses [54,55]. Therefore, it may be possible to enrich transduced T-lymphocytes *ex vivo*, and administer MTX to the host prior and/or during injection of modified T-lymphocytes, allowing for *in vivo* selection of transduced T-cells.

Acknowledgments

The authors thank Sonia Cellot and Simon Girard for technical assistance. This work was supported by the Canadian Institute of Health Research (CIHR) grants 68851 and 154290, as well as NCIC grant 018478.

References

1. Emery DW, Nishino T, Murata K, Fragkos M, Stamatoyannopoulos G (2002) Hematopoietic stem cell gene therapy. Int J Hematol 75:228

2. Fontes AM, Davis BM, Encell LP, *et al.* (2006) Differential competitive resistance to methylating versus chloroethylating agents among five O6-alkylguanine DNA alkyltransferases in human hematopoietic cells. Mol Cancer Ther 5:121

3. Ball CR, Pilz IH, Schmidt M, *et al.* (2007) Stable differentiation and clonality of murine long-term hematopoiesis after extended reduced-intensity selection for MGMT P140K transgene expression. Blood 110:1779

4. Kramer BA, Lemckert FA, Alexander IE, Gunning PW, McCowage GB (2006) Characterisation of a P140K mutant O6-methylguanine-DNA-methyltransferase (MGMT)-expressing transgenic mouse line with drug-selectable bone marrow. J Gene Med 8:1071

5. Gori JL, Podetz-Pedersen K, Swanson D, *et al.* (2007) Protection of mice from methotrexate toxicity by ex vivo transduction using lentivirus vectors expressing drug-resistant dihydrofolate reductase. J Pharmacol Exp Ther 322:989

6. Allay JA, Persons DA, Galipeau J, Riberdy JM, Ashmun RA, Blakley RL, Sorrentino BP (1998) In vivo selection of retrovirally transduced hematopoietic stem cells. Nat Med 4:1136

7. Zhao SC, Li MX, Banerjee D, *et al.* (1994) Long-term protection of recipient mice from lethal doses of methotrexate by marrow infected with a double-copy vector retrovirus containing a mutant dihydrofolate reductase. Cancer Gene Ther 1:27

8. Sorg UR, Kleff V, Fanaei S, *et al.* (2007) O6-methylguanine-DNA-methyltransferase (MGMT) gene therapy targeting haematopoietic stem cells: studies addressing safety issues. DNA Repair (Amst) 6:1197

9. Pinedo HM, Zaharko DS, Bull JM, Chabner BA (1976) The reversal of methotrexate cytotoxicity to mouse bone marrow cells by leucovorin and nucleosides. Cancer Res 36:4418

10. Frei E, 3rd, Blum RH, Pitman SW, *et al.* (1980) High dose methotrexate with leucovorin rescue. Rationale and spectrum of antitumor activity. Am J Med 68:370

11. Chu E, Allegra CJ (1996) Antifolates. In Cancer Chemotherapy and Biotherapy. Philadelphia, PA: Philadelphia, PA

12. Slamon DJ, Romond EH, Perez EA (2006) Advances in adjuvant therapy for breast cancer. Clin Adv Hematol Oncol 4:4

13. Daw NC, Billups CA, Rodriguez-Galindo C, *et al.* (2006) Metastatic osteosarcoma. Cancer 106:403

14. Strojan P, Soba E, Budihna M, Auersperg M (2005) Radiochemotherapy with Vinblastine, Methotrexate, and Bleomycin in the treatment of verrucous carcinoma of the head and neck. J Surg Oncol 92:278

15. Mennes M, Stiers P, Vandenbussche E, *et al.* (2005) Attention and information processing in survivors of childhood acute lymphoblastic leukemia treated with chemotherapy only. Pediatr Blood Cancer 44:478

16. Hashkes PJ, Laxer RM (2006) Update on the medical treatment of juvenile idiopathic arthritis. Curr Rheumatol Rep 8:450

17. Jones G, Crotty M, Brooks P (2000) Interventions for psoriatic arthritis. Cochrane Database Syst Rev:CD000212

18. Das JR, Fryar EB, Epie NN, Southerland WM, Bowen D (2006) Raloxifene attenuation of methotrexate cytotoxicity in human bone marrow by sequence-dependent administration of raloxifene, 5-FU/methotrexate. Anticancer Res 26:1877

19. Warlick CA, Diers MD, Wagner JE, McIvor RS (2002) In vivo selection of antifolate-resistant transgenic hematopoietic stem cells in a murine bone marrow transplant model. J Pharmacol Exp Ther 300:50

20. Zhao SC, Banerjee D, Mineishi S, Bertino JR (1997) Post-transplant methotrexate administration leads to improved curability of mice bearing a mammary tumor transplanted with marrow transduced with a mutant human dihydrofolate reductase cDNA. Hum Gene Ther 8:903

21. Persons DA, Allay JA, Bonifacino A, *et al.* (2004) Transient in vivo selection of transduced peripheral blood cells using antifolate drug selection in rhesus macaques that received transplants with hematopoietic stem cells expressing dihydrofolate reductase vectors. Blood 103:796

22. Mahmud N, Devine SM, Weller KP, *et al.* (2001) The relative quiescence of hematopoietic stem cells in nonhuman primates. Blood 97:3061

23. Antonchuk J, Sauvageau G, Humphries RK (2002) HOXB4-induced expansion of adult hematopoietic stem cells ex vivo. Cell 109:39

24. Sauerbrey A, McPherson JP, Zhao SC, Banerjee D, Bertino JR (1999) Expression of a novel double-mutant dihydrofolate reductase-cytidine deaminase fusion gene confers resistance to both methotrexate and cytosine arabinoside. Hum Gene Ther 10:2495

25. Patel M, Sleep SE, Lewis WS, *et al.* (1997) Comparison of the protection of cells from antifolates by transduced human dihydrofolate reductase mutants. Hum Gene Ther 8:2069

26. Li MX, Banerjee D, Zhao SC, *et al.* (1994) Development of a retroviral construct containing a human mutated dihydrofolate reductase cDNA for hematopoietic stem cell transduction. Blood 83:3403

27. Banerjee D, Schweitzer BI, Volkenandt M, *et al.* (1994) Transfection with a cDNA encoding a Ser31 or Ser34 mutant human dihydrofolate reductase into Chinese hamster ovary and mouse marrow progenitor cells confers methotrexate resistance. Gene 139:269

28. Spencer HT, Sleep SE, Rehg JE, Blakley RL, Sorrentino BP (1996) A gene transfer strategy for making bone marrow cells resistant to trimetrexate. Blood 87:2579

29. Ercikan-Abali EA, Mineishi S, Tong Y, *et al.* (1996) Active site-directed double mutants of dihydrofolate reductase. Cancer Res 56:4142

30. Lewis WS, Cody V, Galitsky N, *et al.* (1995) Methotrexate-resistant variants of human dihydrofolate reductase with substitutions of leucine 22. Kinetics, crystallography, and potential as selectable markers. J Biol Chem 270:5057

31. Capiaux GM, Budak-Alpdogan T, Takebe N, *et al*. (2003) Retroviral transduction of a mutant dihydrofolate reductase-thymidylate synthase fusion gene into murine marrow cells confers resistance to both methotrexate and 5-fluorouracil. Hum Gene Ther 14:435

32. Takebe N, Xu LC, MacKenzie KL, Bertino JR, Moore MA (2002) Methotrexate selection of long-term culture initiating cells following transduction of CD34(+) cells with a retrovirus containing a mutated human dihydrofolate reductase gene. Cancer Gene Ther 9:308

33. Meisel R, Bardenheuer W, Strehblow C, *et al.* (2003) Efficient protection from methotrexate toxicity and selection of transduced human hematopoietic cells following gene transfer of dihydrofolate reductase mutants. Exp Hematol 31:1215

34. Gatlin J, Douglas J, Evans JT, Collins RH, Wendel GD, Garcia JV (2000) In vitro selection of lentivirus vector-transduced human CD34+ cells. Hum Gene Ther 11:1949

35. Havenga MJ, Werner AB, Valerio D, van Es HH (1998) Methotrexate selectable retroviral vectors for Gaucher disease. Gene Ther 5:1379

36. Flasshove M, Banerjee D, Bertino JR, Moore MA (1995) Increased resistance to methotrexate in human hematopoietic cells after gene transfer of the Ser31 DHFR mutant. Leukemia 9 Suppl 1:S34

37. Volpato JP, Fossati E, Pelletier JN (2007) Increasing Methotrexate Resistance by Combination of Active-site Mutations in Human Dihydrofolate Reductase. J Mol Biol 373:599

38. Mamo A, Krosl J, Kroon E, *et al.* (2006) Molecular dissection of Meis1 reveals 2 domains required for leukemia induction and a key role for Hoxa gene activation. Blood 108:622

39. Pineault N, Abramovich C, Ohta H, Humphries RK (2004) Differential and common leukemogenic potentials of multiple NUP98-Hox fusion proteins alone or with Meis1. Mol Cell Biol 24:1907

40. Ory DS, Neugeboren BA, Mulligan RC (1996) A stable human-derived packaging cell line for production of high titer retrovirus/vesicular stomatitis virus G pseudotypes. Proc Natl Acad Sci U S A 93:11400

41. Markowitz D, Goff S, Bank A (1988) A safe packaging line for gene transfer: separating viral genes on two different plasmids. J Virol 62:1120

42. Kiel MJ, Yilmaz OH, Iwashita T, Yilmaz OH, Terhorst C, Morrison SJ (2005) SLAM family receptors distinguish hematopoietic stem and progenitor cells and reveal endothelial niches for stem cells. Cell 121:1109

43. Mareya SM, Sorrentino BP, Blakley RL (1998) Protection of CCRF-CEM human lymphoid cells from antifolates by retroviral gene transfer of variants of murine dihydrofolate reductase. Cancer Gene Ther 5:225

44. Banerjee D, Zhao SC, Tong Y, Steinherz J, Gritsman K, Bertino JR (1994) Transfection of a nonactive site mutant murine DHFR cDNA (the tryptophan 15 mutant) into Chinese hamster ovary and mouse marrow progenitor cells imparts MTX resistance in vitro. Cancer Gene Ther 1:181

45. Allay JA, Spencer HT, Wilkinson SL, Belt JA, Blakley RL, Sorrentino BP (1997) Sensitization of hematopoietic stem and progenitor cells to trimetrexate using nucleoside transport inhibitors. Blood 90:3546

46. Ohta H, Sekulovic S, Bakovic S, *et al.* (2007) Near-maximal expansions of hematopoietic stem cells in culture using NUP98-HOX fusions. Exp Hematol 35:817

47. Nocka K, Tan JC, Chiu E, *et al.* (1990) Molecular bases of dominant negative and loss of function mutations at the murine c-kit/white spotting locus: W37, Wv, W41 and W. Embo J 9:1805

48. Stromhaug A, Slordal L, Warren DJ (1996) Differential effects of the antifolates methotrexate, aminopterin and trimetrexate on murine haemopoietic progenitor cells. Br J Haematol 92:514

49. Zielske SP, Braun SE (2004) Cytokines: value-added products in hematopoietic stem cell gene therapy. Mol Ther 10:211

50. Morgan RA, Dudley ME, Wunderlich JR, *et al.* (2006) Cancer regression in patients after transfer of genetically engineered lymphocytes. Science 314:126

51. Debatin KM, Wei J, Beltinger C (2008) Endothelial progenitor cells for cancer gene therapy. Gene Ther 15:780

52. Aboody KS, Najbauer J, Danks MK (2008) Stem and progenitor cell-mediated tumor selective gene therapy. Gene Ther 15:739

53. Rosenberg SA, Restifo NP, Yang JC, Morgan RA, Dudley ME (2008) Adoptive cell transfer: a clinical path to effective cancer immunotherapy. Nat Rev Cancer 8:299

54. Fairbanks LD, Ruckemann K, Qiu Y, *et al.* (1999) Methotrexate inhibits the first committed step of purine biosynthesis in mitogen-stimulated human T-lymphocytes: a metabolic basis for efficacy in rheumatoid arthritis? Biochem J 342 (Pt 1):143

55. Becker C, Barbulescu K, Hildner K, Meyer zum Buschenfelde KH, Neurath MF (1998) Activation and methotrexate-mediated suppression of the TNF alpha promoter in T cells and macrophages. Ann N Y Acad Sci 859:311

Préface au chapitre 5

La sélection de la banque combinatoire DHFRh 31/34/35 a généré des variantes hautement résistantes au MTX. Les données cinétiques et d'inhibition permettaient de spéculer sur les effets des résidus mutés aux trois positions, mais il restait que les causes moléculaires menant à la résistance ne pouvaient pas être élucidées simplement avec ces données. Nous avons donc entamé des études structurales des variantes résistantes par cristallographie aux rayons X. Nous avons obtenu à ce jour la structure de la double variante F31R/Q35E (RFE) avec le MTX lié au niveau du site actif. L'obtention de la structure cristalline à haute résolution nous a permis d'observer pour la première fois la présence de plus d'un conformère à des résidus clés du site actif, incluant le résidu substitué Arg31. L'orientation des multiples conformères permet d'expliquer certaines causes moléculaires plausibles de l'importante perte d'affinité de ce mutant pour le MTX. De plus, l'introduction d'une charge négative provenant du résidu substitué Glu35 semble créer des interactions electrostatiques non-favorables avec le MTX. Pour mieux comprendre l'effet des substitutions sur la forme la plus oxidée du substrat (folate), nous avons entrepris l'arrimage moléculaire *in silico*. En combinant ces résultats avec la caractérisation cinétique et d'inhibition des variantes ponctuelles F31R, Q35E et de la double variante F31R/Q35E, et nos observations sur la structure de la variante F31R/Q35E lié au MTX, nous avons pu conclure que la perte d'affinité pour le MTX ne se limite pas à des pertes de contacts entre l'inhibiteur et les résidus substitués. Les substitutions pourraient affecter l'étape d'isomérisation de l'enzyme suite à la liaison du MTX, un phénomène uniquement retrouvé lors de la liaison de l'inhibiteur au site actif de l'enzyme native.

Ce chapitre est présenté sous forme d'article scientifique soumis au *Journal of Biological Chemistry* en novembre 2008. Ayant participé à la majorité des aspects de recherches expérimentales et théoriques de cette étude, ma contribution à ce projet est majeure. La résolution du patron de diffraction de la variante F31R/Q35E et des conseils techniques de cristallisations offerts par Brahm Yachnin, étudiant au doctorat au laboratoire de notre collaborateur, le Dr. Albert Berghuis, justifie sa présence en tant que co-premier auteur. Une aide technique pour la détermination des conditions de cristallisation de la

variante F31R/Q35E de la part de Jonathan Blanchet justifie sa présence en tant que deuxième auteur. La caractérisation des variantes ponctuelles F31R et Q35E justifient la présence de Vanessa Guerrero et Elena Fossati en tant que troisième et cinquième auteur respectivement. Le travail de Lucie Poulin pour l'obtention de cristaux pour la structure à basse résolution (Annexe 1) justifie sa présence en tant que quatrième auteure.

Chapitre 5

Structure cristalline de la variante double F31R/Q35E de la dihydrofolate réductase humaine liée au MTX à une résolution de 1.7 Å

5.1 Article 4. Multiple conformers in human dihydrofolate reductase F31R/Q35E double variant suggest structural basis for methotrexate resistance

Multiple conformers in human dihydrofolate reductase F31R/Q35E double variant suggest structural basis for methotrexate resistance

Jordan P. Volpato[1*], Brahm J. Yachnin[2*], Jonathan Blanchet[3], Vanessa Guerrero[3], Lucie Poulin[3], Elena Fossati[1], Albert M. Berghuis[2,4] and Joelle N. Pelletier[1,3]

[*]*Denotes equal contribution*

[1]*Département de Biochimie and* [3]*Département de Chimie*

Université de Montréal

C.P. 6128, Succursale Centre-Ville

Montréal (Québec)

H3C 3J7 CANADA

[2]*Department of Biochemistry and* [4]*Department of Microbiology and Immunology*

McGill University

Montréal (Québec)

Submitted to the *Journal of Biological Chemistry* (November 2008)

ABSTRACT

Methotrexate (MTX) is a slow, tight-binding, competitive inhibitor of human DHFR (hDHFR), an enzyme that provides key metabolites for nucleotide biosynthesis. In an effort to better characterize ligand binding in drug resistance, we have previously developed hDHFR variant F31R/Q35E. This variant displays a > 650-fold decrease in MTX affinity, while maintaining catalytic activity comparable to the native enzyme. To elucidate the molecular basis of decreased MTX affinity in the double variant, we determined kinetic and inhibitory parameters for the F31R and Q35E point variants. This demonstrated that the important decrease of MTX-affinity in variant F31R/Q35E is a result of synergistic effects of the combined point mutations. To better understand the structural cause of this synergy, we obtained the crystal structure of hDHFR double variant F31R/Q35E complexed with MTX at 1.7 Å resolution. A number of active-site residues were observed in more than one conformation, which is not characteristic of the native enzyme. Notably, the substituted residue Arg31 was observed in multiple conformers. This suggests that increased residue disorder underlies the observed MTX resistance. Taken with the introduction of a negative charge by the Q35E substitution, we observe a considerable loss of van der Waals and polar contacts with the *p*-ABA and glutamate moieties. The multiple conformers of Arg31 further suggest that the substitutions may decrease the isomerisation step leading to tight binding of MTX. Molecular docking with folate corroborates this hypothesis.

INTRODUCTION

Human dihydrofolate reductase (hDHFR) catalyzes the reduction of 7,8-dihydrofolate (DHF) to 5,6,7,8-tetrahydrofolate (THF) in a NADPH-dependent manner. THF is used as a cofactor in purine and thymidylate biosynthesis, which are essential metabolites for the maintenance of cell division and proliferation. As a consequence of its essential role in purine and thymidylate biosynthesis, hDHFR has been extensively

exploited as a drug target. The resultant folate antagonists, or antifolates, bind at the active site of the enzyme, thereby arresting cell proliferation. The most effective clinical antifolate to date has been methotrexate (MTX; Figure 5.1), a slow, tight binding competitive inhibitor of hDHFR which displays high affinity for the enzyme (K_i^{MTX} = 3.4 pM). MTX is currently used to treat a variety of diseases, including cancer (1-3) and auto-immune diseases such as juvenile idiopathic arthritis (4). A number of resistance mechanisms to MTX have been observed in cancer cells, namely impaired transport of MTX to the cytoplasm (5), decreased retention of MTX in the cell (6), and mutations in the hDHFR gene which result in an enzyme variant with decreased affinity for MTX (7).

Understanding the molecular interactions that affect tight binding of MTX to the active site of DHFR will contribute to our understanding of drug binding to DHFR, which can in turn contribute to the design of more efficient inhibitors. A considerable number of DHFR active site variants have been identified in MTX-resistant cancer cell lines or engineered *in vitro* to elucidate the role of active site residues in the binding of MTX. Substitutions at residues Ile7 (8), Leu22 (9,10), Phe31 (11), Phe34 (12), Arg70 (13) and Val115 (14) have yielded MTX-resistant variants. These residues are all present in the folate-binding pocket(15). Because MTX and DHF bind to the active site of hDHFR in a similar manner, all known substitutions causing a decrease in MTX-affinity also decrease DHF affinity and overall catalytic efficiency (7,14,16). However, the loss of DHF affinity and catalytic efficiency is generally smaller than the loss of MTX-affinity. This is often attributed to formation of different contacts with either ligand due to the 180° inversion of the pterin ring of bound DHF relative to MTX (15,17).

Crystal structures of MTX-resistant point variants offer insight into the causes of decreased binding of MTX or other antifolates (15,18-22). To this day, crystal structures of MTX-resistant hDHFR variants L22F, L22R, L22Y (10), as well as F31G and F31S (23), complexed to various antifolates, have been reported. Only the L22Y variant has been co-crystallized with MTX. Despite its decreased affinity for MTX (L22Y K_i^{MTX} = 11 nM *vs*

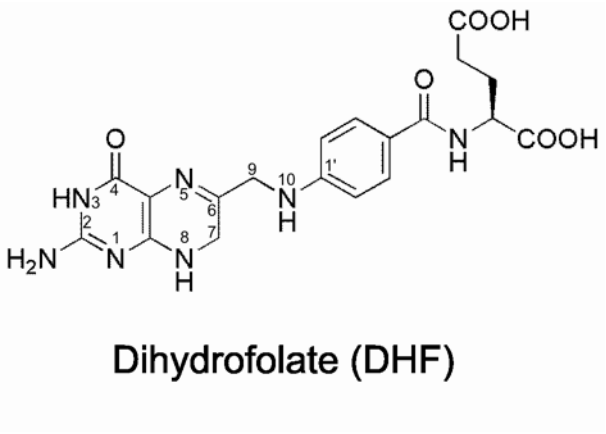

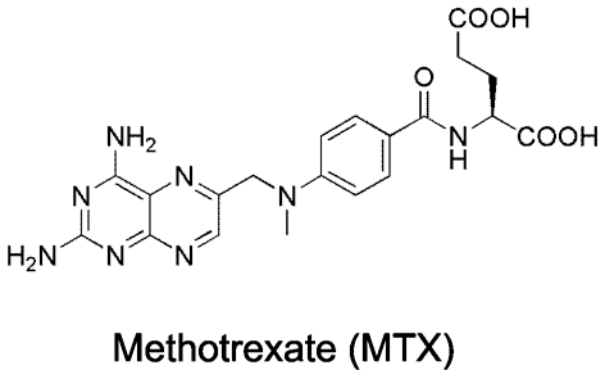

Figure 5.1. Chemical structures of hDHFR ligands. Atom numbering is shown on DHF.

WT K_i^{MTX} = <31 pM (16)), the inhibitor in the variant structure was bound in the same way as in the structure of the native enzyme, making interpretation of decreased affinity difficult to assess. Nonetheless, the low-probability conformation of residue Tyr22 suggested that the presence of a bulky aromatic residue in this area of the folate-binding pocket generated unfavourable hydrophobic interactions with the 2,4-diaminopterin (DAP) moiety of the inhibitor (10). This is also expected to reduce DHF substrate binding. Structures of MTX-resistant variants F31G and F31S were obtained complexed to N-[4-[(2,4-diaminofuro[2,3-*d*]pyrimidin-5-yl)-methyl]-methylamino]-benzoyl]-L-glutamate (MTXO) (23), a MTX analog in which the 2,4-DAP moiety is replaced by a 2,4-diaminofuropyrimidine moiety. Superposition of MTXO-bound variants with MTX-bound WT hDHFR revealed that the ligands bind to the active site in an analogous manner. It was suggested that decreased MTX binding in the variants resulted from the loss of van der Waals and hydrophobic contacts established between the native Phe31 and the *p*-ABA and 2,4-DAP moieties of MTX. F31G and F31S display a 10-fold decrease in affinity for MTX relative to WT hDHFR (K_i^{MTX} < 31 pM (16)). Further F31 variants (*i.e.* F31R ; K_i^{MTX} = 7 nM, 200-fold decrease in MTX-affinity) (8) display larger decreases in affinity relative to F31G and F31S. This cannot be rationalized by reduction of side chain contacts with the inhibitor due to the presence of a smaller side chain. Structural data is required to better understand the molecular mechanisms underlying MTX resistance in these variants.

Combining active-site substitutions in hDHFR has been shown to generate variants with greatly decreased affinity to MTX (16,24). Studying the molecular interactions in highly MTX-resistant hDHFR variants offers the possibility of capturing more important changes in enzyme-ligand interactions. Here, we report detailed observations for the cause of MTX resistance in combinatorial double variant F31R/Q35E (16). Variant F31R/Q35E is a relevant candidate for better understanding of the specific interactions that govern ligand recognition in the folate binding site, as it displays a > 650-fold decrease in MTX affinity (K_i^{MTX} = 21 nM) accompanied by a modest, 9-fold decrease of affinity for the

substrate DHF relative to WT hDHFR. In addition, we have recently shown that this variant is an efficient selectable marker for various mammalian cell types, including murine hematopoietic stem cells ((16), unpublished results). To better understand the effect of either substitution on each ligand, a kinetic double variant cycle was constructed with the F31R and Q35E point variants. The crystal structure of the double variant was obtained with bound MTX at 1.7 Å-resolution, to elucidate the structural basis of MTX-resistance in this variant. In addition, molecular docking was performed with the F31R/Q35E structure to evaluate the role of the two substitutions toward folate binding. Overall, the results reveal synergistic effects of the combined substitutions toward loss of MTX binding, characterized by increased disorder of specific residues within the F31R/Q35E variant.

EXPERIMENTAL PROCEDURES

Construction of vectors hDHFR F31R/Q35E-pET24, hDHFR F31R-pQE32 and hDHFR Q35E-pQE32 – The hDHFR F31R/Q35E gene was amplified by PCR using primer set $^{5'}$ *f* – CACACACCATATGGTTGGTTCGCTAAACTG $^{3'}$ (NdeI restriction site underlined) and $^{5'}$ *r* – GTTCTGAGGTCATTACTGG $^{3'}$ (external primer) from the hDHFR F31R/Q35E-pQE32 template (16). The amplified gene was subcloned in the modified pET24 vector (25) between the *NdeI* and *HindIII* restriction sites using T4 DNA ligase and the ligation mixture was transformed into electrocompetent BL21(DE3) cells. The expected sequence was confirmed by DNA sequencing.

The F31R and Q35E variants were created by megaprimer PCR using external primer set 2 described in (16) and mutagenic primers $^{5'}$ *r* – TCTCTGGAAATATCTACGTTCGTTCCTTAAGG (F31R), and $^{5'}$ *r* – GTTGTGGTCATTTCTTTCGAAATATCTAAATTCGT (Q35E), respectively. The amplified gene was subcloned in the pQE32 vector between the *BamHI* and *HindIII* restriction sites using T4 DNA ligase and the ligation mixture was transformed into

electrocompetent SK037 cells (16). Expression, purification, and determination of kinetic and inhibitory constants was performed as previously described (16).

Expression and purification of hDHFR F31R/Q35E – An overnight preculture of BL21(DE3)/hDHFR F31R/Q35E-pET24 was used to inoculate 1 L of LB medium. The culture was grown at 37°C until the $A_{600\ nm} \approx 0.7$. Protein expression was induced with the addition of 1 mM of isopropyl 1-thio-β-D-galactopyranoside (IPTG), after which the cells were grown for 16 h at 22°C. Induced cells were harvested by centrifugation (4000*g* for 30 min at 4°C). The cell pellet was resuspended in 10 mM Tris-HCl, pH 8.3, at 4°C. The cells were lysed on ice using a Branson sonicator (four pulses at 200 W for 30 s with a tapered micro-tip). The cellular debris was pelleted by centrifugation (4000*g* for 30 min at 4°C) and the supernatant was filtered through a 0.2μm filter before purification.

Purification was performed following a 2-step purification protocol on an AKTA FPLC (GE Healthcare, Piscataway, NJ) at 5°C. First, the supernatant was applied to an anion exchange DEAE-sepharose column (1.6 × 30 cm) followed by a 3 column volumes (CV) wash with 10 mM Tris-HCl, pH 8.3, at 2 mL/min. A linear gradient of 5 CV with NaCl (0-200 mM) in 10 mM Tris-HCl, pH 8.3, was used to elute the F31R/Q35E variant. hDHFR activity was monitored in MATS buffer, pH 7.6, in the presence of 100 μM each NADPH and DHF. Activity was measured in flat-bottom plates (Costar #3595) by monitoring concurrent depletion of NADPH and DHF ($\Delta\varepsilon_{340nm}$ = 12 800 $M^{-1}cm^{-1}$) on a FLUOstar OPTIMA UV-vis plate reader (BMG Laboratories, Offenburg, Germany). Active fractions were pooled and dialysed overnight at 4°C against 50 mM phosphate buffer, pH 7.5. Following dialysis, the sample (45 mL) was concentrated to 1.5 mL using an Amicon concentrator (MCWO 10000, Millipore), for injection on a Superose12 column (1.6 × 55 cm). The sample was eluted with 50 mM phosphate buffer, pH 7.5, at a flowrate of 1.5 mL/min. hDHFR activity was monitored as described above. Enzyme purity was evaluated using separation by SDS-PAGE (15% (w/v) polyacrylamide gel) stained by the zinc-imidazole method (26) and quantified using the public domain image analysis software

Scion Image (NIH, rsb.info.nih.gov/ nih-image). Protein concentration was quantified using the Bradford assay (Biorad, Hercules, CA).

Crystallization and X-ray data collection of hDHFR F31R/Q35E – Purified hDHFR F31R/Q35E enzyme was concentrated to 10 mg/mL using an Amicon concentrator (MCWO 10000). MTX and NADPH were prepared as described previously (16) and were added at a final concentration of 2 mM each (5-fold molar excess) to the protein sample. Crystallization experiments were set up using hanging drop vapour diffusion experiments, with a reservoir volume of 1 mL and a drop size of 4 µL of equal volumes of protein and reservoir solutions. A reservoir solution containing 0.2 M cadmium phosphate and 2.2 M ammonium sulfate yielded crystal-like formations that diffracted poorly. These crystals were crushed using a Hampton Seed Bead Kit and used as seeds (1/10 dilution). Rod-shaped crystals were obtained from crystallization experiments with 0.2 M sodium phosphate and 2.2 M ammonium sulphate as the reservoir solution and with drops containing 1.5 µL of protein, 2 µL reservoir solution, and 0.5 µL seeding solution. The crystals were soaked in the mother liquor supplemented with 15% glycerol as a cryoprotectant and frozen in a nitrogen cryostream (model X-stream 2000). Data were collected using a Rigaku RU-H3R generator, equipped with Osmic focussing mirrors, and an R-axis IV ++ image plate detector, and processed using HKL-2000 (27) (Table 5.1).

Structure Determination and Refinement – The structure was determined by molecular replacement using Phaser (28), which found a single protein molecule in the asymmetric unit (Resolution Range Used: 1.70-25.99; Log Likelihood Gain (refined): 726.123). A lower-quality His-tagged F31R/Q35E-MTX-NADPH structure (Annexe 1) was used as a molecular replacement model. Reciprocal-space refinement was performed using Refmac (29), and included individual isotropic b-factor refinement as well as TLS refinement in the final stages of refinement. Manual model building was performed periodically using Coot (30) (Table 5.1).

Table 5.1. Crystallography data

Data collection statistics	
Space group	$P2_12_12_1$
Number of Molecules per Asymmetric Unit	1
a (Å)	42.348
b (Å)	47.868
c (Å)	90.715
$\alpha = \beta = \gamma$ (°)	90
Wavelength (Å)	1.5418
Resolution Range (Å)	1.70-10.52 (1.70-1.76)
Completeness (%)	97.2 (93.9)
Redundancy	11.7 (9.5)
R_{merge}	6.4 (47.3)
Refinement statistics	
R_{factor}	17.929
R_{free} (10% free test set)	22.297 (2066 reflections)
Number of reflections	20,304
Reflection Cutoff in Refinement	$F > 0\sigma F$
Number of atoms	1719
Protein	1507
Water	138
Ions	41
Inhibitor	33
RMSD	
Bond length (Å)	0.012
Bond angle (°)	1.417
Average atomic B-Factor	16.372
Protein	14.99
Water	30.57
Ions	35.20
Inhibitor	15.78
Wilson B-Factor	21.585
Ramachandran Plot (non-Gly, non-Pro residues)	159 (100%)
Residues in Favoured Positions (%)	146 (91.8%)
Residues in Allowed Positions (%)	13 (8.2%)
Residues in Disallowed Positions (%)	0 (0%)

Items in parentheses refer to the highest resolution shell.

In silico automated docking of folate – The ligands were prepared as .pdb files using ChemDraw 8.0 and Chem3D 8.0 (CambridgeSoft, Cambridge, MA). Energy minimization of ligands was performed with the integrated MM2 energy minimization script in Chem3D. Automated docking experiments were performed using the Autodock 4 software package (Scripps Research Institute, La Jolla, CA). Macromolecules PDB ID 1U72 and 3EIG were stripped of all ligands and heteroatoms, with the exception of the highly conserved active site water molecule (H_2O #216 in 1U72, H_2O #244 in 3EIG), and were prepared using default settings. A box covering the entire folate binding site and more than half the NADPH binding site was generated as a docking grid. Fifty runs of a Lamarckian genetic algorithm using default settings were performed. Following docking, clusters were evaluated according to total binding energies calculated by Autodock 4, and the minimal energy conformation within the lowest energy cluster was retained for comparison with crystal structures.

RESULTS

Kinetic and inhibition double variant cycle of hDHFR double variant F31R/Q35E – In order to determine the effect of each constituent substitution of the F31R/Q35E variant on DHF and MTX binding, the point variants F31R and Q35E were created and their kinetic and inhibition parameters were determined (Table 5.2). The reactivity (k_{cat}) of point variants F31R and Q35E are 5-fold lower (1.9 s^{-1}) and 2-fold lower (4.6 s^{-1}) than WT hDHFR, respectively. The k_{cat} of F31R/Q35E is similar to that of the F31R variant, indicating that loss of reactivity in the double variant is primarily due to the F31R substitution. The Michaelis constants (K_M^{DHF}) of point variants F31R and Q35E are 110 and 250 nM respectively, illustrating a slight decrease in DHF-affinity (1.5 and 3-fold, respectively) relative to the WT. Kinetic data for the F31R variant had previously been reported (8), and compares well with our data, although we determined a K_M^{DHF} value that

Table 5.2. Kinetic and inhibitory parameters of WT hDHFR and hDHFR F31R/Q35E variant

Variant	k_{cat} (s^{-1})	K_M^{DHF} (nM)	$\Delta\Delta G^{DHF}$ (kCal/mol)[b]	IC_{50}^{MTX} (nM)	K_i^{MTX} (nM)	$\Delta\Delta G^{MTX}$ (kCal/mol)[c]
WT [a]	10	<75	0	42	<0.031	0
F31R	1.9 ± 0.3	110 ± 60	0.3	1100 ± 600	1.1 ± 0.6	2.1
Q35E	4.6 ± 0.2	250 ± 90	0.7	19 ± 4	0.048 ± 0.009	0.3
F31R/Q35E[a]	1.3	690	1.3	3100	21	3.8

[a] Values taken from (16)

[b] Calculated using the mathematical relation $\Delta\Delta G = -RT \times \ln(K_m^{DHF}$ WT/ K_m^{DHF} mutant), where $R = 1.9872 \times 10^{-3}$ kCal K^{-1} mol^{-1} and T = 293 K

[c] Calculated using the mathematical relation $\Delta\Delta G = -RT \times \ln(K_i^{MTX}$ WT/ K_i^{MTX} mutant), where $R = 1.9872 \times 10^{-3}$ kCal K^{-1} mol^{-1} and T = 293 K.

is 6-fold lower than previously reported. Because we expected a low value for K_M^{DHF} and a correspondingly low spectrophotometric signal, we used 10-cm cuvettes in K_M^{DHF} determination, rather than 1-cm cuvettes (8). This enabled a more precise measurement in the target range. Inhibition constants for MTX (K_i^{MTX}) revealed that the F31R substitution (K_i^{MTX} = 1.1 nM) confers a 35-fold loss in MTX-affinity, while the Q35E substitution (K_i^{MTX} = 0.048 nM) displays a modest decrease of MTX-affinity relative to WT (1.5-fold decrease). Like the F31R variant, the F31R/Q35E double variant displayed larger decreases in MTX-affinity than DHF-affinity relative to the WT. However, the Q35E substitution modestly decreased DHF affinity, while having a negligible effect on MTX-affinity. The F31R/Q35E double variant presented both of these features, as DHF-affinity decreased 9-fold relative to WT, while MTX-affinity decreased more than > 650-fold relative to the WT. Thus, addition of the Q35E substitution to variant F31R increased the K_M^{DHF} of F31R 6-fold, while increasing the K_i^{MTX} of F31R nearly 20-fold.

To better quantify the effect of the combined substitutions on MTX and DHF binding, we calculated the loss of binding free energy (ΔΔG) for each variant relative to WT hDHFR. For K_M^{DHF}, the sum of the $\Delta\Delta G^{F31R}$ and $\Delta\Delta G^{Q35E}$ values was comparable to the value of $\Delta\Delta G^{F31R/Q35E}$ (Table 5.2; Figure 5.2), indicating additive effects of the two substitutions toward loss of DHF affinity. However, for K_i^{MTX}, $\Delta\Delta G^{F31R/Q35E}$ was considerably greater than the sum of $\Delta\Delta G^{F31R}$ and $\Delta\Delta G^{Q35E}$, indicating a synergistic effect of the two substitutions on loss of MTX affinity (Table 5.2; Figure 5.2). These data demonstrate that the F31R substitution is the most important contributor to the binding properties of the F31R/Q35E double variant, while the addition of the Q35E substitution synergistically decreases MTX-affinity with only a modest, additive reduction of DHF affinity.

Overall structure and general characteristics of hDHFR F31R/Q35E complexed to MTX – To further understand the structural basis of the important loss in MTX-affinity, we

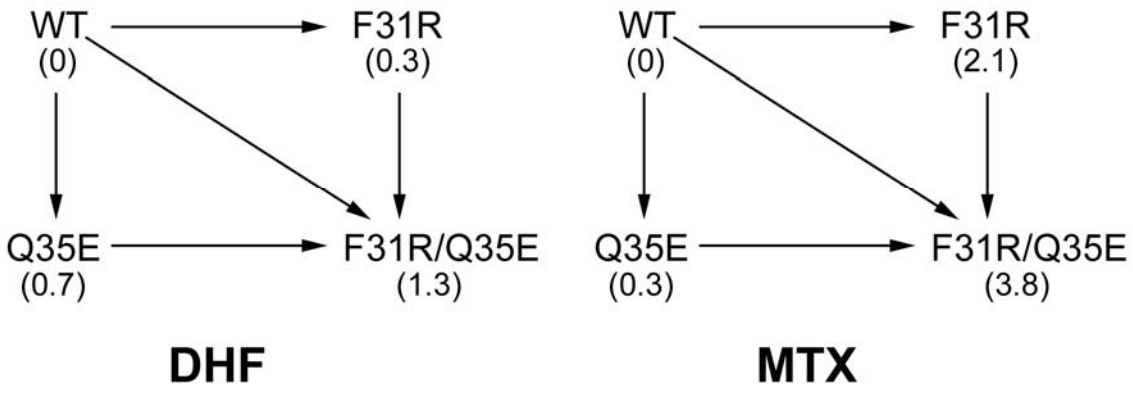

Figure 5.2. Double variant cycle of F31R/Q35E for DHF and MTX affinity. Numbers in parentheses are ΔΔG values for each variant relative to the WT.

obtained two crystal structures of F31R/Q35E double variant. The first structure had bound NADPH and MTX, and contained six hDHFR molecules within the asymmetric unit. However, considerable twinning of the crystal lattice resulted in poor data quality, leading to an inability to refine the crystal structure to acceptable $R_{factors}$ (Annexe 1, Table A1.1). This precluded detailed analysis of molecular contacts; however, we were used this structure to corroborate observations in the second structure. The full length of the hDHFR backbone was modelled from electron density map in the second structure, with several side-chains exhibiting multiple conformations. Some side-chains did not display well-defined electron density, and thus were excluded from the model. A large region of very well-defined electron density was modelled as MTX in the DHF-binding site. There was no electron density in the NADPH-binding site with which to model in NADPH, though two peaks modelled in as sulfate ions were visible where the phosphates of NADPH have been observed in other structures. Six other sulfates, as well as a cadmium ion, were also built into the model.

The overall fold and tertiary structure of variant F31R/Q35E is very similar to that reported for other hDHFRs (10,15,17-23,31,32). hDHFR F31R/Q35E is composed of a central β-sheet containing 7 parallel and 1 anti-parallel strand, and 4 α-helices interconnected by a series of loops (Figure 5.3). Density surrounding the side chains of residues Arg32, Arg36, Glu78, Glu81, His87, Arg91, Lys98, Glu101 and Glu161 was either absent or poorly defined. Those side chains, which are all at the surface of the protein, were not included in the model. Nonetheless, a number of residues were revealed to have two conformers that were clearly visible. Interestingly, these residues are clustered either in the folate (F31R, Tyr33, Met37, Ser41) or NADPH (Ser59, Ser118, Asp145, Thr146) binding sites. Other high-resolution structures have reported two conformers at Ser41, Ser118 and Thr146 when NADPH was not present in the active site (31), but the presence of two conformers at the other residues (F31R, Tyr33, Met37, Ser59, Asp145) has

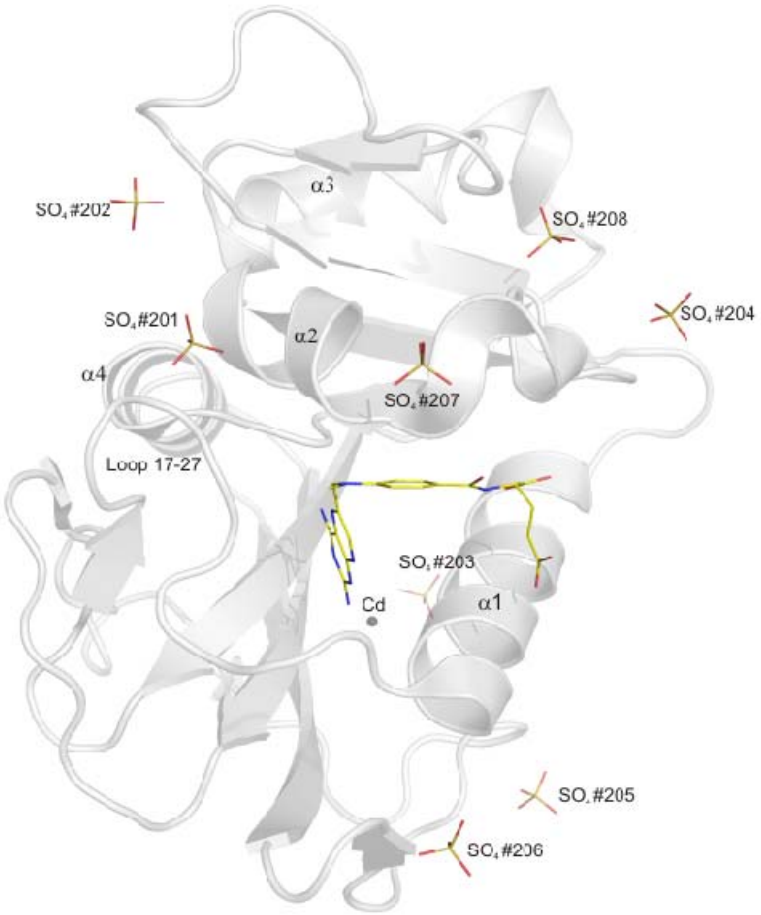

Figure 5.3. Structure of hDHFR variant F31R/Q35E. The macromolecule is shown in cartoon representation, while MTX and sulphate molecules are shown in sticks representation, coloured by atom (C: yellow, N: blue, O: red and S: orange). A Cd atom is shown as a blue sphere.

never been previously reported, and suggests that this is a consequence of the substitutions at residues 31 and/or 35.

Interactions between variant F31R/Q35E and bound MTX at the active site – To identify structural changes in variant F31R/Q35E complexed with MTX, the 1.7 Å resolution structure was superimposed onto WT human DHFR complexed with NADPH and MTX (1U72; 1.9 Å resolution) (15) and WT human DHFR complexed with folate (1DRF; 2.0 Å resolution) (17) (RMSD 0.66 and 0.69 Å, respectively). Those structures were selected because they contain structurally similar ligands in the folate binding site, and because 1DRF lacked NADPH, which enabled identification of structural differences originating from NADPH binding. In contrast to the two WT structures, variant F31R/Q35E displays a considerable shift of loop 17-27 towards the active site (discussed below), in addition to the residues present as two conformers in the NADPH-binding cleft. The low RMSD value (0.304 Å) between 1U72 and 1DRF was also an incentive for comparison with variant F31R/Q35E. MTX binds in a similar fashion in the F31R/Q35E active site (Figure 5.4) as in WT hDHFR (1U72). There was little difference in the orientation of the side chains of residues involved in binding, with the exception of two active site residues, Arg31 and Tyr33, which were each present in two distinct conformations. Therefore, as in the WT enzyme, residues 31 and 35 in variant F31R/Q35E do not form specific contacts with the pterin moiety of MTX.

Binding of the pterin ring involves characteristic H-bonding with specific amino acids and with conserved water molecules (Figure 5.4A). H_2O #210 is also H-bonded to the hydroxyl group of one of the two distinct conformers of Tyr33 observed in the F31R/Q35E structure (Figure 5.4A). To our knowledge, this is the first hDHFR structure that reports two distinct Tyr33 conformers in the same macromolecule, identified as Tyr33A and Tyr33B (Figure 5.5A). The Tyr33A conformer is homologous to that observed in all but one structure of hDHFR, and does not appear to form any contacts. A ~30° rotation around the C_α- C_β bond towards the active site brings the hydroxyl group within H-bonding

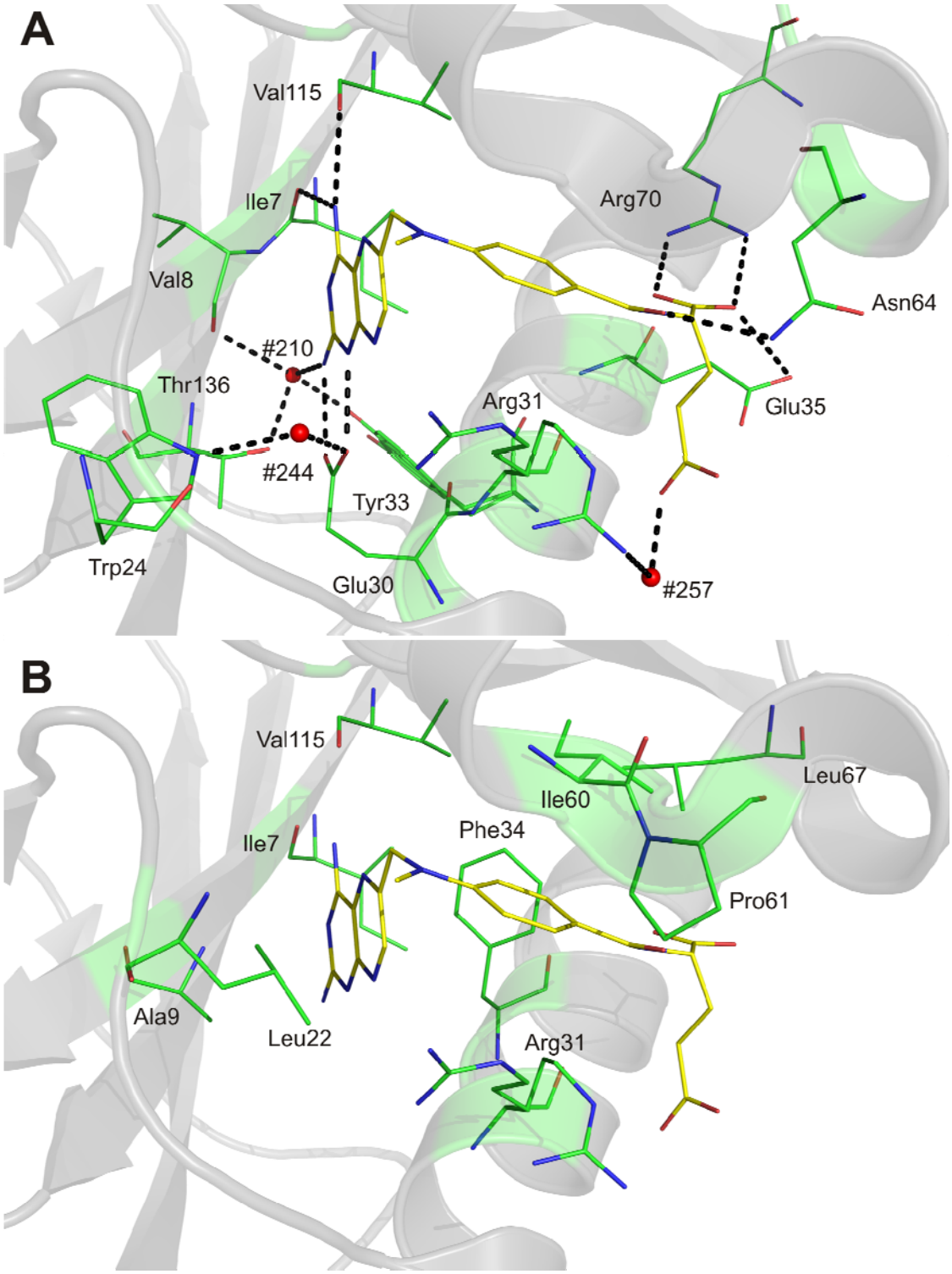
A
Val115
Ile7
Arg70
Val8
Asn64
#210
Thr136
Arg31
Glu35
#244
Tyr33
Trp24
Glu30
#257
B
Val115
Leu67
Ile60
Phe34
Ile7
Pro61
Ala9
Leu22
Arg31

Figure 5.4. Polar (A) and non-polar interactions (B) with bound MTX in hDHFR variant F31R/Q35E. MTX is shown in stick representation, and relevant residues are shown in lines, coloured by atom (C: yellow (MTX), green (active site residues); O: red; N: blue). In (**A**), H-bonds and salt bridges are shown as dashed black lines, while active site water molecules #210, #244 and #257 are shown as red spheres. The backbone carbonyls of Ile7 and Val115 are within H-bonding distance of the pterin 4-amino group, as is the hydroxyl group of Tyr121. The carboxylate of the catalytic Glu30 residue forms a salt bridge with the pterin N_1 and 2-amino group. A conserved active site water molecule (H_2O #257), coordinated *via* H-bonding interactions with the indole ring of Trp24 and the Glu30 carboxylate group, is within H-bonding distance of the pterin N_8. Another highly conserved water molecule (H_2O #210) present in the active site can H-bond with the pterin 2-amino group, the backbone carbonyl of Val8 and the hydroxyl group of Thr136. The *p*-aminobenzoic acid moiety of MTX interacts mainly with residues Phe34, Ile60, Pro61 and Leu67 through hydrophobic contacts. A sole H-bond is formed between the carbonyl group of the *p*-ABA moiety and the γ-amino group of residue Asn64.

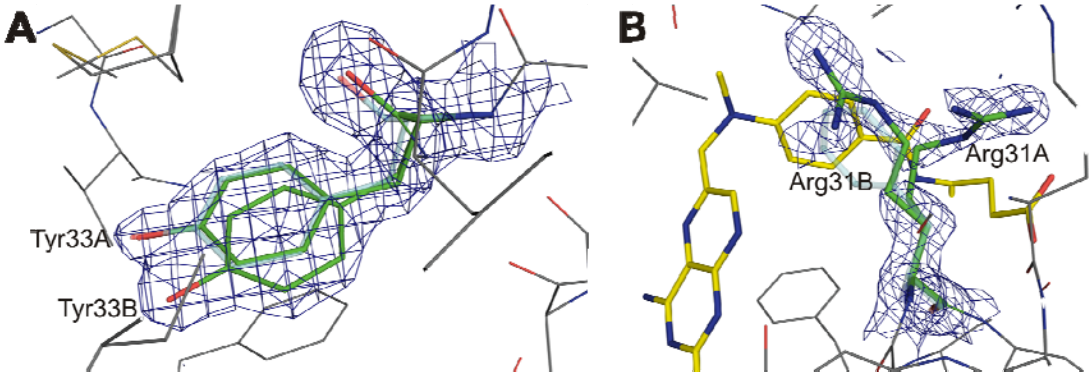

Figure 5.5. Alternate side chain conformers at active site residues Tyr33 (A) and Arg31 (B) in hDHFR variant F31R/Q35E. Residues from the F31R/Q35E and superposed WT hDHFR (1U72) structure are shown in stick representation, coloured by atom (C: green (F31R/Q35E), yellow (MTX), transparent cyan (WT hDHFR); O: red; N: blue). The Tyr33 residue from WT hDHFR is barely visible as it is almost perfectly superposed upon conformer Tyr33A from F31R/Q35E. Superposition was performed by C_α alignment of the crystal structures.

distance of H_2O #210 (Tyr33B; Figure 5.4A). A similar contact is observed in WT hDHFR complexed with NADPH and PT523 (PDB ID 1OHK), a MTX-like inhibitor (22). Hydrophobic and van der Waals interactions are also formed between the pterin moiety of MTX and variant F31R/Q35E (Figure 5.4B). The side chains of Ile7, Ala9, Leu22, Phe34, and Vall15 are all within van der Waals distance of the pterin ring.

Hydrophobic contacts are predominant in binding of the *p*-aminobenzoic acid (*p*-ABA) moiety of MTX, *via* residues Phe34, Ile60, Pro61 and Leu67 (Figure 5.4B). The two side chain conformers of the mutated Arg31 (Arg31A and Arg31B; Figure 5.5B) are also within van der Waals distance of the *p*-ABA phenyl ring. However, Arg31 cannot establish the hydrophobic and possibly edge-to-face aromatic contacts occurring between with WT residue Phe31 and the *p*-ABA phenyl ring, the consequences of which will be discussed below. Importantly, the side chain conformation adopted by four of the six Arg31 residues from the lower resolution structure we obtained clustered about conformation Arg31B (Figure A1.2A in Annexe 1). The other two Arg31 residues from the lower resolution structure clustered together in a new conformation, while none adopted the Arg31A conformation (Figure A1.2B in Annexe 1). The high conformational variation of this residue suggests that the conformers result from the substitutions, rather than from crystallization artifacts.

The glutamate moiety of MTX is mostly solvent exposed and interacts mainly *via* polar contacts with residues of the active site and water molecules at the surface of the protein. The most characteristic contact is the salt bridge formed between the guanidinium group of Arg70 in variant F31R/Q35E and the α-carboxylate of the glutamate moiety. Arg70 is strictly conserved in DHFRs from all species, and this interaction is present in all crystal structures complexed with ligands containing a glutamate moiety. In the F31R/Q35E variant, the α-carboxylate of MTX is also within H-bonding distance of a network involving three water molecules (H_2O #232, 256 and 257) and the carbonyl group of the *p*-ABA moiety. This H-bond network has not been observed in other hDHFR

structures. Molecule H_2O #257 may also H-bond with the γ-carboxylate of MTX and the backbone carbonyl of Arg28. The backbone nitrogen of Arg32 is within H-bonding distance of the γ-carboxylate group of MTX as is the εNH group of mutated Arg31A. The Arg31A conformer places the side-chain in proximity to the glutamate portion of MTX, and enables H-bonding with H_2O #257 and the MTX γ-carboxylate.

Differences in MTX-binding resulting from the F31R and Q35E substitutions – Despite similar interactions formed with MTX in variant F31R/Q35E and WT hDHFR (1U72), differences were observed that are consistent with weakened MTX binding in the variant (Figure 5.6). Table 5.3 lists the distances for apparent polar contacts between the enzyme and the inhibitor, in F31R/Q35E and 1U72. With the exception of unique contacts related to each structure, which mainly involve H-bonds mediated with H_2O #210 and 257, the most important differences were observed in the Trp24-H_2O #244 H-bond (0.8 Å shorter) and the Glu30 εO1- N_8 of MTX H-bond (0.6 Å shorter). The change in distance of the Trp24-H_2O #244 H-bond can be attributed to the shift of residues 17-27 (Figure 5.7). This shift enables closer contacts between the Trp24 indole ring and the conserved water molecule in variant F31R/Q35E. Another difference results from a specific rotation around the C_6-C_9 of the pterin ring of MTX in F31R/Q35E relative to 1U72. The slight rotation (~ 7°) around the C_6-C_9 bond brings the pterin 2-amino group slightly closer (0.6 Å) to the catalytic Glu30 residue. These structural changes in residues that interact with the pterin-moiety appear to be induced by the substitutions at positions 31 and 35, which do not form direct contacts with the pterin moiety.

The *p*-ABA portion of MTX is shifted by ~ 0.6 Å in F31R/Q35E relative to WT hDHFR, bringing this moiety closer to the mutated Arg31, for which two conformers were resolved. Arg31B (Figure 5.5B) points in roughly the same direction as the WT Phe31 residue. Its χ1 angle (-81°) is similar to the WT residue (-84°), such that the guanidinium side chain occupies the area of the active site normally occupied by Phe31. However, a rotation of ~ 90° about the C_β-C_γ bond of Arg31B takes the δCH_2 and εNH groups out of

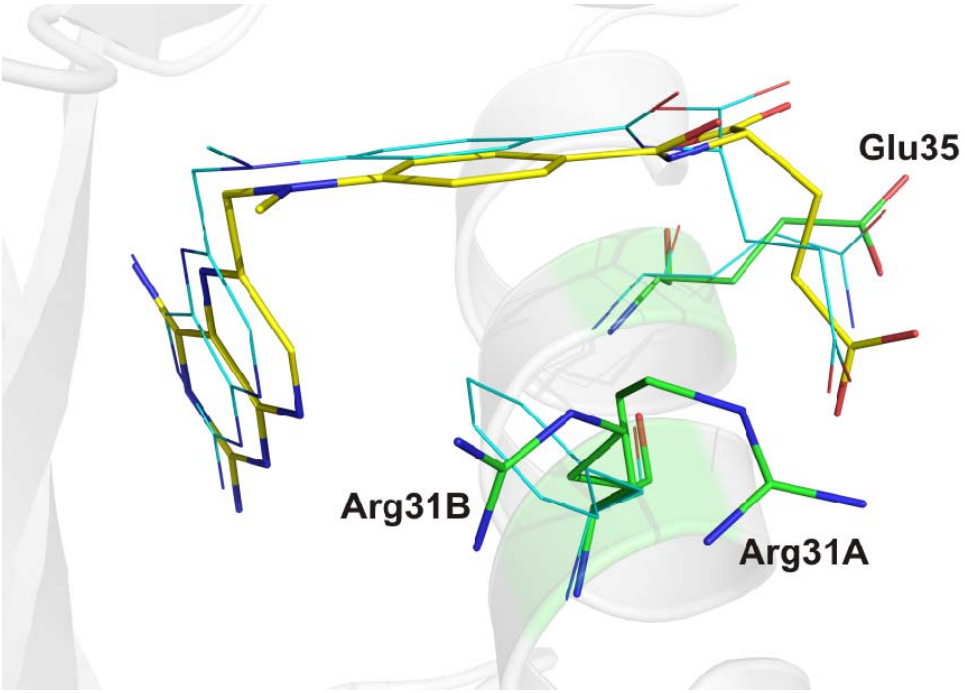

Figure 5.6. Position of MTX, Arg31 and Glu35 in F31R/Q35E relative to the position observed in WT hDHFR (1U72). Residues and MTX from the F31R/Q35E structure are shown in stick representation, while residues and MTX from superposed WT hDHFR (1U72) are shown in lines, coloured by atom (C: green (F31R/Q35E), cyan (WT hDHFR), yellow (MTX from 3eig); O: red; N: blue). Superposition was performed by C_α alignment of the crystal structures.

Table 5.3. Polar interactions in F31R/Q35E and WT hDHFR (1U72) complexed with MTX

Polar contact	Distance F31R/Q35E (Å)	Distance 1U72 (Å) (15)
Ile7 O --- 4-NH_2 MTX	2.9	2.7
Val8 N --- HOH#210	4.1	-
HOH1#210 --- 2-NH_2 MTX	3.1	-
Trp24 N --- HOH#244	3.1	3.9
HOH#244 --- N8 MTX	3.2	3.2
Arg28 O --- HOH#257	2.8	-
HOH#257 --- Oε1 Glu MTX	3.2	-
Glu30 Oε1 --- 2-NH_2 MTX	2.7	3.3
Glu30 Oε2 --- N1 MTX	2.8	2.9
Glu30 Oε2 --- HOH#244	2.8	2.6
Arg31A NH1 --- HOH#257	3.3	-
Arg32 N --- Oε2 Glu MTX	3.2	-
Tyr33B OH --- HOH#210	2.7	-
Gln35 Oε --- O1 Glu MTX	-	3.3
Asn64 Nδ --- O *p*-ABA MTX	2.8	2.8
Arg70 NH1 --- O2 Glu MTX	3.0	2.4
Arg70 NH2 --- O1 Glu MTX	2.8	2.7
Val115 O --- 4-NH_2 MTX	2.9	3.2
Tyr121 O --- 4-NH_2 MTX	3.3	3.3
Thr136 OH --- HOH#210	2.7	-

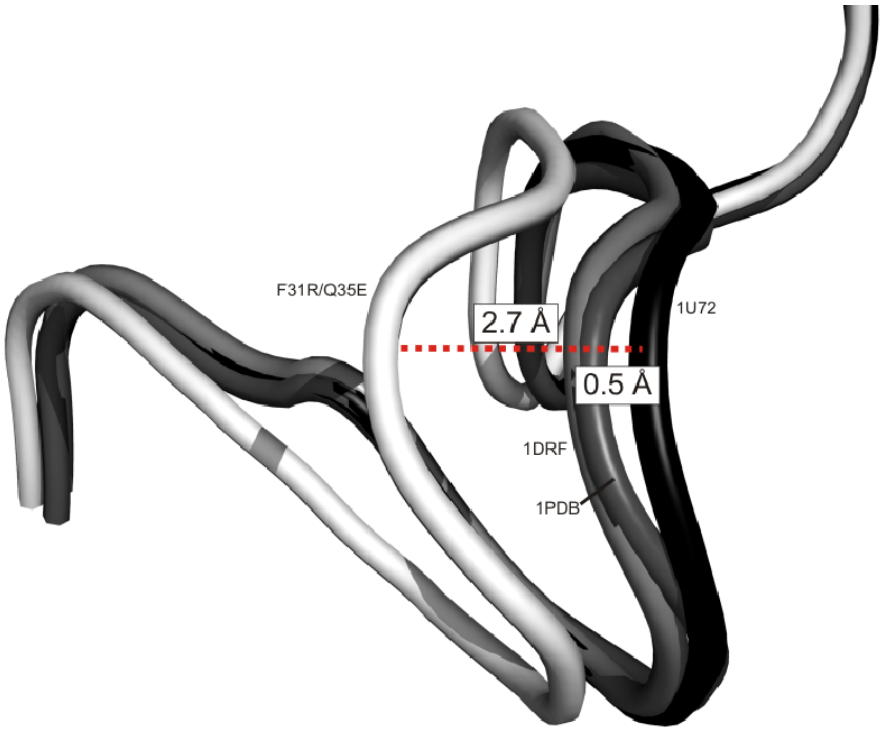

Figure 5.7. Shift of loop 17-27 in hDHFR variant F31R/Q35E. Loops are shown in cartoon representation. Residues 17-27 are shown for variant F31R/Q35E (white), and WT hDHFR from three structures: 1U72 (complexed with NADPH and MTX; black), 1DRF (complexed with folate; light grey) and 1PDB (apoenzyme; dark grey). Distances are calculated between the 1U72 C_α of Gly20 of 1U72 and the respective C_α of Gly20 for the three structures. Superposition was performed by C_α alignment of the crystal structures.

the plane of the Phe31 phenyl group (Figure 5.5B). This results in a loss of hydrophobic and van der Waals contacts, consistent with decreased MTX affinity in F31R/Q35E variant. Nonetheless, the bulky Arg side chain conserved some van der Waals contacts with the *p*-ABA moiety of the inhibitor, and so this may not be sufficient to rationalize the large decrease in MTX-affinity. The shift of the *p*-ABA moiety also brings the MTX N_{10}-methyl group closer to residue 22 in F31R/Q35E as a result of a 7° rotation about the N_{10}-$C_{1'}$ bond. Leu22 belongs to the 17-27 loop, which displays an important shift towards the active site in the double variant structure. This loop shift may be partly attributable to the change of position of residue Leu22 (0.8 Å C_α-C_α distance, relative to 1U72) to maximize van der Waals interactions with MTX, and also with the side chain or Arg31B. In variant F31R/Q35E, one of the ηNH groups of Arg31B is in close proximity to the side chain of Leu22 (Figure 5.8B), mimicking an interaction observed with Phe31 in WT hDHFR (Figure 5.8A). Considering that the van der Waals radius for nitrogen is 0.2 Å smaller than for carbon, Leu22 must therefore be closer to the Arg31 side chain to optimize van der Waals interactions.

The second Arg31 conformer, Arg31A, is rotated about C_α-C_β by more than 70° relative to Arg31B and the native Phe31. This rotation brings the guanidinium side chain closer to the γ-carboxylate group of MTX, where it H-bonds with the γ-carboxylate *via* a water molecule. As shown in Figure 5.6C, considerable hydrophobic and van der Waals contacts with MTX are lost when Arg31 adopts this second conformation, again consistent with the important decrease of MTX-affinity in the variant.

The Gln35Glu substitution also appears to contribute, however slightly, to the decreased MTX-affinity. Residue 35 is located at the surface of the protein. In the WT, the side chain of Gln35 H-bonds with the MTX α-glutamate, but in F31R/Q35E, the variant Glu35 side chain is slightly shifted away from the glutamate moiety of MTX relative to the WT 1U72 structure. As a result, the Glu35 side chain points away from the MTX α-glutamate group such that H-bonding would be weakened or absent. An important rotation

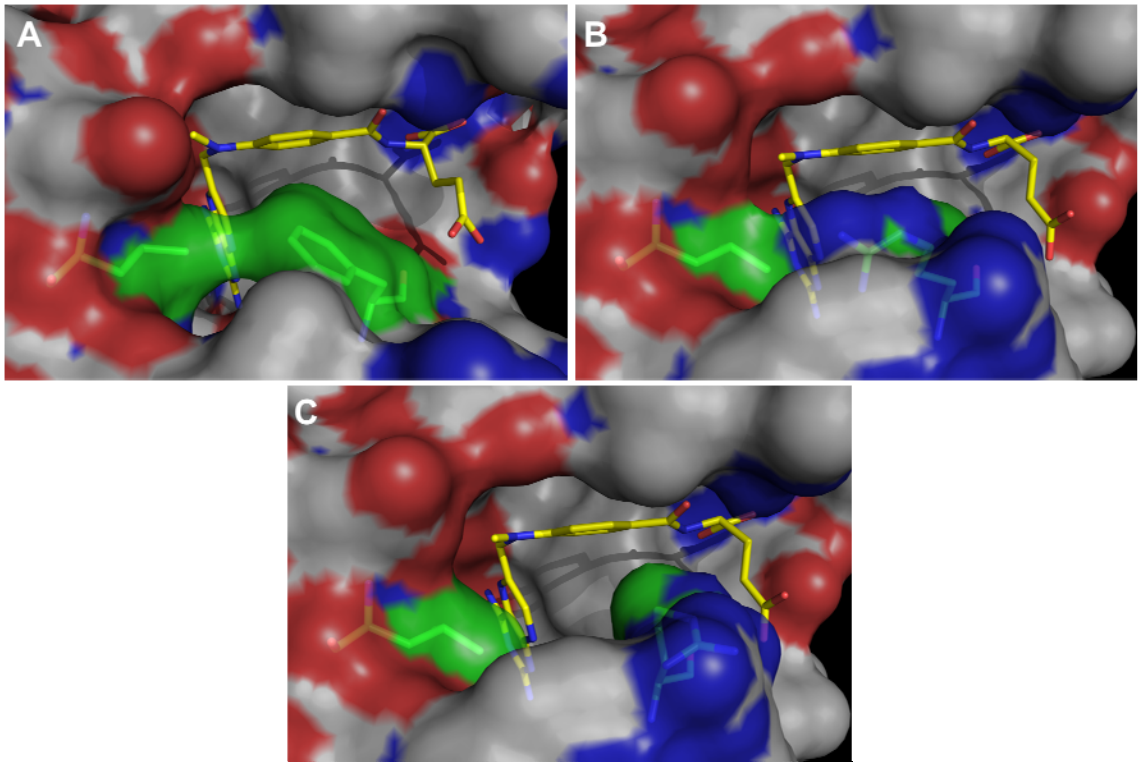

Figure 5.8. Surface representation of the contacts established between residues 22 and 31 in WT hDHFR (A; 1U72), variant F31R/Q35E with Arg31B (B) and variant F31R/Q35E with Arg31A (C) bound to MTX. MTX and residues 22 and 31 are in sticks representation, coloured by atom (C: yellow (MTX); green (residues 22 and 31), O: red, N: blue). Surface is coloured by atoms (C: white, O: red, N: blue).

around the N-C_α bond of the MTX glutamate moiety (34° relative to 1U72), which tilts the α-carboxylate group closer to helix α1, could be caused by unfavourable electrostatic interactions due to two close negative charges (the Glu35 side chain and the glutamate moiety of MTX). This tilt of the MTX glutamate portion results in the lengthening of the salt bridge between Arg70 εNH1 and αO2 of MTX (0.6 Å difference) in variant F31R/Q35E.

A further potential role of the Q35E substitution in reducing MTX-affinity may be a reorientation of Glu35 in the absence of MTX or other ligands, to form a salt bridge with the guanidinium group of Arg70. This speculation is based on the presence of a H-bond between Gln35 and Arg70 in the WT hDHFR apoenzyme structure following repositioning of the Gln35 side chain relative to WT hDHFR bound to MTX (19). An intramolecular salt bridge between Glu35-Arg70 would hinder the binding of the α-carboxylate group of MTX or DHF, thereby decreasing affinity for either compound. However, the kinetic data obtained for the Q35E variant suggests that if these effects are present, they are not the predominant cause for important loss of binding of either ligands.

Docking of folate upon the crystallized F31R/Q35E structure – One of the key features of double variant F31R/Q35E is the more important decrease in MTX affinity relative to DHF affinity. This may be attributed to the flip of the pterin ring of folate relative to MTX, resulting in establishment of different, specific contacts of either ligand with the active-site residues. As mentioned above, the mutated residues 31 and 35 do not interact directly with the pterin moiety of MTX. It is thus unlikely that the selective decrease in MTX affinity relative to DHF could result from different contacts with the mutated residues. The crystal structure presented herein shows that the substitutions mainly perturb interactions with the *p*-ABA and glutamate portions of the bound inhibitor. WT hDHFR structures complexed with folate, the more oxidized form of the substrate, have shown that the *p*-ABA and glutamate portions bind similarly to those of MTX. Therefore, loss of contacts with these portions due to substitutions would be expected to reduce the affinity by a same factor for

either ligand. As our attempts to obtain high-quality crystals of F31R/Q35E with folate were unsuccessful thus far, molecular docking studies were performed with variant F31R/Q35E in order to provide insight into the potential binding mode of folate in the variant enzyme, using the WT hDHFR (PDB ID 1U72) as a reference. As NADPH was not present in the structure of variant F31R/Q35E, it was removed from the 1U72 structure. For variant F31R/Q35E, two independent structures, each containing one of the observed conformers at Arg31 (Figure 5.5B), were created. As the minimal energy conformers for all tested ligands were indistinguishable for the two conformers of Arg31, we report only the results obtained for F31R/Q35E Arg31A.

As a control for the docking protocol, MTX was docked onto 1U72 and F31R/Q35E structures. The docking results confirmed that the protocol enabled good prediction of interactions between MTX and the macromolecules. The minimal energy conformers of docked MTX for WT hDHFR or F31R/Q35E closely resembled the binding observed in the respective crystal structures (RMSD MTX to MTX = 0.9 Å, results not shown). Furthermore, the minimal energy conformer of folate docked onto the 1U72 structure was superimposable with the crystallized folate molecule contained in the 1DRF crystal structure (Figure 5.9A). The orientation of the pterin ring of folate and MTX was correctly predicted in all the minimal energy conformers obtained. Additionally, all known contacts (except when involving non active-site water molecules) were present, including those of the *p*-ABA and glutamate moieties (Figure 5.9B and C). The docking studies with folate suggest that the *p*-ABA and glutamate moieties of folate and MTX bind similarly to the active site of F31R/Q35E variant. If the loss of MTX-affinity in this variant is uniquely attributable to loss of interactions with residues 31 and 35, we would expect the MTX and DHF affinities to decrease by a similar factor. It thus appears that the main effect of substitutions F31R and Q35E is to decrease local order within the active-site area, as evidenced by the number of residues observed as more than one conformer. The resulting active-site composition is more detrimental to MTX affinity than to DHF affinity.

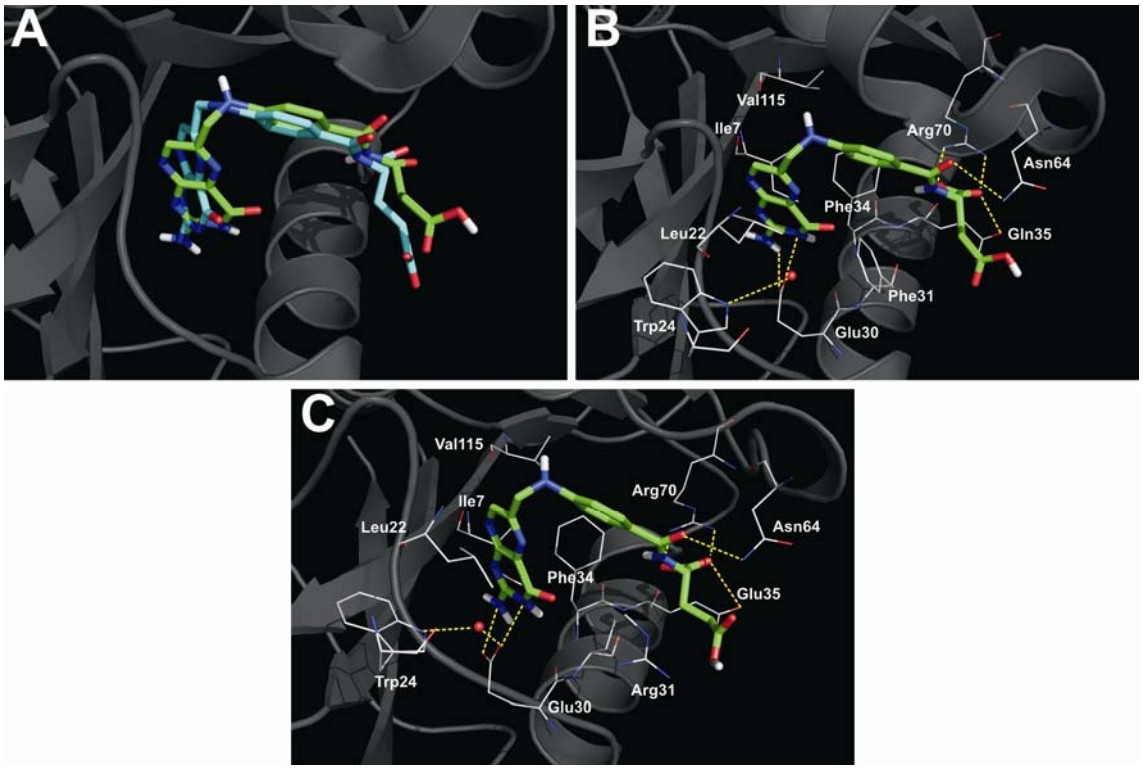

Figure 5.9. Docking of folate onto WT hDHFR and variant F31R/Q35E. (**A**) Superposition of the original crystal structure 1DRF (WT DHFR bound to folate in blue) and the docking model of 1U72 (WT DHFR) docked with folate (in green). Results for the minimum energy binding conformers are shown for folate (**B**) docked onto WT hDHFR (1U72), as well as for folate (**C**) docked onto F31R/Q35E with Arg31A conformer. The ligands are shown in sticks representation while the residues are shown in lines, coloured by atom (C: green (ligands); white (residues), O: red, N: blue). Superposition was performed by C_α alignment of the crystal structures.

DISCUSSION

We report the structure of the highly MTX-resistant hDHFR double variant F31R/Q35E bound to MTX. The decrease of MTX affinity in this variant (> 650-fold relative to WT hDHFR) appears to be attributed to loss of van der Waals contacts between Arg31 and the MTX *p*-ABA moiety resulting in part from multiple conformations adopted by this side-chain, as well as unfavourable electrostatic contacts between Glu35 and the glutamate portion of MTX. These differences could also account for the decrease of DHF affinity (9-fold relative to WT hDHFR), which also contains *p*-ABA and glutamate moieties. Kinetic characterization of the F31R and Q35E point variants showed that the decrease of MTX-affinity in variant F31R/Q35E was attributable to a synergistic effect of the combined substitutions, while the decrease of DHF-affinity was attributable to an additive effect. Docking studies predicted that folate would bind to variant F31R/Q35E in a similar manner to what is observed in WT hDHFR crystal structures bound to folate or MTX (17,32), and that loss of contacts with the *p*-ABA and glutamate moieties of MTX should also be present with DHF or folate. This suggests that the larger decrease in MTX-affinity is not solely caused by loss of contacts between the enzyme and inhibitor.

As indicated by the inhibition constants, the F31R substitution is the main contributor to decreased MTX affinity. Structural data has suggested that the decrease in MTX affinity for variants F31A, F31S and F31G could be due to the loss of van der Waals interactions (11). Although some loss of contacts between MTX and residue 31 is apparent in the F31R/Q35E structure, it is hard to reconcile with the fact that F31R or F31R/Q35E variants display larger decreases in MTX-affinity than the F31G point variant (11), where no contacts can be formed between the ligand and residue 31. This suggests that the basis for the greater decrease of MTX affinity relative to DHF affinity is attributable to a feature that specifically promotes MTX affinity.

It has been shown experimentally that an isomerisation step following initial cofactor and MTX binding increases MTX affinity > 60-fold in the native enzyme, leading to a non-dissociating hDHFR-NADPH-MTX complex (33). It has been suggested that Phe31 is a key residue in this isomerisation (11). This assumption was based on two observations: the presence of a second conformer at the homologous Tyr31 residue in chicken DHFR bound to $NAPD^+$ and biopterin (34); and a non-native-like Phe31 conformer present in one of the two macromolecules observed in WT hDHFR complexed with folate (32). This suggested a possible readjustment of this residue following ligand binding, which would be required for isomerisation.

The structure of variant F31R/Q35E reveals the first-ever evidence of the existence of multiple conformers at residue 31 when MTX is bound to the active site of a variant hDHFR. The presence of these conformers suggests two possibilities. It may result in a decrease in the isomerisation constant (K_{iso}) (33) due to the substitution of Phe31, causing changes in the normal dynamic process related to MTX-binding. Studies have shown that this isomerisation effect exists (33), and leads to tighter binding of MTX in WT hDHFR. However, such an effect has never been reported in the binding of DHF or its more oxidized form, folate; substitutions causing perturbation of K_{iso} would not affect the binding of these ligands as much as it would MTX, consistent with the greater decreases in MTX-affinity observed for variant F31R/Q35E. The F31R substitution, which results in multiple distinct conformers, may perturb K_{iso}, thus reducing MTX-binding. Biophysical data will be required to confirm the disruption of a putative isomerisation step in MTX binding in the F31R and F31R/Q35E variants.

Other residues (Tyr33, Met37, Ser41) in proximity to the folate binding site were represented by two conformers in the F31R/Q35E structure. This has never been observed in any other vertebrate DHFR structure reported to date and suggests that the F31R/Q35E has a more dynamic character than the WT hDHFR. Recent work has shown that variations of ligand binding and catalytic activity can be related to substitutions that change the

dynamics of an enzyme (35,36). Putative dynamic effects related to a substitution, as suggested by the presence of more than one conformer at residue Arg31 and other residues in the F31R/Q35E structure, may lead to selective decrease of inhibitor binding.

ACKNOWLEDGMENTS

This work was supported by the Canadian Institutes of Health Research (CIHR) grants 68851 (J.P.N.) and MOP-13107, NSERC grant 183867-04 (A.M.B.). B.J.Y. is a recipient of a NSERC postgraduate scholarship. A.M.B. is a recipient of the Canada Research Chair in Structural Biology.

REFERENCES

1. Slamon, D. J., Romond, E. H., and Perez, E. A. (2006) *Clin Adv Hematol Oncol* 4, (Suppl. 7), 4-9

2. Daw, N. C., Billups, C. A., Rodriguez-Galindo, C., McCarville, M. B., Rao, B. N., Cain, A. M., Jenkins, J. J., Neel, M. D., and Meyer, W. H. (2006) *Cancer* 106(2), 403-412

3. Strojan, P., Soba, E., Budihna, M., and Auersperg, M. (2005) *J Surg Oncol* 92(4), 278-283

4. Ramanan, A. V., Whitworth, P., and Baildam, E. M. (2003) *Arch Dis Child* 88(3), 197-200

5. Flintoff, W. F., Sadlish, H., Gorlick, R., Yang, R., and Williams, F. M. (2004) *Biochim Biophys Acta* 1690(2), 110-117

6. Takemura, Y., Kobayashi, H., and Miyachi, H. (1999) *Anticancer Drugs* 10(7), 677-683

7. Blakley, R. L., and Sorrentino, B. P. (1998) *Hum Mutat* 11(4), 259-263

8. Patel, M., Sleep, S. E., Lewis, W. S., Spencer, H. T., Mareya, S. M., Sorrentino, B. P., and Blakley, R. L. (1997) *Hum Gene Ther* 8(17), 2069-2077

9. Ercikan-Abali, E. A., Waltham, M. C., Dicker, A. P., Schweitzer, B. I., Gritsman, H., Banerjee, D., and Bertino, J. R. (1996) *Mol Pharmacol* 49(3), 430-437

10. Lewis, W. S., Cody, V., Galitsky, N., Luft, J. R., Pangborn, W., Chunduru, S. K., Spencer, H. T., Appleman, J. R., and Blakley, R. L. (1995) *J Biol Chem* 270(10), 5057-5064

11. Chunduru, S. K., Cody, V., Luft, J. R., Pangborn, W., Appleman, J. R., and Blakley, R. L. (1994) *J Biol Chem* 269(13), 9547-9555

12. Nakano, T., Spencer, H. T., Appleman, J. R., and Blakley, R. L. (1994) *Biochemistry* 33(33), 9945-9952

13. Thompson, P. D., and Freisheim, J. H. (1991) *Biochemistry* 30(33), 8124-8130

14. Fossati, E., Volpato, J. P., Poulin, L., Guerrero, V., Dugas, D. A., and Pelletier, J. N. (2008) *J Biomol Screen* 13(6), 504-514

15. Cody, V., Luft, J. R., and Pangborn, W. (2005) *Acta Crystallogr D Biol Crystallogr* 61(Pt 2), 147-155

16. Volpato, J. P., Fossati, E., and Pelletier, J. N. (2007) *J Mol Biol* 373(3), 599-611

17. Oefner, C., D'Arcy, A., and Winkler, F. K. (1988) *Eur J Biochem* 174(2), 377-385

18. Cody, V., Luft, J. R., Pangborn, W., Gangjee, A., and Queener, S. F. (2004) *Acta Crystallogr D Biol Crystallogr* 60(Pt 4), 646-655

19. Cody, V., Luft, J. R., Pangborn, W., and Gangjee, A. (2003) *Acta Crystallogr D Biol Crystallogr* 59(Pt 9), 1603-1609

20. Cody, V., Galitsky, N., Luft, J. R., Pangborn, W., and Gangjee, A. (2003) *Acta Crystallogr D Biol Crystallogr* 59(Pt 4), 654-661

21. Gangjee, A., Vidwans, A. P., Vasudevan, A., Queener, S. F., Kisliuk, R. L., Cody, V., Li, R., Galitsky, N., Luft, J. R., and Pangborn, W. (1998) *J Med Chem* 41(18), 3426-3434

22. Cody, V., Galitsky, N., Luft, J. R., Pangborn, W., Rosowsky, A., and Blakley, R. L. (1997) *Biochemistry* 36(45), 13897-13903

23. Cody, V., Galitsky, N., Luft, J. R., Pangborn, W., Blakley, R. L., and Gangjee, A. (1998) *Anticancer Drug Des* 13(4), 307-315

24. Ercikan-Abali, E. A., Mineishi, S., Tong, Y., Nakahara, S., Waltham, M. C., Banerjee, D., Chen, W., Sadelain, M., and Bertino, J. R. (1996) *Cancer Res* 56(18), 4142-4145

25. Doucet, N., Savard, P. Y., Pelletier, J. N., and Gagne, S. M. (2007) *J Biol Chem* 282(29), 21448-21459

26. Fernandez-Patron, C., Castellanos-Serra, L., and Rodriguez, P. (1992) *Biotechniques* 12(4), 564-573

27. Otwinowski, Z., and Minor, W. (1997) Processing of X-ray diffraction data collected in oscillation mode. In. *Methods in Enzymology*, Academic Press

28. Storoni, L. C., McCoy, A. J., and Read, R. J. (2004) *Acta Crystallographica, Section D: Biological Crystallography* 60, 432-438

29. Murshudov, G. N., Vagin, A. A., and Dodson, E. J. (1997) *Acta Crystallographica, Section D: Biological Crystallography* D53, 240-255

30. Emsley, P., and Cowtan, K. (2004) *Acta Crystallographica, Section D: Biological Crystallography* D60(12), 2126-2132

31. Klon, A. E., Heroux, A., Ross, L. J., Pathak, V., Johnson, C. A., Piper, J. R., and Borhani, D. W. (2002) *J Mol Biol* 320(3), 677-693

32. Davies, J. F., 2nd, Delcamp, T. J., Prendergast, N. J., Ashford, V. A., Freisheim, J. H., and Kraut, J. (1990) *Biochemistry* 29(40), 9467-9479

33. Appleman, J. R., Prendergast, N., Delcamp, T. J., Freisheim, J. H., and Blakley, R. L. (1988) *J Biol Chem* 263(21), 10304-10313

34. McTigue, M. A., Davies, J. F., 2nd, Kaufman, B. T., and Kraut, J. (1992) *Biochemistry* 31(32), 7264-7273

35. Watt, E. D., Shimada, H., Kovrigin, E. L., and Loria, J. P. (2007) *Proc Natl Acad Sci U S A* 104(29), 11981-11986

36. Eisenmesser, E. Z., Millet, O., Labeikovsky, W., Korzhnev, D. M., Wolf-Watz, M., Bosco, D. A., Skalicky, J. J., Kay, L. E., and Kern, D. (2005) *Nature* 438(7064), 117-121

Préface au chapitre 6

Des mutations dans la DHFR rendant l'enzyme résistante aux antifolates est un mécanisme de résistance retrouvé fréquemment dans des isolats cliniques de diverses espèces de bactéries et de parasites, contrairement aux cellules humaines. Ceci cause un problème d'envergure globale dans le cas de certaines maladies, et le développement de nouveaux antifolates efficaces et spécifiques envers les DHFR mutantes est primordial pour le traitement de ces maladies. Les résidus du site actif ainsi que la structure tridimensionnelle des enzymes parasitaires et bactériennes sont hautement homologues à ceux de la DHFRh. Tout comme chez la DHFRh, les substitutions conférant une résistance aux antifolates chez les bactéries et les parasites se retrouvent majoritairement au niveau du site actif, et la combinaison de substitutions au site actif peut mener à une résistance accrue aux antifolates. Nous avons donc comparé toutes les substitutions du site actif répertoriées chez les DHFR bactériennes et parasitaires à la DHFRh, dans le but de mieux caractériser le rôle de ces résidus par rapport à la reconnaissance des antifolates. La comparaison des séquences, structures et propriétés cinétiques de ces DHFR a permis d'identifier des régions communes du site actif qui, lorsque mutées, menaient à une résistance aux antifolates. L'ensemble des résulats de cette étude comparative offre plusieurs perspectives intéressantes, soit une meilleure compréhension des éléments requis pour la liaison sélective d'antifolates pour la DHFR d'une espèce donnée, une prédiction des régions pouvant être mutées suite à l'administration d'antifolates présentement en phase clinique, ainsi que de nouveaux sites à muter chez la DHFRh pour obtenir des mutants hautement résistants au MTX pour le développement de marqueurs de sélection efficaces.

Ce chapitre est présenté sous forme d'article de revue de littérature soumis au périodique *Drug Resistance Updates* en août 2008. Ayant réalisé la compilation des données et l'ensemble des observations rapportées dans cet ouvrage, ma contribution à ce manuscrit est majeure.

Chapitre 6

Comparaison de séquences et de structures de la dihydrofolate réductase provenant de mammifères, de bactéries et de parasites : identifiaction de régions mutées communes conférant une résistance aux antifolates

6.1 Article 5. Sequence and structural comparison of mammalian, bacterial and parasitic dihydrofolate reductases: cross-species 'hot-spots' provide antifolate resistance

Sequence and structural comparison of mammalian, bacterial and parasitic dihydrofolate reductases: cross-species 'hot-spots' provide antifolate resistance

Jordan P. Volpato[1] and Joelle N. Pelletier[1,2]

[1]Département de Biochimie and [2]Département de Chimie

Université de Montréal

C.P. 6128, Succursale Centre-Ville

Montréal (Québec)

H3C 3J7 CANADA

Submitted to *Drug Resistance Updates* (2008)

Abstract

Human dihydrofolate reductase (DHFR) is a primary target for antifolate drugs in cancer treatment, while DHFR from Plasmodium falciparum, P. vivax and various bacterial species are primary targets in the treatment of malaria and other microbial diseases. Substitutions in each of these DHFRs can yield resistance towards clinically relevant antifolates. We compare the structural and functional impact of active-site substitutions with respect to enzyme activity and antifolate resistance of DHFRs from mammals and from microbes. The high structural homology between DHFRs results in a number of cross-species, active-site 'hot-spots' for broad-based antifolate-resistance. In addition, we identify substitutions that confer species-specific resistance, or yet antifolate-specific resistance. This comprehensive overview of antifolate binding provides new insights into the relation between antifolate design and the advent of mutational resistance in microbes, while presenting avenues for the improvement of antifolate-resistant DHFRs as selective agents for mammalian cells.

Introduction

Antifolates constitute a large family of chemically diverse compounds used in the treatment of a broad range of diseases, the most important of which are various types of cancers as well as parasitic and bacterial infections (Lynch et al., 1982; Mennes et al., 2005; Daw et al., 2006; Bell et al., 2008; Zhanel et al., 2008) (Figure 6.1). These share the common feature of being proliferative diseases. Antifolates inhibit cellular proliferation mainly by interfering with nucleotide biosynthesis. A principal target of antifolates is dihydrofolate reductase (DHFR; E.C.C 1.5.1.3), an essential enzyme found in all living organisms. DHFR catalyzes the reduction of dihydrofolate (DHF) to tetrahydrofolate (THF) using NADPH as a coenzyme. THF is required for the de novo synthesis of purines and thymidylate. Inhibition of DHFR leads to the arrest of cellular proliferation and, eventually, to cellular death.

Antifolates bind to the folate-binding site of DHFR, where they act as competitive inhibitors of the reaction. As a result of high structural homology across species, many antifolates exhibit cross-species inhibition of DHFR. Nonetheless, species-selectivity has also been achieved, as illustrated by trimethoprim (TMP; Figure 6.1), used in the treatment of bacterial infections. Bacterial DHFR exhibits 2500-fold tighter binding for TMP (K_i = 0.08 nM) than the human homolog (K_i = 200 nM), making TMP an effective antibiotic with few or no side effects (Margosiak et al., 1993). Similarly, pyrimethamine (PYR) and cycloguanil (CYC) (Figure 6.1) have proven to be effective antifolates for the treatment of malaria as a result of their higher toxicity towards malarial parasites than human cells (Ferone et al., 1969; Hitchings, 1969). The high structural homology shared by mammalian, parasitic and bacterial chromosomal DHFRs suggests that species-specific inhibition results from slight structural differences within their active site cavities.

Widespread clinical application of antifolates has lead to the development of resistance mechanisms, greatly impairing treatment efficiency. While a number of different

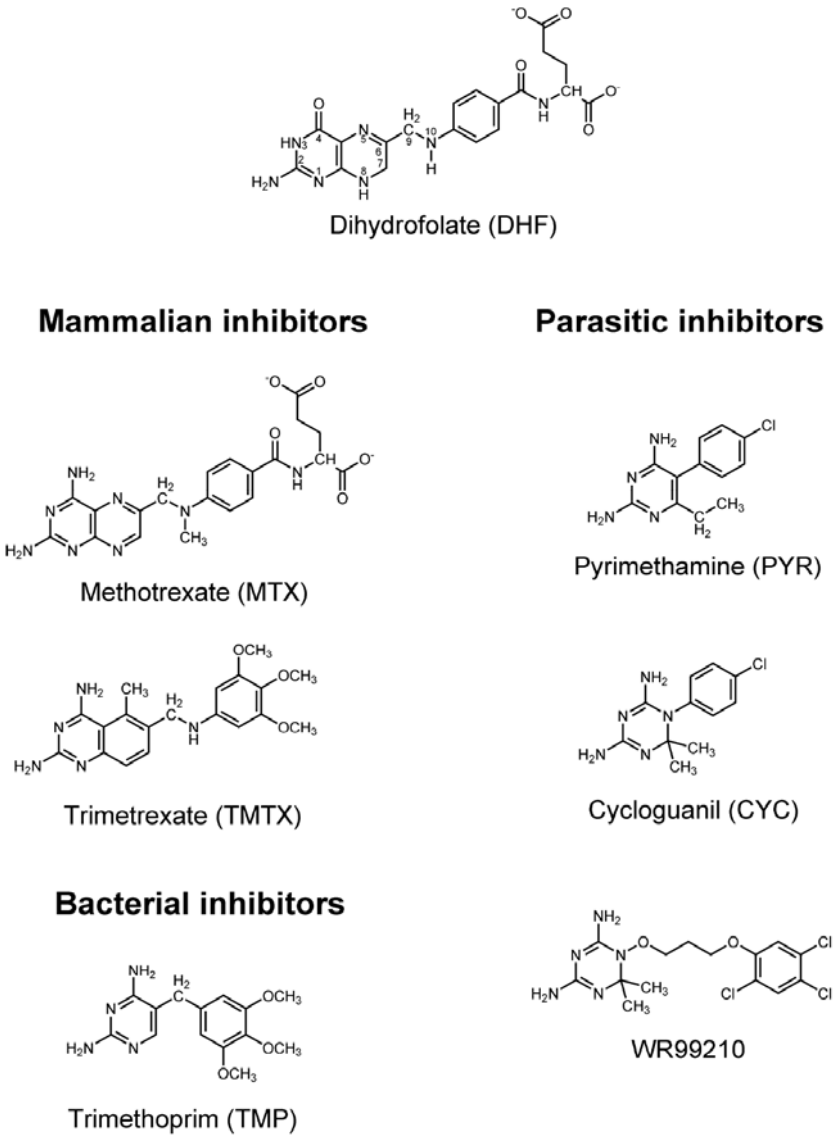

Figure 6.1. Chemical structures of dihydrofolate and antifolates used to inhibit DHFR activity in different species. All antifolates shown are currently used for species-specific treatment. Pterin ring atom numbering is shown on DHF.

resistance mechanisms have been observed, including DHFR gene amplification, decreased cellular permeability toward antifolates and even acquisition of evolutionarily distinct, intrinsically antifolate-resistant variants of DHFR, we focus here on resistance resulting from mutations of the DHFR gene. In parasites and bacteria, the resulting DHFR variants no longer bind the antifolates effectively, yet maintain sufficient catalytic activity to ensure cellular proliferation. As a result, treatment of the microbial infection with the antifolate fails. Because of the slower rate of mutation in human cells relative to microbes, this resistance mechanism is not prevalent in the treatment of proliferative diseases of human cells, such as cancer (Spencer et al., 1996b). Nonetheless, antifolate-resistant variants of human DHFR offer important applications, such as the potential of protecting healthy bone marrow cells from the cytotoxic effects of antifolates used in cancer therapy (Banerjee and Bertino, 2002). Toward this goal, the identification of mutational 'hot-spots' that can lead to antifolate resistance may provide opportunities to engineer the ideal antifolate-resistant DHFR for myeloprotection.

The purpose of this review is to utilize cross-species structural homology, extensive mutational data and inhibition data from a variety of antifolate-resistant DHFRs to map the antifolate-binding requirements at the active site. We strive to highlight cross-species and cross-drug similarities and differences. This will be instrumental in increasing our understanding of the balance struck between binding of the substrate relative to binding of specific antifolates, in clinically-relevant native or mutated DHFR variants.

I Antifolate resistance mechanisms in mammalian cells

Among the antifolates designed to treat proliferative diseases in mammals, no drug has been more useful than methotrexate (MTX) in the clinical field. Since its first synthesis in the 1940's (Farber et al., 1948), MTX has been used to treat various types of cancers and other proliferative diseases (Chu and Allegra, 1996). MTX is a slow, tight binding competitive inhibitor of DHFRs from almost all species. As a result of its lack of

selectivity, MTX is mostly applied to the treatment of human diseases (Jones et al., 2000; Mennes et al., 2005; Strojan et al., 2005; Daw et al., 2006; Hashkes and Laxer, 2006; Slamon et al., 2006). MTX resistance has been observed in mammalian cells exposed ex vivo to MTX. At low doses, substitutions in the Reduced Folate Carrier protein (RFC) (Rothem et al., 2004) and in folylpolyglutamate synthetase (FPGS) reduce cellular uptake of antifolates or allow more rapid efflux of MTX (Zhao et al., 2000), respectively. These MTX-resistance mechanisms have recently been reviewed more extensively (Zhao and Goldman, 2003) and will not be further discussed.

At higher doses, those mechanisms do not sufficiently decrease cytoplasmic MTX concentrations; over-expression and/or amplification of the native DHFR gene are frequently observed (Dolnick et al., 1979; Melera et al., 1982; Chu et al., 1993; Goker et al., 1995). Because MTX binds stoechiometrically to DHFR, increased gene copy number can overcome inhibition. In addition, mammalian DHFR activity is regulated by binding of its cognate mRNA at the active site (Chu et al., 1993). Binding of MTX dislodges the DHFR mRNA, rendering it available for translation.

The above-mentioned MTX resistance mechanisms have all been observed in tumours isolated from patients that relapsed during or following MTX-treatment and have been observed ex vivo by exposing cells to MTX (Lin et al., 1991; Trippett et al., 1992; Goker et al., 1993; Goker et al., 1995). One additional resistance mechanism has solely been observed in ex vivo studies: mutations in the mammalian DHFR gene that encode a DHFR variant with reduced affinity for MTX.

MTX-resistant point variants from mammalian cell lines

Characterization of MTX-resistant variants will increase our understanding of inhibitor binding at the active site of DHFR, critical to the design of novel inhibitors. Early studies exposed mammalian cells to MTX ex vivo, to predict the mutations that would result from the long-term treatment of patients. Among the first substitutions so identified

was the L22R substitution in MTX-resistant fibroblasts from murine embryos (Simonsen and Levinson, 1983). Leu22 is a highly-conserved active site residue that establishes van der Waals contacts with the pterin ring of bound MTX (Cody et al., 2005) (Figure 6.2A). Crystal structure of murine and human L22R variants suggested that introduction the arginine reduces the contact surface with MTX (Cody et al., 2005). A L22F substitution resulted in MTX-resistance in CHO cells (Melera et al., 1988). Characterization of the human L22F variant revealed that it conferred a >100-fold decrease in MTX-affinity, while retaining a catalytic activity slightly lower than WT (Lewis et al., 1995) (Table 6.1).

The first human DHFR substitution was the F31S variant, identified in MTX-resistant human colon cancer cells (Srimatkandada et al., 1989). The F31S substitution increased MTX-resistance 70-fold while decreasing catalytic efficiency < 5-fold relative to WT hDHFR (Table 6.1), providing a further example of increased resistance with little loss of activity. Phe31 establishes van der Waals contacts with the p-aminobenzoyl portion of bound MTX (Oefner et al., 1988) (Figure 6.2A). Ten years earlier, Goldie et al. (Goldie et al., 1980) had identified the murine, MTX-resistant F31W substitution in mouse leukemia cells. Taken together, those results suggested that substitutions at positions 22 and 31 could be 'hot-spots' for MTX-resistance, and that diverse amino acid substitutions may be tolerated at these active site positions of mammalian DHFRs. Further work in MTX-resistant mouse leukemia cells by Dicker et al. (Dicker et al., 1993) revealed the G15W variant. In vitro characterization demonstrated that although MTX-affinity of G15W had decreased by >165-fold relative to WT, the variant was unstable and therefore not the primary cause of resistance.

MTX-resistant mammalian DHFRs from site-directed mutagenesis

While it soon became apparent that MTX-resistant DHFR variants were not the cause of resistance in tumours isolated from patients (Spencer et al., 1996b), MTX-resistant DHFRs became key to a promising application. Because MTX is a myeloablative drug, MTX resistant DHFRs can protect healthy cells from cytotoxicity during high-dose MTX

Table 6.1. Mutations providing MTX-resistance in human DHFR.

hDHFR variant		Catalytic efficiency ($\mu M^{-1}s^{-1}$)	K_i^{MTX} (nM)	References
Native		92	0.0034	(Margosiak *et al.*, 1993)
Position 7	I7F	0.24	24.6	(Patel *et al.*, 1997)
Position 22	L22F	6.1	0.55	(Lewis *et al.*, 1995)
	L22R	0.028	4.6	(Lewis *et al.*, 1995)
	L22W	10	4.3	(Lewis *et al.*, 1995)
	L22Y	12	11	(Lewis *et al.*, 1995)
Position 31	F31A	30	0.27	(Chunduru *et al.*, 1994)
	F31G	26	0.35	(Chunduru *et al.*, 1994)
	F31P	4.3	1.7	(Volpato *et al.*, 2007)
	F31R	1.5	7.2	(Patel *et al.*, 1997)
	F31S	16	0.24	(Chunduru *et al.*, 1994)
Position 34	F34A	0.24[a]	34[b]	(Nakano *et al.*, 1994)
	F34I	0.57[a]	13[b]	(Nakano *et al.*, 1994)
	F34S	0.017[a]	210[b]	(Nakano *et al.*, 1994)
	F34T	0.11[a]	9.6[b]	(Nakano *et al.*, 1994)
	F34V	0.49[a]	10[b]	(Nakano *et al.*, 1994)
Position 115	V115A	0.2	20	(Fossati *et al.*, 2008)
	V115C	0.1	20	(Fossati *et al.*, 2008)
Double mutants	L22F/F31G	3.3	29	(Ercikan-Abali *et al.*, 1996a)
	L22F/F31S	3.6	26	(Ercikan-Abali *et al.*, 1996a)
	L22Y/F31G	1.4	150	(Ercikan-Abali *et al.*, 1996a)
	L22Y/F31S	3.8	42	(Ercikan-Abali *et al.*, 1996a)
	F31R/Q35E	1.9	21	(Volpato *et al.*, 2007)
Triple mutants	F31R/F34T/Q35S	0.6	56	(Volpato *et al.*, 2007)
	F31R/F34T/Q35R	0.5	81	(Volpato *et al.*, 2007)
	F31A/F34V/Q35H	0.3	180	(Volpato *et al.*, 2007)

[a] Derived from plots of rate versus DHF concentration by least-square fit to the equation for substrate inhibition by Nakano *et al.*

[b] Ternary K_D^{MTX} values.

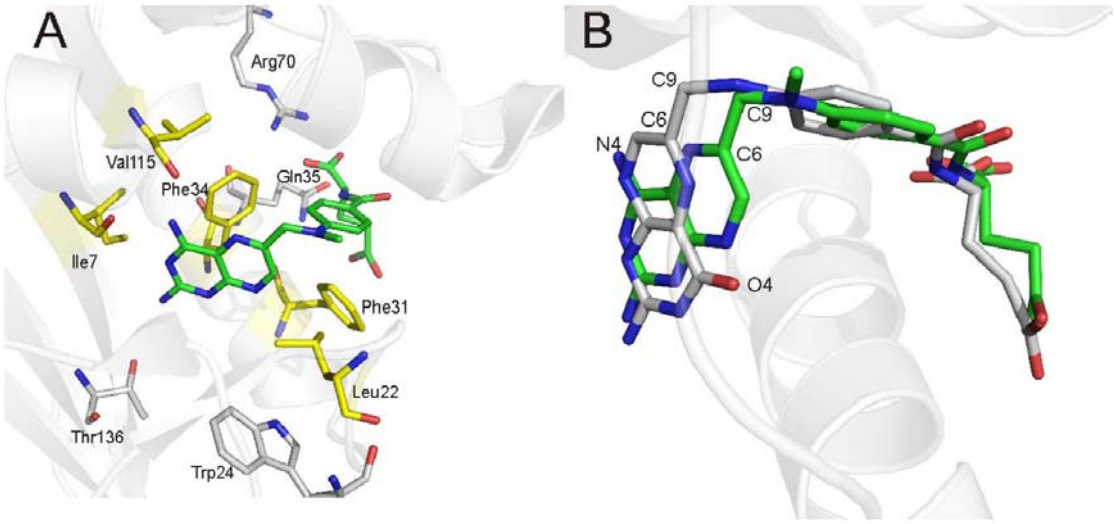

Figure 6.2. Binding of MTX to the active site of human DHFR. A: Principal residues interacting with MTX at the active site (1U72.pdb). Side-chains are shown in stick representation (nitrogen: blue, oxygen: red, carbon: yellow for residues forming non-polar interactions with MTX; white for residues forming polar interactions with MTX; green for MTX. B: Superposition of folate (1DRF.pdb) and MTX (1U72.pdb) at the active site of human DHFR. The pterin ring of MTX is flipped 180º around the C6-C9 bond relative to folate, placing the N4 group of MTX in a different area of the active site than the corresponding O4 group of folate. Only the backbone of 1U72 is shown for clarity.

treatment. The incorporation of MTX-resistant DHFRs in healthy hematopoietic stem cells (HSC) for engraftment in the bone marrow has the potential to ensure myeloprotection of patients during treatment with MTX (Banerjee and Bertino, 2002). Below, we highlight structure-function studies of MTX-resistant variants in mammalian DHFRs, and present the progress made in myeloprotection of human HS cells and in murine models.

Site-directed mutagenesis of murine and human DHFR rapidly demonstrated the potential for decreasing MTX-affinity. Thillet et al. (Thillet et al., 1988) created point substitutions in murine DHFR at active site residues that form specific contacts with bound MTX, including the potential 'hot-spot' positions 22 and 31. The I7S, L22R, W24R, F31S, F31R, F34L, Q35R, Q35P, V115P and T136V point variants were created and characterized. All exhibited decreased MTX-affinity accompanied with loss of catalytic activity generally resulting from reduced DHF affinity. This result is readily rationalized by the fact that MTX and DHF make similar contacts with the enzyme, as illustrated with the highly homologous human DHFR in Figure 6.2B; substitutions affecting binding of MTX are likely to affect DHF binding. The most resistant murine variant was the previously-identified L22R, with MTX-affinity decreased by > 5 orders of magnitude, whereas catalytic efficiency was decreased 1600-fold relative to WT enzyme. Significantly, K_M^{DHF} increased only 25-fold, indicating that DHF binding was modified to a lesser extent than MTX binding. This result underscores the potential for creation of 'efficient' variants for myeloprotection, exhibiting poor MTX binding but retaining significant activity. However, the tight binding of MTX (3.4 pM) relative to DHF (100 nM) in the native human enzyme poses a challenging start point. In another study, Morris and McIvor (Morris and McIvor, 1994) performed saturation mutagenesis at positions 22 and 31 of murine DHFR. At position 22, six residues (A, F, N, W, Y and R) gave higher IC_{50}^{MTX} than the WT enzyme, the highest being variant L22R (2000-fold increase), as seen previously (Thillet et al., 1988). At position 31, eight residues yielded MTX-resistant variants (R, S, Q, E, W, H, G

and N), the most resistant variant being F31N (IC_{50}^{MTX} increased 75-fold). Positions 22 and 31 thus continued to prove their potential for development of resistance.

In accordance with results obtained with murine DHFR, site-directed mutagenesis of human DHFR L22 to F, R, W or Y variants all conferred MTX-resistance (Lewis et al., 1995) (Table 6.1). The L22W and L22Y variants were the most resistant to MTX (K_i^{MTX} increased up to 3200-fold), with a 10-fold reduction in catalytic efficiency. The L22R variant was also highly resistant but showed a greater decrease in catalytic efficiency while the L22F variant was moderately resistant while maintaining catalytic efficiency in the range of the WT.

Although human DHFR residues Phe31 and Phe34 are neighbours, forming similar contacts with bound MTX (Figure 6.3A), their substitution to Ser had differing effects (Schweitzer et al., 1989). The catalytic activity of the F31S variant was comparable to that of the WT while its K_D^{MTX} was increased 100-fold. The F34S substitution had an even higher ternary K_D^{MTX} (> 4 orders of magnitude higher than WT), but had low catalytic activity (4 orders of magnitude lower). Variants F31L, F31V and F31T were not resistant to MTX (Prendergast et al., 1989, Chunduru et al., 1994), while the F31A and F31G displayed MTX-resistance and catalytic efficiencies comparable to the F31S variant (Chunduru et al., 1994) (Table 6.1). While those results suggested that only small amino acids at position 31 confer MTX-resistance, the F31R substitution yielded one of the most resistant hDHFR point variants reported to date, with K_i^{MTX} increased of 3 orders of magnitude relative to WT human DHFR (Patel et al., 1997). Further substitutions at residue F34 also yielded MTX-resistant variants. Like the F34S variant, substitution to A, I, T or V all increased the ternary K_D^{MTX} but greatly impaired catalytic efficiency, mainly due to an increase in K_M^{DHF} (Nakano et al., 1994). Those results highlighted the importance of F34 in folate and antifolate binding in human and murine DHFRs and, consistent with its strict conservation, suggest that this feature may be generalized. Substitution at position 34 in mammalian DHFRs may thus be less prone to development of resistance than positions 22 and 31.

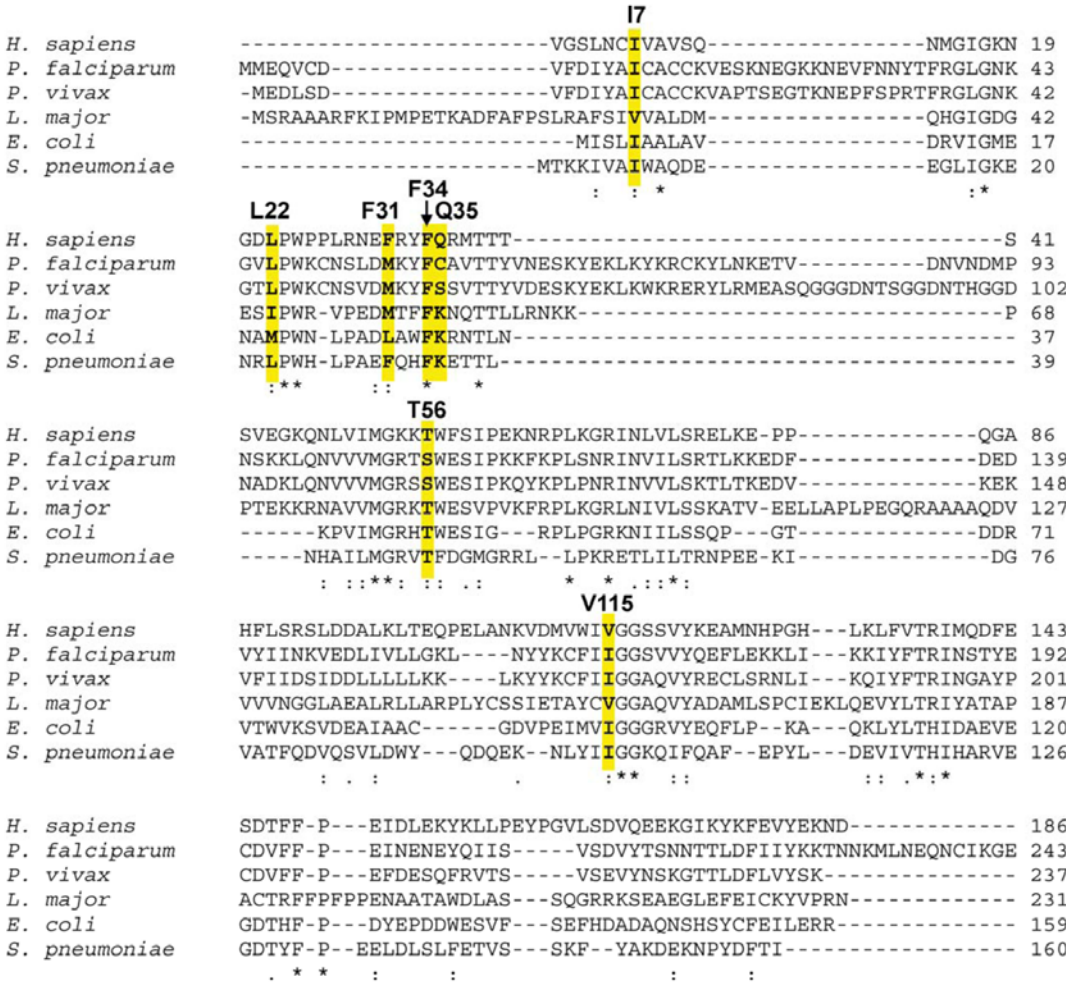

Figure 6.3. Sequence alignment of DHFRs from different species. Highlights identify residues that can be substituted to confer antifolate resistance in more than one species (mammalian numbering). Alignment was generated using Espresso (3Dcoffee alignment; http://www.igs.cnrs-mrs.fr/Tcoffee/). **:** = conserved residues, **.** = semi-conserved residues and * = strickly conserved residues.

Other active site substitutions yielded MTX-resistant hDHFR variants. The I7F substitution generated a 7000-fold increase in K_i^{MTX} (Patel et al., 1997) (Table 6.1). The Ile7 backbone carbonyl has been proposed to H-bond with the 4-amino group of MTX (Figure 6.2A), an interaction that cannot be established with folate given that its pterin ring is flipped 180° around the C_6-C_9 bond relative to MTX (Figure 6.2B). Substitutions that disrupt this H-bond could potentially reduce affinity to MTX while maintaining native-like catalytic efficiencies. However, the catalytic efficiency of the I7F variant dropped 380-fold due to decreased DHF binding, demonstrating that this highly conserved residue plays a role in substrate recognition and catalysis (Patel et al., 1997). This is attributable to formation of van der Waals contacts with the pterin ring of either ligand with residue Ile7. Furthermore, by analogy to 5-deazafolate (Davies et al., 1990), the Ile7 backbone contributes to DHF binding via carbonyl H-bonding with the pterin ring protonated at the N8 atom, which is positioned in the same area of the active site as the 4-amino group of MTX. Arg70 is a highly conserved residue that forms a salt bridge with the glutamate portion of bound ligands. Disruption of this salt bridge in the R70K variant yielded a binary K_D^{MTX} that was 4 orders of magnitude greater than the WT K_i^{MTX}. In counterpart, catalytic efficiency was decreased > 100-fold, mainly due decreased DHF affinity.

More recently, we developed a two-tier screening assay that enables rapid identification and characterization of active and MTX-resistant variants of DHFR (Fossati et al., 2008). Saturation mutagenesis libraries of human DHFR at residues Ile7, Gly15, Trp24, Arg70 and Val115 were selected for activity and MTX-resistance. Position 115 was the most tolerant to substitutions, yielding the MTX-resistant variants V115A and V115C, which displayed high K_i^{MTX} values (6000-fold increase) accompanied by an important loss of catalytic activity (Table 6.1). Like residue I7, the backbone carbonyl of Val115 H-bonds with the 4-amino group of MTX, but not folate. Nonetheless, the data indicate that Val115 is important for binding of both ligands. Saturation mutagenesis at Ile7, Gly15, Trp24 and Arg70 failed to yield MTX-resistant variants according to our screening stringency.

MTX-resistant multiple variants

Highly MTX-resistant mammalian DHFRs were obtained by combining 'hot-spot' Leu22 and Phe31 point variants that individually conferred MTX-resistance (Ercikan-Abali et al., 1996a). All the (L22/F31) double variants tested had higher K_i^{MTX} values than the corresponding Leu22 or Phe31 point variants. Furthermore, the increase was synergistic in some cases, such that the thermodynamic change in MTX-binding ($\Delta\Delta G^{MTX}$) for the double variants was greater than the sum of changes for the corresponding point variants. The increase in MTX-resistance was accompanied by decreased catalytic efficiency in all cases. Nonetheless, those results revealed the potential for increasing MTX resistance by combining substitutions at positions involved in MTX-binding. We recently applied a semi-randomized approach to simultaneously mutate residues Phe31, Phe34 and Gln35 of hDHFR, selecting the most MTX-resistant variants via a bacterial complementation assay. One novel point variant (F31P) and 9 combinatorial variants were identified and characterized (Volpato et al., 2007) (Table 6.1). As with the (Leu22/ Phe31) double variants, the (F31/F34/Q35) double and triple variants were all highly MTX-resistant. A trade-off between increased MTX-resistance and decreased catalytic efficiency was again observed. Triple variant F31A/F34V/Q35H displayed the highest K_i^{MTX} reported for a hDHFR variant (50000-fold increase), accompanied by a relatively modest 180-fold reduction in catalytic efficiency. Thus, while the Leu22/Phe31 hot-spot combination was effective in providing strong MTX-resistance, various combinations of substitutions can provide similar or greater effects.

Applications of MTX-resistant mammalian DHFR variants

MTX-resistant DHFR variants have been tested for their potential in protecting cells from the cytotoxic effects of MTX and other antifolates used in cancer chemotherapy. Antifolates, being antiproliferative drugs, are particularly cytotoxic to rapidly dividing cells such as healthy haematopoietic stem cells (HSC) and other bone marrow cells. The

resulting myeloablation leads to immuno-suppression, inducing secondary infections during chemotherapy (Das et al., 2006). Incorporation of MTX-resistant DHFRs in HSC using retroviral vectors has been shown to provide efficient myeloprotection during antifolate treatment in murine models. In addition, MTX-resistant DHFRs have been shown to be reliable markers for in vivo selection of transduced HSCs (Zhao et al., 1997; Allay et al., 1998) or in vitro selection of transfected or transduced cells (Banerjee et al., 1994a; Banerjee et al., 1994b; Flasshove et al., 1995; Ercikan-Abali et al., 1996b; Havenga et al., 1998; Gatlin et al., 2000; Volpato et al., 2007). For these applications, ideal MTX-resistant DHFR variants should display a high K_i^{MTX} while maintaining a catalytic efficiency that is sufficient to ensure cell proliferation.

Two cell types have mainly been used to evaluate the protection from cytotoxicity conferred by MTX-resistant hDHFRs: CHO DUKX B11 (*dhfr*-) cells and HSC. Human DHFR point variants G15W (Banerjee et al., 1994b), L22F (Ercikan-Abali et al., 1996b), L22R (Banerjee et al., 1994a; Banerjee et al., 1994b), F31S (Banerjee et al., 1994a; Banerjee et al., 1994b) and F34S (Banerjee et al., 1994a) all conferred moderate MTX-protection to CHO *dhfr*- cells at low MTX concentrations (<10% survival of cells at 10μM MTX). The murine DHFR L22R, F31R, F31S and Q35P variants yielded similar results (Thillet and Pictet, 1990). We recently observed greater MTX-protection of CHO *dhfr*- cells with hDHFR variant F31A/F34V/Q35H, which conferred > 70% survival at 200 μM MTX (Volpato et al., 2007). Other double and triple variants also offered efficient protection, conferring > 50% survival at 30 – 56 μM MTX (Volpato et al., 2007).

While CHO *dhfr*- cells offer a convenient model system, they offer no practical applications. HSC constitute a prime target for protection because of their sensitivity to antifolates and their potential as recipients of genetic material for engraftment. Among the MTX-resistant DHFR variants tested for myeloprotection (Hock and Miller, 1986; Banerjee et al., 1994a; Banerjee et al., 1994b; Zhao et al., 1997; Takebe et al., 2002; Warlick et al., 2002), only two variants offered high levels of protection from antifolates to HSC in

culture: L22Y (Spencer et al., 1996a; Allay et al., 1998; Gatlin et al., 2000; Belzile et al., 2003) and the L22F/F31S double variant (Sauerbrey et al., 1999; Takebe et al., 2001; Takebe et al., 2002; Capiaux et al., 2003; Capiaux et al., 2004). The human L22F/F31S variant transduced into human bone marrow cells conferred close to 100 % survival on in vitro myeloid progenitor assays containing 100 nM MTX (Capiaux et al., 2003). In that study, the double variant also contributed to dual-protection against MTX and a thymidylate synthase (TS) inhibitor, 5-fluorouracil (5-FU), when either covalently-linked or independently co-expressed with a 5-FU resistant variant of TS. More recently, those constructs were shown to offer myeloprotection to bone marrow cells exposed to pemetrexed (PMTX), a newer antifolate that inhibits both TS and DHFR activities in cells (Capiaux et al., 2004). Further studies have reported dual protection from MTX and other non-related myeloablative drugs by co-expressing the L22F/F31S double variant with other drug resistance variants (Sauerbrey et al., 1999; Takebe et al., 2001; Takebe et al., 2002). Although the double variant displays good protection of bone marrow cells from the toxic effects of MTX *in vitro*, the concentration of MTX used for selection (100 nM) is lower than the circulating concentration in plasma during treatment with the drug (0.5 to 1 μM) (Goldman, 1974; Cheng, 2007). Therefore, MTX-resistant variants protecting bone marrow cells at higher MTX concentration would be required for myeloprotection applications.

Unlike the L22F/F31S variant, L22Y has mainly been used as an in vivo selection marker for transduced HSC cells. Gene transfer efficiencies using retroviruses or lentiviruses rarely surpass 25%, and transplantation of poorly-transduced bone marrow cell populations is one of the chief limitations to the therapeutic effects of gene therapy (Sorrentino, 2004). MTX-resistant DHFRs can be used as in vivo selection markers against MTX, to enrich the population of transduced cells post-transplantation. Although the L22Y variant was first characterized for its resistance to MTX (Lewis et al., 1995), trimetrexate (TMTX), a non-polyglutamated antifolate that is more cytotoxic to HSC than MTX, has mostly been used as its selective agent in bone marrow cells. In that system, L22Y yielded greater survival rates against TMTX than against MTX (Spencer et al., 1996a).

Transplantation of L22Y-transduced bone marrow cells in mouse recipients followed by TMTX and nucleoside transport inhibitor (NBMPR-P) administration lead to > 50% *in vivo* enrichment of transduced bone marrow cell populations in primary recipients, and this enrichment was maintained in secondary transplant recipients (Allay et al., 1998). However, similar experiments in rhesus macaques (Persons et al., 2004) yielded only transient *in vivo* selection, due to important differences in transduction efficiencies and in vivo HSC cycling in both species. It should be noted that the use of antifolates such as MTX and TMTX as in vivo selective agents is advantageous relative to selection systems such as O^6-methylguanine-DNA-methyltransferase (Kramer et al., 2006) or γ-glutamylcysteine synthtase (Lorico et al., 2005) given that the side-effects of their administration are well characterized and well tolerated by patients.

In vitro selection of bone marrow cells offers the possibility to enrich transduced cell populations prior to transplantation, which would increase the likelyhood of successful engraftment. In vitro selection could be applied to bone marrow cells from virtually any species, regardless of species-specific properties of HSC. However, this application faces a major technical hurdle: HSC can currently be cultured only for a limited number of days, after which they differentiate and cannot repopulate bone marrow populations *in vivo* (Dolznig et al., 2005). The MTX-resistant DHFRs L22Y and L22F/F31S have been tested for this application, with mitigated results. While bone marrow cells could be selected *in vitro* with those DHFR variants (Gatlin et al., 2000; Takebe et al., 2002; Belzile et al., 2003; Capiaux et al., 2003), the HSC viability was considered too poor for engraftment following the period required for efficient in vitro selection. As a result, in vivo repopulation of bone marrow by selected cells was not assessed. We are currently investigating MTX-resistant DHFRs that tolerate a higher dose of MTX during in vitro selection, permitting efficient enrichment of transduced HSC on a shorter timescale that may be compatible with engraftment (J. P. V., N. Mayotte, G. Sauvageau and J. N. P., unpublished results).

II Antifolate resistance mechanisms in parasites and bacteria

Of all parasitic diseases, malaria is the most frequent and the most deadly, causing over one million deaths each year (www.who.int). Malaria is transmitted via the blood by mosquitoes carrying the parasite, and can be caused by four distinct species of Plasmodium: *P. ovale*, *P. malariae*, *P. vivax* and *P. falciparum*, the latter being the most severe and prevalent form. Because of the importance of this disease, we mainly focus on inhibition of the DHFR domain of the bifunctional *P. falciparum* DHFR-thymidylate synthase (DHFR-TS) with pyrimethamine. Although it is an effective antimalarial antifolate, pyrimethamine resistance can result from DHFR mutations. We also discuss resistance to antifolate inhibition in other parasites and in alternative antifolate treatments of Plasmodium, to provide a broad picture of parasitic resistance to antifolates.

Naturally-occurring antifolate resistance in Plasmodium parasites

Discovery of synthetic anti-malarial drugs in the 1930's was stimulated by the decreased abundance of quinine. The first synthetic antifolates were proguanil (which metabolizes to the active compound cycloguanil (CYC) (McGready et al., 2003)) and pyrimethamine (PYR) (Figure 6.1), which efficiently inhibit *P. falciparum* DHFR (Sirawaraporn et al., 1993). The effectiveness of PYR, particularly when administered with sulfadoxine (an inhibitor of dihydropteorate synthase), lead to its widespread use as a first-line treatment for malaria in several countries (Happi et al., 2005; Nzila et al., 2005). However, PYR-resistant *P. falciparum* strains were identified in clinical isolates shortly after the first PYR trials (Chongsuphajaisiddhi and Sabchareon, 1981). The S108N substitution was responsible for the phenotype observed in one PYR-resistant strain (Cowman et al., 1988) (Table 6.2; corresponding residue numbering for DHFRs from other species is provided in Table 6.3). Combination of S108N with the C59R substitution increased PYR resistance 11-fold while combination with a N51I substitution increased resistance 45-fold (Foote et al., 1990). The triple variant C59R/S108N/I164L was more

Table 6.2. Substitutions providing PYR and/or CYC-resistance in *plasmodium* DHFR.

Enzyme		Catalytic efficiency ($\mu M^{-1}s^{-1}$)	K_i^{PYR} (nM)	K_i^{CYC} (nM)	$K_i^{WR99210}$ (nM)	References
Native *pfDHFR*		6.8	1.5	2.6	1	(Sirawaraporn *et al.*, 1997a; Zhang and Rathod, 2002)
Point mutants	A16V	0.01	6.0	570		(Sirawaraporn *et al.*, 1997a)
	N51I	0.81	0.4	4.7		(Sirawaraporn *et al.*, 1997a)
	C59R	76	1.1	4.7		(Sirawaraporn *et al.*, 1997a)
	S108N	3.7	13	15		(Sirawaraporn *et al.*, 1997a)
	I164L	2.4	0.83	9		(Sirawaraporn *et al.*, 1997a)
Double mutants	A16V/S108T	0.64	3.6	2100		(Sirawaraporn *et al.*, 1997a)
	N51I/S108N	13	37	24		(Sirawaraporn *et al.*, 1997a)
	C59R/S108N	0.18	72	82	0.6	(Hekmat-Nejad and Rathod, 1997; Sirawaraporn *et al.*, 1997a)
Triple mutants	N51I/C59R/S108N	0.53	120	100		(Sirawaraporn *et al.*, 1997a)
	C59R/S108N/I164L	0.17	380	1141		(Sirawaraporn *et al.*, 1997a)
Quadruple mutant	N51I/C59R/S108N/I164L	1.1	860	730	1.9	(Sirawaraporn *et al.*, 1997a; Chusacultanachai *et al.*, 2002)
Native *pvDHFR*		3.3	0.16	0.6	6	(Leartsakulpanich *et al.*, 2002)
Point mutants	F57L	0.0015	130	740	160	(Leartsakulpanich *et al.*, 2002)
	S58R	1.1	1.8	8.5	13	(Leartsakulpanich *et al.*, 2002)
	S117N	0.02	650	980	51	(Leartsakulpanich *et al.*, 2002)
	I173L	3.7	1.8	19	21	(Leartsakulpanich *et al.*, 2002)
Double mutant	S58R/S117N	0.25	930	743	8.1	(Leartsakulpanich *et al.*, 2002)

Table 6.3. Homologous active site residues in DHFRs from different species.

Species	Corresponding residues						
H. sapiens	I7	L22	F31	F34	Q35	T56	V115
P. falciparum	I14	L46	M55	F58	C59	S108	I164
P. vivax	I13	L45	M54	F57	S58	S117	I173
L. major	V30	L45	M53	F56	K57	T83	V156
E. coli	I5	M20	L28	F31	K32	T46	I94
S. pneumonia	I8	L23	F31	F34	K35	T49	I100
M. tuberculosis	I5	I20	Q28	F31	R32	T46	I94

resistant than the double variants (250-fold > WT; Table 6.2), suggesting that the conservative I164L substitution also played a role in PYR-resistance (Foote et al., 1990). These results, along with corroborating observations (Peterson et al., 1988; Zolg et al., 1989), suggested that an initial substitution (S108N) was necessary for acquisition of PYR resistance. Furthermore, these findings highlight a fundamental difference between antifolate resistance in parasites, where DHFR substitutions are a primary source of resistance, and antifolate resistance in mammalian cells.

Further studies of antifolate-resistant strains of *P. falciparum* highlighted a general trend, where most PYR-resistant DHFR variants were also resistant to CYC (Table 6.2), suggesting that cross-resistance would be a barrier to the design of novel antifolates to treat PYR-resistant malaria (Foote et al., 1990; Peterson et al., 1990). However, the same studies identified combinations of substitutions that correlated with selective antifolate resistance. Whereas the IC_{50}^{PYR} for a strain containing the A16V/S108T substitutions was comparable to that of the sensitive strain, the IC_{50}^{CYC} was increased by more than two orders of magnitude. The role of the A16V/S108T substitutions in CYC resistance remained unclear because those tests had been undertaken in *P. falciparum* rather than *in vitro*, such that DHFR-independent resistance mechanisms could not be ruled out.

In vitro characterization of the PYR-resistant *P. falciparum* DHFRs helped to elucidate of role of substitutions in resistance. The activity and inhibitory constants determined for the isolated domains of the WT *pf*DHFR-TS were similar to the bifunctional enzyme (Sirawaraporn et al., 1990). Using the mutated *P. falciparum* DHFR domain, the S108N substitution was shown to provide a 10-fold increase in K_i^{PYR} and a 5-fold increase in K_i^{CYC}, with a 2-fold reduction in catalytic efficiency relative to the WT solely due to increased K_M^{DHF} (Sirawaraporn et al., 1993). Interestingly, combination of S108N and N51I not only increased K_i^{PYR} and K_i^{CYC} (30- and 10-fold relative to WT, respectively), but re-established catalytic efficiency (and K_M^{DHF}) to the level of the WT (Table 6.2). This clearly illustrates the impact of cumulative substitutions on the efficacy of resistant variants.

Further naturally-occurring PYR and/or CYC-resistant double to quadruple variants, all containing S108N, were also characterized (Sirawaraporn et al., 1997a). K_i^{PYR} and K_i^{CYC} increased synergistically in all combinatorial variants relative to S108N, such that K_i^{PYR} was highest in the N51I/C59R/S108N/I164L quadruple variant (a 570-fold increase relative to WT). This gain in resistance was associated with a 6-fold loss in catalytic efficiency. The quadruple variant was also one of the most CYC-resistant variants in the study. Nonetheless, the aforementioned double variant A16V/S108T had the highest K_i^{CYC} but remained sensitive to PYR. This observation confirmed that the A16V/S108T substitutions was solely responsible for the CYC-resistant phenotype observed in the strain of *P. falciparum* (Foote et al., 1990), and demonstrated that a specific subset of substitutions can confer selective antifolate resistance. The basis for selectivity would be rationalized later, when structural data became available (*vide infra*).

The impact of each mutation occurring in those multiple variants of *pf*DHFR was assessed (Sirawaraporn et al., 1997a). The C59R and I164L variants did not decrease the affinity for PYR, but slightly decreased affinity for CYC (2 to 5-fold). Importantly, the equivalent positions in mammalian DHFRs (Gln35 and Val115, see Table 6.3) have yielded MTX-resistant variants (Thillet et al., 1988; Fossati et al., 2008), identifying these positions as cross-species hot-spots for selective antifolate resistance. The only point variant that conferred moderate resistance to PYR and CYC was S108N. These observations support the hypothesis that the S108N substitution is essential in conferring PYR-resistance, as it remains the only point variant that it is present in all naturally-occurring PYR-resistant variants. In a parallel study (Sirawaraporn et al., 1997b), kinetic characterization of the 19 possible substitutions at *pf*DHFR position 108 confirmed that variant S108N exhibited the most efficient balance between loss of catalytic efficiency and gain of PYR-resistance, justifying its prevalence in PYR-resistant isolates. Homology models of the *P. falciparum* DHFR domain (Santos-Filho et al., 2001; Delfino et al., 2002), based on the structure of avian DHFR, yielded telling results regarding PYR and CYC drug-selectivity (Delfino et

al., 2002): the modelled S108N point variant created steric clashes of greater magnitude between bound PYR and other active site residues than when CYC was bound. Selective CYC-resistance of the A16V variant could also be rationalized by differential steric clashes.

The first structure of a parasitic DHFR was reported in 1994, for the *Leishmania major* DHFR-TS (Knighton et al., 1994). The DHFR domain was structurally homologous to *E. coli* and mammalian DHFR structures (Knighton et al., 1994; Cody et al., 1997; Sawaya and Kraut, 1997). Crystal structure resolution of *P. falciparum* DHFR-TS with bound PYR (Yuvaniyama et al., 2003) confirmed that the *P. falciparum* DHFR model of Delfino et al. (Delfino et al., 2002) was a good prediction of the crystal structure. Superimposition of WT *P. falciparum*, *E. coli* and human DHFR structures (Figure 6.4) shows that despite additional loops and helices found far from the active site in *P. falciparum*, the NADPH and folate binding sites are homologous in the three species. This suggests that positions involved in Plasmodium antifolate resistance may be relevant to bacterial and mammalian antifolate resistance, and vice-versa.

Second generation antifolates are currently being tested on clinical isolates of PYR and CYC-resistant *P. falciparum* strains. The most promising compound to date is WR99210 (Figure 6.1), a triazine drug that inhibits growth of WT *P. falciparum* and strains containing PYR and CYC-resistant DHFR double to quadruple variants (Hankins et al., 2001). In vitro characterization of variant C59R/S108N in presence of WR99210 demonstrated effective inhibition (Hekmat-Nejad and Rathod, 1997). Consistent with this observation, WR99210 was readily docked into the active site of modeled PYR-sensitive and PYR-resistant *pf*DHFRs with no steric hindrance (Delfino et al., 2002). Furthermore, comparison of crystal structures of WT *pf*DHFR and its quadruple variant N51I/C59R/S108N/I164L complexed with WR99210 suggested that the additional flexiblity conferred by the 3-carbon linker to the trichlorophenyl moiety of the ligand was a key feature in its potency toward the different DHFR variants (Yuvaniyama et al., 2003).

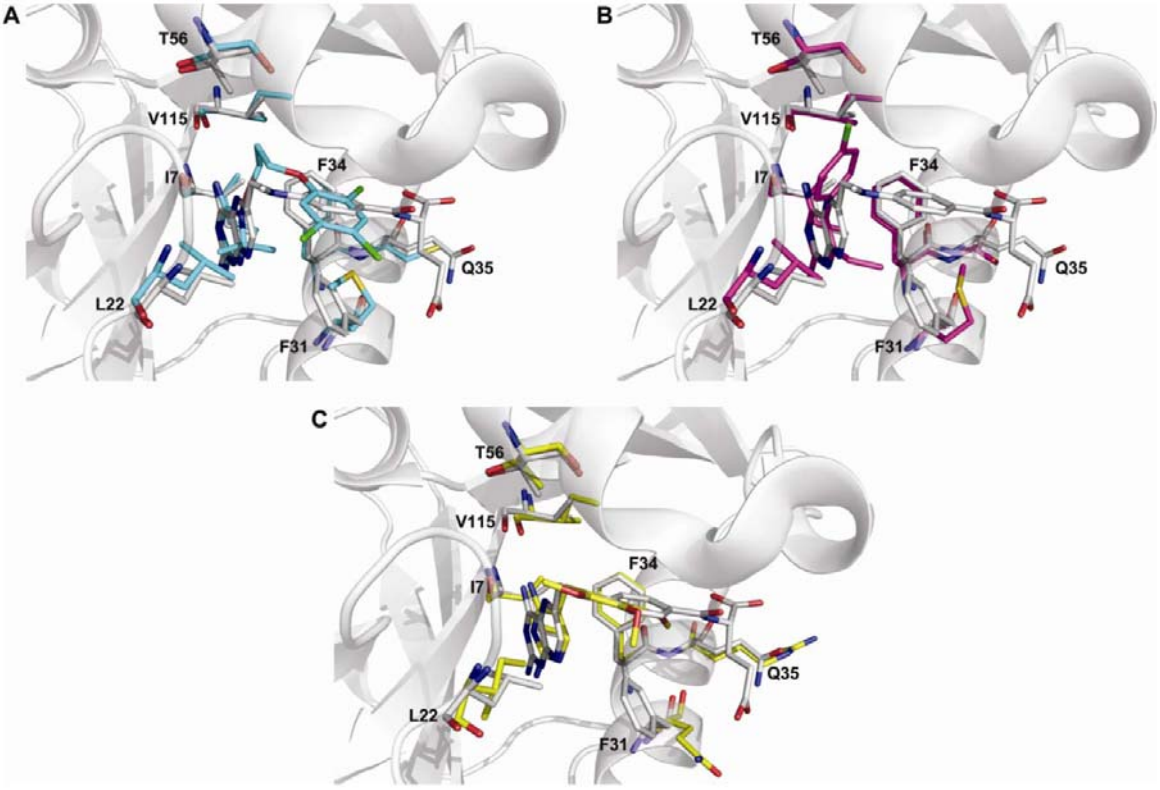

Figure 6.4. Superposition of hDHFR (1U72) with *pf*DHFR (A; 1J3I), *pv*DHFR (B; 1BL9) and *mt*DHFR (C; 1DG5). For clarity only the backbone of human DHFR is shown (cartoon representation). Residues mutated in the different DHFRs are shown in sticks. hDHFR is complexed with MTX, while the *pf*, *pv* and *mt* DHFRs are complexed with WR99210, PYR and TMP respectively. The RSMDs for all-atom superpositions were between 1.3 and 1.8 Å.

Because PYR, CYC and WR99210 all carry a 2,4-diaminopyrimidine moiety, mammalian and parasitic DHFRs have comparable K_i values (Ma and Kovacs, 2000). For example, $K_i^{WR99210}$ for human DHFR is only 10-fold higher than for *pf*DHFR (K_i = 12 nM and 1 nM respectively (Zhang and Rathod, 2002)). Nonetheless, those compounds display *in vivo* selectivity: growth of *P. falciparum* was inhibited at WR99210 concentrations 8000-fold lower than those required to inhibit human fibroblasts. The *in vivo* selectivity was recently shown to be due to differences in regulation of DHFR expression (Zhang and Rathod, 2002). In mammalian cells, DHFR mRNA binds to the DHFR active site to regulate expression. This regulation is relieved when inhibitors bind to the active site and dislodge the bound mRNA, making it available for translation. The resulting overexpression constitutes a commonly-observed antifolate-resistance mechanism in mammalian cells (Chu et al., 1993). The parasitic DHFR-TS mRNA also binds its cognate enzyme, but not at the DHFR active site (Zhang and Rathod, 2002). Thus, antifolate binding at the active site does not induce overexpression of *pf*DHFR which may explain the selectivity of drugs such as WR99210 towards parasites.

Laboratory-generated antifolate resistance in Plasmodium falciparum

Directed evolution of *pf*DHFR was performed to predict the onset of mutations conferring resistance towards WR99210, PYR and its analog, m-Cl-PYR (Chusacultanachai et al., 2002). Selection of random mutations for PYR-resistance yielded the well-characterized S108N, C59R/S108N and N51I/C59R/S108N/I164L variants, as well novel combinatorial variants at previously uncharacterized positions (Table 6.2). Random mutagenesis on the quadruple N51I/C59R/S108N/I164L variant also yielded novel combinations, including the introduction of a F58L substitution, accompanied by a switch of substitution S108N to N108T. The resulting variant, N51I/F58L/C59R/N108T/I164L was also identified when the quadruple variant library was selected against WR99210. In fact, many WR99210-selected variants from the quadruple variant library contained the F58L substitution, often accompanied by a N108S reversion, consistent with earlier

observations that the S108N substitution did not confer resistance to WR99210. This suggests that F58L is a key actor in WR99210 resistance, and also suggests that substitution N108T offers broader-based antifolate resistance than S108N.

Consistent with this hypothesis, further variations at position 58 were observed. Both the F58C substitution added to the quadruple N51I/C59R/S108N/I164L variant, and the F58L point variant, conferred resistance to WR99210. All Phe58 variants exhibited low catalytic activities relative to the WT or quadruple variant enzymes, but high resistance to all the inhibitors tested. Phe58 is homologous to Phe34 in mammalian DHFR (Figure 6.3; Table 6.3), a highly conserved active-site residue involved in van der Waals interactions with bound substrate as well as 2,4-diaminopterin and 2,4-diaminopyrimidine inhibitors. Substituting Phe34 with hydrophobic residues in human or murine DHFR conferred high resistance towards MTX, but reduced catalytic activity (Nakano et al., 1994), (Thillet et al., 1988). This illustrates the similarities between the active sites of Plasmodium and mammalian DHFR enzymes with respect to substrate and inhibitor binding and is consistent with the high structural homology of their active sites, despite the fact that these enzymes share only between 25 and 40% sequence identity (Zhang and Rathod, 2002).

Antifolate resistance in Plasmodium vivax

Plasmodium vivax, the second most frequent type of malaria, is rarely fatal. Nonetheless, important morbidity and mortality related to *P. vivax* in certain areas of the world justify the requirement for efficient treatment (Mendis et al., 2001). It was initially believed that *P. vivax* was intrinsically antifolate-resistant as it proved resistant to PYR and CYC treatment (Young and Burgess, 1959). De Pécoulas et al. (de Pecoulas et al., 1998) identified polymorphisms at five residues of the *P. vivax dhfr-ts* gene from strains originating from regions where PYR had been extensively used to treat *P. falciparum*. As the two *Plasmodium* strains often co-exist, those studies suggested that resistance to PYR was not intrinsic, but had been acquired by *P. vivax* following drug exposure during treatment of *P. falciparum*. The PYR-exposed strains all contained single or combinatorial

substitutions at positions 58, 117 and 173 (positions 59, 108 and 164, respectively, in *pf*DHFR; Table III). In particular, the substitutions constituting the *P. vivax* variants S58R/S117N and S58L/S117N/I173L are the homologs of the *pf*DHFR substitutions C59R, S108N and I164L that contribute to PYR resistance (Table 6.2). In vitro characterization of the *P. vivax* S58R and S117N point variants confirmed that they were slightly resistant to PYR and CYC, and that their combination increased resistance to both drugs (Tahar et al., 2001) as observed for the *P. falciparum* C59R/S108N variant. A recent study showed that this double variant was the most frequent polymorphism identified in antifolate-resistant clinical isolates for both malarial species (*pf* DHFR C59R/S108N and *pv*DHFR S58R/S117N) (Alam et al., 2007).

Despite the high prevalence of the S58R/S117N double variant, Phe57 substitutions (= hDHFR Phe34; Table 6.3) were also identified (de Pecoulas et al., 1998). The F57L variant conferred resistance to all antifolates tested, including WR99210 (Imwong et al., 2001; Hastings and Sibley, 2002; Leartsakulpanich et al., 2002). This again demonstrates the cross-species contribution of this strictly conserved residue in antifolate binding, where substitution of the phenyl ring confers antifolate resistance in mammalian as well as parasitic DHFRs. A larger screen identified triple to quintuple variants including F57L/S58R with the further substitutions I13L, S117N (Imwong et al., 2001), S117T (Imwong et al., 2003) and/or T61M (Imwong et al., 2003). Thr61 is homologous to Thr38 in mammalian DHFRs, which is an important active site residue involved in inhibitor recognition (Cody et al., 2005). Ile13 is homologous to residue Ile7 in mammalian DHFR, which specifically interacts with the 4-amino group of bound inhibitor (Table 6.3). Similarly, the human DHFR I7L substitution can give rise to MTX-resistant variants when combined with additional active site substitutions, including substitutions at residues F34 (F57 in *pv*DHFR) and Q35 (S58 in *pv*DHFR) (J. P. V., L. Poulin and J. N. P., unpublished results). Ile7, Phe34 and Gln35 are thus cross-species hot-spots for antifolate resistance (Figure 6.5).

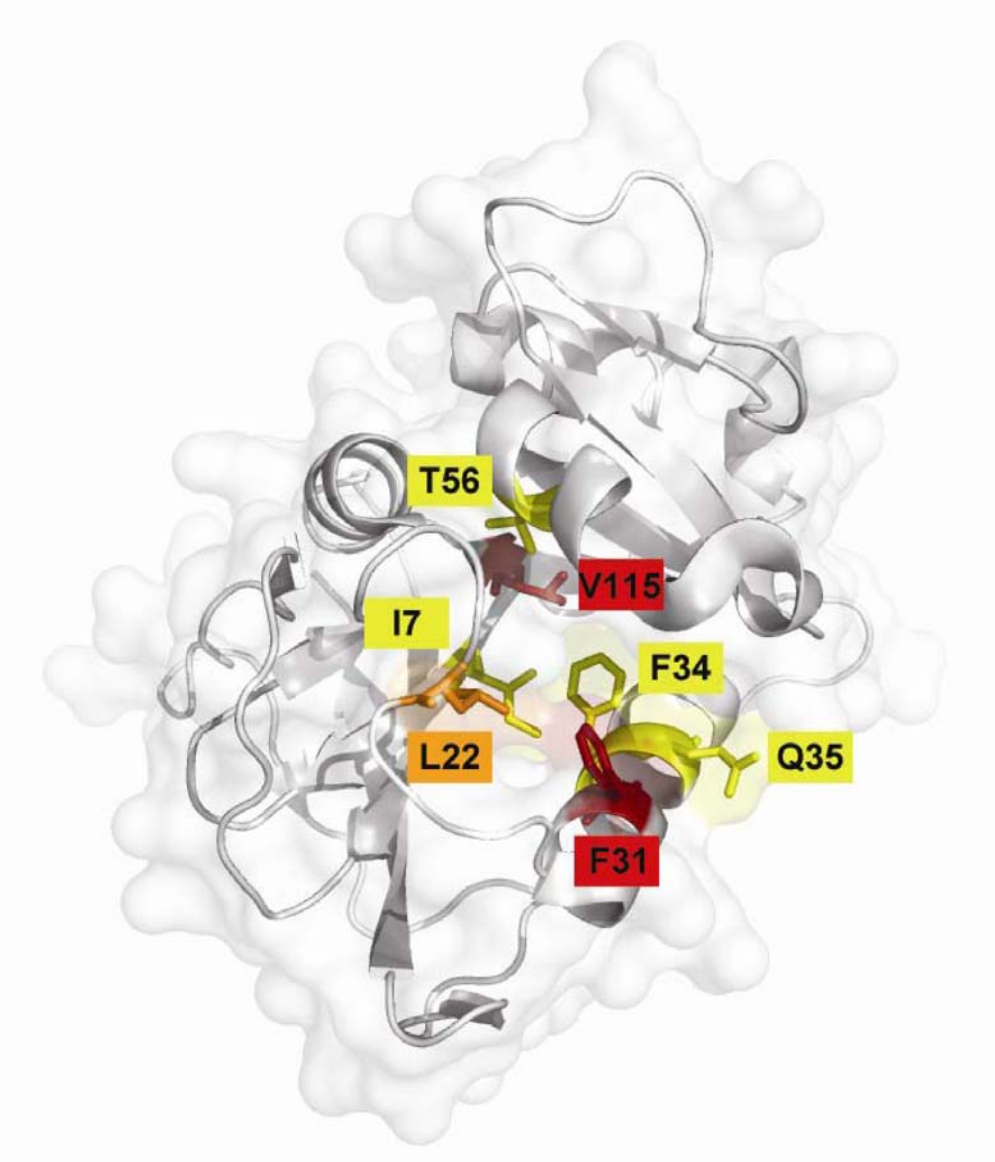

Figure 6.5. 'Hot-spots' for mutations conferring resistance to antifolates in DHFRs from different species plotted on human DHFR (1U72). The positions conferring antifolate resistance when mutated are represented as follows: yellow: positions conferring antifolate resistance in mammalian and parasitic DHFRs; orange; in mammalian and bacterial DHFRs; red: in mammalian, parasitic and bacterial DHFRs.

Comparison of the substitutions that confer antifolate resistance in the two Plasmodium DHFRs illustrates that despite their high sequence and structural homologies (Kongsaeree et al., 2005), certain substitutions or combinations of substitutions provide species-specific antifolate resistance. The homologs of the *P. vivax* variants I13L and T61M have not been reported in *pf* DHFR (Ile14 and Thr62, respectively; Table 6.3) for resistance to antifolates. Substitutions equivalent to Phe57 substitutions (Phe58 of *pf* DHFR) were not identified in PYR-resistant clinical isolates of *P. falciparum*. Conversely, substitutions at residues Ala15 or Asn50 in *pv*DHFR (residues Ala16 and Asn51 in *pf* DHFR ; Table 6.3) have not been reported in PYR or CYC-resistant strains. While the above studies were not exhaustive, it appears that these mutational variations result from subtle structural differences in the active site of each species (Kongsaeree et al., 2005).

Other parasites and bacteria

Antifolates are also applied to treatment of other human parasites, such as *Leishmania*. PYR and CYC are inefficient for treatment of *Leishmania* due to lack of specificity for its DHFR (Gilbert, 2002). Therefore, antifolates exhibiting cross-species inhibition, such as MTX, are used to treat infections caused by *Leishmania*. As with mammalian cells, *Leishmania* have developed MTX resistance mechanisms. Amplification of the *Leishmania* DHFR-TS gene has been observed, suggesting that, as for the mammalian enzymes, the mRNA binds to its cognate active site (Coderre *et al.*, 1983). Reduced drug-permeability combined with overexpression of DHFR has also been reported in *Leishmania* (Ellenberger and Beverley, 1989). These resistance mechanisms form parallels with resistance in mammalian systems and contrast with the advent of mutations, which constitute the main cause of resistance in *Plasmodium* parasites. Arrebola *et al.* reported a strain of *Leishmania major* that was resistant to MTX due to a M53R substitution in DHFR (Arrebola *et al.*, 1994). Met53 is analogous to Phe31 in mammalian DHFR (Table 6.3), where the F31R substitution importantly decreases the affinity for MTX (Patel *et al.*, 1997). This *L. major* variant exhibited a 30-fold decrease in MTX-affinity, and

like the F31R variant of human DHFR, the catalytic efficiency was mainly decreased due to loss in reactivity (k_{cat}) relative to the WT. Conversely, some bacterial DHFRs exhibit intrinsically low affinity for MTX. This is the case of *Mycobacterium tuberculosis* DHFR, where the K_i^{MTX} is 11 nM, which is within the range of highly resistant hDHFR variants (Table 6.1). The *mt*DHFR active-site residues are highly homologous to mammalian DHFR, with the exception of Q28 (F31 in hDHFR) and R32 (Q35 in hDHFR) (Figure 6.4C). Interestingly, the F31Q (Morris and McIvor, 1994) and Q35R (Thillet *et al.*, 1988) substitutions confer MTX-resistance in murine DHFR. Although we have shown that combining human DHFR substitutions at residues 31 and 35 can yield high MTX-resistance (Volpato *et al.*, 2007), those point variants (F31Q, Q35R) were not characterized.

Trimethoprim (TMP) has been the antifolate of choice for the treatment of bacterial infections such as urinary tract infections and is still widely used (Hawser *et al.*, 2006). TMP is a competitive inhibitor that is selective towards chromosomal bacterial DHFR, as its affinity is > 2500-fold higher for *E. coli* DHFR than for mammalian DHFR (Margosiak *et al.*, 1993). Resistance to TMP was reported shortly after its clinical introduction. Unlike parasitic and mammalian resistances, the main TMP resistance mechanism involves the acquisition of a secondary DHFR that is insensitive to TMP (reviewed in (Huovinen *et al.*, 1995)). These resistance enzymes are either plasmid or integron encoded and are generally evolutionarily unrelated to chromosomal DHFR. Nonetheless, TMP-resistant chromosomal DHFRs have been reported in different bacterial species. Baccanari *et al.* (Baccanari *et al.*, 1981) reported a L28R substitution in *E. coli* DHFR which decreased TMP affinity 100-fold. Leu28 corresponds to Phe31 in mammalian DHFR and Met53 in *L. Major* (Table 6.3), where substitution to Arg confers resistance to MTX and other related antifolates (Arrebola *et al.*, 1994; Patel *et al.*, 1997). More recently, directed evolution of *E. coli* DHFR followed by *in vivo* selection for TMP resistance in a bacterial complementation assay (Watson *et al.*, 2007) yielded multiple single and combinatorial variants. The most frequently observed substitutions occurred at residues Met20 (Leu22 in hDHFR) and Trp30 (Tyr33 in hDHFR), two active site residues located in the folate-binding site. Substitution of Leu22 in

mammalian DHFRs can confer antifolate resistance. The *E. coli* M20V point variant conferred the highest resistance to TMP, while its combination with other substitutions conferred lower TMP-resistance (Watson *et al.*, 2007). Surprisingly, that point variant showed no decrease in catalytic activity, unlike substitutions of hDHFR L22. Trp30 was also frequently mutated in TMP-resistant variants: substitution W30G was identified in a TMP-resistant clinical isolate (Flensburg and Skold, 1987) and the W30R substitution was also shown to confer TMP resistance (Watson *et al.*, 2007). Trp30 occurs on the α-helix that plays a key role in antifolate binding. In *E. coli* DHFR (Sawaya and Kraut, 1997), the side-chain amine of Trp30 is involved in a hydrogen bonding network with a water molecule, residue T113 and the 2-amino group of bound MTX. As the 2,4-diaminopyrimidine moieties of MTX and TMP bind in similar fashions (Matthews *et al.*, 1985), it is likely that Trp30 substitutions reduce TMP binding by disrupting this hydrogen bonding network. Nonetheless, no mammalian DHFR substitutions have been reported at the homologous position 33, suggesting that this position confers antifolate specificity. One further residue also confered TMP-resistance when mutated: the I94L substitution was identified in TMP-resistant *E. coli* (Watson *et al.*, 2007), and its homolog in *Streptococcus pneumoniae* (I100L) has been identified in clinical isolates (Pikis *et al.*, 1998). The backbone carbonyl of Ile94 is within hydrogen bonding distance of the 4-amino group of TMP (Matthews *et al.*, 1985) (Figure 6.4). In mammalian DHFR, the backbone carbonyl of the homologous Val115 is within hydrogen bonding distance of the 4-amino group of MTX (Cody *et al.*, 2005). As mentioned previously, substitutions at this 'hot-spot' position, including the hDHFR V115L variant (Fossati *et al.*, 2008), give rise to MTX resistance.

III Parallels between mutations that confer antifolate resistance in mammalian, parasitic and bacterial DHFRs.

As made evident above, a number of homologous positions confer cross-species antifolate resistance in mammalian, parasitic and bacterial DHFRs (Figure 6.5). Some positions confer broad antifolate resistance, suggesting that they are essential for binding

common features of clinically-relevant antifolates. Those cases highlight the cross-species similarities at the DHFR active site, allowing mapping of mutational 'hot-spots' (Figure 6.5). Residue Phe34 of mammalian DHFR constitutes such a hot-spot, as a result of its key interactions with the 2,4-diaminopterin ring and the *p*-aminobenzoyl (*p*ABA) portion of MTX. Substitution of Phe34 has yielded point variants with the lowest reported affinity to MTX (Thillet *et al.*, 1988; Nakano *et al.*, 1994). Low affinity to PYR, CYC and WR99210 has been associated with substitutions at the homologous residue (Phe57 (*P. vivax*) and Phe58 (*P. falciparum*)) in parasitic DHFRs, suggesting a similar role for the phenyl ring. In fact, substitutions of *pv*DHFR Phe57 appear to be essential for resistance to WR99210: the trichlorophenyl portion of WR99210 is bound in the same active site area as the *p*ABA of MTX (Figure 6.6), suggesting the establishment of van der Waals and/or edge-to-face aromatic contacts between the Phe58 phenyl of *pf*DHFR and the WR99210 trichlorophenyl in the WT enzyme. On this basis, we may foresee that *pf*DHFR substitutions at residue 58 will eventually be reported if WR99210 or related compounds are used to treat PYR and CYC-resistant malarias.

Val115 of mammalian DHFRs (*E. coli* Ile94, *P. falciparum* Ile164 and *P. vivax* Ile173) is also a hot-spot for antifolate-resistance. In all cases studied, substitution to leucine results in decreased affinity for antifolates. As its backbone carbonyl H-bonds with the 4-amino group of antifolates, substitution to leucine may displace the backbone to weaken this interaction. Inversely, the V115I substitution in human DHFR (which encodes the native residue found in bacterial and parasitic DHFRs) yielded an enzyme with increased affinity for MTX compared to the native enzyme (Fossati *et al.*, 2008).

Ile7 of mammalian DHFR is also involved in specific H-bonding with the 4-amino group of antifolates. Again, this feature is conserved in all species, and substitutions at this residue in combination with other substitutions can provide antifolate resistance (Patel *et al.*, 1997; Imwong *et al.*, 2003). It thus constitutes a hot-spot for resistance, but not as a point variant.

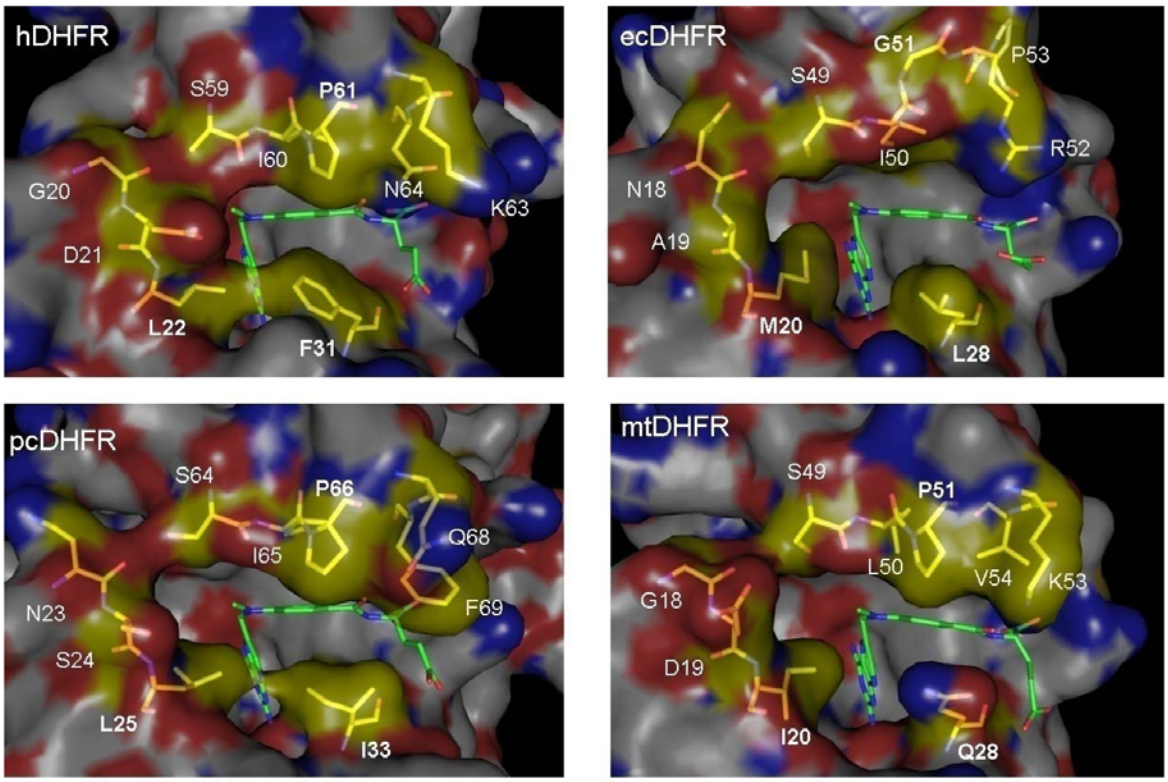

Figure 6.6. Surface representation of hDHFR, *ec*DHFR, *pc*DHFR and *mt*DHFR complexed with MTX. A semi-transparent surface was generated for hDHFR (1U72), *ec*DHFR (1RH3), *pc*DHFR (3CD2) and *mt*DHFR (1DF7). The surface representation is colored by atom (oxygen: red, nitrogen: blue and carbon: white). Residues surrounding the active site cavity and MTX are shown in sticks representation and colored by atom (oxygen: red, nitrogen: blue, carbon: residues in yellow, MTX in green). RSMDs for complete superpositions were < 1.0 Å.

Other substitution sites confer selective antifolate resistance. Drugs such as MTX are 'classical' antifolates, of chemical structure very similar to the substrate, DHF. Phe31 of mammalian DHFR establishes specific van der Waals contacts with the *p*ABA portion of DHF or MTX. Substitutions at this position are only observed for antifolates containing a *p*ABA moiety or a functional group that occupies the same active site space. Therefore, substitutions at this position may eventually arise in malarial DHFRs (Met55 in *P. falciparum*, Met54 in *P. vivax*; Table 6.3) following treatment with drugs such as WR99210, since the tricholorophenyl moiety binds in a similar space and orientation as does the *p*ABA moiety (Yuvaniyama *et al.*, 2003; Cody *et al.*, 2005). A substitution at the homologous position (M53R) has been reported for the parasite *L. major* following treatment with MTX (Arrebola *et al.*, 1994). This position may provide antifolate-specific resistance; it also confers species specificity (see below).

In malarial DHFR, the S108N substitution in *P. falciparum* (S117N in *P. vivax*) provides PYR and CYC resistance while remaining sensitive to WR99210 (Hankins *et al.*, 2001). This results from the proximity of Ser108 with the structurally-constrained chlorophenyl moiety of CYC and PYR; WR99210 does not form close contacts with this residue, such that its substitution would have little effect on binding of the drug. There is evidence only of weak resistance upon substitution of the equivalent position in mammalian DHFRs (hDHFR Thr56) (Schweitzer *et al.*, 1990), suggesting that this position may confer species specificity.

Cross-species mapping of DHFR active site substitutions has also yielded insight into TMP binding. TMP displays high affinity and selectivity towards certain bacterial DHFRs, including *E. coli* DHFR, but binds less efficiently to other bacterial, parasitic and mammalian DHFRs. The crystal structure of *ec*DHFR complexed with TMP (Matthews *et al.*, 1985) (for which coordinates are not available) suggests that binding of the TMP 2,4-diaminopyrimidine is similar to binding of the MTX 2,4-diaminopterin, involving the same active site residues in hydrophobic, van der Waals and hydrogen bonding interactions. It

follows that those interactions cannot account for the observed species selectivity, given that MTX binding is homologous between *E. coli* (Sawaya and Kraut, 1997) and hDHFR (Cody *et al.*, 2005). The selectivity of TMP was attributed to binding of the trimethoxybenzyl group. It mainly interacts with helices αB and αC of *ec*DHFR, which harbour sequence differences relative to human DHFR. In particular, Leu28 of helix αB (hDHFR Phe 31) was reported to form major contacts with the TMP trimethoxybenzyl. In contrast, Phe31 of avian DHFR produced unfavorable interactions with the TMP trimethoxybenzyl (Matthews *et al.*, 1985). It was thus proposed that a Phe31Leu substitution would increase the affinity of hDHFR for TMP. However, that substitution did not give the expected result, indicating that this residue was not solely responsible for the species selectivity of TMP (Prendergast *et al.*, 1989).

Watson *et al.* (Watson *et al.*, 2007) recently reported the M20V substitution in *ec*DHFR (hDHFR Leu22), responsible for the greatest observed decrease in TMP binding in that enzyme. Interestingly, most bacterial, protozoan and mammalian DHFRs encode a leucine or isoleucine at that position (Figure 6.3; Table 6.3), suggesting that a non-polar β-branched amino acid at this position may account for the intrinsic TMP-resistance observed in most DHFRs. The side-chain of Met20 is positioned at the interface of the folate and NADPH binding pockets in *ec*DHFR (Figure 6.6). Baccanari *et al.* (Baccanari *et al.*, 1982) reported a 3000-fold increase in TMP binding to the *E. coli* enzyme when NADPH is present, an effect not observed in mammalian DHFRs. The difference in cooperative binding between *E. coli* and hDHFR correlates with the difference in TMP affinity. Modelling NADPH into *ec*DHFR complexed with TMP (Matthews *et al.*, 1985) suggested that this cooperativity was related to direct interactions between the two ligands. However, recent NMR studies of hDHFR in complex with NADPH and TMP suggest that the cooperativity is mainly caused by interactions between the ligands and protein side-chains (Kovalevskaya *et al.*, 2005). Thus, contacts with Met20 appear to promote cooperativity between ligands in *ec*DHFR in a manner that cannot be reproduced by β-branched amino acids. While this suggests that the cooperativity observed in *ec*DHFR could be introduced

into hDHFR by the L22M substitution, that variant did not yield a TMP-sensitive hDHFR (J.P.V. and J.N.P., unpublished data).

It thus appears that TMP-selectivity in *ec*DHFR is the consequence of multiple active-site features. In the absence of the coordinates for TMP-bound *E. coli* DHFR, we compared protein surfaces of human (Cody *et al.*, 2005), *E. coli* (Sawaya and Kraut, 1997), *M. tuberculosis* (Li *et al.*, 2000)and *P. carinii* (Cody *et al.*, 1999) DHFRs bound to MTX (Figure 6.6). This constitutes a good comparative model since MTX and TMP display similar binding in *ec*DHFR (reported in (Matthews *et al.*, 1985)) and in *P. carinii* (Champness *et al.*, 1994) and *M. tuberculosis* (Li *et al.*, 2000) DHFRs (TMP-bound structures overlayed with the respective MTX-bound structures; RMSD < 0.3 Å for each overlay, results not shown). *P. carinii* and *M. tuberculosis* DHFRs are TMP-resistant (K_i^{TMP} 0.21 μM (Ma and Kovacs, 2000) and 88 μM (Li *et al.*, 2000), respectively), as is hDHFR (Table 6.4). We identifed features shared among the TMP-insensitive DHFRs that are not found in *ec*DHFR. Pro61, located at the C-terminus of hDHFR helix α2, is also present in *pc*DHFR (Pro66) and *mt*DHFRs (Pro51) where it creates a bulge near the *p*-ABA moiety of MTX. The proline is replaced by Gly51 in *ec*DHFR, which has also been shown to interact with the trimethoxybenzyl ring of TMP. The presence of a proline in this helix may induce unfavorable interactions with TMP, decreasing binding.

While hDHFR Leu22, alone, was not sufficient to determine TMP sensitivity, we observed a correlation between residues 22, 31 and 61 (hDHFR numbering) and TMP binding (Table 6.4). Close contacts are formed between the side chains of hDHFR L22 and F31, restricting the volume of the active site cavity (Figure 6.6). Those interactions are also present with the homologous residues of *pc*DHFR (L25 and I33) but are not as constrictive in *ec*DHFR (M20 and L28) and seem to be absent in *mt*DHFR (I20 and Q28), which displays the lowest affinity for MTX and TMP (Table 6.4). A combination of the above active-site elements may generate landscapes that are either ideal (*ec*DHFR), too constrained (*pc* and hDHFR) or else non-specific (*mt*DHFR) for TMP-binding. More

Table 6.4. Cross-species comparison of K_i for TMP and MTX, and identity at positions 22, 31 and 61

Species	22[a]	31	61	K_i^{TMP} (nM)	K_i^{MTX} (nM)
E. coli	M	L	G	0.080	0.0010
H. influenza	M	L	G	0.082	
S. aureus	L	L	G	0.539	
S. pneumoniae	L	L	G	1	
P. vivax	L	M	P	98	5.2
L. major	I	M	P	120	0.180
P. carinii	L	I	P	152	0.0081
P. falciparum	L	M	P	160	1.3
H. sapiens	L	F	P	200	0.0034
M. tuberculosis	I	Q	P	88000	11

[a] Residue numbering according to human DHFR.

structural information combined with determination of inhibitory constants from a greater number of DHFRs is required to confirm these hypotheses.

Information about mutations conferring antifolate resistance in parasitic and bacterial enzymes may provide knowledge toward engineering high resistance in mammalian DHFRs while maintaining native-like catalytic efficiency. These properties are desirable for myeloprotection applications (Nakano *et al.*, 1994). Practically all highly MTX-resistant mammalian DHFRs display poor catalytic activities. Combinatorial hDHFR variants display the lowest affinity to MTX, but have significantly reduced catalytic efficiencies (Table 6.1). In contrast, combinatorial variants of *pf*DHFR maintain native-like activity (Sandefur *et al.*, 2007) while antifolate resistance to PYR and CYC is increased with every additional mutation as a result of the N51I, C59R, S108N and I164L substitutions (Table 6.2). Point mutations of Gln35 (Cys59 in *pf*DHFR) and Val115 (Ile164 in *pf*DHFR) of human and murine DHFRs have led to antifolate resistance (Thillet *et al.*, 1988; Fossati *et al.*, 2008), and the T56N substitution (S108N in *pf* DHFR) slightly decreased the MTX affinity in human DHFR (Schweitzer *et al.*, 1990). The contribution of the N51I substitution in *pf*DHFR is of particular interest: while having little effect on antifolate binding, it reestablishes the loss of catalytic efficiency of the S108N variant to native levels. Would the homologous variant of hDHFR possess similar properties? We are currently combining hDHFR substitutions according to this cross-species information to generate highly MTX-resistant DHFRs with high catalytic efficiencies for use in myeloprotection.

Understanding the similarities and differences for antifolate binding in DHFR across species is the key to understanding specific properties essential for inhibitor binding, contributing to the knowledge required for future drug design. By comparing structure-based sequence alignments, mutational data and kinetic data for evolutionarily distant DHFRs, we provide compelling evidence that identifies active site positions across species which provide general antifolate resistance, and further active site positions providing

species-specificity or antifolate-specificity. Increasing throughput of structural and functional characterizations will provide additional data to flesh out the framework we have begun to lay down, to fully elucidate the requirements for antifolate binding and resistance in DHFR. Finally, this work serves to illustrate the interest of studying further relevant drug targets via high-throughput mutational screening and structural determination.

Acknowledgments

The authors would like to thank Elena Fossati for critical reading of this manuscript.

References

Alam, M. T., Bora, H., Bharti, P. K., Saifi, M. A., Das, M. K., Dev, V., Kumar, A., Singh, N., Dash, A. P., Das, B., Wajihullah, and Sharma, Y. D. (2007). Similar trends of pyrimethamine resistance-associated mutations in Plasmodium vivax and P. falciparum. *Antimicrob Agents Chemother* **51**, 857-863.

Allay, J. A., Persons, D. A., Galipeau, J., Riberdy, J. M., Ashmun, R. A., Blakley, R. L., and Sorrentino, B. P. (1998). In vivo selection of retrovirally transduced hematopoietic stem cells. *Nat Med* **4**, 1136-1143.

Arrebola, R., Olmo, A., Reche, P., Garvey, E. P., Santi, D. V., Ruiz-Perez, L. M., and Gonzalez-Pacanowska, D. (1994). Isolation and characterization of a mutant dihydrofolate reductase-thymidylate synthase from methotrexate-resistant Leishmania cells. *J Biol Chem* **269**, 10590-10596.

Baccanari, D. P., Daluge, S., and King, R. W. (1982). Inhibition of dihydrofolate reductase: effect of reduced nicotinamide adenine dinucleotide phosphate on the selectivity and affinity of diaminobenzylpyrimidines. *Biochemistry* **21**, 5068-5075.

Baccanari, D. P., Stone, D., and Kuyper, L. (1981). Effect of a single amino acid substitution on Escherichia coli dihydrofolate reductase catalysis and ligand binding. *J Biol Chem* **256**, 1738-1747.

Banerjee, D., and Bertino, J. R. (2002). Myeloprotection with drug-resistance genes. *Lancet Oncol* **3**, 154-158.

Banerjee, D., Schweitzer, B. I., Volkenandt, M., Li, M. X., Waltham, M., Mineishi, S., Zhao, S. C., and Bertino, J. R. (1994a). Transfection with a cDNA encoding a Ser31 or Ser34 mutant human dihydrofolate reductase into Chinese hamster ovary and mouse marrow progenitor cells confers methotrexate resistance. *Gene* **139**, 269-274.

Banerjee, D., Zhao, S. C., Tong, Y., Steinherz, J., Gritsman, K., and Bertino, J. R. (1994b). Transfection of a nonactive site mutant murine DHFR cDNA (the tryptophan 15 mutant) into Chinese hamster ovary and mouse marrow progenitor cells imparts MTX resistance in vitro. *Cancer Gene Ther* **1**, 181-184.

Bell, D. J., Nyirongo, S. K., Mukaka, M., Zijlstra, E. E., Plowe, C. V., Molyneux, M. E., Ward, S. A., and Winstanley, P. A. (2008). Sulfadoxine-pyrimethamine-based combinations for malaria: a randomised blinded trial to compare efficacy, safety and selection of resistance in Malawi. *PLoS ONE* **3**, e1578.

Belzile, J. P., Karatzas, A., Shiu, H. Y., Letourneau, S., Palerme, J. S., and Cournoyer, D. (2003). Increased resistance to nitrogen mustards and antifolates following in vitro selection of murine fibroblasts and primary hematopoietic cells transduced with a bicistronic retroviral vector expressing the rat glutathione S-transferase A3 and a mutant dihydrofolate reductase. *Cancer Gene Ther* **10**, 637-646.

Capiaux, G. M., Budak-Alpdogan, T., Alpdogan, O., Bornmann, W., Takebe, N., Banerjee, D., Maley, F., and Bertino, J. R. (2004). Protection of hematopoietic stem cells from pemetrexed toxicity by retroviral gene transfer with a mutant dihydrofolate reductase-mutant thymidylate synthase fusion gene. *Cancer Gene Ther* **11**, 767-773.

Capiaux, G. M., Budak-Alpdogan, T., Takebe, N., Mayer-Kuckuk, P., Banerjee, D., Maley, F., and Bertino, J. R. (2003). Retroviral transduction of a mutant dihydrofolate reductase-thymidylate synthase fusion gene into murine marrow cells confers resistance to both methotrexate and 5-fluorouracil. *Hum Gene Ther* **14**, 435-446.

Champness, J. N., Achari, A., Ballantine, S. P., Bryant, P. K., Delves, C. J., and Stammers, D. K. (1994). The structure of Pneumocystis carinii dihydrofolate reductase to 1.9 A resolution. *Structure* **2**, 915-924.

Cheng, K. K.-F. (2007). Association of plasma methotrexate, neutropenia, hepatic dysfunction, nausea/vomiting and oral mucositis in children with cancer. *European Journal of Cancer Care* **In press**.

Chongsuphajaisiddhi, T., and Sabchareon, A. (1981). Sulfadoxine-pyrimethamine resistant falciparum malaria in Thai children. *Southeast Asian J Trop Med Public Health* **12**, 418-421.

Chu, E., and Allegra, C. J. (1996). *Antifolates. In Cancer Chemotherapy and Biotherapy*. Lippincott-Raven, Philadelphia, PA.

Chu, E., Takimoto, C. H., Voeller, D., Grem, J. L., and Allegra, C. J. (1993). Specific binding of human dihydrofolate reductase protein to dihydrofolate reductase messenger RNA in vitro. *Biochemistry* **32**, 4756-4760.

Chunduru, S. K., Cody, V., Luft, J. R., Pangborn, W., Appleman, J. R., and Blakley, R. L. (1994). Methotrexate-resistant variants of human dihydrofolate reductase. Effects of Phe31 substitutions. *J Biol Chem* **269**, 9547-9555.

Chusacultanachai, S., Thiensathit, P., Tarnchompoo, B., Sirawaraporn, W., and Yuthavong, Y. (2002). Novel antifolate resistant mutations of Plasmodium falciparum dihydrofolate reductase selected in Escherichia coli. *Mol Biochem Parasitol* **120**, 61-72.

Coderre, J. A., Beverley, S. M., Schimke, R. T., and Santi, D. V. (1983). Overproduction of a bifunctional thymidylate synthetase-dihydrofolate reductase and DNA amplification in methotrexate-resistant Leishmania tropica. *Proc Natl Acad Sci U S A* **80**, 2132-2136.

Cody, V., Galitsky, N., Luft, J. R., Pangborn, W., Rosowsky, A., and Blakley, R. L. (1997). Comparison of two independent crystal structures of human dihydrofolate reductase ternary complexes reduced with nicotinamide adenine dinucleotide phosphate and the very tight-binding inhibitor PT523. *Biochemistry* **36**, 13897-13903.

Cody, V., Galitsky, N., Rak, D., Luft, J. R., Pangborn, W., and Queener, S. F. (1999). Ligand-induced conformational changes in the crystal structures of Pneumocystis carinii dihydrofolate reductase complexes with folate and NADP+. *Biochemistry* **38**, 4303-4312.

Cody, V., Luft, J. R., and Pangborn, W. (2005). Understanding the role of Leu22 variants in methotrexate resistance: comparison of wild-type and Leu22Arg variant mouse and human dihydrofolate reductase ternary crystal complexes with methotrexate and NADPH. *Acta Crystallogr D Biol Crystallogr* **61**, 147-155.

Cowman, A. F., Morry, M. J., Biggs, B. A., Cross, G. A., and Foote, S. J. (1988). Amino acid changes linked to pyrimethamine resistance in the dihydrofolate reductase-thymidylate synthase gene of Plasmodium falciparum. *Proc Natl Acad Sci U S A* **85**, 9109-9113.

Das, J. R., Fryar, E. B., Epie, N. N., Southerland, W. M., and Bowen, D. (2006). Raloxifene attenuation of methotrexate cytotoxicity in human bone marrow by sequence-dependent administration of raloxifene, 5-FU/methotrexate. *Anticancer Res* **26**, 1877-1883.

Davies, J. F., 2nd, Delcamp, T. J., Prendergast, N. J., Ashford, V. A., Freisheim, J. H., and Kraut, J. (1990). Crystal structures of recombinant human dihydrofolate reductase complexed with folate and 5-deazafolate. *Biochemistry* **29**, 9467-9479.

Daw, N. C., Billups, C. A., Rodriguez-Galindo, C., McCarville, M. B., Rao, B. N., Cain, A. M., Jenkins, J. J., Neel, M. D., and Meyer, W. H. (2006). Metastatic osteosarcoma. *Cancer* **106**, 403-412.

de Pecoulas, P. E., Tahar, R., Ouatas, T., Mazabraud, A., and Basco, L. K. (1998). Sequence variations in the Plasmodium vivax dihydrofolate reductase-thymidylate synthase gene and their relationship with pyrimethamine resistance. *Mol Biochem Parasitol* **92**, 265-273.

Delfino, R. T., Santos-Filho, O. A., and Figueroa-Villar, J. D. (2002). Molecular modeling of wild-type and antifolate resistant mutant Plasmodium falciparum DHFR. *Biophys Chem* **98**, 287-300.

Dicker, A. P., Waltham, M. C., Volkenandt, M., Schweitzer, B. I., Otter, G. M., Schmid, F. A., Sirotnak, F. M., and Bertino, J. R. (1993). Methotrexate resistance in an in vivo mouse tumor due to a non-active-site dihydrofolate reductase mutation. *Proc Natl Acad Sci U S A* **90**, 11797-11801.

Dolnick, B. J., Berenson, R. J., Bertino, J. R., Kaufman, R. J., Nunberg, J. H., and Schimke, R. T. (1979). Correlation of dihydrofolate reductase elevation with gene amplification in a homogeneously staining chromosomal region in L5178Y cells. *J Cell Biol* **83**, 394-402.

Dolznig, H., Kolbus, A., Leberbauer, C., Schmidt, U., Deiner, E. M., Mullner, E. W., and Beug, H. (2005). Expansion and differentiation of immature mouse and human hematopoietic progenitors. *Methods Mol Med* **105**, 323-344.

Ellenberger, T. E., and Beverley, S. M. (1989). Multiple drug resistance and conservative amplification of the H region in Leishmania major. *J Biol Chem* **264**, 15094-15103.

Ercikan-Abali, E. A., Mineishi, S., Tong, Y., Nakahara, S., Waltham, M. C., Banerjee, D., Chen, W., Sadelain, M., and Bertino, J. R. (1996a). Active site-directed double mutants of dihydrofolate reductase. *Cancer Res* **56**, 4142-4145.

Ercikan-Abali, E. A., Waltham, M. C., Dicker, A. P., Schweitzer, B. I., Gritsman, H., Banerjee, D., and Bertino, J. R. (1996b). Variants of human dihydrofolate reductase with substitutions at leucine-22: effect on catalytic and inhibitor binding properties. *Mol Pharmacol* **49**, 430-437.

Farber, S., Diamond, L. K., Mercer, R. D., Sylvester, R. F., and Wolff, V. A. (1948). *N. Engl. J. Med.* **238**, 787-793.

Ferone, R., Burchall, J. J., and Hitchings, G. H. (1969). Plasmodium berghei dihydrofolate reductase. Isolation, properties, and inhibition by antifolates. *Mol Pharmacol* **5**, 49-59.

Flasshove, M., Banerjee, D., Mineishi, S., Li, M. X., Bertino, J. R., and Moore, M. A. (1995). Ex vivo expansion and selection of human CD34+ peripheral blood progenitor cells after introduction of a mutated dihydrofolate reductase cDNA via retroviral gene transfer. *Blood* **85**, 566-574.

Flensburg, J., and Skold, O. (1987). Massive overproduction of dihydrofolate reductase in bacteria as a response to the use of trimethoprim. *Eur J Biochem* **162**, 473-476.

Foote, S. J., Galatis, D., and Cowman, A. F. (1990). Amino acids in the dihydrofolate reductase-thymidylate synthase gene of Plasmodium falciparum involved in cycloguanil resistance differ from those involved in pyrimethamine resistance. *Proc Natl Acad Sci U S A* **87**, 3014-3017.

Fossati, E., Volpato, J. P., Poulin, L., Guerrero, V., Dugas, D. A., and Pelletier, J. N. (2008). Two-tier bacterial and in vitro selection of active and methotrexate-resistant variants of human dihydrofolate reductase. *J Biomol Screen* **13**, 504-514.

Gatlin, J., Douglas, J., Evans, J. T., Collins, R. H., Wendel, G. D., and Garcia, J. V. (2000). In vitro selection of lentivirus vector-transduced human CD34+ cells. *Hum Gene Ther* **11**, 1949-1957.

Gilbert, I. H. (2002). Inhibitors of dihydrofolate reductase in Leishmania and trypanosomes. *Biochim Biophys Acta* **1587**, 249-257.

Goker, E., Lin, J. T., Trippett, T., Elisseyeff, Y., Tong, W. P., Niedzwiecki, D., Tan, C., Steinherz, P., Schweitzer, B. I., and Bertino, J. R. (1993). Decreased polyglutamylation of methotrexate in acute lymphoblastic leukemia blasts in adults compared to children with this disease. *Leukemia* **7**, 1000-1004.

Goker, E., Waltham, M., Kheradpour, A., Trippett, T., Mazumdar, M., Elisseyeff, Y., Schnieders, B., Steinherz, P., Tan, C., Berman, E., and et al. (1995). Amplification of the dihydrofolate reductase gene is a mechanism of acquired resistance to methotrexate in patients with acute lymphoblastic leukemia and is correlated with p53 gene mutations. *Blood* **86**, 677-684.

Goldie, J. H., Krystal, G., Hartley, D., Gudauskas, G., and Dedhar, S. (1980). A methotrexate insensitive variant of folate reductase present in two lines of methotrexate-resistant L5178Y cells. *Eur J Cancer* **16**, 1539-1546.

Goldman, I. D. (1974). The mechanism of action of methotrexate. I. Interaction with a low-affinity intracellular site required for maximum inhibition of deoxyribonucleic acid synthesis in L-cell mouse fibroblasts. *Mol Pharmacol* **10**, 257-274.

Hankins, E. G., Warhurst, D. C., and Sibley, C. H. (2001). Novel alleles of the Plasmodium falciparum dhfr highly resistant to pyrimethamine and chlorcycloguanil, but not WR99210. *Mol Biochem Parasitol* **117**, 91-102.

Happi, C. T., Gbotosho, G. O., Folarin, O. A., Akinboye, D. O., Yusuf, B. O., Ebong, O. O., Sowunmi, A., Kyle, D. E., Milhous, W., Wirth, D. F., and Oduola, A. M. (2005). Polymorphisms in Plasmodium falciparum dhfr and dhps genes and age related in vivo sulfadoxine-pyrimethamine resistance in malaria-infected patients from Nigeria. *Acta Trop* **95**, 183-193.

Hashkes, P. J., and Laxer, R. M. (2006). Update on the medical treatment of juvenile idiopathic arthritis. *Curr Rheumatol Rep* **8**, 450-458.

Hastings, M. D., and Sibley, C. H. (2002). Pyrimethamine and WR99210 exert opposing selection on dihydrofolate reductase from Plasmodium vivax. *Proc Natl Acad Sci U S A* **99**, 13137-13141.

Havenga, M. J., Werner, A. B., Valerio, D., and van Es, H. H. (1998). Methotrexate selectable retroviral vectors for Gaucher disease. *Gene Ther* **5**, 1379-1388.

Hawser, S., Lociuro, S., and Islam, K. (2006). Dihydrofolate reductase inhibitors as antibacterial agents. *Biochem Pharmacol* **71**, 941-948.

Hekmat-Nejad, M., and Rathod, P. K. (1997). Plasmodium falciparum: kinetic interactions of WR99210 with pyrimethamine-sensitive and pyrimethamine-resistant dihydrofolate reductase. *Exp Parasitol* **87**, 222-228.

Hitchings, G. H. (1969). Species differences among dihydrofolate reductases as a basis for chemotherapy. *Postgrad Med J* **45**, Suppl:7-10.

Hock, R. A., and Miller, A. D. (1986). Retrovirus-mediated transfer and expression of drug resistance genes in human haematopoietic progenitor cells. *Nature* **320**, 275-277.

Huovinen, P., Sundstrom, L., Swedberg, G., and Skold, O. (1995). Trimethoprim and sulfonamide resistance. *Antimicrob Agents Chemother* **39**, 279-289.

Imwong, M., Pukrittakayamee, S., Looareesuwan, S., Pasvol, G., Poirreiz, J., White, N. J., and Snounou, G. (2001). Association of genetic mutations in Plasmodium vivax dhfr with resistance to sulfadoxine-pyrimethamine: geographical and clinical correlates. *Antimicrob Agents Chemother* **45**, 3122-3127.

Imwong, M., Pukrittayakamee, S., Renia, L., Letourneur, F., Charlieu, J. P., Leartsakulpanich, U., Looareesuwan, S., White, N. J., and Snounou, G. (2003). Novel point mutations in the dihydrofolate reductase gene of Plasmodium vivax: evidence for sequential selection by drug pressure. *Antimicrob Agents Chemother* **47**, 1514-1521.

Jones, G., Crotty, M., and Brooks, P. (2000). Interventions for psoriatic arthritis. *Cochrane Database Syst Rev*, CD000212.

Knighton, D. R., Kan, C. C., Howland, E., Janson, C. A., Hostomska, Z., Welsh, K. M., and Matthews, D. A. (1994). Structure of and kinetic channelling in bifunctional dihydrofolate reductase-thymidylate synthase. *Nat Struct Biol* **1**, 186-194.

Kongsaeree, P., Khongsuk, P., Leartsakulpanich, U., Chitnumsub, P., Tarnchompoo, B., Walkinshaw, M. D., and Yuthavong, Y. (2005). Crystal structure of dihydrofolate reductase from Plasmodium vivax: pyrimethamine displacement linked with mutation-induced resistance. *Proc Natl Acad Sci U S A* **102**, 13046-13051.

Kovalevskaya, N. V., Smurnyy, Y. D., Polshakov, V. I., Birdsall, B., Bradbury, A. F., Frenkiel, T., and Feeney, J. (2005). Solution structure of human dihydrofolate reductase in its complex with trimethoprim and NADPH. *J Biomol NMR* **33**, 69-72.

Kramer, B. A., Lemckert, F. A., Alexander, I. E., Gunning, P. W., and McCowage, G. B. (2006). Characterisation of a P140K mutant O6-methylguanine-DNA-methyltransferase (MGMT)-expressing transgenic mouse line with drug-selectable bone marrow. *J Gene Med* **8**, 1071-1085.

Leartsakulpanich, U., Imwong, M., Pukrittayakamee, S., White, N. J., Snounou, G., Sirawaraporn, W., and Yuthavong, Y. (2002). Molecular characterization of dihydrofolate reductase in relation to antifolate resistance in Plasmodium vivax. *Mol Biochem Parasitol* **119**, 63-73.

Lewis, W. S., Cody, V., Galitsky, N., Luft, J. R., Pangborn, W., Chunduru, S. K., Spencer, H. T., Appleman, J. R., and Blakley, R. L. (1995). Methotrexate-resistant variants of human dihydrofolate reductase with substitutions of leucine 22. Kinetics, crystallography, and potential as selectable markers. *J Biol Chem* **270**, 5057-5064.

Li, R., Sirawaraporn, R., Chitnumsub, P., Sirawaraporn, W., Wooden, J., Athappilly, F., Turley, S., and Hol, W. G. (2000). Three-dimensional structure of M. tuberculosis dihydrofolate reductase reveals opportunities for the design of novel tuberculosis drugs. *J Mol Biol* **295**, 307-323.

Lin, J. T., Tong, W. P., Trippett, T. M., Niedzwiecki, D., Tao, Y., Tan, C., Steinherz, P., Schweitzer, B. I., and Bertino, J. R. (1991). Basis for natural resistance to methotrexate in human acute non-lymphocytic leukemia. *Leuk Res* **15**, 1191-1196.

Lorico, A., Bratbak, D., Meyer, J., Kunke, D., Krauss, S., Plott, W. E., Solodushko, V., Baum, C., Fodstad, O., and Rappa, G. (2005). Gamma-glutamylcysteine synthetase and L-buthionine-(S,R)-sulfoximine: a new selection strategy for gene-transduced neural and hematopoietic stem/progenitor cells. *Hum Gene Ther* **16**, 711-724.

Lynch, G., Magill, G. B., Sordillo, P., and Golbey, R. B. (1982). Combination chemotherapy of advanced sarcomas in adults with "CYOMAD" (S7). *Cancer* **50**, 1724-1727.

Ma, L., and Kovacs, J. A. (2000). Expression and characterization of recombinant human-derived Pneumocystis carinii dihydrofolate reductase. *Antimicrob Agents Chemother* **44**, 3092-3096.

Margosiak, S. A., Appleman, J. R., Santi, D. V., and Blakley, R. L. (1993). Dihydrofolate reductase from the pathogenic fungus Pneumocystis carinii: catalytic properties and interaction with antifolates. *Arch Biochem Biophys* **305**, 499-508.

Matthews, D. A., Bolin, J. T., Burridge, J. M., Filman, D. J., Volz, K. W., Kaufman, B. T., Beddell, C. R., Champness, J. N., Stammers, D. K., and Kraut, J. (1985). Refined crystal structures of Escherichia coli and chicken liver dihydrofolate reductase containing bound trimethoprim. *J Biol Chem* **260**, 381-391.

McGready, R., Stepniewska, K., Seaton, E., Cho, T., Cho, D., Ginsberg, A., Edstein, M. D., Ashley, E., Looareesuwan, S., White, N. J., and Nosten, F. (2003). Pregnancy and use of oral contraceptives reduces the biotransformation of proguanil to cycloguanil. *Eur J Clin Pharmacol* **59**, 553-557.

Melera, P. W., Davide, J. P., and Oen, H. (1988). Antifolate-resistant Chinese hamster cells. Molecular basis for the biochemical and structural heterogeneity among dihydrofolate reductases produced by drug-sensitive and drug-resistant cell lines. *J Biol Chem* **263**, 1978-1990.

Melera, P. W., Hession, C. A., Davide, J. P., Scotto, K. W., Biedler, J. L., Meyers, M. B., and Shanske, S. (1982). Antifolate-resistant Chinese Hamster Cells. mRNA directed overproduction of multiple dihydrofolate reductases from a series of independently derived sublines containing amplified dihydrofolate reductase genes. *J Biol Chem* **257**, 12939-12949.

Mendis, K., Sina, B. J., Marchesini, P., and Carter, R. (2001). The neglected burden of Plasmodium vivax malaria. *Am J Trop Med Hyg* **64**, 97-106.

Mennes, M., Stiers, P., Vandenbussche, E., Vercruysse, G., Uyttebroeck, A., De Meyer, G., and Van Cool, S. W. (2005). Attention and information processing in survivors of childhood acute lymphoblastic leukemia treated with chemotherapy only. *Pediatr Blood Cancer* **44**, 478-486.

Morris, J. A., and McIvor, R. S. (1994). Saturation mutagenesis at dihydrofolate reductase codons 22 and 31. A variety of amino acid substitutions conferring methotrexate resistance. *Biochem Pharmacol* **47**, 1207-1220.

Nakano, T., Spencer, H. T., Appleman, J. R., and Blakley, R. L. (1994). Critical role of phenylalanine 34 of human dihydrofolate reductase in substrate and inhibitor binding and in catalysis. *Biochemistry* **33**, 9945-9952.

Nzila, A., Ochong, E., Nduati, E., Gilbert, K., Winstanley, P., Ward, S., and Marsh, K. (2005). Why has the dihydrofolate reductase 164 mutation not consistently been found in Africa yet? *Trans R Soc Trop Med Hyg* **99**, 341-346.

Oefner, C., D'Arcy, A., and Winkler, F. K. (1988). Crystal structure of human dihydrofolate reductase complexed with folate. *Eur J Biochem* **174**, 377-385.

Patel, M., Sleep, S. E., Lewis, W. S., Spencer, H. T., Mareya, S. M., Sorrentino, B. P., and Blakley, R. L. (1997). Comparison of the protection of cells from antifolates by transduced human dihydrofolate reductase mutants. *Hum Gene Ther* **8**, 2069-2077.

Persons, D. A., Allay, J. A., Bonifacino, A., Lu, T., Agricola, B., Metzger, M. E., Donahue, R. E., Dunbar, C. E., and Sorrentino, B. P. (2004). Transient in vivo selection of transduced peripheral blood cells using antifolate drug selection in rhesus macaques that received transplants with hematopoietic stem cells expressing dihydrofolate reductase vectors. *Blood* **103**, 796-803.

Peterson, D. S., Milhous, W. K., and Wellems, T. E. (1990). Molecular basis of differential resistance to cycloguanil and pyrimethamine in Plasmodium falciparum malaria. *Proc Natl Acad Sci U S A* **87**, 3018-3022.

Peterson, D. S., Walliker, D., and Wellems, T. E. (1988). Evidence that a point mutation in dihydrofolate reductase-thymidylate synthase confers resistance to pyrimethamine in falciparum malaria. *Proc Natl Acad Sci U S A* **85**, 9114-9118.

Pikis, A., Donkersloot, J. A., Rodriguez, W. J., and Keith, J. M. (1998). A conservative amino acid mutation in the chromosome-encoded dihydrofolate reductase confers trimethoprim resistance in Streptococcus pneumoniae. *J Infect Dis* **178**, 700-706.

Prendergast, N. J., Appleman, J. R., Delcamp, T. J., Blakley, R. L., and Freisheim, J. H. (1989). Effects of conversion of phenylalanine-31 to leucine on the function of human dihydrofolate reductase. *Biochemistry* **28**, 4645-4650.

Rothem, L., Stark, M., Kaufman, Y., Mayo, L., and Assaraf, Y. G. (2004). Reduced folate carrier gene silencing in multiple antifolate-resistant tumor cell lines is due to a

simultaneous loss of function of multiple transcription factors but not promoter methylation. *J Biol Chem* **279**, 374-384.

Sandefur, C. I., Wooden, J. M., Quaye, I. K., Sirawaraporn, W., and Sibley, C. H. (2007). Pyrimethamine-resistant dihydrofolate reductase enzymes of Plasmodium falciparum are not enzymatically compromised in vitro. *Mol Biochem Parasitol* **154**, 1-5.

Santos-Filho, O. A., de Alencastro, R. B., and Figueroa-Villar, J. D. (2001). Homology modeling of wild type and pyrimethamine/cycloguanil-cross resistant mutant type Plasmodium falciparum dihydrofolate reductase. A model for antimalarial chemotherapy resistance. *Biophys Chem* **91**, 305-317.

Sauerbrey, A., McPherson, J. P., Zhao, S. C., Banerjee, D., and Bertino, J. R. (1999). Expression of a novel double-mutant dihydrofolate reductase-cytidine deaminase fusion gene confers resistance to both methotrexate and cytosine arabinoside. *Hum Gene Ther* **10**, 2495-2504.

Sawaya, M. R., and Kraut, J. (1997). Loop and subdomain movements in the mechanism of Escherichia coli dihydrofolate reductase: crystallographic evidence. *Biochemistry* **36**, 586-603.

Schweitzer, B. I., Dicker, A. P., and Bertino, J. R. (1990). Dihydrofolate reductase as a therapeutic target. *Faseb J* **4**, 2441-2452.

Schweitzer, B. I., Srimatkandada, S., Gritsman, H., Sheridan, R., Venkataraghavan, R., and Bertino, J. R. (1989). Probing the role of two hydrophobic active site residues in the human dihydrofolate reductase by site-directed mutagenesis. *J Biol Chem* **264**, 20786-20795.

Simonsen, C. C., and Levinson, A. D. (1983). Isolation and expression of an altered mouse dihydrofolate reductase cDNA. *Proc Natl Acad Sci U S A* **80**, 2495-2499.

Sirawaraporn, W., Prapunwattana, P., Sirawaraporn, R., Yuthavong, Y., and Santi, D. V. (1993). The dihydrofolate reductase domain of Plasmodium falciparum thymidylate synthase-dihydrofolate reductase. Gene synthesis, expression, and anti-folate-resistant mutants. *J Biol Chem* **268**, 21637-21644.

Sirawaraporn, W., Sathitkul, T., Sirawaraporn, R., Yuthavong, Y., and Santi, D. V. (1997a). Antifolate-resistant mutants of Plasmodium falciparum dihydrofolate reductase. *Proc Natl Acad Sci U S A* **94**, 1124-1129.

Sirawaraporn, W., Sirawaraporn, R., Cowman, A. F., Yuthavong, Y., and Santi, D. V. (1990). Heterologous expression of active thymidylate synthase-dihydrofolate reductase from Plasmodium falciparum. *Biochemistry* **29**, 10779-10785.

Sirawaraporn, W., Yongkiettrakul, S., Sirawaraporn, R., Yuthavong, Y., and Santi, D. V. (1997b). Plasmodium falciparum: asparagine mutant at residue 108 of dihydrofolate reductase is an optimal antifolate-resistant single mutant. *Exp Parasitol* **87**, 245-252.

Slamon, D. J., Romond, E. H., and Perez, E. A. (2006). Advances in adjuvant therapy for breast cancer. *Clin Adv Hematol Oncol* **4**, 4-9.

Sorrentino, B. P. (2004). Clinical strategies for expansion of haematopoietic stem cells. *Nat Rev Immunol* **4**, 878-888.

Spencer, H. T., Sleep, S. E., Rehg, J. E., Blakley, R. L., and Sorrentino, B. P. (1996a). A gene transfer strategy for making bone marrow cells resistant to trimetrexate. *Blood* **87**, 2579-2587.

Spencer, H. T., Sorrentino, B. P., Pui, C. H., Chunduru, S. K., Sleep, S. E., and Blakley, R. L. (1996b). Mutations in the gene for human dihydrofolate reductase: an unlikely cause of clinical relapse in pediatric leukemia after therapy with methotrexate. *Leukemia* **10**, 439-446.

Srimatkandada, S., Schweitzer, B. I., Moroson, B. A., Dube, S., and Bertino, J. R. (1989). Amplification of a polymorphic dihydrofolate reductase gene expressing an enzyme with decreased binding to methotrexate in a human colon carcinoma cell line, HCT-8R4, resistant to this drug. *J Biol Chem* **264**, 3524-3528.

Strojan, P., Soba, E., Budihna, M., and Auersperg, M. (2005). Radiochemotherapy with Vinblastine, Methotrexate, and Bleomycin in the treatment of verrucous carcinoma of the head and neck. *J Surg Oncol* **92**, 278-283.

Tahar, R., de Pecoulas, P. E., Basco, L. K., Chiadmi, M., and Mazabraud, A. (2001). Kinetic properties of dihydrofolate reductase from wild-type and mutant Plasmodium vivax expressed in Escherichia coli. *Mol Biochem Parasitol* **113**, 241-249.

Takebe, N., Xu, L. C., MacKenzie, K. L., Bertino, J. R., and Moore, M. A. (2002). Methotrexate selection of long-term culture initiating cells following transduction of CD34(+) cells with a retrovirus containing a mutated human dihydrofolate reductase gene. *Cancer Gene Ther* **9**, 308-320.

Takebe, N., Zhao, S. C., Adhikari, D., Mineishi, S., Sadelain, M., Hilton, J., Colvin, M., Banerjee, D., and Bertino, J. R. (2001). Generation of dual resistance to 4-hydroperoxycyclophosphamide and methotrexate by retroviral transfer of the human aldehyde dehydrogenase class 1 gene and a mutated dihydrofolate reductase gene. *Mol Ther* **3**, 88-96.

Thillet, J., Absil, J., Stone, S. R., and Pictet, R. (1988). Site-directed mutagenesis of mouse dihydrofolate reductase. Mutants with increased resistance to methotrexate and trimethoprim. *J Biol Chem* **263**, 12500-12508.

Thillet, J., and Pictet, R. (1990). Transfection of DHFR- and DHFR+ mammalian cells using methotrexate-resistant mutants of mouse dihydrofolate reductase. *FEBS Lett* **269**, 450-453.

Trippett, T., Schlemmer, S., Elisseyeff, Y., Goker, E., Wachter, M., Steinherz, P., Tan, C., Berman, E., Wright, J. E., Rosowsky, A., and et al. (1992). Defective transport as a mechanism of acquired resistance to methotrexate in patients with acute lymphocytic leukemia. *Blood* **80**, 1158-1162.

Volpato, J. P., Fossati, E., and Pelletier, J. N. (2007). Increasing Methotrexate Resistance by Combination of Active-site Mutations in Human Dihydrofolate Reductase. *J Mol Biol* **373**, 599-611.

Warlick, C. A., Diers, M. D., Wagner, J. E., and McIvor, R. S. (2002). In vivo selection of antifolate-resistant transgenic hematopoietic stem cells in a murine bone marrow transplant model. *J Pharmacol Exp Ther* **300**, 50-56.

Watson, M., Liu, J. W., and Ollis, D. (2007). Directed evolution of trimethoprim resistance in Escherichia coli. *Febs J* **274**, 2661-2671.

Young, M. D., and Burgess, R. W. (1959). Pyrimethamine resistance in Plasmodium vivax malaria. *Bull World Health Organ* **20**, 27-36.

Yuvaniyama, J., Chitnumsub, P., Kamchonwongpaisan, S., Vanichtanankul, J., Sirawaraporn, W., Taylor, P., Walkinshaw, M. D., and Yuthavong, Y. (2003). Insights into antifolate resistance from malarial DHFR-TS structures. *Nat Struct Biol* **10**, 357-365.

Zhanel, G. G., Decorby, M., Laing, N., Weshnoweski, B., Vashisht, R., Tailor, F., Nichol, K. A., Wierzbowski, A., Baudry, P. J., Karlowsky, J. A., Lagace-Wiens, P., Walkty, A., McCracken, M., Mulvey, M. R., Johnson, J., and Hoban, D. J. (2008). Antimicrobial

Resistant Pathogens in Intensive Care Units in Canada: Results of the Canadian National Intensive Care Unit (CAN-ICU) Study, 2005/2006. *Antimicrob Agents Chemother*.

Zhang, K., and Rathod, P. K. (2002). Divergent regulation of dihydrofolate reductase between malaria parasite and human host. *Science* **296**, 545-547.

Zhao, R., and Goldman, I. D. (2003). Resistance to antifolates. *Oncogene* **22**, 7431-7457.

Zhao, R., Titus, S., Gao, F., Moran, R. G., and Goldman, I. D. (2000). Molecular analysis of murine leukemia cell lines resistant to 5, 10-dideazatetrahydrofolate identifies several amino acids critical to the function of folylpolyglutamate synthetase. *J Biol Chem* **275**, 26599-26606.

Zhao, S. C., Banerjee, D., Mineishi, S., and Bertino, J. R. (1997). Post-transplant methotrexate administration leads to improved curability of mice bearing a mammary tumor transplanted with marrow transduced with a mutant human dihydrofolate reductase cDNA. *Hum Gene Ther* **8**, 903-909.

Zolg, J. W., Plitt, J. R., Chen, G. X., and Palmer, S. (1989). Point mutations in the dihydrofolate reductase-thymidylate synthase gene as the molecular basis for pyrimethamine resistance in Plasmodium falciparum. *Mol Biochem Parasitol* **36**, 253-262.

CHAPITRE 7

Conclusions et perspectives

7.0 – Conclusions générales

La dihydrofolate reductase humaine est une cible très convoitée pour le traitement de maladies à caractère prolifératif tel le cancer. Plusieurs inhibiteurs ont été développés au fil des ans pour contrer l'activité DHFR et arrêter la prolifération cellulaire, mais l'utilisation clinique de ces inhibiteurs a toujours été limitée par l'apparition de mécanismes de résistance. La compréhension des causes moléculaires reliées à l'un de ces mécanismes, soit la perte d'affinité pour l'antifolate MTX suite à des mutations dans le gène de la DHFR, peut générer une quantité d'informations pouvant être utiles pour le design de nouveaux médicaments ayant la capacité de contourner les mécanismes de résistance cellulaire. Centré sur cette problématique générale, le thème principal de cette thèse fut d'entreprendre une étude structure-fonction détaillée de la majorité des résidus du site actif de la DHFR humaine ayant comme objectif d'améliorer la compréhension de leur rôle au niveau de la reconnaissance et de la liaison d'un inhibiteur clinique utilisé couramment pour le traitement de divers cancers, soit le MTX. En ce sens, nous avons contribué, en substituant la majorité des résidus du site actif de la DHFR humaine de manière ponctuelle ou combinatoire (Chapitre 2, 3 et 5), à mieux comprendre le rôle des différents résidus dans la liaison du MTX.

Au chapitre 2, nous avons créé une banque de mutants combinatoires contenant des mutations aux résidus du site actif Phe31, Phe34 et/ou Gln35. En développant un système de criblage par sélection chez la bactérie, nous avons observé que les variantes conférrant les plus hauts taux de résistance (ou les plus importantes pertes d'affinité pour le MTX) étaient principalement des variantes combinatoires contenant des mutations aux résidus 31 et 35 ou 31, 34 et 35. Dans l'échantillon sélectionné, les variantes triples démontraient des plus grandes pertes d'affinité pour le MTX que les variantes doubles. Ces derniers ne comportant pas de mutation au résidu 34, ceci suggère que le résidu Phe34 est important pour la reconnaisance du MTX. Une étude de modélisation moléculaire avec la triple

variante F31A/F34V/Q35H suggérait que l'importante perte d'affinité pour le MTX présente chez cette variante était reliée à des pertes de contacts hydrophobes importants entre les résidus 31 et 34 et certains groupements du MTX.

Au chapitre 3, nous avons développé une méthodologie à deux étapes pour sélectionner les variantes actives, ou actives et résistantes au MTX, et caractériser rapidement certains paramètres cinétiques et d'inhibition. Les banques de mutants ponctuels aux résidus du site actif Ile7, Trp24, Arg70 et Val115, ainsi qu'au résidu Gly15, ont été soumises à cette procédure de sélection et caractérisation. Ce système nous a permis d'éliminer les faux-positifs obtenus suite à l'étape de sélection bactérienne. De plus, il peut être facilement adapté pour le criblage à haut débit de plus grandes banques de mutants. D'une autre part, nous avons généré des informations structure-fonction concernant le rôle des résidus mutés. Aucune variante active n'a été obtenu au résidu 70, démontrant l'implication essentielle du résidu natif Arg70 tant au niveau de la catalyse enzymatique que la reconnaissance des ligands de la DHFR humaine. Seules des mutations conservatrices permettaient de garder un certain niveau d'activité enzymatique aux résidus 7, 15, 24 et 115, démontrant l'importance de ces résidus dans la reconnaissance des ligands et la catalyse de la DHFR humaine. Toutefois, la banque Val115 a généré des variantes actives et résistantes au MTX, suggérant que ce résidu était impliqué de façon plus importante dans la reconnaissance du MTX que dans la réaction catalysée par la DHFR humaine.

Les paramètres cinétiques et d'inhibition rapportés aux chapitres 2 et 3 ont permis d'émettre des hypothèses sur le rôle des différents résidus mutés par rapport à la liaison du MTX, mais ne permettaient pas de voir l'effet des mutations sur la reconnaissance du MTX et sur l'intégrité de la structure de la DHFR humaine. Au chapitre 5, nous avons décrit une première structure cristalline pour la double variante F31R/Q35E, issu de la banque 31/34/35, avec le MTX lié au site actif. La variante F31R/Q35E était un candidat idéal pour la compréhension moléculaire de la discrimination de reconnaissance observée entre le

substrat DHF et le MTX. Chez cette variante, l'affinité pour le DHF est réduite par un ordre de grandeur par rapport à l'enzyme native, alors que l'affinité pour le MTX est réduite par près de trois ordres de grandeur par rapport l'enzyme native. La détermination des paramètres cinétiques et d'inhibition pour les variantes ponctuelles F31R et Q35E a révélé que la perte d'affinité pour le DHF chez la variante F31R/Q35E était le résultat d'un effet additif des deux mutations, alors que la perte d'affinité pour le MTX résultait d'un phénomène synergique. Dans la structure de la double variante, nous observons la présence de deux conformères distincts de divers résidus du site actif, dont le résidu substitué Arg31. La position de la chaîne latérale d'un des conformères Arg31 résulte en la perte de contacts van der Waals et hydrophobes importants avec les parties *p*-ABA et ptérine du MTX. Des études d'arrimage moléculaire avec le folate ont suggéré que ce conformère résulterait en des pertes similaires pour le substrat. Ces pertes de contacts ne pouvaient donc pas expliquer l'effet discriminatoire de la double mutation sur les deux ligands. La présence d'un bon nombre de résidus représentés par deux conformères dans la structure cristalline de la double variante suggère plutôt la présence d'un phénomène dynamique, avec un effet plus important sur la liaison du MTX que sur le cycle catalytique de l'enzyme. Ainsi, il est possible que la combinaison des substitutions F31R et Q35E perturbent la constante d'isomérisation de la DHFR humaine, un phénomène qui mène à une liaison plus forte du MTX au site actif de l'enzyme native.

En plus de générer une meilleure compréhension des interactions entre le MTX et la DHFR humaine, la création de variantes résistantes au MTX offre des applications intéressantes en tant que marqueurs de sélection pour plusieurs systèmes cellulaires. Ainsi, nous avons pu démontrer aux chapitres 2 et 4, que certains variantes de la DHFR humaine hautement résistantes au MTX issus de la banque 31/34/35 conférraient une meilleure protection aux cellules contre les effets cytotoxiques du MTX que les variantes précédemment décrites dans la littérature. Les résultats obtenus dans les cellules CHO *dhfr*$^-$ pour les variantes SFE, RFE, RTS et AVH nous ont incités à tester le potentiel de ces variantes en tant que marqueurs de sélection pour les cellules hématopoïétiques, qui offrent

plusieurs perspectives de traitements thérapeutiques[171-173]. Dans le chapitre 4, nous démontrons que la variante F31R/Q35E offre la meilleure protection aux cellules hématopoïétiques exposées à une dose élevée de MTX pendant un court laps de temps. Dans des expériences de compétition *ex vivo*, il a été possible de démontrer qu'une petite population de cellules hématopoïétiques transduites avec la double variante contenues dans une plus grande population de cellules non-transduites étaient les seules à survivre et à proliférer suite à une courte exposition à une forte concentration de MTX. En applicant l'expérience de compétition sur des cellules HS et en greffant les cellules sélectionnées chez des souris irradiées, nous avons démontré que les cellules HS transduites avec la variante F31R/Q35E survivent à la sélection au MTX et avaient la capacité de repeupler la moelle osseuse de souris à des pourcentages plus élevés qu'attendus si les cellules n'avaient pas été soumises à une étape de sélection avec le MTX. En plus de procurer un enrichissement des cellules HS avant leur transplantation, pouvant pallier à un des problèmes principaux de la thérapie génique, les variantes de la DHFRh hautement résistantes pourraient servir de marqueurs de sélection pour de nouvelles thérapies basées sur la création par transduction de lymphocytes T cytotoxiques pour le traitement ciblé de certains types de cancers[171, 174].

Le chapitre 6 comporte une compilation des travaux effectués par nous et d'autres groupes par rapport aux mutations permettant la résistance aux antifolates, tout en étant un préambule aux différentes perspectives pouvant découler des résultats présentés dans cette thèse. En comparant les séquences et les structures de variantes de la DHFR conférant une résistance aux antifolates chez différents organismes, nous avons observé une forte corrélation au niveau des sites de mutations donnant lieu à la résistance. En même temps, nous avons identifié de nouveaux sites à muter chez la DHFR humaine, qui pourraient générer des variantes aussi actives que l'enzyme native, tout en ayant une importante diminution de l'affinité pour le MTX. Finalement, notre étude comparative nous a permis d'émettre une nouvelle hypothèse sur la liaison spécifique de l'antifolate trimethoprime (TMP), qui se lie plus fortement à l'enzyme bactérienne qu'à l'enzyme humaine. La

combinaison des informations traitant de données cinétiques et d'inhibition pour différents antifolates, de résidus mutés procurant une résistance aux antifolates et de la structure des DHFR de différentes espèces sera d'une grande utilité pour élucider les bases moléculaires pour la reconnaissance et la liaison des antifolates chez la DHFR.

7.1 – Perspectives

7.1.1 – Effets des mutations sur la liaison d'autres antifolates

La compréhension des éléments moléculaires essentiels à la liaison du MTX peuvent nous mener à mieux comprendre ce qui est essentiel dans la liaison de cet inhibiteur. Toutefois, une plus grande compréhension générale de la liaison de molécules au site actif de la DHFR humaine serait possible en testant comment la liaison d'autres antifolates est affectée par les mutations intégrées à différentes régions du site actif. Plusieurs antifolates classiques et non-classiques sont disponibles pour ce type d'étude. Nous avons entamé la détermination des valeurs de constantes d'inhibition pour le pemetrexed, un antifolate contenant plus d'homologie chimique avec le folate qu'avec le MTX (**Tableau 7.1**). Malgré ces différences chimiques, nous observons une corrélation quasi-linéaire entre la perte d'affinité pour le PMTX et le MTX, suggérant que des mécanismes moléculaires communs sont responsables pour la moins bonne liaison des deux inhibiteurs (**Figure 7.1A**). Des études d'arrimage moléculaire nous suggèrent que le PMTX se lierait au site actif de la DHFRh native avec son noyau pyrrolopyrimidine dans la même orientation que le noyau ptérine du folate (**Figure 7.1B**). En supposant que ce modèle est juste, les différentes interactions moléculaires dues à l'orientation du noyau ptérine du folate par rapport au MTX ne seraient pas suffisantes pour expliquer en entier la perte d'affinité plus importante pour le MTX par rapport au DHF chez les variantes combinatoires.

Tableau 7.1. Constantes d'affinité pour différents ligands chez les variantes combinatoires 31/34/35 de la DHFRh.

Enzyme	K_M^{DHF} (µM)[a]	K_i^{MTX} (nM)[a]	K_i^{PMTX} (nM)[b]
WT	0.075	≤ 0.031	≤ 0.48 ± 0.06
F31R/Q35E	0.69	21	170 ± 77
F31S/Q35E	3.3	30	97 ± 2
F31P/Q35E	2.7	12	49 ± 6
F31P/Q35H	2.1	10	50 ± 5
F31G/Q35N	1.7	9	41 ± 11
F31R/F34T/Q35S	1.7	59	110 ± 3
F31R/F34T/Q35R	2.0	86	87 ± 12
F31A/F34V/Q35H	4.3	180	260 ± 20

[a] Valeurs tirées du chapitre 2.

[b] Valeurs calculées à partir du IC_{50}^{PMTX} et l'équation pour l'inhibition compétitive[160].

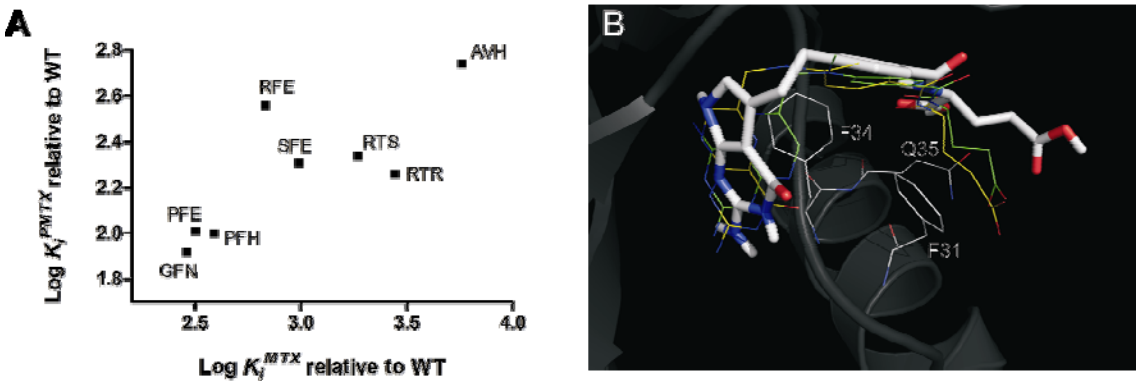

Figure 7.1. A) Relation entre la perte d'affinité pour le MTX et le PMTX chez les variantes combinatoires 31/34/35 de la DHFRh. Les valeurs sur les axes correspondent au logarithme du rapport de $K_i^{variante}/K_i^{native}$ pour le MTX et le PMTX. B) Arrimage moléculaire du PMTX (en bâtonnets ; C : blanc, N : bleu, O : rouge) sur la structure de la DHFRh native (1U72.pdb). Le positionnement du MTX (en lignes ; C : vert, N : bleu, O : rouge; 1U72.pdb) et du folate (en lignes ; C : jaunes, N : bleu, O : rouge; 1DRF.pdb) dans des structures cristallines de la DHFRh native est montré à titre comparatif. Les résidus F31, F34 et Q35 sont aussi représentés (lignes ; C : blanc, N : bleu, O : rouge).

Ceci suggère la présence d'autres facteurs moléculaires pouvant être affectés par l'introduction de mutations au site actif de la DHFRh.

7.1.2 – Caractérisation des constantes d'isomérisation pour les mutants hautement résistantes au MTX

Il a été démontré que la liaison du MTX au site actif de la DHFR humaine induisait un effet d'isomérisation de l'enzyme, qui augmente l'affinité de l'enzyme pour le MTX de 60 fois, menant à un complexe enzyme-inhibiteur pratiquement indissociable[175] (**Figure 7.2**). Ce phénomène n'a pas été rapporté lors de la liaison du folate ou du DHF, et ceci pourrait constituer la base des différences de pertes d'affinité observées entre l'inhibiteur et le substrat. Bien que l'effet d'isomérisation ait été caractérisé physiquement, aucune information n'est disponible quant aux résidus participant à cette étape chez la DHFR humaine. Une des conséquences possibles de mutations aux résidus 31, 34 et 35 serait la réduction de l'effet d'isomérisation de la protéine suite à la liaison du MTX, ne permettant la formation d'un complexe enzyme-inhibiteur indissociable. Il serait donc intéressant de caractériser l'effet des mutations chez les variantes résistantes de la banque 31/34/35 sur l'étape d'isomérisation menant à une forte affinité pour le MTX. Pour ce faire, les constantes de vitesses thermodynamiques (k_{on}, k_{off}, k_{iso}, $k_{r\ iso}$) devront être déterminées pour le complexe ternaire (DHFRh•NADPH•MTX) des différentes variantes à l'aide d'un fluorimètre couplé à un injecteur rapide ('stopped-flow'). La décroissance du signal de fluorescence de l'enzyme suite à la liaison du MTX au site actif permet l'évaluation de la valeur des constantes de vitesse dictant la liaison de l'inhibiteur. Les résultats de cette étude nous donneraient une meilleure idée du rôle des mutations sur la liaison thermodynamique du MTX, ce qui nous permettrait de mieux caractériser le rôle des résidus natifs dans l'étape d'isomérisation.

Figure 7.2. Schéma de l'étape d'isomérisation menant à une forte affinité entre l'enzyme (E) et l'inhibiteur (I). * signifie un changement conformationnel de l'enzyme menant à une plus forte liaison avec l'inhibiteur.

7.1.3 – Création de nouvelles banques de la DHFR humaine

Bien que plusieurs résidus du site actif aient été caractérisés lors de ce projet, il reste à explorer le rôle d'autres résidus situés à d'autres endroits du site actif de la DHFR humaine pour mieux comprendre les bases moléculaires de la liaison de l'inhibiteur. Par exemple, notre étude comparative a révélé que le résidu humain homologue à Thr56 chez le parasite *Plasmodium falciparum* est le résidu principalement responsable pour la résistance aux antifolates pyriméthamine (PYR) et cycloguanyl (CYC). Chez l'enzyme humaine, ce résidu est situé dans une région du site actif que nous n'avons pas encore exploré, situé à moins de 5 Å du MTX (**Figure 7.3**). À proximité de ce résidu se trouvent les résidus Ile60, Pro61 et Asn64, également à moins de 5 Å du MTX (**Figure 7.3**). Les résidus Ile60 et Pro61 peuvent former des contacts hydrophobes avec la partie *p*-ABA du MTX, alors que le résidu Asn64 peut former un pont hydrogène avec le carbonyl du *p*-ABA. Il est plausble que des mutations à ces résidus puissent perturber la liaison du MTX. Il serait donc d'un grand intérêt de créer une banque combinatoire, *via* la mutagénèse par saturation, à l'ensemble de ces résidus. La méthodologie de criblage décrite au chapitre 3 serait idéale pour cribler une banque de cette taille (qui contiendra > 1 000 000 combinaisons de mutations).

L'approche de mutagénèse décrite dans nos travaux peut être considérée comme étant locale, puisque les banques créées, incluant la banque combinatoire, exploraient une région du site actif à la fois. Chez *Plasmodium falciparum*, des mutations combinatoires aux résidus homologues à Gln35, Thr56 et Val115 ont généré une variante enzymatique hautement résistante aux antifolates PYR et CYC, tout en ramenant les constantes catalytiques de l'enzyme, diminuées chez les variantes ponctuelles et les doubles variantes, au niveau de l'enzyme native[176]. Ces trois résidus se retrouvent dans trois régions distinctes du site actif. L'introduction de mutations combinatoires à différentes régions du site actif de la DHFR humaine aurait le potentiel de générer des variantes ayant uniquement perdu de

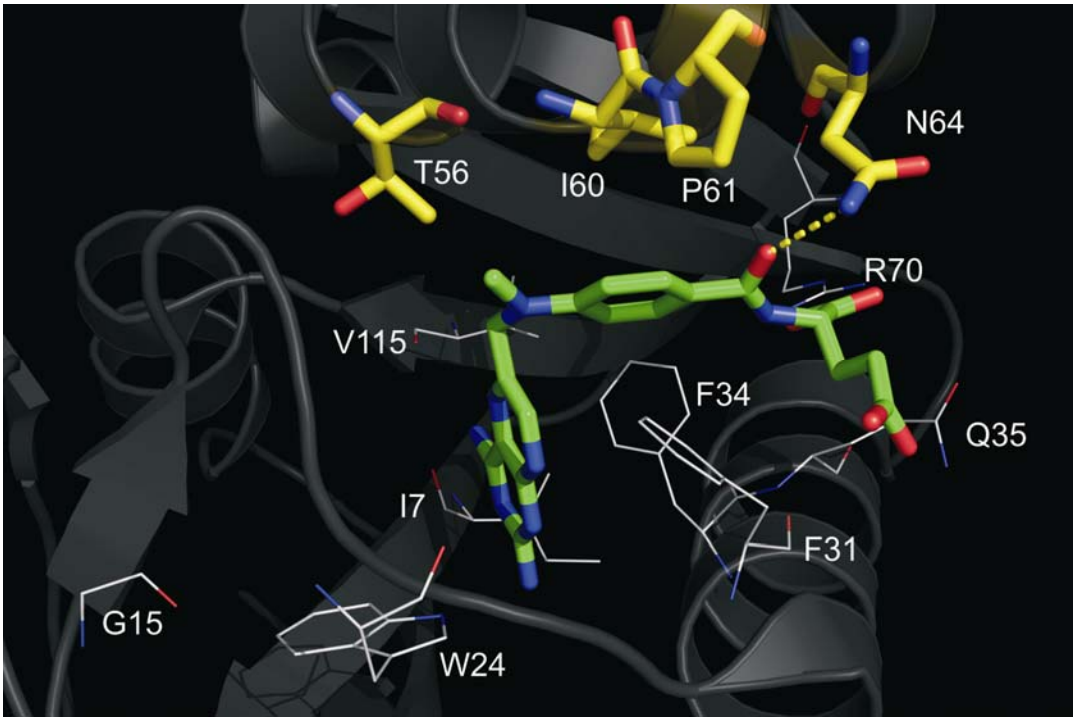

Figure 7.3. Futurs sites à muter chez la DHFRh pour l'étude de la liaison du MTX. Les résidus Thr56, Ile60, Pro61, Asn64 (en bâtonnets ; C : jaune, N : bleu, O : rouge) sont à proximité du MTX lié (en lignes ; C : vert, N : bleu, O : rouge; 1U72.pdb) et se retrouvent dans une région du site actif dont le rôle dans la liaison de l'inhibiteur n'a pas été exploré. Les résidus mutés lors de nos travaux sont également représentés (lignes ; C : blanc, N : bleu, O : rouge).

l'affinité pour le MTX, ce qui serait intéressant d'un point de vue structure-fonction et pour le développement de marqueurs de sélection plus efficaces que ceux obtenus à ce jour. Nous allons combiner les banques 31/34/35, 56 et 115 entre elles dans le but d'identifier des variantes avec un comportement cinétique semblable à l'enzyme native, tout en ayant une importante perte d'affinité pour le MTX. Ce type de variante pourrait potentiellement corriger un des problèmes rencontré lors du développement de marqueurs de sélection pour les cellules HS. Les pourcentages de reconstitution de la moelle osseuse de souris ayant reçues démontrait un enrichissement des cellules HS transduites avec la variante F31R/Q35E suite à une sélection avec du MTX (Chapitre 4). Toutefois, nous espérions obtenir des pourcentages de reconstitutions plus élevés, étant donné l'incorporation du facteur prolifératif Nup98-HoxA10 suite à la sélection et avant la greffe chez les souris (Chapitre 4). La reconstitution moderée que nous avons obtenue pourrait être attribuable à la concentration de MTX utilisée lors de la sélection, qui aurait pu être légèrement toxique pour la croissance des cellules HS transduites avec la variante F31R/Q35E. Il aurait été envisageable de réduire la concentration de MTX pour alléger la toxicité aux cellules transduites, mais ceci aurait pu réduire l'efficacité de l'effet cytotoxique du MTX sur les cellules non-transduites. La variante F31R/Q35E a une efficacité catalytique (k_{cat}/K_M^{DHF}) près de deux ordres de grandeurs plus petite que l'enzyme native. Une moins bonne efficacité catalytique de cette enzyme chez les cellules HS transduite pourrait être à la base de la légère toxicité suggérée par les résultats de reconstitutions *in vivo*. Une enzyme hautement efficace et hautement résistante au MTX pourrait permettre de maintenir des conditions de sélection stringentes tout en allégeant l'effet potentiellement cytotoxique de hautes concentrations de MTX sur les cellules transduites.

7.1.4 – Obtention d'autres structures cristallines pour les variantes de la DHFR humaine hautement résistantes au MTX

L'obtention d'une première structure cristalline nous a permis de suggérer certaines causes moléculaires reliées à la perte d'affinité pour le MTX chez la variantes F31R/Q35E de la DHFR humaine. Malgré ces observations, il reste plusieurs questions non-résolues quant à la perte d'affinité plus importante observée pour le MTX par rapport au substrat DHF. La majorité des variantes sélectionnées de la banque 31/34/35 présentent ce phénotype, suggérant que la combinaison de mutations aux résidus 31, 34 et/ou 35 promouvrait une plus grande perte d'affinité pour le MTX. Il serait donc primordial de caractériser structurellement l'ensemble de ces variantes dans le but de mieux élucider ce phénomène. Ayant déterminé des conditions de cristallisation pour la variante F31R/Q35E, nous avons tenté de cristalliser d'autres variantes combinatoires de la banque 31/34/35 dans les mêmes conditions, sans succès. Il faudra identifier d'autres conditions potentielles de cristallisation, en ciblant de nouvelles conditions de criblage avec les variantes combinatoires. Aussi, la cristallisation en présence du folate devra être réalisée pour obtenir une structure des différentes variantes en présence de ce substrat. Bien que nous ayons obtenu un modèle représentatif de la liaison du folate à l'enzyme F31R/Q35E par arrimage moléculaire (Chapitre 5), il reste que plusieurs interactions (*e.g.* formation de ponts hydrogènes entre ligands et/ou résidus avec plusieurs molécules d'eau cristallographiques) ne peuvent être élucidées par ce type de modélisation. L'obtention de structures de variantes liées au folate faciliterait la comparaison avec des structures des mêmes variantes liées au MTX, permettant de mieux élucider la cause des pertes d'affinité différentes entre l'inhibiteur et le substrat chez une variante donnée.

7.1.5. – Études dynamiques des variantes de la DHFR humaine

La résonance magnétique nucléaire (RMN) est une technique efficace pour évaluer des différences dynamiques entre des variantes et une enzyme native, en absence et en présence de ligands. Des études récentes ont démontré que les mouvements dynamiques retrouvés chez une enzyme pouvaient dicter la spécificité de reconnaissance d'un ligand et la catalyse enzymatique, et que la perte d'affinité pour un ligand et la diminution d'activité catalytique suite à une mutation pouvait être correlée avec un changement de dynamique dans une variante enzymatique[177, 178]. Le nombre élevé de résidus observés sous plus d'un conformère dans le site actif de la variante F31R/Q35E suggère que cette enzyme a un caractère dynamique différent de la DHFRh native. Cette différence structurale pourrait être la base de la perte d'affinité pour le MTX chez les variantes combinatoires. Ainsi, il serait possible de vérifier l'effet des mutations aux résidus 31, 34 et/ou 35 sur la dynamique de la DHFRh en absence et en présence de ligands. Le spectre HSQC de la DHFRh native liée au MTX a été assigné et est disponible publiquement[179], ainsi que certains spectres 3D pour la DHFRh complexée au NADPH et au PT523, un antifolate semblable au MTX[180]. Ces données pourraient faciliter l'assignation de spectres 2D et 3D de variantes marqués au $^{13}C/^{15}N$, en absence et en présence du co-facteur NADPH et du MTX liés. La superposition des spectres HSQC assignés de l'enzyme native et d'enzymes variantes permettraient d'observer les différences de déplacements chimiques du squelette peptidique résultant des mutations. Des expériences de pulses CPMG[181] permettraient d'observer la dynamique globale sur l'échelle des picosecondes-nanosecondes et microsecondes-millisecondes des enzymes variantes et native, donnant ainsi des informations structurales sur la dynamique moléculaire des variantes par rapport à l'enzyme native. En combinant ces informations avec une structure cristalline et les paramètres d'inhibition d'une variante donnée, il serait possible d'identifier l'ensemble des causes moléculaires dictant la liaison du MTX au site actif de la DHFR.

Bibliographie

1. Willis, L., Treatment of "pernicious anemia of pregnancy" and "tropical anemia" with special reference to yeast extract as curative agent. *British Medical Journal* **1931,** 1, 1059-1064.

2. Mitchell, H. K.; Snell, E. E.; Williams, R. J., The concentration of "folic acid". *Journal of the American Chemistry Society* **1941,** 63, (8), 2284-2284.

3. Jukes, T. H.; Stokstad, E. L. R., Pteroylglutamic acid and related compounds. *Physiol. Rev.* **1948,** 28, 51-106.

4. Zhao, R.; Goldman, I. D., Resistance to antifolates. *Oncogene* **2003,** 22, (47), 7431-57.

5. Ratnam, M.; Marquardt, H.; Duhring, J. L.; Freisheim, J. H., Homologous membrane folate binding proteins in human placenta: cloning and sequence of a cDNA. *Biochemistry* **1989,** 28, (20), 8249-54.

6. McGuire, J. J.; Hsieh, P.; Coward, J. K.; Bertino, J. R., Enzymatic synthesis of folylpolyglutamates. Characterization of the reaction and its products. *J Biol Chem* **1980,** 255, (12), 5776-88.

7. Moran, R. G.; Werkheiser, W. C.; Zakrzewski, S. F., Folate metabolism in mammalian cells in culture. I Partial characterization of the folate derivatives present in L1210 mouse leukemia cells. *J Biol Chem* **1976,** 251, (12), 3569-75.

8. Schirch, V.; Strong, W. B., Interaction of folylpolyglutamates with enzymes in one-carbon metabolism. *Arch Biochem Biophys* **1989,** 269, (2), 371-80.

9. Pelletier, J. N.; MacKenzie, R. E., Binding and interconversion of tetrahydrofolates at a single site in the bifunctional methylenetetrahydrofolate dehydrogenase/cyclohydrolase. *Biochemistry* **1995,** 34, (39), 12673-80.

10. Nichol, C. A.; Anton, A. H.; Zakrzewski, S. F., A labile precursor of citrovorum factor. *Science* **1955,** 121, (3139), 275-9.

11. Broquist, H. P.; Kohler, A. R.; Hutchison, D. J.; Burchenal, J. H., Studies on the enzymatic formation of citrovorum factor by Streptococcus faecalis. *J Biol Chem* **1953,** 202, (1), 59-66.

12. Nichol, C. A.; Welch, A. D., Synthesis of citrovorum factor from folic acid by liver slices; augmentation by ascorbic acid. *Proc Soc Exp Biol Med* **1950,** 74, (1), 52-5.

13. Osborn, M. J.; Huennekens, F. M., Enzymatic reduction of dihydrofolic acid. *J Biol Chem* **1958,** 233, (4), 969-74.

14. Maurer, B. J.; Barker, P. E.; Masters, J. N.; Ruddle, F. H.; Attardi, G., Human dihydrofolate reductase gene is located in chromosome 5 and is unlinked to the related pseudogenes. *Proc Natl Acad Sci U S A* **1984,** 81, (5), 1484-8.

15. Gudewicz, T. M.; Morhenn, V. B.; Kellems, R. E., The effect of polyoma virus, serum factors, and dibutyryl cyclic AMP on dihydrofolate reductase synthesis, and the entry of quiescent cells into S phase. *J Cell Physiol* **1981,** 108, (1), 1-8.

16. Hentze, M. W., Enzymes as RNA-binding proteins: a role for (di)nucleotide-binding domains? *Trends Biochem Sci* **1994,** 19, (3), 101-3.

17. Nagy, E.; Henics, T.; Eckert, M.; Miseta, A.; Lightowlers, R. N.; Kellermayer, M., Identification of the NAD(+)-binding fold of glyceraldehyde-3-phosphate dehydrogenase as a novel RNA-binding domain. *Biochem Biophys Res Commun* **2000,** 275, (2), 253-60.

18. Chu, E.; Takimoto, C. H.; Voeller, D.; Grem, J. L.; Allegra, C. J., Specific binding of human dihydrofolate reductase protein to dihydrofolate reductase messenger RNA in vitro. *Biochemistry* **1993,** 32, (18), 4756-60.

19. Appleman, J. R.; Beard, W. A.; Delcamp, T. J.; Prendergast, N. J.; Freisheim, J. H.; Blakley, R. L., Unusual transient- and steady-state kinetic behavior is predicted by the kinetic scheme operational for recombinant human dihydrofolate reductase. *J Biol Chem* **1990,** 265, (5), 2740-8.

20. Beard, W. A.; Appleman, J. R.; Delcamp, T. J.; Freisheim, J. H.; Blakley, R. L., Hydride transfer by dihydrofolate reductase. Causes and consequences of the wide range of rates exhibited by bacterial and vertebrate enzymes. *J Biol Chem* **1989,** 264, (16), 9391-9.

21. Villafranca, J. E.; Howell, E. E.; Voet, D. H.; Strobel, M. S.; Ogden, R. C.; Abelson, J. N.; Kraut, J., Directed mutagenesis of dihydrofolate reductase. *Science* **1983,** 222, (4625), 782-8.

22. Appleman, J. R.; Tsay, J. T.; Freisheim, J. H.; Blakley, R. L., Effect of enzyme and ligand protonation on the binding of folates to recombinant human dihydrofolate reductase: implications for the evolution of eukaryotic enzyme efficiency. *Biochemistry* **1992,** 31, (14), 3709-15.

23. Posner, B. A.; Li, L.; Bethell, R.; Tsuji, T.; Benkovic, S. J., Engineering specificity for folate into dihydrofolate reductase from Escherichia coli. *Biochemistry* **1996,** 35, (5), 1653-63.

24. Oefner, C.; D'Arcy, A.; Winkler, F. K., Crystal structure of human dihydrofolate reductase complexed with folate. *Eur J Biochem* **1988,** 174, (2), 377-85.

25. Cody, V.; Galitsky, N.; Luft, J. R.; Pangborn, W.; Blakley, R. L.; Gangjee, A., Comparison of ternary crystal complexes of F31 variants of human dihydrofolate reductase with NADPH and a classical antitumor furopyrimidine. *Anticancer Drug Des* **1998,** 13, (4), 307-15.

26. Cody, V.; Luft, J. R.; Pangborn, W.; Gangjee, A., Analysis of three crystal structure determinations of a 5-methyl-6-N-methylanilino pyridopyrimidine antifolate complex with human dihydrofolate reductase. *Acta Crystallogr D Biol Crystallogr* **2003,** 59, (Pt 9), 1603-9.

27. Cody, V.; Galitsky, N.; Luft, J. R.; Pangborn, W.; Gangjee, A., Analysis of two polymorphic forms of a pyrido[2,3-d]pyrimidine N9-C10 reversed-bridge antifolate binary complex with human dihydrofolate reductase. *Acta Crystallogr D Biol Crystallogr* **2003,** 59, (Pt 4), 654-61.

28. Cody, V.; Galitsky, N.; Luft, J. R.; Pangborn, W.; Rosowsky, A.; Blakley, R. L., Comparison of two independent crystal structures of human dihydrofolate reductase ternary complexes reduced with nicotinamide adenine dinucleotide phosphate and the very tight-binding inhibitor PT523. *Biochemistry* **1997,** 36, (45), 13897-903.

29. Lewis, W. S.; Cody, V.; Galitsky, N.; Luft, J. R.; Pangborn, W.; Chunduru, S. K.; Spencer, H. T.; Appleman, J. R.; Blakley, R. L., Methotrexate-resistant variants of human dihydrofolate reductase with substitutions of leucine 22. Kinetics, crystallography, and potential as selectable markers. *J Biol Chem* **1995,** 270, (10), 5057-64.

30. Reynolds, R. C.; Campbell, S. R.; Fairchild, R. G.; Kisliuk, R. L.; Micca, P. L.; Queener, S. F.; Riordan, J. M.; Sedwick, W. D.; Waud, W. R.; Leung, A. K.; Dixon, R. W.; Suling, W. J.; Borhani, D. W., Novel boron-containing, nonclassical antifolates: synthesis and preliminary biological and structural evaluation. *J Med Chem* **2007,** 50, (14), 3283-9.

31. Klon, A. E.; Heroux, A.; Ross, L. J.; Pathak, V.; Johnson, C. A.; Piper, J. R.; Borhani, D. W., Atomic structures of human dihydrofolate reductase complexed with NADPH and two lipophilic antifolates at 1.09 a and 1.05 a resolution. *J Mol Biol* **2002,** 320, (3), 677-93.

32. Gangjee, A.; Vidwans, A. P.; Vasudevan, A.; Queener, S. F.; Kisliuk, R. L.; Cody, V.; Li, R.; Galitsky, N.; Luft, J. R.; Pangborn, W., Structure-based design and synthesis of lipophilic 2,4-diamino-6-substituted quinazolines and their evaluation as inhibitors of dihydrofolate reductases and potential antitumor agents. *J Med Chem* **1998,** 41, (18), 3426-34.

33. Cody, V.; Luft, J. R.; Pangborn, W.; Gangjee, A.; Queener, S. F., Structure determination of tetrahydroquinazoline antifolates in complex with human and Pneumocystis carinii dihydrofolate reductase: correlations between enzyme selectivity and stereochemistry. *Acta Crystallogr D Biol Crystallogr* **2004,** 60, (Pt 4), 646-55.

34. Cody, V.; Luft, J. R.; Pangborn, W., Understanding the role of Leu22 variants in methotrexate resistance: comparison of wild-type and Leu22Arg variant mouse and human dihydrofolate reductase ternary crystal complexes with methotrexate and NADPH. *Acta Crystallogr D Biol Crystallogr* **2005,** 61, (Pt 2), 147-55.

35. Davies, J. F., 2nd; Delcamp, T. J.; Prendergast, N. J.; Ashford, V. A.; Freisheim, J. H.; Kraut, J., Crystal structures of recombinant human dihydrofolate reductase complexed with folate and 5-deazafolate. *Biochemistry* **1990,** 29, (40), 9467-79.

36. Kovalevskaya, N. V.; Smurnyy, Y. D.; Polshakov, V. I.; Birdsall, B.; Bradbury, A. F.; Frenkiel, T.; Feeney, J., Solution structure of human dihydrofolate reductase in its complex with trimethoprim and NADPH. *J Biomol NMR* **2005,** 33, (1), 69-72.

37. Meiering, E. M.; Li, H.; Delcamp, T. J.; Freisheim, J. H.; Wagner, G., Contributions of tryptophan 24 and glutamate 30 to binding long-lived water molecules in the ternary complex of human dihydrofolate reductase with methotrexate and NADPH studied by site-directed mutagenesis and nuclear magnetic resonance spectroscopy. *J Mol Biol* **1995,** 247, (2), 309-25.

38. Gready, J. E., Theoretical studies on the activation of the pterin cofactor in the catalytic mechanism of dihydrofolate reductase. *Biochemistry* **1985,** 24, (18), 4761-6.

39. McGuire, J. J., Anticancer antifolates: current status and future directions. *Curr Pharm Des* **2003,** 9, (31), 2593-613.

40. Nair, M. G.; Fayard, M. L.; Lariccia, J. M.; Amato, A. E.; McGuire, J. J.; Galivan, J. H.; Kisliuk, R. L., Metabolism blocked classical folate analog inhibitors of dihydrofolate reductase-1: Synthesis and biological evaluation of mobiletrex. *Medicinal Chemistry Research* **1999,** 9, (3), 176-185.

41. Williams, E. A.; Morrison, J. F., Human dihydrofolate reductase: reduction of alternative substrates, pH effects, and inhibition by deazafolates. *Biochemistry* **1992,** 31, (29), 6801-11.

42. Rosowsky, A., PT523 and other aminopterin analogs with a hemiphthaloyl-L-ornithine side chain: Exceptionally tight-binding inhibitors of dihydrofolate reductase which are transported by the reduced folate carrier but cannot form polyglutamates [Review]. *Current Medicinal Chemistry* **1999,** 6, (4), 329-352.

43. Gangjee, A.; Yu, J.; McGuire, J. J.; Cody, V.; Galitsky, N.; Kisliuk, R. L.; Queener, S. F., Design, synthesis, and X-ray crystal structure of a potent dual inhibitor of thymidylate synthase and dihydrofolate reductase as an antitumor agent. *J Med Chem* **2000,** 43, (21), 3837-51.

44. Gangjee, A.; Jain, H. D.; Kurup, S., Recent advances in classical and non-classical antifolates as antitumor and antiopportunistic infection agents: part I. *Anticancer Agents Med Chem* **2007,** 7, (5), 524-42.

45. Auliff, A.; Wilson, D. W.; Russell, B.; Gao, Q.; Chen, N.; Anh le, N.; Maguire, J.; Bell, D.; O'Neil, M. T.; Cheng, Q., Amino acid mutations in Plasmodium vivax DHFR and DHPS from several geographical regions and susceptibility to antifolate drugs. *Am J Trop Med Hyg* **2006,** 75, (4), 617-21.

46. van Merode, T.; Nys, S.; Raets, I.; Stobberingh, E., Acute uncomplicated lower urinary tract infections in general practice: clinical and microbiological cure rates after three- versus five-day treatment with trimethoprim. *Eur J Gen Pract* **2005,** 11, (2), 55-8.

47. Burchall, J. J.; Hitchings, G. H., Inhibitor binding analysis of dihydrofolate reductases from various species. *Mol Pharmacol* **1965,** 1, (2), 126-36.

48. Volz, K. W.; Matthews, D. A.; Alden, R. A.; Freer, S. T.; Hansch, C.; Kaufman, B. T.; Kraut, J., Crystal structure of avian dihydrofolate reductase containing phenyltriazine and NADPH. *J Biol Chem* **1982,** 257, (5), 2528-36.

49. Matthews, D. A.; Bolin, J. T.; Burridge, J. M.; Filman, D. J.; Volz, K. W.; Kaufman, B. T.; Beddell, C. R.; Champness, J. N.; Stammers, D. K.; Kraut, J., Refined crystal structures of Escherichia coli and chicken liver dihydrofolate reductase containing bound trimethoprim. *J Biol Chem* **1985,** 260, (1), 381-91.

50. Taira, K.; Benkovic, S. J., Evaluation of the importance of hydrophobic interactions in drug binding to dihydrofolate reductase. *J Med Chem* **1988,** 31, (1), 129-37.

51. Piper, J. R.; McCaleb, G. S.; Montgomery, J. A.; Kisliuk, R. L.; Gaumont, Y.; Sirotnak, F. M., Syntheses and antifolate activity of 5-methyl-5-deaza analogues of aminopterin, methotrexate, folic acid, and N10-methylfolic acid. *J Med Chem* **1986,** 29, (6), 1080-7.

52. Fidock, D. A.; Wellems, T. E., Transformation with human dihydrofolate reductase renders malaria parasites insensitive to WR99210 but does not affect the intrinsic activity of proguanil. *Proc Natl Acad Sci U S A* **1997,** 94, (20), 10931-6.

53. Matherly, L. H.; Hou, Z.; Deng, Y., Human reduced folate carrier: translation of basic biology to cancer etiology and therapy. *Cancer Metastasis Rev* **2007,** 26, (1), 111-28.

54. Whetstine, J. R.; Flatley, R. M.; Matherly, L. H., The human reduced folate carrier gene is ubiquitously and differentially expressed in normal human tissues: identification of seven non-coding exons and characterization of a novel promoter. *Biochem J* **2002,** 367, (Pt 3), 629-40.

55. Sierra, E. E.; Brigle, K. E.; Spinella, M. J.; Goldman, I. D., pH dependence of methotrexate transport by the reduced folate carrier and the folate receptor in L1210 leukemia cells. Further evidence for a third route mediated at low pH. *Biochem Pharmacol* **1997,** 53, (2), 223-31.

56. Pompei, A.; Cordisco, L.; Amaretti, A.; Zanoni, S.; Matteuzzi, D.; Rossi, M., Folate production by bifidobacteria as a potential probiotic property. *Appl Environ Microbiol* **2007,** 73, (1), 179-85.

57. Kopytek, S. J.; Dyer, J. C.; Knapp, G. S.; Hu, J. C., Resistance to methotrexate due to AcrAB-dependent export from Escherichia coli. *Antimicrob Agents Chemother* **2000,** 44, (11), 3210-2.

58. McGuire, J. J.; Bertino, J. R., Enzymatic synthesis and function of folylpolyglutamates. *Mol Cell Biochem* **1981,** 38 Spec No, (Pt 1), 19-48.

59. Daw, N. C.; Billups, C. A.; Rodriguez-Galindo, C.; McCarville, M. B.; Rao, B. N.; Cain, A. M.; Jenkins, J. J.; Neel, M. D.; Meyer, W. H., Metastatic osteosarcoma. *Cancer* **2006,** 106, (2), 403-12.

60. Slamon, D. J.; Romond, E. H.; Perez, E. A., Advances in adjuvant therapy for breast cancer. *Clin Adv Hematol Oncol* **2006,** 4, (Suppl. 7), 4-9.

61. Strojan, P.; Soba, E.; Budihna, M.; Auersperg, M., Radiochemotherapy with Vinblastine, Methotrexate, and Bleomycin in the treatment of verrucous carcinoma of the head and neck. *J Surg Oncol* **2005,** 92, (4), 278-83.

62. Walling, J., From methotrexate to pemetrexed and beyond. A review of the pharmacodynamic and clinical properties of antifolates. *Invest New Drugs* **2006,** 24, (1), 37-77.

63. Jones, G.; Crotty, M.; Brooks, P., Interventions for psoriatic arthritis. *Cochrane Database Syst Rev* **2000**, (3), CD000212.

64. Ramanan, A. V.; Whitworth, P.; Baildam, E. M., Use of methotrexate in juvenile idiopathic arthritis. *Arch Dis Child* **2003,** 88, (3), 197-200.

65. Seeger, D. R.; Smith, J. M.; Hultquist, M. E., Antagonist for pteroylglutamic acid. *Journal of the American Chemistry Society* **1947,** 69, 2567.

66. Farber, S.; Diamond, L. K.; Mercer, R. D.; Sylvester, R. F.; Wolff, V. A., Temporary remissions in acute leukemia in children produced by folic acid antagonist, 4-aminopteroyl-glutamic acid (aminopterin). *New England Journal of Medicine* **1948,** 238, 787-793.

67. Werkheiser, W. C.; Zakrzewski, S. F.; Nichol, C. A., Assay for 4-amino folic acid analogues by inhibition of folic acid reductase. *J Pharmacol Exp Ther* **1962,** 137, 162-6.

68. Lavoie, J.; Drouin, R., Lymphoblasts already in the DNA synthesis phase of the cell cycle can be reversibly arrested at the R/G transition. *Chromosoma* **2001,** 110, (7), 501-10.

69. Banerjee, D.; Zhao, S. C.; Li, M. X.; Schweitzer, B. I.; Mineishi, S.; Bertino, J. R., Gene therapy utilizing drug resistance genes: a review. *Stem Cells* **1994,** 12, (4), 378-85.

70. Sorrentino, B. P., Clinical strategies for expansion of haematopoietic stem cells. *Nat Rev Immunol* **2004,** 4, (11), 878-88.

71. Mitchell, M. S.; Wawro, N. W.; DeConti, R. C.; Kaplan, S. R.; Papac, R.; Bertino, J. R., Effectiveness of high-dose infusions of methotrexate followed by leucovorin in carcinoma of the head and neck. *Cancer Res* **1968,** 28, (6), 1088-94.

72. Sawaya, M. R.; Kraut, J., Loop and subdomain movements in the mechanism of Escherichia coli dihydrofolate reductase: crystallographic evidence. *Biochemistry* **1997,** 36, (3), 586-603.

73. Rosowsky, A.; Forsch, R. A.; Wright, J. E., Synthesis and in vitro antifolate activity of rotationally restricted aminopterin and methotrexate analogues. *J Med Chem* **2004,** 47, (27), 6958-63.

74. Vaidya, C. M.; Wright, J. E.; Rosowsky, A., Synthesis and in vitro antitumor activity of new deaza analogues of the nonpolyglutamatable antifolate N(alpha)-(4-amino-4-deoxypteroyl)-N(delta)-hemiphthaloyl-L-ornithine (PT523). *J Med Chem* **2002,** 45, (8), 1690-6.

75. Miyachi, H.; Takemura, Y.; Kobayashi, H.; Ando, Y., Expression of variant dihydrofolate reductase with decreased binding affinity to antifolates in MOLT-3 human leukemia cell lines resistant to trimetrexate. *Cancer Lett* **1995,** 88, (1), 93-9.

76. Stone, S. R.; Montgomery, J. A.; Morrison, J. F., Inhibition of dihydrofolate reductase from bacterial and vertebrate sources by folate, aminopterin, methotrexate and their 5-deaza analogues. *Biochem Pharmacol* **1984,** 33, (2), 175-9.

77. Shih, C.; Chen, V. J.; Gossett, L. S.; Gates, S. B.; MacKellar, W. C.; Habeck, L. L.; Shackelford, K. A.; Mendelsohn, L. G.; Soose, D. J.; Patel, V. F.; Andis, S. L.; Bewley, J. R.; Rayl, E. A.; Moroson, B. A.; Beardsley, G. P.; Kohler, W.; Ratnam, M.; Schultz, R. M., LY231514, a pyrrolo[2,3-d]pyrimidine-based antifolate that inhibits multiple folate-requiring enzymes. *Cancer Res* **1997,** 57, (6), 1116-23.

78. Tinoco, I., Jr., Sauer, K., Wang, J.C., *Physical chemistry: Principles and applications in biological sciences*. 3rd Edition ed.; Prentice-Hall: Upper Saddle River, NJ, 1995; p 762.

79. Fischer, G. A., Defective transport of amethopterin (methotrexate) as a mechanism of resistance to the antimetabolite in L5178Y leukemic cells. *Biochem Pharmacol* **1962,** 11, 1233-4.

80. Serra, M.; Reverter-Branchat, G.; Maurici, D.; Benini, S.; Shen, J. N.; Chano, T.; Hattinger, C. M.; Manara, M. C.; Pasello, M.; Scotlandi, K.; Picci, P., Analysis of dihydrofolate reductase and reduced folate carrier gene status in relation to methotrexate resistance in osteosarcoma cells. *Ann Oncol* **2004,** 15, (1), 151-60.

81. Dixon, K. H.; Lanpher, B. C.; Chiu, J.; Kelley, K.; Cowan, K. H., A novel cDNA restores reduced folate carrier activity and methotrexate sensitivity to transport deficient cells. *J Biol Chem* **1994,** 269, (1), 17-20.

82. Brigle, K. E.; Spinella, M. J.; Sierra, E. E.; Goldman, I. D., Characterization of a mutation in the reduced folate carrier in a transport defective L1210 murine leukemia cell line. *J Biol Chem* **1995,** 270, (39), 22974-9.

83. Jansen, G.; Mauritz, R.; Drori, S.; Sprecher, H.; Kathmann, I.; Bunni, M.; Priest, D. G.; Noordhuis, P.; Schornagel, J. H.; Pinedo, H. M.; Peters, G. J.; Assaraf, Y. G., A structurally altered human reduced folate carrier with increased folic acid transport mediates a novel mechanism of antifolate resistance. *J Biol Chem* **1998,** 273, (46), 30189-98.

84. Gong, M.; Yess, J.; Connolly, T.; Ivy, S. P.; Ohnuma, T.; Cowan, K. H.; Moscow, J. A., Molecular mechanism of antifolate transport-deficiency in a methotrexate-resistant MOLT-3 human leukemia cell line. *Blood* **1997,** 89, (7), 2494-9.

85. Gong, M.; Cowan, K. H.; Gudas, J.; Moscow, J. A., Isolation and characterization of genomic sequences involved in the regulation of the human reduced folate carrier gene (RFC1). *Gene* **1999,** 233, (1-2), 21-31.

86. Argiris, A.; Longo, G. S.; Gorlick, R.; Tong, W.; Steinherz, P.; Bertino, J. R., Increased methotrexate polyglutamylation in acute megakaryocytic leukemia (M7) compared to other subtypes of acute myelocytic leukemia. *Leukemia* **1997,** 11, (6), 886-9.

87. Flintoff, W. F.; Sadlish, H.; Gorlick, R.; Yang, R.; Williams, F. M., Functional analysis of altered reduced folate carrier sequence changes identified in osteosarcomas. *Biochim Biophys Acta* **2004,** 1690, (2), 110-7.

88. Hooijberg, J. H.; Broxterman, H. J.; Kool, M.; Assaraf, Y. G.; Peters, G. J.; Noordhuis, P.; Scheper, R. J.; Borst, P.; Pinedo, H. M.; Jansen, G., Antifolate resistance

mediated by the multidrug resistance proteins MRP1 and MRP2. *Cancer Res* **1999,** 59, (11), 2532-5.

89. Norris, M. D.; De Graaf, D.; Haber, M.; Kavallaris, M.; Madafiglio, J.; Gilbert, J.; Kwan, E.; Stewart, B. W.; Mechetner, E. B.; Gudkov, A. V.; Roninson, I. B., Involvement of MDR1 P-glycoprotein in multifactorial resistance to methotrexate. *Int J Cancer* **1996,** 65, (5), 613-9.

90. Higgins, C. F., Multiple molecular mechanisms for multidrug resistance transporters. *Nature* **2007,** 446, (7137), 749-57.

91. Zeng, H.; Chen, Z. S.; Belinsky, M. G.; Rea, P. A.; Kruh, G. D., Transport of methotrexate (MTX) and folates by multidrug resistance protein (MRP) 3 and MRP1: effect of polyglutamylation on MTX transport. *Cancer Res* **2001,** 61, (19), 7225-32.

92. Morrison, P. F.; Allegra, C. J., The kinetics of methotrexate polyglutamation in human breast cancer cells. *Arch Biochem Biophys* **1987,** 254, (2), 597-610.

93. McGuire, J. J.; Hsieh, P.; Coward, J. K.; Bertino, J. R., In vitro methotrexate polyglutamate synthesis by rat liver folylpolyglutamate synthetase and inhibition by bromosulfophthalein. *Adv Exp Med Biol* **1983,** 163, 199-214.

94. Pizzorno, G.; Chang, Y. M.; McGuire, J. J.; Bertino, J. R., Inherent resistance of human squamous carcinoma cell lines to methotrexate as a result of decreased polyglutamylation of this drug. *Cancer Res* **1989,** 49, (19), 5275-80.

95. McGuire, J. J.; Russell, C. A., Folylpolyglutamate synthetase expression in antifolate-sensitive and -resistant human cell lines. *Oncol Res* **1998,** 10, (4), 193-200.

96. Takemura, Y.; Kobayashi, H.; Miyachi, H., Variable expression of the folylpolyglutamate synthetase gene at the level of mRNA transcription in human leukemia cell lines sensitive, or made resistant, to various antifolate drugs. *Anticancer Drugs* **1999,** 10, (7), 677-83.

97. Lin, J. T.; Tong, W. P.; Trippett, T. M.; Niedzwiecki, D.; Tao, Y.; Tan, C.; Steinherz, P.; Schweitzer, B. I.; Bertino, J. R., Basis for natural resistance to methotrexate in human acute non-lymphocytic leukemia. *Leuk Res* **1991,** 15, (12), 1191-6.

98. Longo, G. S.; Gorlick, R.; Tong, W. P.; Ercikan, E.; Bertino, J. R., Disparate affinities of antifolates for folylpolyglutamate synthetase from human leukemia cells. *Blood* **1997,** 90, (3), 1241-5.

99. Frei, E., 3rd; Rosowsky, A.; Wright, J. E.; Cucchi, C. A.; Lippke, J. A.; Ervin, T. J.; Jolivet, J.; Haseltine, W. A., Development of methotrexate resistance in a human squamous cell carcinoma of the head and neck in culture. *Proc Natl Acad Sci U S A* **1984,** 81, (9), 2873-7.

100. Wolman, S. R.; Craven, M. L.; Grill, S. P.; Domin, B. A.; Cheng, Y. C., Quantitative correlation of homogeneously stained regions on chromosome 10 with dihydrofolate reductase enzyme in human cells. *Proc Natl Acad Sci U S A* **1983,** 80, (3), 807-9.

101. Saito, H.; Kishi, K.; Narita, M.; Furukawa, T.; Nagura, E.; Maekawa, T.; Abe, T.; Shibata, A., A new myeloblastic leukemia cell line with double minute chromosomes. Induction of methotrexate resistance and dihydrofolate reductase gene amplification. *Leuk Res* **1992,** 16, (3), 217-26.

102. Hall, M. J.; Lawrence, D. A.; Lansiedel, J. C.; Walsh, A. C.; Comstock, L. L.; Kremer, J. M., Long-term exposure to methotrexate induces immunophenotypic changes, decreased methotrexate uptake and increased dihydrofolate gene copy number in Jurkat T cells. *Int J Immunopharmacol* **1997,** 19, (11-12), 709-20.

103. Carman, M. D.; Schornagel, J. H.; Rivest, R. S.; Srimatkandada, S.; Portlock, C. S.; Duffy, T.; Bertino, J. R., Resistance to methotrexate due to gene amplification in a patient with acute leukemia. *J Clin Oncol* **1984,** 2, (1), 16-20.

104. Horns, R. C., Jr.; Dower, W. J.; Schimke, R. T., Gene amplification in a leukemic patient treated with methotrexate. *J Clin Oncol* **1984,** 2, (1), 2-7.

105. Goker, E.; Waltham, M.; Kheradpour, A.; Trippett, T.; Mazumdar, M.; Elisseyeff, Y.; Schnieders, B.; Steinherz, P.; Tan, C.; Berman, E.; et al., Amplification of the dihydrofolate reductase gene is a mechanism of acquired resistance to methotrexate in patients with acute lymphoblastic leukemia and is correlated with p53 gene mutations. *Blood* **1995,** 86, (2), 677-84.

106. Anagnou, N. P.; O'Brien, S. J.; Shimada, T.; Nash, W. G.; Chen, M. J.; Nienhuis, A. W., Chromosomal organization of the human dihydrofolate reductase genes: dispersion, selective amplification, and a novel form of polymorphism. *Proc Natl Acad Sci U S A* **1984,** 81, (16), 5170-4.

107. Masters, J.; Keeley, B.; Gay, H.; Attardi, G., Variable content of double minute chromosomes is not correlated with degree of phenotype instability in methotrexate-resistant human cell lines. *Mol Cell Biol* **1982,** 2, (5), 498-507.

108. Pauletti, G.; Lai, E.; Attardi, G., Early appearance and long-term persistence of the submicroscopic extrachromosomal elements (amplisomes) containing the amplified DHFR genes in human cell lines. *Proc Natl Acad Sci U S A* **1990,** 87, (8), 2955-9.

109. Ercikan-Abali, E. A.; Banerjee, D.; Waltham, M. C.; Skacel, N.; Scotto, K. W.; Bertino, J. R., Dihydrofolate reductase protein inhibits its own translation by binding to dihydrofolate reductase mRNA sequences within the coding region. *Biochemistry* **1997,** 36, (40), 12317-22.

110. Skacel, N.; Menon, L. G.; Mishra, P. J.; Peters, R.; Banerjee, D.; Bertino, J. R.; Abali, E. E., Identification of amino acids required for the functional up-regulation of human dihydrofolate reductase protein in response to antifolate Treatment. *J Biol Chem* **2005,** 280, (24), 22721-31.

111. Jackson, R. C.; Hart, L. I.; Harrap, K. R., Intrinsic resistance to methotrexate of cultured mammalian cells in relation to the inhibition kinetics of their dihydrololate reductases. *Cancer Res* **1976,** 36, (6), 1991-7.

112. Simonsen, C. C.; Levinson, A. D., Isolation and expression of an altered mouse dihydrofolate reductase cDNA. *Proc Natl Acad Sci U S A* **1983,** 80, (9), 2495-9.

113. Haber, D. A.; Beverley, S. M.; Kiely, M. L.; Schimke, R. T., Properties of an altered dihydrofolate reductase encoded by amplified genes in cultured mouse fibroblasts. *J Biol Chem* **1981,** 256, (18), 9501-10.

114. Melera, P. W.; Davide, J. P.; Oen, H., Antifolate-resistant Chinese hamster cells. Molecular basis for the biochemical and structural heterogeneity among dihydrofolate reductases produced by drug-sensitive and drug-resistant cell lines. *J Biol Chem* **1988,** 263, (4), 1978-90.

115. Dicker, A. P.; Volkenandt, M.; Schweitzer, B. I.; Banerjee, D.; Bertino, J. R., Identification and characterization of a mutation in the dihydrofolate reductase gene from the methotrexate-resistant Chinese hamster ovary cell line Pro-3 MtxRIII. *J Biol Chem* **1990,** 265, (14), 8317-21.

116. Srimatkandada, S.; Schweitzer, B. I.; Moroson, B. A.; Dube, S.; Bertino, J. R., Amplification of a polymorphic dihydrofolate reductase gene expressing an enzyme with decreased binding to methotrexate in a human colon carcinoma cell line, HCT-8R4, resistant to this drug. *J Biol Chem* **1989,** 264, (6), 3524-8.

117. McIvor, R. S.; Simonsen, C. C., Isolation and characterization of a variant dihydrofolate reductase cDNA from methotrexate-resistant murine L5178Y cells. *Nucleic Acids Res* **1990,** 18, (23), 7025-32.

118. Chunduru, S. K.; Cody, V.; Luft, J. R.; Pangborn, W.; Appleman, J. R.; Blakley, R. L., Methotrexate-resistant variants of human dihydrofolate reductase. Effects of Phe31 substitutions. *J Biol Chem* **1994,** 269, (13), 9547-55.

119. Dicker, A. P.; Waltham, M. C.; Volkenandt, M.; Schweitzer, B. I.; Otter, G. M.; Schmid, F. A.; Sirotnak, F. M.; Bertino, J. R., Methotrexate resistance in an in vivo mouse tumor due to a non-active-site dihydrofolate reductase mutation. *Proc Natl Acad Sci U S A* **1993,** 90, (24), 11797-801.

120. Farnum, M. F.; Magde, D.; Howell, E. E.; Hirai, J. T.; Warren, M. S.; Grimsley, J. K.; Kraut, J., Analysis of hydride transfer and cofactor fluorescence decay in mutants of

dihydrofolate reductase: possible evidence for participation of enzyme molecular motions in catalysis. *Biochemistry* **1991,** 30, (49), 11567-79.

121. Li, L.; Falzone, C. J.; Wright, P. E.; Benkovic, S. J., Functional role of a mobile loop of Escherichia coli dihydrofolate reductase in transition-state stabilization. *Biochemistry* **1992,** 31, (34), 7826-33.

122. Prendergast, N. J.; Delcamp, T. J.; Smith, P. L.; Freisheim, J. H., Expression and site-directed mutagenesis of human dihydrofolate reductase. *Biochemistry* **1988,** 27, (10), 3664-71.

123. Patel, M.; Sleep, S. E.; Lewis, W. S.; Spencer, H. T.; Mareya, S. M.; Sorrentino, B. P.; Blakley, R. L., Comparison of the protection of cells from antifolates by transduced human dihydrofolate reductase mutants. *Hum Gene Ther* **1997,** 8, (17), 2069-77.

124. Ercikan-Abali, E. A.; Waltham, M. C.; Dicker, A. P.; Schweitzer, B. I.; Gritsman, H.; Banerjee, D.; Bertino, J. R., Variants of human dihydrofolate reductase with substitutions at leucine-22: effect on catalytic and inhibitor binding properties. *Mol Pharmacol* **1996,** 49, (3), 430-7.

125. Spencer, H. T.; Sorrentino, B. P.; Pui, C. H.; Chunduru, S. K.; Sleep, S. E.; Blakley, R. L., Mutations in the gene for human dihydrofolate reductase: an unlikely cause of clinical relapse in pediatric leukemia after therapy with methotrexate. *Leukemia* **1996,** 10, (3), 439-46.

126. Thillet, J.; Absil, J.; Stone, S. R.; Pictet, R., Site-directed mutagenesis of mouse dihydrofolate reductase. Mutants with increased resistance to methotrexate and trimethoprim. *J Biol Chem* **1988,** 263, (25), 12500-8.

127. Nakano, T.; Spencer, H. T.; Appleman, J. R.; Blakley, R. L., Critical role of phenylalanine 34 of human dihydrofolate reductase in substrate and inhibitor binding and in catalysis. *Biochemistry* **1994,** 33, (33), 9945-52.

128. Schweitzer, B. I.; Srimatkandada, S.; Gritsman, H.; Sheridan, R.; Venkataraghavan, R.; Bertino, J. R., Probing the role of two hydrophobic active site residues in the human dihydrofolate reductase by site-directed mutagenesis. *J Biol Chem* **1989,** 264, (34), 20786-95.

129. Thompson, P. D.; Freisheim, J. H., Conversion of arginine to lysine at position 70 of human dihydrofolate reductase: generation of a methotrexate-insensitive mutant enzyme. *Biochemistry* **1991,** 30, (33), 8124-30.

130. Fischer, A., Severe combined immunodeficiencies. *Immunodefic Rev* **1992,** 3, (2), 83-100.

131. Blaese, R. M.; Culver, K. W.; Chang, L.; Anderson, W. F.; Mullen, C.; Nienhuis, A.; Carter, C.; Dunbar, C.; Leitman, S.; Berger, M.; et al., Treatment of severe combined immunodeficiency disease (SCID) due to adenosine deaminase deficiency with CD34+ selected autologous peripheral blood cells transduced with a human ADA gene. Amendment to clinical research project, Project 90-C-195, January 10, 1992. *Hum Gene Ther* **1993,** 4, (4), 521-7.

132. Cavazzana-Calvo, M.; Hacein-Bey, S.; de Saint Basile, G.; Gross, F.; Yvon, E.; Nusbaum, P.; Selz, F.; Hue, C.; Certain, S.; Casanova, J. L.; Bousso, P.; Deist, F. L.; Fischer, A., Gene therapy of human severe combined immunodeficiency (SCID)-X1 disease. *Science* **2000,** 288, (5466), 669-72.

133. Hacein-Bey-Abina, S.; Le Deist, F.; Carlier, F.; Bouneaud, C.; Hue, C.; De Villartay, J. P.; Thrasher, A. J.; Wulffraat, N.; Sorensen, R.; Dupuis-Girod, S.; Fischer, A.; Davies, E. G.; Kuis, W.; Leiva, L.; Cavazzana-Calvo, M., Sustained correction of X-linked severe combined immunodeficiency by ex vivo gene therapy. *N Engl J Med* **2002,** 346, (16), 1185-93.

134. Aiuti, A.; Slavin, S.; Aker, M.; Ficara, F.; Deola, S.; Mortellaro, A.; Morecki, S.; Andolfi, G.; Tabucchi, A.; Carlucci, F.; Marinello, E.; Cattaneo, F.; Vai, S.; Servida, P.; Miniero, R.; Roncarolo, M. G.; Bordignon, C., Correction of ADA-SCID by stem cell gene therapy combined with nonmyeloablative conditioning. *Science* **2002,** 296, (5577), 2410-3.

135. Hacein-Bey-Abina, S.; Von Kalle, C.; Schmidt, M.; McCormack, M. P.; Wulffraat, N.; Leboulch, P.; Lim, A.; Osborne, C. S.; Pawliuk, R.; Morillon, E.; Sorensen, R.; Forster, A.; Fraser, P.; Cohen, J. I.; de Saint Basile, G.; Alexander, I.; Wintergerst, U.; Frebourg, T.; Aurias, A.; Stoppa-Lyonnet, D.; Romana, S.; Radford-Weiss, I.; Gross, F.; Valensi, F.; Delabesse, E.; Macintyre, E.; Sigaux, F.; Soulier, J.; Leiva, L. E.; Wissler, M.; Prinz, C.; Rabbitts, T. H.; Le Deist, F.; Fischer, A.; Cavazzana-Calvo, M., LMO2-associated clonal T cell proliferation in two patients after gene therapy for SCID-X1. *Science* **2003,** 302, (5644), 415-9.

136. Hacein-Bey-Abina, S.; von Kalle, C.; Schmidt, M.; Le Deist, F.; Wulffraat, N.; McIntyre, E.; Radford, I.; Villeval, J. L.; Fraser, C. C.; Cavazzana-Calvo, M.; Fischer, A., A serious adverse event after successful gene therapy for X-linked severe combined immunodeficiency. *N Engl J Med* **2003,** 348, (3), 255-6.

137. Giordano, F. A.; Hotz-Wagenblatt, A.; Lauterborn, D.; Appelt, J. U.; Fellenberg, K.; Nagy, K. Z.; Zeller, W. J.; Suhai, S.; Fruehauf, S.; Laufs, S., New bioinformatic strategies to rapidly characterize retroviral integration sites of gene therapy vectors. *Methods Inf Med* **2007,** 46, (5), 542-7.

138. Bauer, T. R., Jr.; Allen, J. M.; Hai, M.; Tuschong, L. M.; Khan, I. F.; Olson, E. M.; Adler, R. L.; Burkholder, T. H.; Gu, Y. C.; Russell, D. W.; Hickstein, D. D., Successful

treatment of canine leukocyte adhesion deficiency by foamy virus vectors. *Nat Med* **2008,** 14, (1), 93-7.

139. Chalmers, D.; Ferrand, C.; Apperley, J. F.; Melo, J. V.; Ebeling, S.; Newton, I.; Duperrier, A.; Hagenbeek, A.; Garrett, E.; Tiberghien, P.; Garin, M., Elimination of the truncated message from the herpes simplex virus thymidine kinase suicide gene. *Mol Ther* **2001,** 4, (2), 146-8.

140. Zaiss, A. K.; Son, S.; Chang, L. J., RNA 3' readthrough of oncoretrovirus and lentivirus: implications for vector safety and efficacy. *J Virol* **2002,** 76, (14), 7209-19.

141. Hirata, R.; Chamberlain, J.; Dong, R.; Russell, D. W., Targeted transgene insertion into human chromosomes by adeno-associated virus vectors. *Nat Biotechnol* **2002,** 20, (7), 735-8.

142. Sawai, N.; Persons, D. A.; Zhou, S.; Lu, T.; Sorrentino, B. P., Reduction in hematopoietic stem cell numbers with in vivo drug selection can be partially abrogated by HOXB4 gene expression. *Mol Ther* **2003,** 8, (3), 376-84.

143. Kramer, B. A.; Lemckert, F. A.; Alexander, I. E.; Gunning, P. W.; McCowage, G. B., Characterisation of a P140K mutant O6-methylguanine-DNA-methyltransferase (MGMT)-expressing transgenic mouse line with drug-selectable bone marrow. *J Gene Med* **2006,** 8, (9), 1071-85.

144. Yam, P.; Jensen, M.; Akkina, R.; Anderson, J.; Villacres, M. C.; Wu, J.; Zaia, J. A.; Yee, J. K., Ex vivo selection and expansion of cells based on expression of a mutated inosine monophosphate dehydrogenase 2 after HIV vector transduction: effects on lymphocytes, monocytes, and CD34+ stem cells. *Mol Ther* **2006,** 14, (2), 236-44.

145. Taub, J. W.; Huang, X.; Ge, Y.; Dutcher, J. A.; Stout, M. L.; Mohammad, R. M.; Ravindranath, Y.; Matherly, L. H., Cystathionine-beta-synthase cDNA transfection alters the sensitivity and metabolism of 1-beta-D-arabinofuranosylcytosine in CCRF-CEM leukemia cells in vitro and in vivo: a model of leukemia in Down syndrome. *Cancer Res* **2000,** 60, (22), 6421-6.

146. Lorico, A.; Bratbak, D.; Meyer, J.; Kunke, D.; Krauss, S.; Plott, W. E.; Solodushko, V.; Baum, C.; Fodstad, O.; Rappa, G., Gamma-glutamylcysteine synthetase and L-buthionine-(S,R)-sulfoximine: a new selection strategy for gene-transduced neural and hematopoietic stem/progenitor cells. *Hum Gene Ther* **2005,** 16, (6), 711-24.

147. Allay, J. A.; Persons, D. A.; Galipeau, J.; Riberdy, J. M.; Ashmun, R. A.; Blakley, R. L.; Sorrentino, B. P., In vivo selection of retrovirally transduced hematopoietic stem cells. *Nat Med* **1998,** 4, (10), 1136-43.

148. Hock, R. A.; Miller, A. D., Retrovirus-mediated transfer and expression of drug resistance genes in human haematopoietic progenitor cells. *Nature* **1986,** 320, (6059), 275-7.

149. Banerjee, D.; Zhao, S. C.; Tong, Y.; Steinherz, J.; Gritsman, K.; Bertino, J. R., Transfection of a nonactive site mutant murine DHFR cDNA (the tryptophan 15 mutant) into Chinese hamster ovary and mouse marrow progenitor cells imparts MTX resistance in vitro. *Cancer Gene Ther* **1994,** 1, (3), 181-4.

150. Banerjee, D.; Schweitzer, B. I.; Volkenandt, M.; Li, M. X.; Waltham, M.; Mineishi, S.; Zhao, S. C.; Bertino, J. R., Transfection with a cDNA encoding a Ser31 or Ser34 mutant human dihydrofolate reductase into Chinese hamster ovary and mouse marrow progenitor cells confers methotrexate resistance. *Gene* **1994,** 139, (2), 269-74.

151. Cheng, K. K.-F., Association of plasma methotrexate, neutropenia, hepatic dysfunction, nausea/vomiting and oral mucositis in children with cancer. *European Journal of Cancer Care* **2007,** In press.

152. Goldman, I. D., The mechanism of action of methotrexate. I. Interaction with a low-affinity intracellular site required for maximum inhibition of deoxyribonucleic acid synthesis in L-cell mouse fibroblasts. *Mol Pharmacol* **1974,** 10, (2), 257-74.

153. Spencer, H. T.; Sleep, S. E.; Rehg, J. E.; Blakley, R. L.; Sorrentino, B. P., A gene transfer strategy for making bone marrow cells resistant to trimetrexate. *Blood* **1996,** 87, (6), 2579-87.

154. Ercikan-Abali, E. A.; Mineishi, S.; Tong, Y.; Nakahara, S.; Waltham, M. C.; Banerjee, D.; Chen, W.; Sadelain, M.; Bertino, J. R., Active site-directed double mutants of dihydrofolate reductase. *Cancer Res* **1996,** 56, (18), 4142-5.

155. Sauerbrey, A.; McPherson, J. P.; Zhao, S. C.; Banerjee, D.; Bertino, J. R., Expression of a novel double-mutant dihydrofolate reductase-cytidine deaminase fusion gene confers resistance to both methotrexate and cytosine arabinoside. *Hum Gene Ther* **1999,** 10, (15), 2495-504.

156. Takebe, N.; Xu, L. C.; MacKenzie, K. L.; Bertino, J. R.; Moore, M. A., Methotrexate selection of long-term culture initiating cells following transduction of CD34(+) cells with a retrovirus containing a mutated human dihydrofolate reductase gene. *Cancer Gene Ther* **2002,** 9, (3), 308-20.

157. Capiaux, G. M.; Budak-Alpdogan, T.; Takebe, N.; Mayer-Kuckuk, P.; Banerjee, D.; Maley, F.; Bertino, J. R., Retroviral transduction of a mutant dihydrofolate reductase-thymidylate synthase fusion gene into murine marrow cells confers resistance to both methotrexate and 5-fluorouracil. *Hum Gene Ther* **2003,** 14, (5), 435-46.

158. Zhao, H.; Arnold, F. H., Optimization of DNA shuffling for high fidelity recombination. *Nucleic Acids Res* **1997,** 25, (6), 1307-8.

159. Chica, R. A.; Doucet, N.; Pelletier, J. N., Semi-rational approaches to engineering enzyme activity: combining the benefits of directed evolution and rational design. *Curr Opin Biotechnol* **2005,** 16, (4), 378-84.

160. Segel, I. H., *In Enzyme Kinetics : Behavior and Analysis of rapid Equilibrium and Steady-State Enzyme Systems*. Wiley Classics Library ed.; John Wiley and sons: 1993; p 957.

161. Hawley, R. G.; Lieu, F. H.; Fong, A. Z.; Hawley, T. S., Versatile retroviral vectors for potential use in gene therapy. *Gene Ther* **1994,** 1, (2), 136-8.

162. Ory, D. S.; Neugeboren, B. A.; Mulligan, R. C., A stable human-derived packaging cell line for production of high titer retrovirus/vesicular stomatitis virus G pseudotypes. *Proc Natl Acad Sci U S A* **1996,** 93, (21), 11400-6.

163. Horn, P. A.; Topp, M. S.; Morris, J. C.; Riddell, S. R.; Kiem, H. P., Highly efficient gene transfer into baboon marrow repopulating cells using GALV-pseudotype oncoretroviral vectors produced by human packaging cells. *Blood* **2002,** 100, (12), 3960-7.

164. Neff, T.; Beard, B. C.; Kiem, H. P., Survival of the fittest: in vivo selection and stem cell gene therapy. *Blood* **2006,** 107, (5), 1751-60.

165. Persons, D. A.; Allay, J. A.; Bonifacino, A.; Lu, T.; Agricola, B.; Metzger, M. E.; Donahue, R. E.; Dunbar, C. E.; Sorrentino, B. P., Transient in vivo selection of transduced peripheral blood cells using antifolate drug selection in rhesus macaques that received transplants with hematopoietic stem cells expressing dihydrofolate reductase vectors. *Blood* **2004,** 103, (3), 796-803.

166. Sorg, U. R.; Kleff, V.; Fanaei, S.; Schumann, A.; Moellmann, M.; Opalka, B.; Thomale, J.; Moritz, T., O6-methylguanine-DNA-methyltransferase (MGMT) gene therapy targeting haematopoietic stem cells: studies addressing safety issues. *DNA Repair (Amst)* **2007,** 6, (8), 1197-209.

167. Dolznig, H.; Kolbus, A.; Leberbauer, C.; Schmidt, U.; Deiner, E. M.; Mullner, E. W.; Beug, H., Expansion and differentiation of immature mouse and human hematopoietic progenitors. *Methods Mol Med* **2005,** 105, 323-44.

168. Jhoti, H.; Cleasby, A.; Verdonk, M.; Williams, G., Fragment-based screening using X-ray crystallography and NMR spectroscopy. *Curr Opin Chem Biol* **2007,** 11, (5), 485-93.

169. Scapin, G., Structural biology and drug discovery. *Curr Pharm Des* **2006,** 12, (17), 2087-97.

170. Banerjee, D.; Bertino, J. R., Myeloprotection with drug-resistance genes. *Lancet Oncol* **2002,** 3, (3), 154-8.

171. Rosenberg, S. A.; Restifo, N. P.; Yang, J. C.; Morgan, R. A.; Dudley, M. E., Adoptive cell transfer: a clinical path to effective cancer immunotherapy. *Nat Rev Cancer* **2008,** 8, (4), 299-308.

172. Nienhuis, A. W., Development of gene therapy for blood disorders. *Blood* **2008,** 111, (9), 4431-44.

173. Miccio, A.; Cesari, R.; Lotti, F.; Rossi, C.; Sanvito, F.; Ponzoni, M.; Routledge, S. J.; Chow, C. M.; Antoniou, M. N.; Ferrari, G., In vivo selection of genetically modified erythroblastic progenitors leads to long-term correction of beta-thalassemia. *Proc Natl Acad Sci U S A* **2008,** 105, (30), 10547-52.

174. Dudley, M. E.; Yang, J. C.; Sherry, R.; Hughes, M. S.; Royal, R.; Kammula, U.; Robbins, P. F.; Huang, J.; Citrin, D. E.; Leitman, S. F.; Wunderlich, J.; Restifo, N. P.; Thomasian, A.; Downey, S. G.; Smith, F. O.; Klapper, J.; Morton, K.; Laurencot, C.; White, D. E.; Rosenberg, S. A., Adoptive Cell Therapy for Patients With Metastatic Melanoma: Evaluation of Intensive Myeloablative Chemoradiation Preparative Regimens. *J Clin Oncol* **2008**.

175. Appleman, J. R.; Prendergast, N.; Delcamp, T. J.; Freisheim, J. H.; Blakley, R. L., Kinetics of the formation and isomerization of methotrexate complexes of recombinant human dihydrofolate reductase. *J Biol Chem* **1988,** 263, (21), 10304-13.

176. Sandefur, C. I.; Wooden, J. M.; Quaye, I. K.; Sirawaraporn, W.; Sibley, C. H., Pyrimethamine-resistant dihydrofolate reductase enzymes of Plasmodium falciparum are not enzymatically compromised in vitro. *Mol Biochem Parasitol* **2007,** 154, (1), 1-5.

177. Watt, E. D.; Shimada, H.; Kovrigin, E. L.; Loria, J. P., The mechanism of rate-limiting motions in enzyme function. *Proc Natl Acad Sci U S A* **2007,** 104, (29), 11981-6.

178. Eisenmesser, E. Z.; Millet, O.; Labeikovsky, W.; Korzhnev, D. M.; Wolf-Watz, M.; Bosco, D. A.; Skalicky, J. J.; Kay, L. E.; Kern, D., Intrinsic dynamics of an enzyme underlies catalysis. *Nature* **2005,** 438, (7064), 117-21.

179. Stockman, B. J.; Nirmala, N. R.; Wagner, G.; Delcamp, T. J.; DeYarman, M. T.; Freisheim, J. H., Methotrexate binds in a non-productive orientation to human dihydrofolate reductase in solution, based on NMR spectroscopy. *FEBS Lett* **1991,** 283, (2), 267-9.

180. Johnson, J. M.; Meiering, E. M.; Wright, J. E.; Pardo, J.; Rosowsky, A.; Wagner, G., NMR solution structure of the antitumor compound PT523 and NADPH in the ternary complex with human dihydrofolate reductase. *Biochemistry* **1997,** 36, (15), 4399-411.

181. Loria, J. P.; Berlow, R. B.; Watt, E. D., Characterization of enzyme motions by solution NMR relaxation dispersion. *Acc Chem Res* **2008,** 41, (2), 214-21.

Annexe 1: Matériel supplémentaire

Chapitre 4

Ex vivo MTX selection in BM liquid media - Infected BM cells were plated in 35 mm dishes at a concentration of 1×10^6 cells/mL in liquid BM media in presence or absence of 1 μM MTX. Cells were incubated for 4 days at 37°C / 5% CO_2. Myeloid clonogenic progenitor assays were conducted on day 0 and day 4 to evaluate infection rate (day 0) and survival of cells after selection (day 4). For these assays, cells were plated on MC medium at 2×10^3 and 5×10^3 cells/mL in 35 mm dishes. Colonies were scored after 10 days incubation at 37°C / 5% CO_2 using normal and GFP-fluorescence lamp microscopy.

Competitive repopulation assay of BM cells in murine recipients following MTX-selection in BM medium - Co-cultured BM cells were analyzed by flow cytometry to assess the percentage of infection of each construct (monitoring GFP signal). Infected BM cells were diluted to 25% with mock-infected co-cultured BM cells, and plated at 1×10^6 cells/mL in 35 mm plates, in 3 mL BM medium in presence or absence of 1 μM MTX. Following incubation for 4 days at 37°C / 5% CO_2, lethally-irradiated recipient C57BL/6J mice were injected intravenously with a mix of 2×10^5 selected cells and 1×10^5 C57BL/6J helper cells. In parallel, myeloid clonogenic progenitor assays were conducted on day 0 and day 4 as described above.

Repopulation by BM cells in murine recipients was evaluated by monitoring GFP signalling in peripheral blood samples isolated from the tail-vein of recipient mice, at 12 and 16 weeks post-injection. Blood samples (1 capillary) were treated with 1× erythrocyte lysis buffer (155 mM NH_4Cl, 10 mM $NaHCO_3$, 0.1 mM EDTA) for 10 minutes on ice and washed twice with PBS + 2% FCS before flow cytometry analysis.

Mice were sacrificed at 17 weeks post transplantation and integrity of the provirus, genomic DNA from BM and spleen cells was prepared with the DNAzol reagent (Invitrogen) and 15 ug DNA digested with KpnI, wich cleave in the LTRs, thus releasing identical fragments for all proviruses unless rearrangement occurred. Southern blot analyses were performed as described previously (Chapitre 4). ^{32}P probes of GFP were generated using standard techniques. Morphology was assessed by Wright staining of cytospin preparations of BM cells.

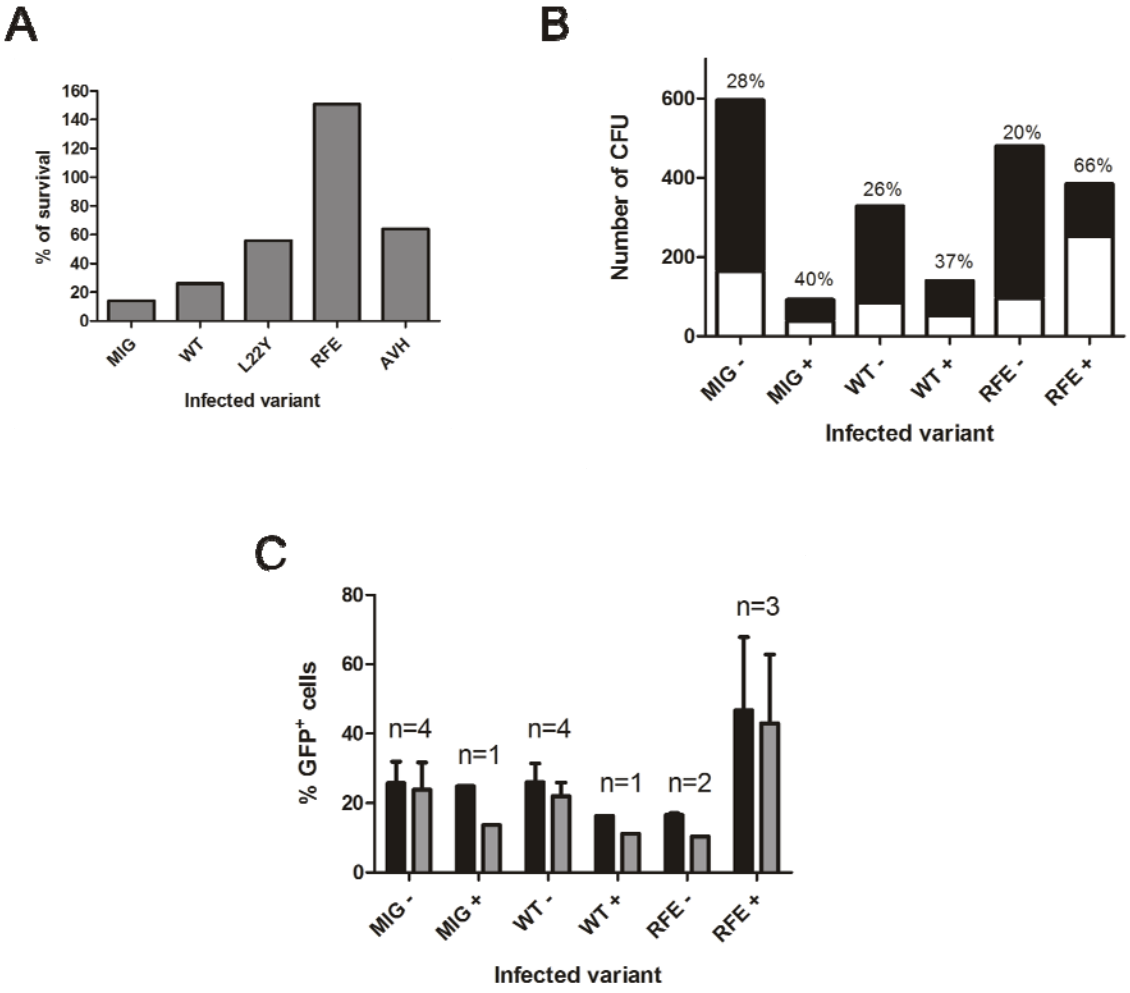

Figure A1.1. Preliminary experiments to evaluate the efficiency of highly MTX-resistant hDHFR double and triple mutants as *ex vivo* selection markers for hematopoietic cells. A) Clonogenic progenitor assays following 4-day MTX-selection of infected BM cells in liquid culture with 1 μM MTX. BM cells infected with WT hDHFR and variants L22Y, SFE, RFE, RTS or AVH were plated at 1×10^6 cells/mL in BM medium in the presence and absence of 1000 nM MTX. After 4 days, cells were plated on semi-solid MC media at 5×10^3 cells/mL. The surviving colonies were scored after 12 days with normal and GFP-fluoresence microscopy. The percentage of survival is the ratio of GFP-fluorescent colonies counted in presence *vs* absence of MTX. The results shown are for a single experiment.

MTX selection and engraftment of infected murine BM cells in recipient C57BL/6J mice. BM cells infected with MIG, WT hDHFR and hDHFR variant RFE were diluted to approximately 25% with non-infected BM cells, according to GFP fluorescence. Cells were plated in BM medium in the presence (+) or absence (-) of 1 μM MTX. B. After 4 days of selection, a myeloid progenitor assay was performed. The colonies were scored after 10 days with normal (black bars) and GFP-fluorescence (white bars) microscopy (single experiment). Percentage of GFP^+ cells in each population is reported above the bars. Only the cells infected with the MTX-resistant RFE variant showed strong survival following MTX-selection. C. After 4 days of selection, 3×10^5 cells were injected in the tail vein of lethally irradiated C57BL/6J mouse recipients. Percentage of GFP^+ cells from blood samples isolated 13 weeks (black bars) and 17 weeks (grey bars) post-injection are reported. The number of mice per condition tested is given above the bars. One mouse displayed 88% and 82% GFP^+ cells at 13 weeks and 17 weeks post-engraftment respectively, while the other two displayed 20 and 33% GFP^+ cells, respectively, both at 13 or 17 weeks post-engraftment. These percentages were substantially higher than those observed in control mice engrafted with cells exposed to MTX (MIG: 14%; WT hDHFR: 11% at 17 weeks post-engraftment).

Chapitre 5

Expression and purification of His_6-hDHFR F31R/Q35E – An overnight preculture of SK037/His_6-hDHFR F31R/Q35E-pQE32 was used to inoculate 1 L of LB medium. The culture was grown at 37°C until the $A_{600\ nm} \approx 0.7$. Protein expression was induced with the addition of 1 mM of isopropyl 1-thio-β-D-galactopyranoside (IPTG), after which the cells were grown for 3 h at 37°C. Induced cells were harvested by centrifugation (4000*g* for 30 min at 4°C). The cell pellet was resuspended in 0.1 M phosphate buffer, pH 8.0, at 4°C. The cells were lysed on ice using a Branson sonicator (four pulses at 200 W for 30 s with a tapered micro-tip). The cellular debris was pelleted by centrifugation (4000*g* for 30 min at 4°C) and the supernatant was filtered through a 0.2µm filter before purification.

Purification was performed following a 2-step purification protocol on an AKTA FPLC (GE Healthcare, Piscataway, NJ) at 5°C. First, the supernatant was applied to a HisTrap FF 1 mL prepacked cartridge (GE Healthcare) followed by a 10 column volumes (CV) wash with 0.1 M phosphate buffer, pH 8.0, at 1 mL/min. A step-wise gradient of imidazole (10, 20, 50 and 200 mM; 5 CV for each step) in 0.1 M phosphate buffer, pH 8.0, was used to elute the F31R/Q35E mutant. hDHFR activity was monitored in MATS buffer, pH 7.6, in the presence of 100 µM each NADPH and DHF. Activity was measured in flat-bottom plates (Costar #3595) by monitoring concurrent depletion of NADPH and DHF ($\Delta\varepsilon_{340nm}$ = 12 800 $M^{-1}cm^{-1}$) on a FLUOstar OPTIMA UV-vis plate reader (BMG Laboratories, Offenburg, Germany). Active fractions were pooled and dialysed overnight at 4°C against 50 mM phosphate buffer, pH 7.5. Following dialysis, the sample (15 mL) was concentrated to 1.5 mL using an Amicon concentrator (MCWO 10000, Millipore), for injection on a Superose12 column (1.6 × 55 cm). The sample was eluted with 50 mM phosphate buffer, pH 7.5, at a flowrate of 1.5 mL/min. hDHFR activity was monitored as described above. Enzyme purity was evaluated following separation by SDS-PAGE (15% (w/v) polyacrylamide gel) stained by the zinc-imidazole method (1) and quantified using

the public domain image analysis software Scion Image (NIH, rsb.info.nih.gov/ nih-image). Protein concentration was quantified using the Bradford assay (Biorad, Hercules, CA).

Crystallization and X-ray data collection of His_6-hDHFR F31R/Q35E – Purified His_6-hDHFR F31R/Q35E enzyme was buffer-exchanged into 50 mM Imidazole pH 7.5 and concentrated to 20 mg/mL using an Amicon concentrator (MCWO 10000). MTX and NADPH were prepared as described previously (2) and were added at a final concentration of 4 mM each (5-fold molar excess) to the protein sample. Crystallization experiments were set up using hanging drop vapour diffusion experiments, with a reservoir volume of 1 mL and a drop size of 4 μL of equal volumes of protein and reservoir solutions. A reservoir solution containing 0.1 M Tris pH 8.5, 0.01 M $NiCl_2$ and 21% PEG 2000 MME yielded crystals that diffracted at 2.2 Å. The crystals were soaked in the mother liquor supplemented with 30% PEG 400 as a cryoprotectant, frozen in a nitrogen cryostream (model X-stream 2000), and stored in liquid nitrogen. Data collection was performed with a X8C beam at the National Synchrotron Light Source, Brookhaven National Laboratory, and processed using HKL2000 (3). (Table A1.1).

Structure Determination and Refinement – The structure was determined by molecular replacement using Phaser (4), which found six protein molecules in the asymmetric unit (Resolution Range Used: 2.21-40.89; Log Likelihood Gain (Refined): 1932.291). PDB ID 1U72 was used as a molecular replacement model. Reciprocal-space refinement was performed using Refmac (5), and included individual isotropic B-factor refinement. Manual model building was performed periodically using Coot (6) (Table A1.1). The full length of the hDHFR backbone could be modelled from the electron density mapin all six molecules in the asymmetric unit, as could some portion of the N-terminal His_6-tag. For all six protein molecules in the asymmetric unit, large regions of electron density were observed in the DHF- and NADPH-binding sites. MTX and NADPH were modelled into these sites, respectively.

Table A1.1. Crystallographic data for His_6-hDHFR F31R/Q35E

Data collection statistics	
Space group	P1
Number of Molecules per Asymmetric Unit	6
a (Å)	62.605
b (Å)	83.334
c (Å)	83.272
α (º)	62.92
β (º)	78.68
γ (º)	71.81
Wavelength (Å)	1.100
Resolution Range (Å)	2.21-40.89 (2.21-2.29)
Completeness (%)	92.1 (94.2)
Redundancy	3.6 (3.1
R_{merge}	6.2 (15.6)
Refinement statistics	
R_{factor}	31.420
R_{free} (5% free test set)	40.028 (3284 reflections)
Number of reflections	65,777
Reflection Cutoff in Refinement	$F > 0\sigma F$
Number of atoms	10446
Protein	9720
Water	240
Co-factor	288
Inhibitor	198
RMSD	
Bond length (Å)	0.010
Bond angle (º)	1.847
Average atomic B-Factor	32.789
Protein	32.85
Water	22.74
Co-factor	41.01
Inhibitor	30.06
Wilson B-Factor	32.253
Ramachandran Plot (non-Gly, non-Pro residues)	1026 (100)
Residues in Favoured Positions (%)	822 (80.1)
Residues in Allowed Positions (%)	137 (13.4)
Residues in Generously Allowed Positions (%)	34 (3.3)
Residues in Disallowed Positions (%)	33 (3.2)

Items in parentheses refer to the highest resolution shell.

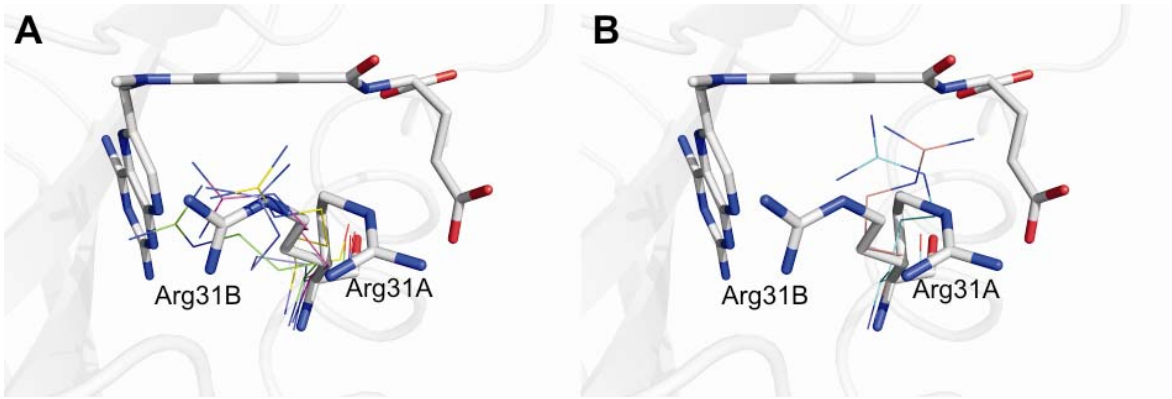

Figure A1.2. Multiple conformers of Arg31 in the lower resolution His_6-hDHFR F31R/Q35E (in lines) relative to 1.7 Å resolution hDHFR F31R/Q35E (in sticks). (A) Four of the six Arg31 residues found in the lower resolution structure adopt a conformation that clusters with Arg31B. (B) Two Arg31 residues found in the lower resolution structure adopt a conformation that neither resembles that of Arg31A or Arg31B.

References

1. Fernandez-Patron, C., Castellanos-Serra, L., and Rodriguez, P. (1992) *Biotechniques* 12(4), 564-573

2. Volpato, J. P., Fossati, E., and Pelletier, J. N. (2007) *J Mol Biol* 373(3), 599-611

3. Otwinowski, Z., and Minor, W. (1997) Processing of X-ray diffraction data collected in oscillation mode. In. *Methods in Enzymology*, Academic Press

4. Storoni, L. C., McCoy, A. J., and Read, R. J. (2004) *Acta Crystallographica, Section D: Biological Crystallography* 60, 432-438

5. Murshudov, G. N., Vagin, A. A., and Dodson, E. J. (1997) *Acta Crystallographica, Section D: Biological Crystallography* D53, 240-255

6. Emsley, P., and Cowtan, K. (2004) *Acta Crystallographica, Section D: Biological Crystallography* D60(12), 2126-2132